Characterisation of ice particle residuals and aerosol particles in laboratory and field experiments by scanning electron microscopy during INUIT (Ice Nuclei research UnIT)

Submitted in fulfilment of the requirements for the degree of
Doctor rerum naturalium (Dr. rer. nat.)
Dissertation by Stine Eriksen Hammer
At the Department of Materials and Earth Sciences
TU Darmstadt - D17

TECHNISCHE UNIVERSITÄT DARMSTADT

1. Examiner: Professor Dr. Stephan Weinbruch

2. Examiner: Professor Dr. Konrad Kandler

Darmstadt 2019

Characterisation of ice particle residuals and aerosol particles in laboratory and field experiments by scanning electron microscopy during INUIT (Ice Nuclei research UnIT)

By
Stine Eriksen Hammer

Institute of Applied Geosciences
Department of Materials and Earth Sciences
Technische Universität Darmstadt

Submitted: 06.02.2019
Year of publication in TUprints: 2019
URN: urn:nbn:de:tuda-tuprints-86113
Date of disputation: 29.03.2019

Darmstadt 2019

Characterisation of ice particle residuals and aerosol particles in laboratory and field experiments by scanning electron microscopy during INUIT (Ice Nuclei research UnIT)

Stine Eriksen Hammer

ABSTRACT

Ice nucleating particles are necessary for formation of ice crystals in mixed-phase clouds, but there are still uncertainties regarding physico-chemical properties, variability and concentration of these particles in the environment. The ice nuclei research unit (INUIT), funded by the German research foundation (DFG), has thoroughly investigated ice nucleation in laboratory, model and field studies. This thesis contains research from a field study (Jungfraujoch, Switzerland) and a laboratory experiment (of coal fly ash) as well as a methodological part to study the performance of single particle techniques applied. Scanning electron microscopy (SEM) with energy dispersive X-ray microanalysis (EDX) was used as main technique in this thesis. The capability of SEM-EDX in ice nucleation research is demonstrated in the following chapters and in the corresponding papers to this thesis.

Single particle analysis by SEM-EDX can be performed operator controlled (opSEM) or computer controlled (ccSEM). In this thesis, it is shown that the technique of choice is dependent on the research question and the particle composition. A comparison of the techniques for different types of aerosol samples provided valuable information about the differences and was further used as a guide to the technique of choice in the remaining studies.

Ice particle residuals were studied in mixed-phase clouds at Jungfraujoch in February 2017. The results show that different silicate groups were the most important ice nucleating particles, consistent with previous literature. However, in our study, soot and complex secondary particles were not found in the ice particle residual fraction which is inconsistent with previous results. Furthermore, an upgraded sampling procedure gave the opportunity to determine enrichment and depletion of particle groups in the ice particle residual fraction relative to total aerosol, as well as to identify sampling artefacts.

The ice nucleation properties of coal fly ash particles were investigated in a laboratory study. In this study, SEM-EDX was applied to characterise the fly ash particles before and after suspension in water. Anhydrite and CaO, in one of the fly ash samples, reacted to gypsum, calcium hydroxide and calcite needles after suspension. This change led to an overestimation of the ice nucleation active surface site density, which was later corrected for because of the morphological information from SEM.

Last, a newly developed method for phase determination by single particle mass spectrometry (SP-MS) was tested and compared to SEM-EDX. Both techniques show the same differences in chemical composition of mineral dust from North-Africa. SP-MS could characterise the phase composition of the particles. Still, SP-MS was limited by matrix effects which was seen from a higher abundance of Ca- and Mg-rich silicates obtained by SEM-EDX. A better understanding of these matrix effects is needed to improve the application of the former method to ice particle research.

Rasterelektronenmikroskopische Charakterisierung von Eispartikel-residuen und Aerosolpartikeln in Labor- und Feldexperimenten während INUIT (Ice Nuclei research UnIT)

KURZFASSUNG

Für die Bildung von Eiskristallen in Mischphasenwolken ist die Anwesenheit von Partikeln notwendig. Es bestehen jedoch immer noch Unsicherheiten hinsichtlich der physikalisch-chemischen Eigenschaften, der Variabilität und der Konzentration dieser Partikel. Im Rahmen der DFG-Forschergruppe INUIT (Ice Nuclei reseach UnIT) wurde die Eiskeimbildung in Labor-, Modell- und Feldstudien detailliert untersucht. Die vorliegende Arbeit enthält Ergebnisse einer Feldstudie (Jungfraujoch, Schweiz), einem Laborexperiment (Flugaschen aus der Kohleverbrennung) sowie einen methodischen Teil zur Untersuchung der Leistungsfähigkeit der verwendeten Messtechniken. Als Hauptmethode wurde in dieser Arbeit Rasterelektronenmikroskopie (SEM) gekoppelt mit energie-dispersiver Röntgenmikroanalyse (EDX) verwendet. Das Potential von SEM-EDX in der Eisnukleationsforschung wird in den folgenden Kapiteln und in den entsprechenden Veröffentlichungen zu dieser Dissertation demonstriert.

Die Einzelpartikelanalyse mit SEM-EDX kann bediener- (opSEM) oder computergesteuert (ccSEM) durchgeführt werden. In dieser Arbeit wird gezeigt, dass je nach Fragestellung und Partikelzusammensetzung beide Ansätze Vor- und Nachteile haben. Dementsprechend wurde in den nachfolgenden Studien die jeweilig beste Technik eingesetzt.

In dem Feldexperiment auf dem Jungfraujoch (Februar 2017) wurden Eispartikelresiduen in Mischphasenwolken untersucht. Verschiedene Gruppen von Silikaten waren (in Übereinstimmung mit früheren Arbeiten) die wichtigsten Eiskeime. In unserer Studie wurden jedoch keine Ruß- und komplexen Sekundärpartikel bei den Eispartikelresiduen gefunden, was im Gegensatz zu früheren Veröffentlichungen steht. Ein verbessertes Probenahmeverfahren eröffnete die Möglichkeit, die An- bzw. Abreicherung von Partikelgruppen in der Eisresiduenfraktion relativ zum Gesamtaerosol zu bestimmen. Außerdem erlaubte dieses Probenahmeverfahren eine bessere Identifikation von Artefakten.

Die Eiskeimfähigkeit von Flugaschepartikeln aus der Kohleverbrennung wurde in einer Laborstudie untersucht. Hierbei wurde SEM-EDX eingesetzt, um die Flugascheteilchen vor und nach der Suspension in Wasser zu charakterisieren. In einem Flugaschetyp reagierten Anhydrit und CaO zu nadelförmigem Gips, Calciumhydroxid und Calcit. Die Änderung der Morphologie während dieser Reaktion führte zunächst zu einer Überschätzung der Oberflächedichte aktiver Stellen für die Eisnukleation, die jedoch durch die SEM-Untersuchungen korrigiert wurde.

Abschließend wurde eine neue Methode zur Phasenbestimmung mit Einzelpartikel-Massenspektrometrie (SP-MS) durch den Vergleich mit SEM-EDX überprüft. Beide Techniken zeigten die selben Unterschiede in der chemischen Zusammensetzung von nordafrikanischen Mineralstaubproben. SP-MS ermöglichte zusätzlich die Bestimmung der Phasenzusammensetzung. SEM-EDX konnte jedoch nachweisen, dass Ca und Mg-reiche Silikate in der SP-MS aufgrund von Matrixeffekten unvollständig detektiert wurden. Ein Verständnis der Matrixeffekte ist jedoch erforderlich, um die Anwendung dieser Methode in der Eispartikelforschung zu verbessern.

Karakterisering av iskjerner og aerosolpartikler i laboratorie- og feltforsøk med sveipeelektronmikroskopi som en del av INUIT-prosjektet (Ice Nuclei research UnIT)

SAMMENDRAG

Iskjerner er nødvendig for at iskrystaller skal dannes i blandede-faseskyer. Det er stor usikkerhet knyttet til iskjernenes fysisk-kjemiske egenskaper, variabilitet og konsentrasjon i miljøet. Prosjektet INUIT (Ice Nuclei research UnIT), finansiert av det tyske forskningsrådet (DFG), har gjennom laboratoriearbeid, modellering og feltarbeid undersøkt isdannelse i sammenheng med skydannelse. Denne avhandlingen omhandler en feltstudie (Jungfraujoch, Sveits) og et laboratorieexperiment (av flyveaske fra kullforbrenning), i tillegg til en metodisk del der ytelsen til forskjellige enkeltpartikkel-analyseteknikker er diskutert. Hovedmetoden i denne avhandlingen er sveipeelektronmikroskop (SEM) med energidispersiv Røntgenanalyse (EDX). Potensialet til SEM-EDX i forskning på isdannelse er demonstrert i de følgende kapitlene og i de tilhørende artiklene.

Enkelpartikkelanalyse med SEM-EDX kan utføres manuelt av en operatør (opSEM) eller datastyrt (ccSEM). I dette arbeidet er det vist at begge teknikkene har fordeler og ulemper avhengig av forskningsspørsmålet og partikkelsammensetningen. Sammenlikningen av de to ulike teknikkene gav grunnlag for å bestemme hvilken teknikk som passet best i de tre andre presenterte studiene.

Iskjerner ble studert i blandede-faseskyer på Jungfraujoch (Februar 2017). Resultatene viste at forskjellige typer silikater utpekte seg som de viktigste iskjernene. Dette sammensvarte med tidligere resultater. I motsetning til tidligere resultater fant vi hverken sot eller komplekse sekundære partikler i prøvene. Et forbedret prøvetakingsoppsett gav muligheten til å bestemme anrikning og reduksjon i iskjernefraksjonen relativt til total aerosol, og muligheten til å identifisere artefakter fra prøvetakingen.

Isdannelsesegenskapene til flyveaske fra kull ble undersøkt i en laboratoriestudie. I denne studien ble SEM-EDX bruk til å karakterisere flyveaskeprøvene før og etter den ble suspendert i vann. I en av prøvene reagerte anhydritt og CaO til nålformede gips, kasliumhydroksid og kalsitt etter suspension i vann. Denne endringen førte til en overestimering av isdannelsesegenskapene til denne typen flyveaske fra kullforbrenning. Denne overestimeringen ble korrigert for etter at den morfologiske endringen ble oppdaget med SEM.

En nyutviklet metode for å bestemme mineralfaser med enkelt-partikkel massespektrometer (SP-MS) ble testet og sammeliknet med SEM-EDX. Begge teknikkene viste samme forskjeller i den kjemiske sammensetningen til mineralstøvet fra Nord-Afrika. SP-MS kunne karakterisere mineralfasene. Utenom dette viste sammenlikningen at SP-MS-teknikken var begrenset av matrikseffekter sett av en høyere konsentrasjon Mg- og Ca-rike silikater detektert med SEM-EDX. En bedre forståelse av disse matrikseffektene er nødvendig for å forbedre anvendelsen i ispartikkelforskning.

DECLARATION OF AUTHORSHIP

Hereby I, Stine Eriksen Hammer, declare that I authored the present PhD-thesis alone and exclusively under the use of the literature denoted. The present PhD-thesis has by now not been used in any exam.

Darmstadt 06.02.2019 Stine Eriksen Hammer

ACKNOWLEDGMENT

I would like to thank all the participants of the INUIT group and collaborating institutes for the educational campaigns, as well as all the nice discussions afterwards within the INUIT meetings. A special thank you to the INUIT organizing committee and all the participants of the INUIT summer school and the INUIT Final Conference. I am grateful to have been a part of the INUIT project and for everything I learned. I acknowledge the German research foundation for financial support (INUIT FOR-1525, EB 383/3-1 and 264907654; 264912134; 416816480 KA 2280) and the Open Access Publishing Fund of the Technical University Darmstadt. This project also received funding from the European Union's Horizon 2020 research and innovation programme under grant agreement number 654109.

I would like to express my deep gratitude to my supervisors Prof. Dr. Stephan Weinbruch and Prof. Dr. Martin Ebert for the patient guidance during my PhD period. One extra thank you to Stephan Weinbruch for the useful critique in the writing phase, your enthusiasm and inspiration. To Martin Ebert, thank you for the guidance at the microscope and support when analysing the results.

I would like to thank all my co-authors for the collaboration and interesting discussions, I really value all your comments. A special thank you to Prof. Dr. Konrad Kandler for all help with the impactor set-up, the dilution unit and for always answering my questions during the campaigns and after. Thank you STAMI and Dr. Torunn Kringlen Ervik for the time at the SEM in Oslo, and for teaching me EBSD.

I am grateful to everyone who has been there during my PhD period. Thank you Thomas Dirsch for all your technical support, and to Astrid Kern for helping me get settle in Germany. To Dr. Nathalie Benker, thank you for staying in Cyprus the first week of my PhD to help me set-up the samples, and for all your help and nice words thereafter. A very special gratitude goes to my colleagues and former colleagues Dr. Dirk Scheuvens, Dr. Anette Worringen, Andebo Waza, Dr. Aryasree Sudharaj, Mark Scerri and Dr. Katharina Schütze, for all questions, answers and good times at the work-group seminars.

I am grateful to my host-family, Carolin and David Weygandt, for taking care of me and for teaching me German, and also all the dinners, talks and general help.

To my family and friends in Norway, thank you for your visits, your calls, the encouragement and all the love. A special thank you to my mom, Cathrine N. Eriksen, and dad, Bjørn-Erik Hammer, for your kind words, for backing me up during my stay, and for encouraging me to move to Germany back in 2016. Thank you, Aunt Elisabeth N. Eriksen, for always being there to cheer me up, and to my Gradma Jorun Grethe Eriksen for cheering me on. To Bjørn-Jostein Singstad, thanks for always listening and being there for me.

Last, as we say in Norwegian, "*Takk for meg*" (thanks for me). I enjoyed the time in Darmstadt, and I can hardly wait to use the things I learned in the time to come.

TABLE OF CONTENTS

ABSTRACT

DECLARATION OF AUTHORSHIP

ACKNOWLEDGMENT

1 ABOUT THIS THESIS 1

2 INTRODUCTION 3

2.1 Aerosol characterisation 3
2.1.1 Scanning electron microscopy 3
2.1.2 Single particle mass spectrometry 4
2.2 Ice nucleation 4
2.2.1 Ice nucleating particles and cloud interactions 4
2.2.2 Ice nucleating particle research 5
2.2.3 Ice particle residual selective inlets 6
2.2.4 Aerosol cloud chambers 7
2.3 Coal fly ash as ice nucleating particles 8
2.4 A new method in single particle mass spectrometry to study phase composition of mineral dust 9

3 MATERIAL AND METHODS 10

3.1 Sampling 10
3.1.1 Sampling in the ambient environment 10
3.1.2 Sampling in the laboratory 11
3.2 Scanning electron microscopy analysis 11
3.2.1 Operator controlled analysis 11
3.2.2 Computer controlled analysis 11
3.3 Statistical analysis 12

4 RESULTS AND DISCUSSION 13

4.1 Comparison of operator- and computer controlled scanning electron microscopy 13
4.1.1 Differences in particle group abundance 13
4.1.2 Which technique is better suited for which aerosol types? 14
4.2 Ice particle residuals in mixed-phase clouds at Jungfraujoch 15
4.2.1 Single particle analysis of ice particle residuals and total aerosol collected in parallel 16
4.2.2 Enrichment and depletion of ice particle residuals 17
4.3 Ice nucleation of coal fly ash particles 18
4.3.1 Morphology of dry and wet dispersed coal fly ash particles 18
4.3.2 Contribution of scanning electron microscopy analysis to the ice nucleation experiment of coal fly ash 21
4.4 Mineral dust identification by single particle mass spectrometry compared to computer controlled scanning electron microscopy 22
4.4.1 Chemical composition of the North-African mineral dust samples 22
4.4.2 Phase determination by single particle mass spectrometry 24

5 CONCLUSION AND FURTHER WORK 25

REFERENCES **27**

ABBREVIATIONS **36**

LIST OF FIGURES **37**

LIST OF TABLES **38**

SHORT CV **39**

PUBLICATIONS **41**

1 ABOUT THIS THESIS

This thesis is written cumulative based on the following papers, the first two papers as first-author and the next two as co-author. All the papers are attached in the back of this thesis.

Paper I

Eriksen Hammer, S., Mertes, S., Schneider, J., Ebert, M., Kandler, K., and Weinbruch, S.: Composition of ice particle residuals in mixed-phase clouds at Jungfraujoch (Switzerland): enrichment and depletion of particle groups relative to total aerosol, Atmospheric Chemistry and Physics, doi: 10.5194/acp-18-13987-2018, 2018.

Paper II

Eriksen Hammer, S., Ebert, M., and Weinbruch, S.: Comparison of operator- and computer-controlled scanning electron microscopy of particles from different atmospheric aerosol types, Analytical and Bioanalytical chemistry, doi: 10.1007/s00216-019-01614-7, 2019.

Paper III

Grawe, S., Augustin-Bauditz, S., Clemen, H. C., Ebert, M., Eriksen Hammer, S., Lubitz, J., Reicher, N., Rudich, Y., Schneider, J., Staacke, R., Stratmann, F., Welti, A., and Wex, H.: Coal fly ash: linking immersion freezing behavior and physicochemical particle properties, Atmospheric Chemistry and Physics, doi: 10.5194/acp-18-13903-2018, 2018.

Paper IV

Marsden, N. A., Ullrich, R., Möhler, O., Eriksen Hammer, S., Kandler, K., Cui, Z., Williams, P. I., Flynn, M. J., Liu, D., Allan, J. D., and Coe, H.: Mineralogy and mixing state of North African mineral dust by on-line single-particle mass spectrometry, Atmospheric Chemistry and Physics, doi: 10.5194/acp-19-2259-2019, 2019.

The main goal of this thesis was to apply scanning electron microscopy (SEM) with energy dispersive X-ray microanalysis (EDX) in ice nucleation research. This involves particle sampling behind ice selective inlets, as well as complementing single particle analysis with other ice nucleation experiments, and further develop and evaluate instrumentations already in use in ice research. In the following introduction, ice nucleation research is presented together with techniques in use to measure single particles. This thesis is based upon four scientific articles which can be divided in two main topics, 1) Study of ice nucleating particles (**paper I and III**), and 2) method validation and determination (**Paper II and IV**).

Paper I investigates ice particle residuals sampled in mixed-phase clouds during the INUIT campaign at Jungfraujoch 2017. The sampling method used during this campaign is an upgraded version of previous set-ups. Particles collected during this campaign were characterised with SEM. The most important ice particle residual groups were silica, aluminosilicates and other aluminosilicates at site temperatures between -10 and -18 °C.

The second scientific article (**paper II**) characterises the differences between operator- and computer controlled SEM. Aerosol particle samples from different areas were analysed to highlight the differences between the two SEM-EDX techniques. The result of this paper was used for method selection of the SEM-EDX technique applied in the other research articles in this thesis.

A description of coal fly ash particles in an immersion freezing experiment is presented in the third paper (**paper III**). This paper clearly illustrates the importance of morphological information on single particles in ice nucleation research, even for known bulk chemical composition.

In the fourth paper (**Paper IV**), North African mineral dust particles were investigated. This paper demonstrates a newly developed method for mineral classification in SP-MS. Computer controlled SEM was applied for method validation. A comparison of SP-MS and SEM-EDX is important to understand matrix effects in SP-MS which are limiting this technique in ice nucleation research.

2 INTRODUCTION

2.1 Aerosol characterisation

Aerosol characterisation is a scientifically important task. A special focus is set on human health research in respect to air quality measurement, as well as in atmospheric science in respect to climate change. In climate research, aerosols are under intensive investigations to study their influence on earths radiative forcing (Kulkarni et al., 2011). Aerosol in the atmosphere will influence the radiative forcing in three different ways, (1) directly by scattering and/ or absorbing the radiation, (2) semi-directly when absorption influences the vertical temperature profile, and (3) by the ability to interact with cloud formation as cloud condensation nuclei (CCN) or as ice nucleating particle (INP) (Storelvmo, 2017). Knowledge on chemical composition and morphology of single particles is crucial in terms of source identification to distinguish between i.e. anthropogenic and natural sources, as well as to understand the ice nucleation mechanisms (Kanji et al., 2017;Cziczo et al., 2017).

Different analytical techniques are in use to study atmospheric aerosol (McMurry, 2000). Single particle mass spectrometry (SP-MS) is often used to investigate single particles online (Trimborn et al., 2000;Bente et al., 2008;Roth et al., 2016). Other techniques like micro Raman spectroscopy (Craig et al., 2015), Fourier-transform infrared-spectrometry (Paton-Walsh et al., 2014) and X-ray photo electron spectroscopy (Craig et al., 1974;Zhu et al., 2001) are also applied in aerosol research, but these techniques are either specialised towards few specific particle groups, surface characteristics or not used solely as a single particle technique.

2.1.1 Scanning electron microscopy

Scanning electron microscopy with energy dispersive X-ray microanalysis (SEM-EDX) is an established approach for single particle analysis applied in many studies of ambient aerosol from different environments (Ebert et al., 2000;Ebert et al., 2002;Laskin et al., 2006;Targino et al., 2006;Kandler et al., 2007;Weinbruch et al., 2012;O'Brien et al., 2015;Gunsch et al., 2017;Wagner et al., 2017). With SEM-EDX, particles can be characterised based on morphology, chemical composition, size and stability under the electron beam. Particles can be studied either manually, herby referred to as operator controlled (opSEM), or automatically with the use of a specialised software, termed computer controlled (ccSEM) analysis. In aerosol science, both techniques are frequently applied (Laskin et al., 2006;Weinbruch et al., 2010;O'Brien et al., 2015;Ebert et al., 2016;Gunsch et al., 2017;Kandler et al., 2018). There are, to this date, no certified procedure for single particle analysis with SEM in environmental samples. Thus, operators can choose between several set-ups optimized to the research questions when investigating single particles (i.e. spot-/line-/ mapping- analysis, operator or computer controlled). A study of the performance and results of the two techniques, opSEM and ccSEM, analysing the same samples are presented in **paper II**. This study was conducted to emphasise the strengths and differences of both techniques. The work is expected to guide future investigators to settle upon the best suited technique for their specific research. Additionally, the restriction of closed data is accentuated in **paper II**. This last point does not only apply to SEM-EDX users, but to interdisciplinary readers who compare relative particle composition (sometimes unintentionally) independent of the analytical technique.

In the papers presented in this thesis, the SEM-EDX technique is solely used for classification based on the presence of chemical elements (without a precise quantification). A quantification can be reached with SEM-EDX, but in these cases specific care needs to be taken in correction of geometric and matrix effects. A possibility is to use specialised procedures like particle ZAF correction - at least for particles larger than 1 μm (Weinbruch et al., 1997), or the interpolation method described in (Kandler et al., 2018).

2.1.2 Single particle mass spectrometry

Single particle mass spectrometry is known to yield high real-time output data on single particles. Two different instruments are presented in this thesis (**Paper III** and **IV**), the laser ablation aerosol particles time of flight (LAAPTOF) mass spectrometer and aircraft-based laser ablation aerosol mass spectrometer (ALABAMA). Both SP-MS instruments use the same ionisation principle (laser desorption ionisation -LDI) and mass separation unit (Time of Flight -TOF). The mass separation includes bipolar TOF units which give the possibility of simultaneous measurement of negative and positive ion spectra. An obvious difference between the instruments is the actual size as ALABAMA is made for aircraft measurement and is hence smaller. Also, there is a slight difference in the size range which is investigated, ALABAMA [0.2-2.5μm] and LAAPTOF [0.4-2.5μm].

SP-MS has been applied in ice particle residual (IR) research in several field campaigns (Cziczo et al., 2003;DeMott et al., 2003;Kamphus et al., 2010;Baustian et al., 2012;Worringen et al., 2015;Schmidt et al., 2017). Generally, this technique is limited by particle loss related to specific size or shape (particle matrix effects), poor reproducibility as well as instrumentation variation e.g. difference in ionisation efficiency (Hatch et al., 2014;Marsden et al., 2018). This often leads to a systematic error for some particle types and an overall different sampling efficiency between instruments which are usually not reported (Marsden et al., 2016). As a result, a relatively low number of successfully collected particles behind ice-selective inlets are presented (Worringen et al., 2015).

2.2 Ice nucleation

In nature, water must overcome an energy barrier to transform from gas or liquid phase to ice crystals. This phase transition can occur in different ways depending on the surrounding conditions. Spontaneous freezing of supersaturated droplets, termed homogeneous ice nucleation (Vali et al., 2015), occurs at temperatures below -38°C and relative humidity (RH) with respect to ice > ~140 % (Kanji et al., 2017). At higher temperatures, as most often for mixed-phase clouds, a surface - like an INP - can lower the free energy leading to ice formation, termed heterogeneous ice nucleation.

2.2.1 Ice nucleating particles and cloud interactions

Ice nucleating particles play an important role in cloud formation. First, there are two main types of clouds where IRs are studied: cirrus and mixed-phase clouds. The focus of the field work study presented in **paper I** is of mixed-phase clouds. This type of cloud is important because they impact the hydrological cycle, serve as platform for cloud electrification, and

regulate radiation to earth (Korolev et al., 2017). A mixed-phase cloud consists of water droplets and ice crystals, and the partitioning between these two fractions determines its optical properties. In fact, a dense area of liquid will be optical thicker than a dense area of ice (Storelvmo, 2017). Initiation and deactivation of glaciation (diffusional growth when INPs interact with liquid water) in mixed-phase clouds will influence the cloud lifetime and precipitation (Myhre et al., 2013). Deactivation of cloud glaciation may occur when gases condense to INPs changing their ice forming ability temporarily or permanently.

2.2.2 Ice nucleating particle research

The fact that particles interact with clouds has been known for more than a century (Dufour, 1862;Aitken, 1923). Since the beginning, scientists have tried to figure out which particle types contribute to ice nucleation, along with understanding the detailed interaction between particle and the surrounding water. Today, the focus of many studies is quantification of INP concentrations in the environment, as well as the characterisation of the particles in terms of chemical composition (**paper I**) and surface characteristics. Different particle types have been tested in laboratory studies to investigate the ice nucleation activity (Hoose and Möhler, 2012;Atkinson et al., 2013;Grawe et al., 2016). This is also the work of **paper III** where the ice nucleation properties of coal fly ash were studied.

Several theories are discussed in previous literature regarding the active sites where particle and water interact to form an ice crystal. These includes surface morphology in terms of cracks, cavities, pores or steps (Hiranuma et al., 2014;Wagner et al., 2016;Kiselev et al., 2017) or the angle of these imperfections allowing more available hydroxyl groups (Freedman, 2015). Ice nucleation efficiency is also hypothesised to be enhanced by organic molecules like cellulose serving as the active site (Hiranuma et al., 2015), as well as gene expression of ice nucleating proteins (Hartmann et al., 2013) or other macromolecules (Pummer et al., 2015).

The outcome so far, from laboratory and field studies of INPs and IRs, is that mineral dust particles appear as the most important INP, due to their presence in the atmosphere and their ice nucleating efficiency (Kanji et al., 2017). Still, the mineral dust types diverge in ice nucleation efficiency, hence, a lot of work is performed to study different minerals (Zimmermann et al., 2008;Atkinson et al., 2013;Boose et al., 2016). **Paper IV** is a contribution to this work by studying a better procedure for characterisation of mineral dust using mass spectrometry with the aim to apply this method in ice nucleation research.

At relatively high temperatures (above -10 °C), biological particles (i.e. fungi, lichens, leaf litter and plankton) are the dominating INPs in laboratory studies (Després et al., 2012;Hoose and Möhler, 2012;Pummer et al., 2015;O'Sullivan et al., 2015). The atmospheric relevance of these particles as INPs under ambient conditions still needs to be confirmed as most research of mixed-phase clouds was performed at Jungfraujoch during winter, in free tropospheric conditions where biological particles are scarce. Due to the relatively large size of primary biological particles, the atmospheric relevance of these particles might be limited to the local scale. Still, the biological relevance to ice nucleation is intensively studied in regards to e.g. particle coatings of ice nucleating macromolecules (INMs) and in the relation to organic matter in sea spray (Wilson et al., 2015;DeMott et al., 2016;Augustin-Bauditz et al., 2016;Wolf et al., 2018). Sea salt particles are widely discussed when it comes to associated ice nucleation ability, as crystalline salts seem to activate ice under only cirrus conditions and the probability that

aging/ mixing does not occur before reaching this altitude is low (Kanji et al., 2017). Still, over the oceans, about 25 % of the IRs collected were classified as sea salt (Cziczo et al., 2013). Extensive studies are therefor made to clarify the contribution of sea salt to INPs, like the mentioned studies of the organic fraction in sea spray. Secondary aerosol particles are, in laboratory studies, investigated at more or less idealised cases of organic particles. This particle group is found to only nucleate ice at the lower end of the temperature range of mixed-phase clouds, close to homogenous freezing. Bearing in mind the constrains in the laboratory work, the results so far are uncertain because they do not incorporate atmospheric relevant parameters like variable particle types, mixing state, particle-generation, viscosity and time. From field experiments, secondary particles are reported in the IR fraction in both cirrus and mixed-phase clouds, notably often with a lower relative number than in total aerosol (Ebert et al., 2011;Cziczo et al., 2013;Worringen et al., 2015). Finally, particles originating from fossil fuel like soot and coal fly ash particles are reported as ice active in laboratory studies at similar temperatures as secondary aerosol particles (Hoose and Möhler, 2012;Grawe et al., 2016). In field studies, soot particles were reported in the IR fraction in both cirrus and mixed-phase clouds (Cozic et al., 2008;Ebert et al., 2011;Cziczo et al., 2013;Worringen et al., 2015). **Paper III** is dedicated to the study of ice nucleation ability of coal fly ash particles.

2.2.3 Ice particle residual selective inlets

An ice selective inlet is a requirement when studying INPs in the environment. The first ice selective inlet was developed by Ogren et al. (1985), a counter flow virtual impactor (CVI). The working principle of the CVI being an inlet with an opposite air stream to stop the relatively small interstitial particles from entering. This size selective inlet has later been applied in IR research of cirrus clouds in many air-craft campaigns (Heintzenberg et al., 1996;Twohy and Poellot, 2005;Targino et al., 2006;Froyd et al., 2010;Cziczo et al., 2013). A CVI is insufficient to study IRs in mixed-phase clouds because liquid droplets and ice have similar size range. This technique would, hence, not be able to separate the one from the other. Thus, two other inlets have been developed to work in mixed-phase clouds, the ice selective inlet (ISI) by Kupiszewski et al. (2015) and the Ice-CVI (Mertes et al., 2007). In **Paper I**, the Ice-CVI was applied for IRs sampling. With this inlet, ice particles between 5-20 µm are selected. The restricted lower cut off is set to be able to separate ice particles from interstitial particles. There are three reasons for the restricted upper cut-off size, (1) to restrict rimed particles from sampling, and (2) to only sample freshly produced ice particles. In rimed and large old particles, there is a higher risk of having particles that have experienced impaction scavenging by interstitial particles– secondary ice process - which can add more particles to the ice crystals. The last reason (3) is the technical reason that larger particles can shatter and abrade the inner surface of the Ice-CVI. A scheme based on the schematic drawing in Mertes et al. (2007) of Ice-CVI is shown in Fig. 1.

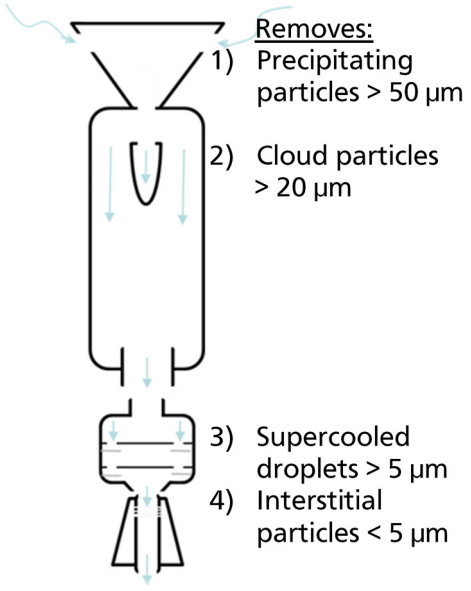

Figure 1: The Ice-CVI based on Mertes et al. (2007)

2.2.4 Aerosol cloud chambers

There exists several ice nucleation chambers for laboratory and in-situ measurements i.e. Lacher et al. (2017);Bundke et al. (2008);Garimella et al. (2016). A general limitation when investigating INP on-line in the environment is the low concentration of these particles combined with a relatively low sampling rate of the instruments. In laboratory studies, the limit of detection (LOD) restriction is overcome by increasing the particle concentrations. Another advantage in the laboratory is that several influencing factors like size- or temperature dependence as well as different interactions like coatings can be investigated under controlled conditions (Cziczo et al., 2017).

The following described cloud chambers are stationary, built in special facilities to house these huge cloud chambers.

LACIS - Leipzig Aerosol Cloud Interaction Simulator

LACIS is used to investigate immersion freezing (**Paper III**), and homogenous freezing experiments. The supersaturation in the chamber is set by the gas phase, which gives a better opportunity than traditional cold stage set-ups to study single particles with a lower risk of contamination from water impurities (Grawe et al., 2016). LACIS is a continuous flow chamber where particles pass through exposure sections (total of ~7 meter), at supersaturated conditions and variable temperature. The advantage of being up scaled, is the possibility to study ice nucleation at atmospheric relevant conditions and time scale (Stratmann et al., 2004). In LACIS, the ice fraction is discriminated from the droplets by their different light scattering ability with a special designed optical particle counter, the TOPS-Ice. The non-spherical ice particles will scatter the light more strongly than the spherical droplets (Clauss et al., 2013).

AIDA - Aerosol interaction and dynamics in the atmosphere

In AIDA, homogenous freezing, as well as deposition nucleation, immersion and condensation freezing can be studied (Cziczo et al., 2017). The AIDA chamber is a 7 m tall, 4 m wide cylindrical chamber of aluminium with the possibility to be cooled down to -90 °C (Möhler et al., 2003). The large operating temperature span gives the opportunity to investigate various cloud types, like liquid-, mixed-phase and cirrus clouds (Möhler et al., 2001). Both temperature and saturation with respect to ice can vary, depending of the research question. Supersaturation with respect to ice is set by expansion cooling. The pressure in the chamber can be reduced to mimic the atmospheric cooling rates. Different instruments are attached to the chamber to control and describe the conditions and to characterise the aerosol. A laser through the middle of the chamber, and light scattering detectors yield information on the particle phase, size and volume, and hence allows for determination of onset ice nucleation. An optical particle spectrometer (OPS) is located at the bottom of the chamber for size distribution measurements, and a Fourier-transform infrared-spectrometer is located in the middle of the chamber to analyse chemical composition, size and phase - all in continuous measurements (Möhler et al., 2001). Additional instrumentations for size selection and/or particle characterisation can be attached to inlets (as for **Paper IV**) and at the outlet. Altogether, the AIDA facility provides a unique possibility to study particle interaction to cloud formation.

2.3 Coal fly ash as ice nucleating particles

In the atmosphere, coal fly ash particles are often overlooked in analysis. The reason for this is that the composition of these particles is often similar to mineral dust particles (Weinbruch et al., 2010) as they consist of the non-combustible constituents of wood and fossil fuels (Damle et al., 1981). In some cases, trace elements like Cr, Pb, Ni, Ba, Sr, V and Zn have been reported in coal fly ash (Yao et al., 2015). In many cases, coal fly ash are spherical because of the generation at high temperatures (Fisher et al., 1976). Occasionally, also microcrystals have been observed associated with coal fly ash particles (Fisher et al., 1976;Grawe et al., 2016;Grawe et al., 2018).

Only a few studies were performed investigating the ice nucleation efficiency of coal fly ash, and the results are inconclusive. Summarised, immersion freezing was found to be less efficient than deposition nucleation by Havlíček et al. (1993), but later the opposite was reported by Garimella et al. (2016). Beside, Umo et al. (2015) report that coal fly ash was more efficient than bottom ash in immersion freezing experiments, but the effect is more than one order of magnitude lower than reported by Garimella et al. (2016). In addition, Garimella et al. (2016) found that 300 nm particles were more efficient per surface area than 700 nm particles leading to the hypothesis that this was due to the heavy metal trace elements being enriched in the smaller particles. Furthermore, Grawe et al. (2016) report a decrease in the immersion freezing efficiency of wet generated brown coal particles compared to dry generated particles, which contradicts the size dependence hypothesis by Garimella et al. (2016). Inspired by the inconsistent results from previous literature, a new study (**Paper III**) was carried out to answer the following questions:

"1) *Do coal fly ash samples from different power plants feature a similar immersion freezing behaviour?*

2) Is the deactivation in transition from dry to wet particle generation observable for different coal fly ash samples?

3) Is it possible to find a connection between physicochemical sample properties and the observed immersion freezing behaviour?

4) Which particle generation technique (dry or wet particle generation) or measurement method (single particle vs. cold stage) is appropriate for representing atmospheric processes after coal fly ash emission?" (From **paper III**)

2.4 A new method in single particle mass spectrometry to study phase composition of mineral dust

Single particle mass spectrometry has proven to be a useful tool for in-situ on-line characterisation of particle composition. The aim of the study in **paper IV** was to test a new LAAPTOF technique developed by Marsden et al. (2018). This technique allows to determine the mineral phase based on chemistry and mass spectra characteristic, reflecting the behaviour of minerals after ionisation by laser ablation. A study of single particle mass spectrometry is important because this technique has suffered from poor reproducibility, matrix effects and insufficient instrument functions analysing mineral particles (Reilly et al., 2000;Sullivan and Prather, 2005;Murphy, 2007;Shen et al., 2018).

Marsden et al. (2018) show that interchangeable cations in the crystal structure influenced the travel time of two fragmentation ions (O^- and SiO_3^-) in the TOF (Fig. 2). In e.g. kaolinite, silicon-oxygen or aluminium- oxygen/ hydroxyl layers are bound together to form the three dimensional crystal structure (1:1 layer). Illite is composed of a more complex crystal structure, bound up by relatively large cations (potassium, sodium and calcium) which needs to be charge balanced by an additional layer (2:1 layer). The illite structure is the clean form of a clay mineral, where all the interstitial cations are changed. In nature, the 2:1 clay minerals can be composed of different interstitial cations throughout the crystal structure, complicating the phase determination of minerals. K-feldspars consist of interstitial cations in cavities stabilised by layers in three dimensions. As a result of the charge stabilisation, these cations are not so easy to interchange and a dissolution of the cations will lead to a change of the mineral phase.

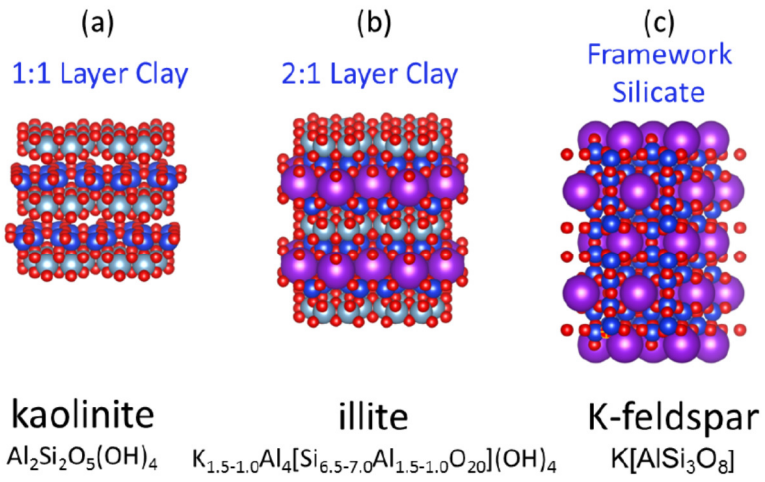

Figure 2: The mineral structure of a) kaolinite, b) illite and c) K-feldspar. Figure 1 in *"Mineralogy and mixing state of North African mineral dust by on-line single-particle mass spectrometry"* by Marsden et al. (2019)

The result of the laboratory experiments in Marsden et al. (2018) was the framework for this new study (**Paper IV**) performed on laboratory suspended soil from North Africa and in-situ investigation of North African mineral dust aerosol.

3 MATERIAL AND METHODS

In this chapter, details on particle sampling on substrates, as well as the two different SEM-EDX analysis techniques (opSEM and ccSEM) are presented. In **Paper III** and **Paper IV**, other instruments were additionally operated. A detailed description of these instruments can be found in the corresponding papers.

3.1 Sampling

The environmental particle samples were collected in-situ, either with the use of an impactor only or attached behind another particle inlet. In the laboratory experiments, particles were sampled behind different particle distributers. All samples are collected with a cascade impactor- either the Micro Inertial Impactor (MINI) (see Kandler et al. (2007) for details) or the multi MINI impactor (see Ebert et al. (2016) for details).

3.1.1 Sampling in the ambient environment

The various sample set-ups for the environmental samples involving two different cascade impactors are described in Table 1. The MINI is a small, easy to handle impactor which only requires a battery driven pump, but can only operate with one sample at the time. Please note that one sample can contain several substrates when collecting particles with more than one cut-off size stage. The multi MINI is a larger particle sampler which requires electrical power. Nevertheless, this impactor has the possibility to hold up to 12 samples and to flush the system before/after each sampling. Using the multi MINI, at least 5 min of flushing the system were performed before each sampling. This impactor was used at Jungfraujoch (Switzerland) and the Cyprus observatory. In some cases, a longer sampling time was required to have a more representative sample, like when comparing total aerosol and IR (**Paper I**) and during the sampling in Cyprus (**Paper II**). In these cases, a dilution unit was attached to the sampling line (for details see **Paper I**).

Table 1: Samples and sampler set-up

Sample	Sampler	Inlet	Nozzle 50 % cut off size diameter (μm)
All IR samples*	Multi MINI	Ice-CVI	0.1
Urban background**	Multi MINI	Steel inlet	0.1
Total aerosol at Jungfraujoch*	Multi MINI + Dilution	Heated total inlet (Weingartner et al., 1999)	0.1
Rural background/ marine – Cyprus**	Multi MINI + Dilution	Size selective inlet (DMA) ~1.5 μm, roof of laboratory	0.1
Traffic hotspot/ Essen – Germany**	Single stage nozzle impactor	Impactor inlet	1.0
Rural background/ Odenwald – Germany**	Single stage nozzle impactor	Impactor inlet	1.0

*Paper I **Paper II

3.1.2 Sampling in the laboratory

In the laboratory experiments investigating four different coal fly ash samples, particles were collected behind a particle distributor, after a size selecting step (300 nm) with a differential mobility analyser (DMA). The particles were sampled on boron substrates with the multi MINI (50% cut-off diameter at 0.1 μm). The system was always flushed for at least 5 minutes before sampling. A detailed description of the particle distribution set-up can be found in **Paper III.**

The mineral particles investigated for method validation (**Paper IV**) were sampled with a MINI onto nickel TEM grids before distribution into the AIDA chamber. The particles were collected with a 50 % cut-off diameter at 0.1 μm, and a sampling time between 12-16 min.

3.2 Scanning electron microscopy analysis

All samples were investigated with SEM-EDX for single particle characterisation. Size, morphology, chemical composition, mixing state and the stability (under electron bombardment) of the particles were investigated using a FEI Quanta 400 FEG instrument (FEI, Eindhoven, The Netherlands) equipped with an X-Max150 energy-dispersive silicon drift X-ray detector (Oxford, Oxfordshire, United Kingdom) allowing analysis of all elements with $Z > 3$ (Li). All boron substrate samples were investigated under high vacuum conditions ($\sim 10^{-5}$ mbar chamber pressure), at an acceleration voltage of 15 kV, spot size 4 and a working distance of 10 mm. The TEM grid samples (**Paper IV**) and the coal fly ash samples were investigated at the same working distance and chamber pressure, but with an acceleration voltage of 12.5 kV and spot size 5. The Oxford software Aztec (version 3.3. SP1) was used for all analyses.

3.2.1 Operator controlled analysis

Approximately 500 particles per sample were investigated operator controlled in **Paper I** and **Paper II**. The analysis was performed by the "point & ID" feature of the software and all particles with an equivalent projected area diameter ≥ 100 nm in an image frame were selected for X-ray microanalysis (5 seconds live time) to minimize a systematic selection bias by the operator. In **Paper III**, only 20-30 particles per sample were selected for X-ray microanalysis. A longer acquisition time (20 seconds live time) was set in this analysis to detect minor amounts of heavy metals observed by the parallel SP-MS investigation.

3.2.2 Computer controlled analysis

In the computer controlled analysis, particles were selected based on their contrast in the backscattered electron (BSE) images. Particles with an equivalent projected area diameter ≥ 100 nm were selected for X-ray microanalysis (5 seconds live time). The electron beam was scanned over the whole particle. The acquisition area was defined by the operator before the analysis. Secondary electron (SE) images were acquired additionally to have the possibility to investigate the sample manually after ccSEM.

In **Paper IV**, ccSEM was performed on TEM grids. A post-analysis sorting step was required to sort out features of the grid and particles with low X-ray counts due to shading effects.

3.3 Statistical analysis

The statistical parameter and figures presented in this thesis and the corresponding papers of single particle analysis with SEM-EDX were realised with RStudio, version 3.3.0 (2016) and Microsoft Excel (2016).

Results of single particle analysis is often presented as closed data in a given interval like 0-100 (%) or 0-1 (Aitchison, 2003). When the data have a given sum, the components of the data only carry relative information. A dataset should be sub-compositional coherent, meaning that the ratio between groups are independent if the analysis is of sub-compositions or the full composition (Van den Boogaart and Tolosana-Delgado, 2013). Sub-compositions can be presented as scatter plots (two components, seen in Fig. 11) or ternary diagrams (three components), both ways are presented in **Paper IV**.

To overcome the problems related to comparing closed datasets, the results were normalised either to another particle group (**Paper I**) or the substrate area analysed (**Paper II**). In the first case (**Paper I**), a normalisation to a certain particle group (termed odds ratio in literature) gave the opportunity to compare the IR and the total aerosol fraction by the calculation of enrichment and depletion of the IR group (Fig. 7).

The odds ratio (OR) was calculated in the following way:

$$(OR_i) = \frac{(\frac{n_i}{n_{AlSi}})_{IR}}{(\frac{n_i}{n_{AlSi}})_{Total}} \qquad (1),$$

with n_i the absolute number of particles in particle group i, n_{AlSi} the absolute number of particles in the group of aluminosilicates in the IR or total aerosol fraction. By using odds ratio, we avoid the problem of sampling loss as long as the particle groups are normalised to a group which can be assumed not to be lost during sampling and/or analysis. The aluminosilicate group can be assumed to be collected with same efficiency in the IR and total aerosol fraction, and the particles of this group is stable during analysis. The confidence interval of the odds ratio was calculated with the Fisher exact test. The Fisher exact test rather than Chi-squared test was performed in **Paper I** because of the limited number of particles in the different groups.

In the second case, the number of particles in the given group was normalised to the substrate area analysed (**Paper II**). Arguably, particle per volume sampled would yield a more intuitive value which can be compared to other literature. On the other hand, a normalisation to volume sampled would not include the sample loss during particle collection and as a result contain large uncertainty. As the aim of the paper was to compare two SEM-EDX analysis techniques (opSEM vs. ccSEM), it was decided to use the parameter measured - the substrate area. One assumption made is that the particles analysed are representative of the sample. As the impaction spot has a slight gradient distribution of particles, either the whole impaction spot (for ccSEM) or a circular sector relative to the impaction spot (opSEM) was analysed.

The confidence intervals in **Paper II** (also seen in Fig. 3, 4 and 5) were calculated based on the method described by Quesenberry and Hurst (1964) implemented in the R package CoinMinD (Subbiah, 2013).

4 RESULTS AND DISCUSSION

In the following sub-sections, results and discussion of the SEM-EDX analyses are presented. Starting with the comparison between opSEM and ccSEM (**Paper II**). The next two subsections deal with IR research at Jungfraujoch (**Paper I**) and the ice nucleating ability of coal fly ash (**Paper III**). Finally, the comparison between SP-MS and ccSEM (**Paper IV**) is addressed. In **Papers III** and **IV** the SEM-EDX work makes up only a part of the results. Please, refer to the relevant paper for more results and detailed discussion of the other techniques.

4.1 Comparison of operator- and computer controlled scanning electron microscopy

4.1.1 Differences in particle group abundance

To be able to choose the best suited SEM-EDX technique for the purpose of analysing different ambient particle samples, a comprehensive comparison between opSEM and ccSEM was performed (**Paper II**). The following results show the advantages and disadvantages of the techniques highlighted from analysis of different environmental samples, characterised as urban background, rural background/marine, free tropospheric, traffic hotspot and rural background.

A considerable fraction of mixed particles, fly ash and soot was found in the urban background and rural background/marine sample (Fig. 3). These three particle groups can only be classified by the opSEM technique.

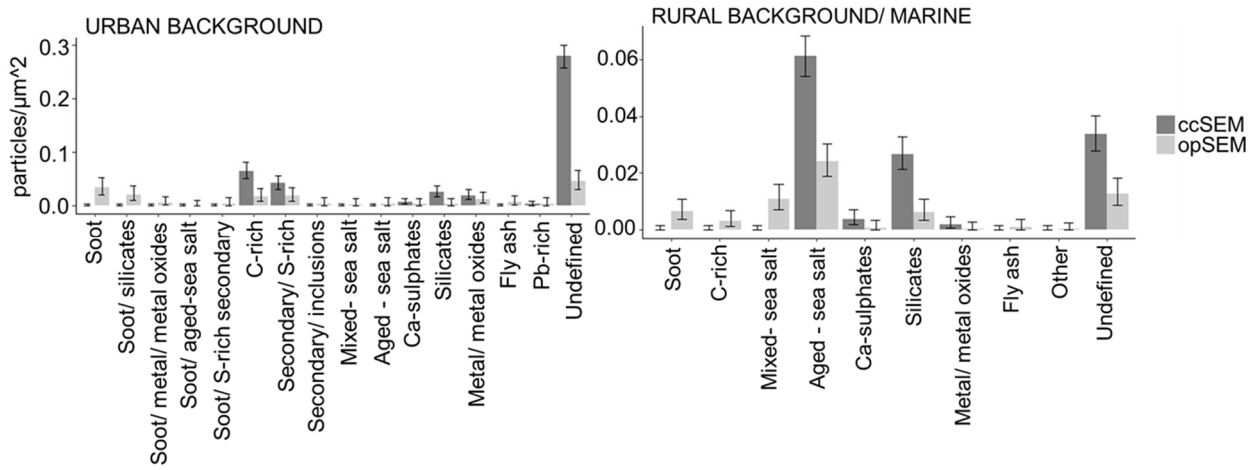

Figure 3: Comparison between opSEM and ccSEM of an urban background sample in Mainz (n=2751 in ccSEM, and n=523 in opSEM) and rural background/marine sample from Cyprus (n=1348 in ccSEM, and n=503 in opSEM). The particles were sampled with a 50 % cut off diameter at 0.1µm. The relative number abundance of each particle group was normalised by the substrate area analysed. From figure 2 in Eriksen Hammer et al. (2019).

In samples with high content of unstable particles, like in the free tropospheric sample (Fig. 4), ccSEM is limited to the stable fraction. Information on heterogeneous inclusions within a particle is also lost because of the particle instability under electron bombardment.

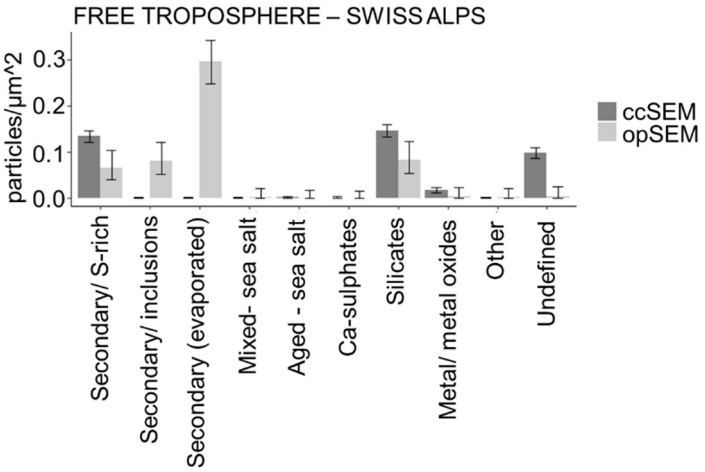

Figure 4: ccSEM (n=3751) and opSEM (n=529) analysis of a sample from the free troposphere- Swiss Alps. Particles were sampled with a (sampled with 50 % cut off diameter at 0.1µm). The relative number abundance of each particle group was normalised by the substrate area analysed. From figure 2 in Eriksen Hammer et al. (2019).

Environmental samples with larger particles, or generally particles with a higher contrast relative to background are suited for ccSEM analysis. This can be seen in the samples from a traffic hotspot in Essen and rural background in Odenwald/ Germany (Fig. 5). Still, all particle groups where morphology is necessary for an accurate classification will be misclassified or overlooked with ccSEM.

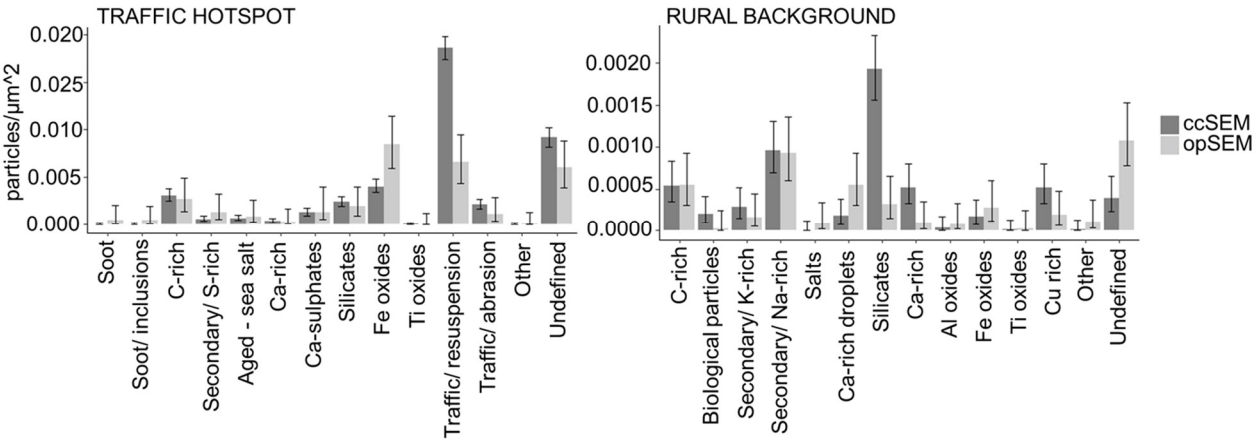

Figure 5: Comparison of opSEM and ccSEM of a traffic hotspot sample – Essen, Germany (n=6940 in ccSEM, and n=552 in opSEM) and a rural background sample – Odenwald, Germany (n=1103 in ccSEM, and n=501 in opSEM). Particles were sampled with 50 % cut-off diameter at 1.0 µm. The relative number abundance of each particle group was normalised by the substrate area analysed. From figure 2 in Eriksen Hammer et al. (2019).

4.1.2 Which technique is better suited for which aerosol types?

The comparison between opSEM and ccSEM clearly demonstrates and quantifies the differences between the two techniques. Even though ccSEM yields much better statistics from the higher number of particles analysed at a reasonable expenditure of time, the results show that some particle groups were not detected and/or not classified by the ccSEM procedure. The higher degree of complexity a sample has - in terms of morphology, mixing state and beam stability - the more opSEM becomes the appropriate technique. For example, in samples where mixed particles, fly ash particles and/or soot content have a significant contribution to the

composition, ccSEM is a limited technique because of the strict chemical based classification compared to the more detailed classification with opSEM. This is clearly seen in the urban background from Mainz and the rural background/ marine sample from Cyprus (Fig. 3).

In samples with beam sensitive particles with or without inclusions, only opSEM represent sufficient detailed results. Evidently, this is the case for the free tropospheric sample from the Swiss Alps (Fig. 4). For this reason, opSEM was the technique of choice in **paper I**. A detailed analysis of single particles is required when investigating IRs for several reasons. First, information on soot, unstable particles, possible mixing state and morphology is acquired. Second, a better understanding of ice nucleation is enabled from information on surface structure, coatings and mixing state, additionally to the particle chemistry. Third, morphological information is useful for other analytical techniques like SP-MS because the detection efficiency is highly dependent on the particle shape (Marsden et al., 2016). Last, for rare and expensive samples, as detailed information as possible should be obtained.

Other samples, with larger particles and a higher fraction of stable unmixed particles, are suitable for ccSEM. In literature, mineral dust particles are analysed by ccSEM in several cases (Kandler et al., 2007;Kandler et al., 2011). The result of **paper II**, support that mineral dust can be analysed by ccSEM and that this is the advantageous technique. On these grounds, in **paper IV,** ccSEM was the technique of choice to analyse mineral particles impacted on TEM grids.

4.2 Ice particle residuals in mixed-phase clouds at Jungfraujoch

Prior to SEM-EDX investigation of IRs, an accurate particle selection step is essential. An ice selective inlet needs to have an exceptional separation efficiency to be able to separate INPs from the rest, 1 out of 10^5 other particles (DeMott et al., 2010). In **Paper I** the Ice-CVI was used. Previous studies from Jungfraujoch with a similar set up (Mertes et al., 2007;Ebert et al., 2011;Worringen et al., 2015) have shown that the Ice-CVI had an acceptable separation efficiency but the collected samples were still contaminated by other particles. To manage this contamination, a new set-up was built before the INUIT Jungfraujoch 2017 campaign. First, this included a coating of all inner surfaces of the inlet, the virtual impactor and the droplet pre-impactor with nickel to have a better control of any particles arriving from the inlet system. Second, parallel sampling of total aerosol particles and IRs was performed. This was done to be able to compare the particle groups of both, and to study the enrichment/ depletion of the ice particle residual fraction. The results from the INUIT Jungfraujoch campaign 2017 shows that the effort of getting rid of contamination particles was rather unsuccessful. Compared to previous studies, we found a higher relative abundance of contamination. This can be explained by different meteorological conditions during sampling leading to different ice particle residual concentration, or the different sampling stage used in the latest campaign with another particle size cut-off and/or the different sampling time. Nevertheless, the parallel set up gave the opportunity to characterise the contamination particles and later to remove the particles from further analysis. IRs could be recognised unambiguously as the artefact particles had a distinct chemical composition.

4.2.1 Single particle analysis of ice particle residuals and total aerosol collected in parallel

A detailed study of IRs in mixed-phase clouds at Jungfraujoch is presented in **Paper I**. Based on the results of **Paper II,** opSEM was the technique of choice for the investigation of the mixing state as well as possible contribution of soot and complex secondary particles.

In Fig. 6, total aerosol particle group abundance and ice residual particle group abundance sampled in parallel are presented. Even though a dilution unit was applied during sampling, in some cases, the parallel total aerosol sampling was unsuccessful (overloaded or insufficient particle number on the substrate), and hence, resulting in fewer total aerosol than IR samples.

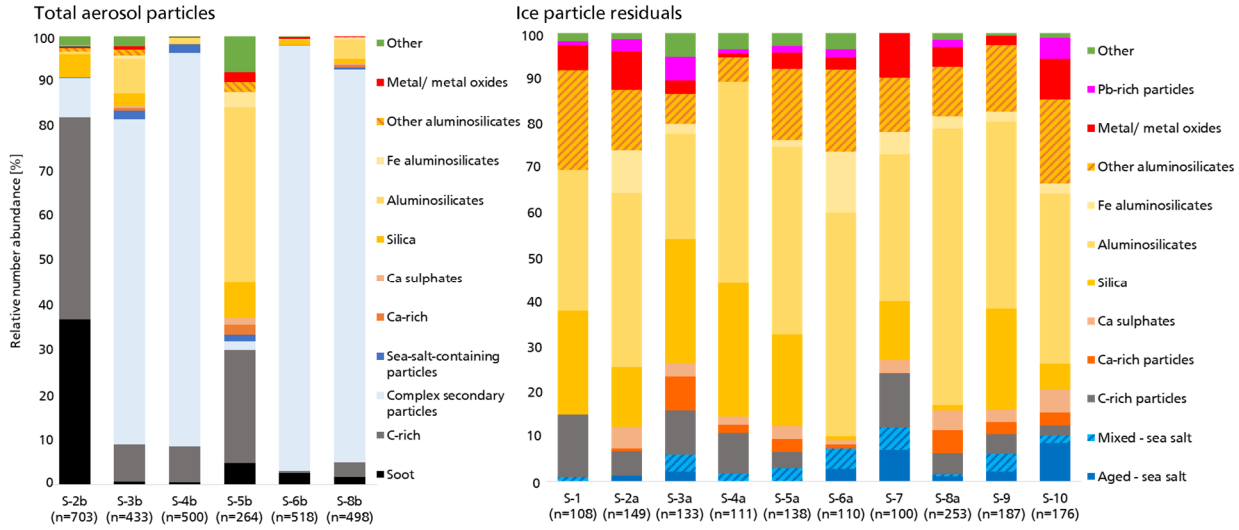

Figure 6: Relative number abundance of different particle groups in total aerosol and ice particle residuals sampled during Jungfraujoch campaign 2017. The samples marked with a/b behind number are parallel sampled. Figure 4 and 6 in Eriksen Hammer et al. (2018)

The chemical composition of total aerosol particles and IRs is clearly different. The major difference is that soot and complex particles are not present in the IR fraction. In both fractions, C-rich and Ca-rich particles, sea salt-containing particles (mixed- and aged- sea salt), Ca sulphates, silica, aluminosilicates, Fe aluminosilicates, other aluminosilicates (consisting of variable amounts of Na, K, Ca, Si, Al, O, Ti and Fe) as well as metal/metal oxide particles are present. Also, a small fraction of particles that could not be classified in any of the above mentioned groups are found in both fractions. Pb-rich particles are only present in the IR fraction.

In the total aerosol fraction, a typical particle composition for the free troposphere was found in three of the five samples. This includes a significant contribution of complex secondary aerosol and a smaller contribution of soot and C-rich particles. The rest consist of different mineral particles (silica, aluminosilicates, Fe aluminosilicates, other aluminosilicates, Ca sulphates and Ca-rich particles), metal/ metal oxides and sea salt-containing particles. The first atypical sample is from air masses arriving from the Po-Valley containing a large combustion component (seen in footprint plots, **Paper I**). The second peculiar sample is influenced by an analytical artefact from particle loss during analysis. As the odds ratios are shown, this artefact

does not influence the results of all other particle groups other than complex secondary particles. This group would be even more depleted relative to aluminosilicates.

In the IR fraction, the relative composition of the particle groups showed little variation. The highest relative number abundance was aluminosilicates. This particle group was also relatively abundant in the total aerosol fraction. For a further investigation of the difference between the two fractions, the odds ratio was plotted. In the odds ratio plot (Fig. 7), all particles are normalised to aluminosilicate because this group was found in both fractions in relatively high abundance, and can be expected not to be lost/ or partly lost during sampling and analysis.

4.2.2 Enrichment and depletion of ice particle residuals

Enrichment and depletion of IRs are presented in Fig. 7. Complex secondary particles and soot were strongly depleted in the IR fraction. These groups show a high relative abundance in the total aerosol fraction, and in contrast, not a single particle was detected in the IR fraction. C-rich particles were found in both fractions, but were less enriched than aluminosilicates. Other aluminosilicates and Pb-rich particles were somewhat more enriched than aluminosilicates. The rest of the particle groups – silica, Fe aluminosilicates, Ca-rich, Ca sulphates, sea-salt-containing and metal/metal oxide particles – showed a similar enrichment as aluminosilicates.

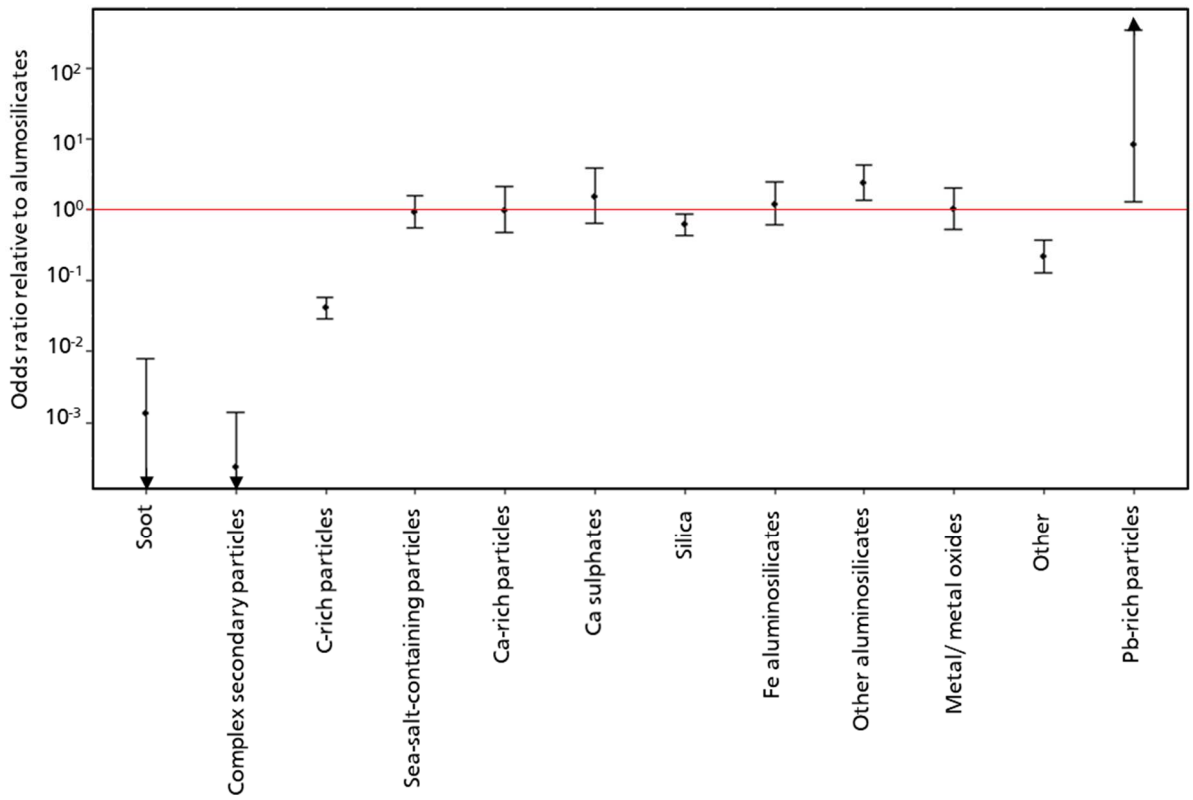

Figure 7: Enrichment or depletion of the different particle groups within the IR fraction relative to the aluminosilicate group expressed as odds ratio. Confidence intervals (95%) are presented as error bars, and the arrows indicates undefined upper/ lower limits due to counting statistics. Figure 8 from Eriksen Hammer et al. (2018)

Comparable to laboratory and field studies, the IR fraction in our study was dominated by mineral dust. Our results also fit relatively well with what is reported in the IR fraction at Jungfraujoch previously (Cozic et al., 2008;Ebert et al., 2011;Kamphus et al., 2010;Worringen et al., 2015;Schmidt et al., 2017) except the fact that soot and complex secondary particles were not present in the IR fraction in our study. This discrepancy can, to some extent, be explained by counting statistics, but also by the different site temperatures at Jungfraujoch during the respective campaigns.

The groups of other aluminosilicates and Pb-rich particles were more enriched than aluminosilicates. This indicates that these particle groups are more ice active than the rest. The other aluminosilicate group most likely include feldspars, illite and smectite. K-feldspar is reported as one of the most ice active mineral dust particles (Atkinson et al., 2013). To understand the ice nucleation efficiency, K-feldspar was thoroughly investigated in a laboratory study (Kiselev et al., 2017). Pb-rich particles were reported at Jungfraujoch previously (Ebert et al., 2011), and the ice nucleation efficiency of these particles was investigated in a laboratory study as well (Cziczo et al., 2009). In the INUIT 2017 campaign at Jungfraujoch, no Pb-rich particles were detected in the total aerosol – resulting in a very high enrichment of this particle group relative to aluminosilicates in the IR fraction. Further research is needed to identify the sources of Pb-rich particles. If these particles originate from helicopters and/ or small aircrafts, as proposed by Kamphus et al. (2010), these particles can be expected to act as ice nuclei only on a rather local scale compared to mineral dust particles. For a better overview of INPs globally, investigations of IRs at different locations are needed.

4.3 Ice nucleation of coal fly ash particles

4.3.1 Morphology of dry and wet dispersed coal fly ash particles

In the coal fly ash experiment, opSEM was performed to investigate the morphology of different coal fly ash particles both dry and wet dispersed. Overview images of the samples show the differences in morphology between dry and wet (from suspension) dispersed particles (Fig. 8 and Fig. 9).

A clear difference between dry and wet particles was observed for the first coal fly ash sample (coal fly ash 1), seen in Fig. 8. In this sample, wet dispersed particles were needle shaped as a result of the reaction of anhydrite to gypsum and quick-lime (CaO) to calcium hydroxide and calcite.

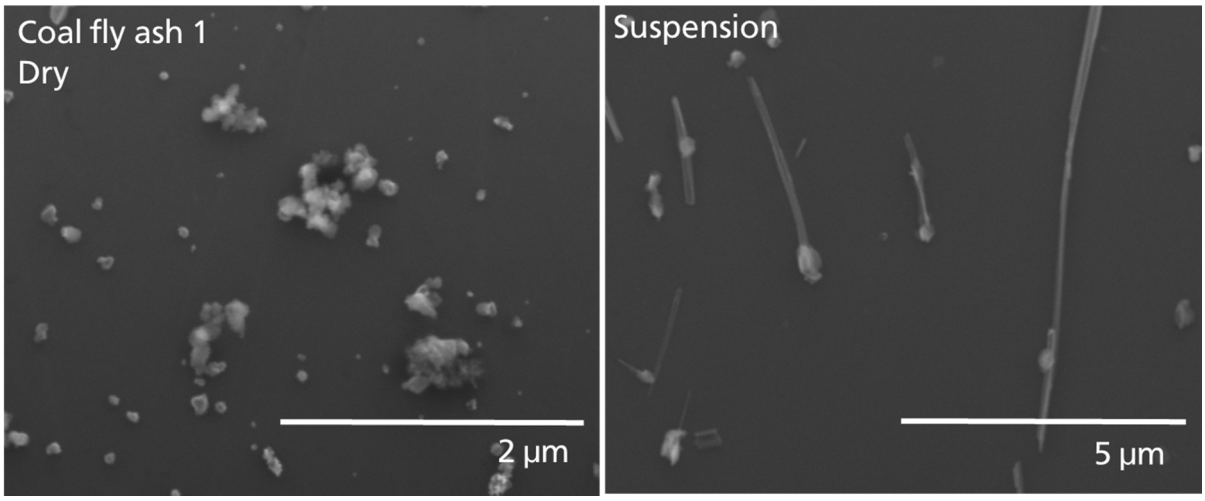

Figure 8: Secondary electron image of coal fly ash sample 1 dispersed dry and after suspension in distilled water

For all samples (Fig. 9) except the first coal fly ash sample (Fig. 8), the two fractions look similar. Respectively in these samples, wet dispersed particles had a somewhat smoother surface than the dry dispersed particles.

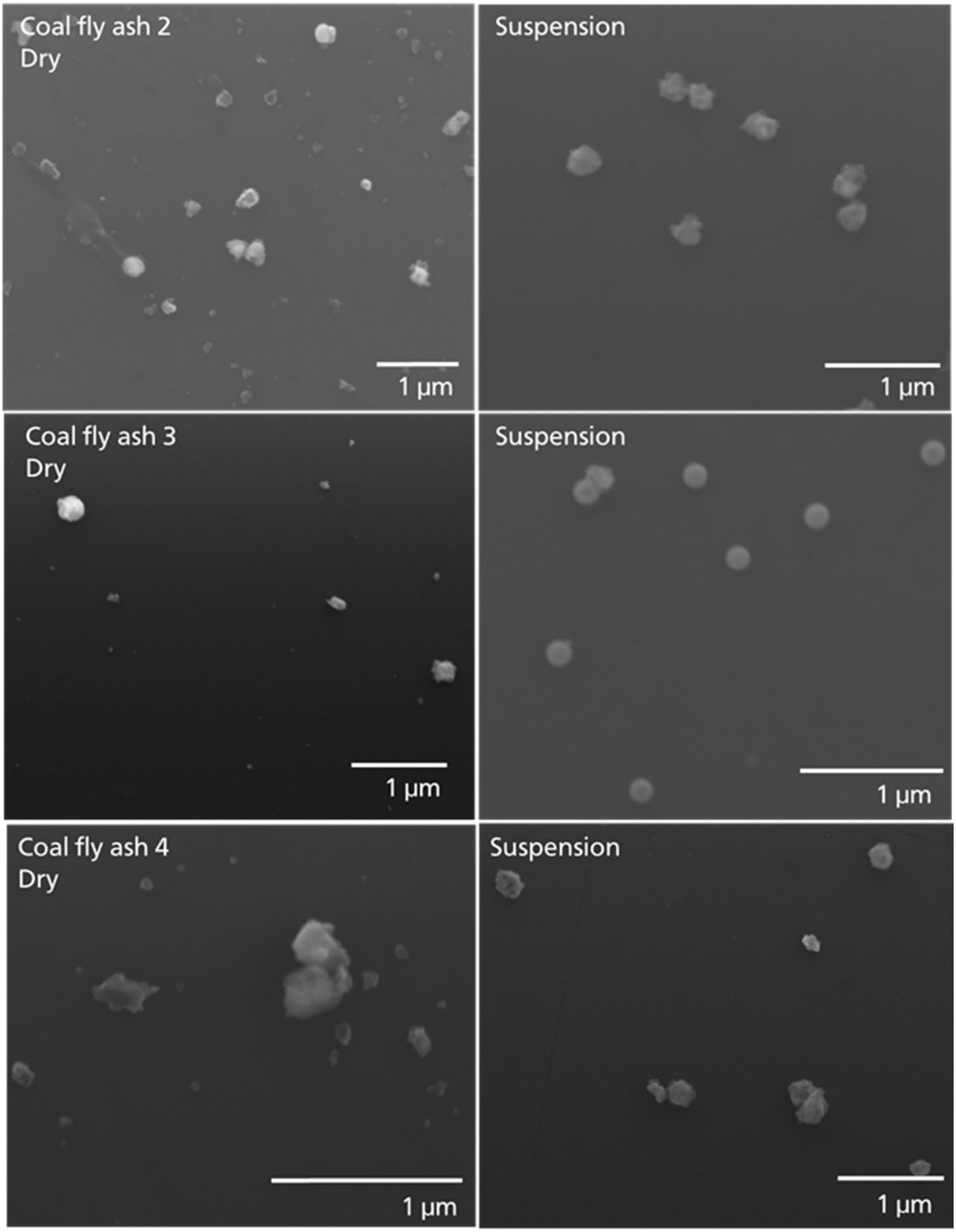

Figure 9: Secondary electron image of different coal fly ash samples dispersed dry and after suspension in distilled water

4.3.2 Contribution of scanning electron microscopy analysis to the ice nucleation experiment of coal fly ash

Coal fly ash particles were studied by opSEM with the focus on morphology and the difference between wet and dry dispersed particles. The SP-MS ALABAMA was applied for chemical characterisation of the particles, together with ICP-MS and XRD for bulk chemistry and minerology information. Still, a few particles (between 20 and 30 per sample) were investigated per samples with opSEM yielding a comparable composition to the SP-MS result.

In three of the four coal fly ash samples, there was little change in morphology between the dry and wet dispersed samples. On the contrary, the particles in the first coal fly ash sample reacted to needles after suspension in water (seen in Fig. 8). Many of these needles were larger than 300 nm, but could - due to the fact that the dynamic shape factor of the needles differ significantly from unity - cross the size selection step in the DMA. This led to needles larger than 5 μm being introduced in LACIS which is the same size as the ice crystals and droplets detected with the TOPS-Ice. The thin layer of water surrounding the needle shaped particles resulted in an overestimation of the frozen fraction of the wet dispersed particles from coal fly ash 1. This was later proved when a similar ice nucleation active surface site density (n_s) was observed at T > 0 °C. The same sample (coal fly ash 1) was investigated in Grawe et al. (2016) and our new results led to the conclusion that the ice nucleation efficiency was overestimated for the wet dispersed particles due to the needle formation. The new results contradict the previous conclusion by Grawe et al. (2016) stating that the difference in immersion freezing efficiency of coal fly ash is caused by a change in particle property between dry and wet generated particles.

The overall results from the LACIS experiments show that all the coal fly ash samples have a similar n_s value and curve shape. Furthermore, the samples showed a decrease in ice nucleation efficiency when the samples were suspended in water. Based on the chemical composition of the samples (high amount of Ca and S), it was hypothesised that anhydrite and/or quick-lime contributes to the ice nucleation efficiency. Following, a comparability test between the dry generated coal fly ash samples and reference particles of anhydrite and quick-lime supported this hypothesis. Additionally, tests of the hydration and carbonisation products of the particles, i.e. gypsum and calcite, compares well to the wet generated coal fly ash samples. In one of the samples (coal fly ash 3) the Si content is higher than the Ca content. The n_s value of this sample compares to the n_s efficiency of quartz measured in a previous experiment in LACIS. This sample also show the lowest efficiency of the coal fly ash samples and the smallest difference between dry and wet dispersed particles. The results indicate that coal fly ash play a smaller role as INP in the environment than first supposed. This still needs to be further investigated by in-situ sampling, assuming that the particle characterisation of coal fly ash improves. In **paper III**, it is pointed out that selection of coal fly ash samples is rather limited and hence it is still need for further investigations.

4.4 Mineral dust identification by single particle mass spectrometry compared to computer controlled scanning electron microscopy

4.4.1 Chemical composition of the North-African mineral dust samples

The samples were first classified (Fig. 10) following the classification scheme of Kandler et al. (2011). Between approximately 40-75 % of the particles in the samples can, based on chemistry, be classified into the mineral groups of interest (kaolinite, illite, Na/K-feldspar and montmorillonite). This classification showed that the SP-MS method is less efficient in determining Mg and Ca containing silicates due to matrix effects. Thus, SEM-EDX analysis gives valuable additional information, as it includes particle groups which SP-MS did not detect.

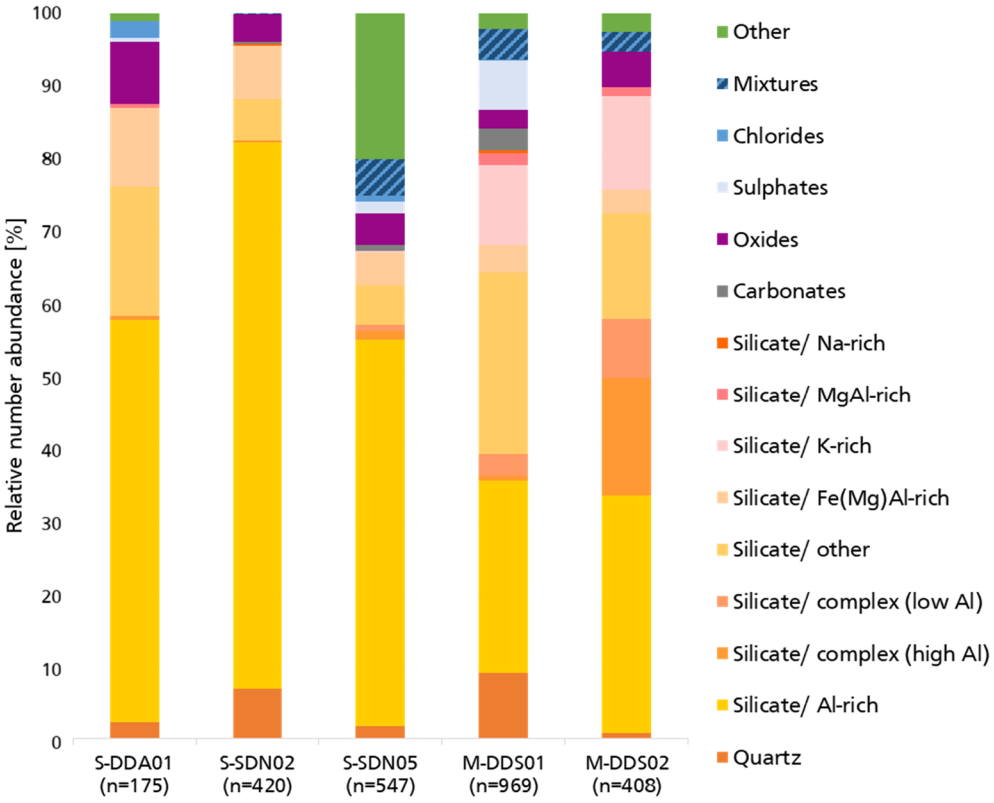

Figure 10: Relative number abundance of particle groups from mineral dust samples, S- in front of the sample name indicates Sahelian and M- Moroccan sample

A scatterplot of the proportion between (Na+K)/Si, Al/Si and (Mg+Fe)/Si (Fig. 11) can to some extend show the different mineral types compared to reference values (average compositions from literature) of nominally pure minerals.

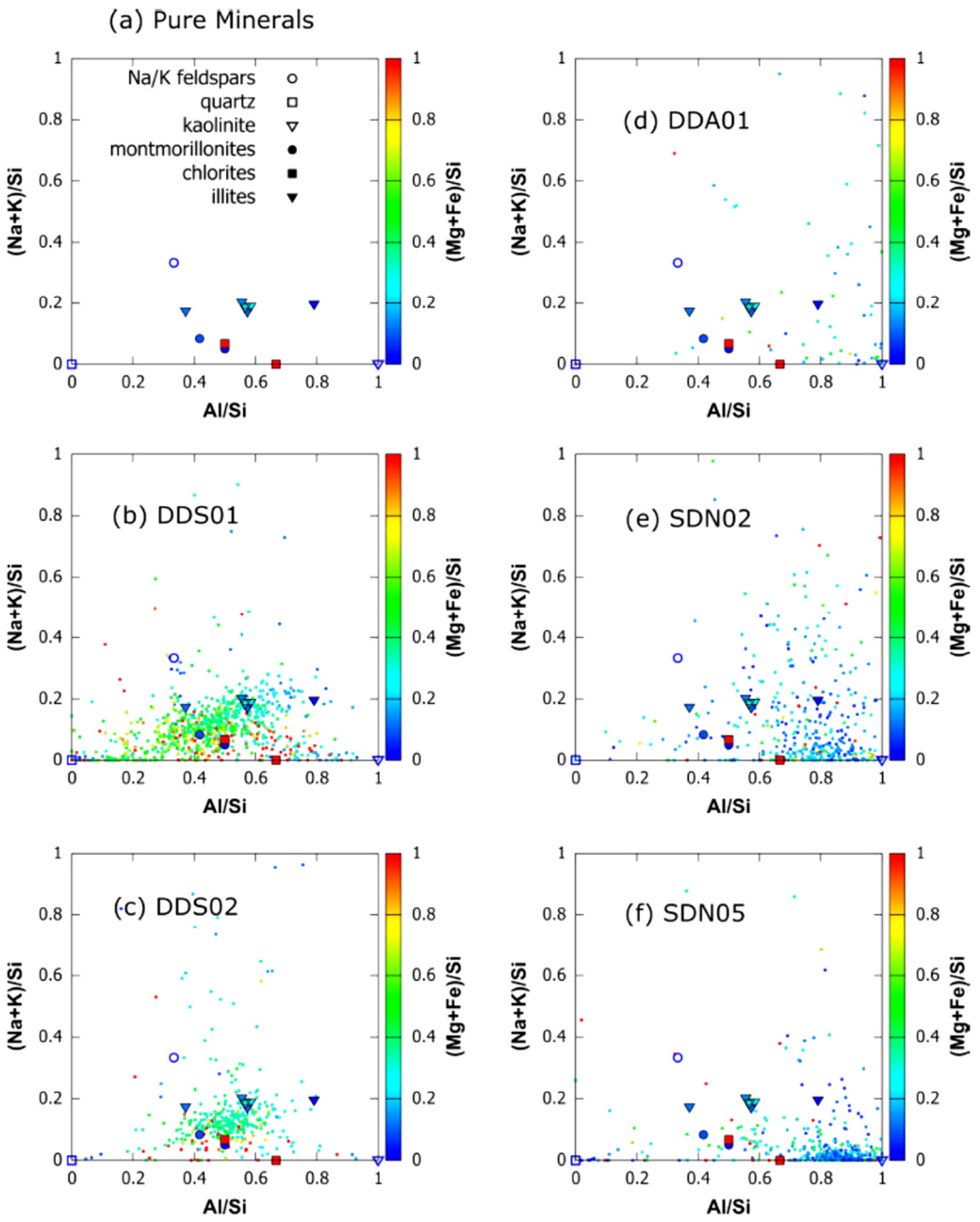

Figure 11: Average composition of nominally pure minerals from the literature (a), SEM-EDX analysis (atomic %) of the Moroccan samples (b, c), and the Sahelian samples (d, e, f). Figure 5 in Marsden et al. (2019)

The frequency of particles with sub-composition of Al+Si relative to Al+Si+K+Na, of two North-African mineral dust samples, were plotted in histograms for a direct comparison between SP-MS and SEM-EDX. The results in Fig. 12 clearly illustrates the different detection efficiency of Al+Si in in the two techniques. The high detection efficiency for K and Na (due to the low ionisation potential of these elements) is an advantage of the SP-MS technique as it allows differentiation of various mineral dust phases.

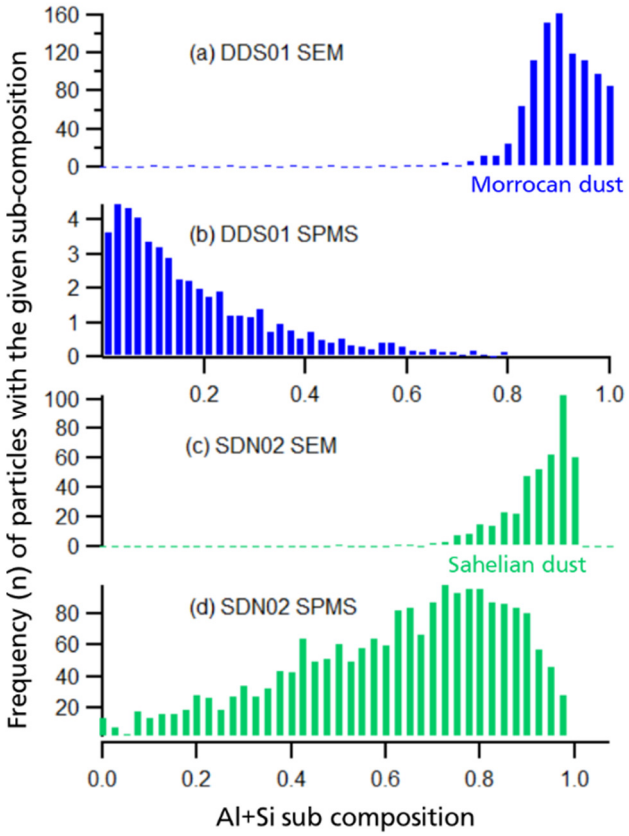

Figure 12: Histograms of the Al+Si sub-composition with respect to the alkali metals (Al+Si)/ (Al+Si+K+Na) in single particles of Moroccan (a and b) and Sahelian (c,d) samples comparing SEM-EDX and SP-MS technique. From figure 8 in Marsden et al., (2019)

4.4.2 Phase determination by single particle mass spectrometry

In general, illite and K-feldspars cannot be distinguished by SEM-EDX because they contain the same chemical components. However, the scatterplot (Fig. 11) shows that ratios can yield some hints about the minerology, keeping in mind that the reference in the plot is of average nominally pure minerals. Still, ccSEM provide valuable results of the different composition of Moroccan and Sahelian dust samples (Fig. 10).

Due to the low ionisation potential of K and Na, and the new characterisation method based on the time delay characteristic, different minerals (kaolinite, Na-montmorillonite, illite, Na-feldspar and K-feldspar) can be characterised by SP-MS. Being an on-line method, the new SP-MS technique has demonstrated that it can be used for real time output of mineralogy with high temporal resolution. Additionally, information about the mixing state of organic materials formed on the surface of the mineral dust particles yields knowledge of the particle history. With this newly developed technique it is concluded that the information have the potential to give a better image on dust emission, transport and deposition. Due to the still uncertain extent of matrix effects, it is recommended that the new method with LAAPTOF should be always complemented by SEM-EDX analysis.

5 CONCLUSION AND FURTHER WORK

In this thesis with the corresponding papers, the utility and necessity of SEM-EDX analysis in ice nucleating research has been outlined and discussed. Even though there are limitations regarding statistics and temporal resolution generally by SEM-EDX, the technique should complement other techniques for quality assurance in both laboratory and field studies.

First, opSEM and ccSEM were investigated to characterise the different techniques and to report strengths and limitations (**Paper II**). This study showed that opSEM is the only suitable technique to use in IR studies because it yields detailed information about particle groups including soot and fly ash, as well as the mixing state and beam stability. CcSEM has high potential to be used for single particle analysis independent of aerosol composition, but there is still a need for an automatic classification procedure for morphology. Machine learning was applied for aerosol particle classification by SP-MS (Christopoulos et al., 2018). This may also be a helpful tool when applied to particle images and adjacent spectra for a better classification of for example soot particles by ccSEM.

Ice particle residuals from mixed-phase clouds and cirrus clouds can be investigated with SEM-EDX. One advantage by collecting IR and total aerosol particles in parallel is the possibility to directly compare the samples, as is shown in **Paper I**. This is important because the measurement of IRs have shown to be influenced by artefacts (Murphy et al., 2004;Pekour and Cziczo, 2011;Worringen et al., 2015;Cziczo et al., 2017). Further study of enrichment and depletion of IRs will lead to a better understanding of the ice nucleation efficiency of different particle groups in both mixed-phase and cirrus clouds - especially for groups with conflicting result i.e. soot. These studies should also include temperature measurements of the clouds to get an estimate of the initiating ice nucleation temperature compared to the on-site temperature. In addition, more research of IRs in mixed-phase clouds in other areas of the world is highly needed.

In laboratory studies of ice nucleation, particles are often size selected in a preselection step. The ice activity is reported from the particles detected after growth. SEM can in these cases be used to validate the size selection step because the particle collection is much less influenced by particle shape or surface charge (**Paper III**). SEM-EDX can also be applied to make sure the system is clean and without leakage of other particles. Additionally, particles can be sampled before and after ice nucleation experiments if a pumped-CVI is attached behind the ice nucleation chamber (Hiranuma et al., 2016). This will give information about possible particle change (both morphological and chemical) after ice nucleation. These results are valuable for IR investigations in the environment to be able to classify IRs correctly - as IRs are assumed to represent the original INP in these studies. In future research of ice nucleation in laboratory studies, information about potential particle change between INP and IR should hence be investigated.

Another advantage of sampling on filters is the sampling efficiency compared to the successfully ablated particles by SP-MS (Kamphus et al., 2010;Worringen et al., 2015;Schmidt et al., 2017). The low number of IR successfully ablated by SP-MS in mixed-phase clouds restricts this analytical technique. In further research, it is important to investigate and understand these limiting effects and improve the SP-MS technique which has high potential in IR research, like the possibility to provide information on the mineral phase composition for some mineral dust

particles as seen in **Paper IV**. To fully understand and quantify the matrix effects in SP-MS, comparing parallel measurement with SEM-EDX will give valuable information which may help to find out if these effects are mainly influenced by the particle size, morphology or chemical composition.

REFERENCES

Aitchison, J.: A concise guide to compositional data analysis, Cairndow, United Kingdom, 2003.

Aitken, J.: Collected scientific papers of John Aitken, edited by: Knott, C. G., for The Royal society of Edinburg, Cambridge University Press, Great Britan, 1923.

Atkinson, J. D., Murray, B. J., Woodhouse, M. T., Whale, T. F., Baustian, K. J., Carslaw, K. S., Dobbie, S., O'Sullivan, D., and Malkin, T. L.: The importance of feldspar for ice nucleation by mineral dust in mixed-phase clouds, Nature, doi: 10.1038/nature12278, 2013.

Augustin-Bauditz, S., Wex, H., Denjean, C., Hartmann, S., Schneider, J., Schmidt, S., Ebert, M., and Stratmann, F.: Laboratory-generated mixtures of mineral dust particles with biological substances: characterization of the particle mixing state and immersion freezing behavior, Atmospheric chemistry and Physics, doi: 10.5194/acp-16-5531-2016, 2016.

Baustian, K. J., Cziczo, D. J., Wise, M. E., Pratt, K. A., Kulkarni, G., Hallar, A. G., and Tolbert, M. A.: Importance of aerosol composition, mixing state, and morphology for heterogeneous ice nucleation: A combined field and laboratory approach, Journal of Geophysical Research: Atmospheres, doi: 10.1029/2011JD016784, 2012.

Bente, M., Sklorz, M., Streibel, T., and Zimmermann, R.: Online Laser Desorption-Multiphoton Postionization Mass Spectrometry of Individual Aerosol Particles: Molecular Source Indicators for Particles Emitted from Different Traffic-Related and Wood Combustion Sources, Analytical Chemistry, doi: 10.1021/ac801295f, 2008.

Boose, Y., Welti, A., Atkinson, J., Ramelli, F., Danielczok, A., Bingemer, H. G., Plötze, M., Sierau, B., Kanji, Z. A., and Lohmann, U.: Heterogeneous ice nucleation on dust particles sourced from nine deserts worldwide-Part 1: Immersion freezing, Atmospheric Chemistry and Physics, doi: 10.5194/acp-2016-438, 2016.

Bundke, U., Nillius, B., Jaenicke, R., Wetter, T., Klein, H., and Bingemer, H.: The fast Ice Nucleus chamber FINCH, Atmospheric Research, doi: 10.1016/j.atmosres.2008.02.008, 2008.

Christopoulos, C. D., Garimella, S., Zawadowicz, M. A., Möhler, O., and Cziczo, D. J.: A machine learning approach to aerosol classification for single-particle mass spectrometry, Atmospheric Measurement Techniques, doi: 10.5194/amt-11-5687-2018, 2018.

Clauss, T., Kiselev, A., Hartmann, S., Augustin, S., Pfeifer, S., Niedermeier, D., Wex, H., and Stratmann, F.: Application of linear polarized light for the discrimination of frozen and liquid droplets in ice nucleation experiments, Atmospheric Measurement Techniques, doi: 10.5194/amt-6-1041-2013, 2013.

Cozic, J., Mertes, S., Verheggen, B., Cziczo, D. J., Gallavardin, S. J., Walter, S., Baltensperger, U., and Weingartner, E.: Black carbon enrichment in atmospheric ice particle residuals observed in lower tropospheric mixed phase clouds, Journal of Geophysical Research: Atmospheres, doi: 10.1029/2007JD009266, 2008.

Craig, N., Harker, A., and Novakov, T.: Determination of the chemical states of sulfur in ambient pollution aerosols by X-ray photoelectron spectroscopy, Atmospheric Environment (1967), doi: 10.1016/0004-6981(74)90108-5, 1974.

Craig, R. L., Bondy, A. L., and Ault, A. P.: Surface Enhanced Raman Spectroscopy Enables Observations of Previously Undetectable Secondary Organic Aerosol Components at the Individual Particle Level, Analytical Chemistry, doi: 10.1021/acs.analchem.5b01507, 2015.

Cziczo, D. J., DeMott, P. J., Brock, C., Hudson, P. K., Jesse, B., Kreidenweis, S. M., Prenni, A. J., Schreiner, J., Thomson, D. S., and Murphy, D. M.: A Method for Single Particle Mass Spectrometry of Ice Nuclei, Aerosol Science and Technology, doi: 10.1080/02786820300976, 2003.

Cziczo, D. J., Stetzer, O., Worringen, A., Ebert, M., Weinbruch, S., Kamphus, M., Gallavardin, S. J., Curtius, J., Borrmann, S., and Froyd, K. D.: Inadvertent climate modification due to anthropogenic lead, Nature geoscience, doi: 10.1038/NGEO499, 2009.

Cziczo, D. J., Froyd, K. D., Hoose, C., Jensen, E. J., Diao, M., Zondlo, M. A., Smith, J. B., Twohy, C. H., and Murphy, D. M.: Clarifying the Dominant Sources and Mechanisms of Cirrus Cloud Formation, Science, doi: 10.1126/science.1234145, 2013.

Cziczo, D. J., Ladino, L., Boose, Y., Kanji, Z. A., Kupiszewski, P., Lance, S., Mertes, S., and Wex, H.: Measurements of Ice Nucleating Particles and Ice Residuals, Meteorological Monographs, doi: 10.1175/amsmonographs-d-16-0008.1, 2017.

Damle, A. S., Ensor, D. S., and Ranade, M. B.: Coal Combustion Aerosol Formation Mechanisms: A Review, Aerosol Science and Technology, doi: 10.1080/02786828208958582, 1981.

DeMott, P., Cziczo, D., Prenni, A., Murphy, D., Kreidenweis, S., Thomson, D., Borys, R., and Rogers, D.: Measurements of the concentration and composition of nuclei for cirrus formation, Proceedings of the National Academy of Sciences, doi: 10.1073/pnas.2532677100, 2003.

DeMott, P. J., Prenni, A. J., Liu, X., Kreidenweis, S. M., Petters, M. D., Twohy, C. H., Richardson, M. S., Eidhammer, T., and Rogers, D. C.: Predicting global atmospheric ice nuclei distributions and their impacts on climate, Proceedings of the National Academy of Sciences, doi: 10.1073/pnas.0910818107, 2010.

DeMott, P. J., Hill, T. C. J., McCluskey, C. S., Prather, K. A., Collins, D. B., Sullivan, R. C., Ruppel, M. J., Mason, R. H., Irish, V. E., Lee, T., Hwang, C. Y., Rhee, T. S., Snider, J. R., McMeeking, G. R., Dhaniyala, S., Lewis, E. R., Wentzell, J. J. B., Abbatt, J., Lee, C., Sultana, C. M., Ault, A. P., Axson, J. L., Diaz Martinez, M., Venero, I., Santos-Figueroa, G., Stokes, M. D., Deane, G. B., Mayol-Bracero, O. L., Grassian, V. H., Bertram, T. H., Bertram, A. K., Moffett, B. F., and Franc, G. D.: Sea spray aerosol as a unique source of ice nucleating particles, Proceedings of the National Academy of Sciences, doi: 10.1073/pnas.1514034112, 2016.

Després, V., Huffman, J. A., Burrows, S. M., Hoose, C., Safatov, A., Buryak, G., Fröhlich-Nowoisky, J., Elbert, W., Andreae, M., Pöschl, U., and Jaenicke, R.: Primary biological aerosol particles in the atmosphere: a review, Tellus B: Chemical and Physical Meteorology, doi: 10.3402/tellusb.v64i0.15598, 2012.

Dufour, L.: Ueber das Gefrieren des Wassers und über die Bildung des Hagels, Annalen der Physik, doi: 10.1002/andp.18621901203, 1862.

Ebert, M., Weinbruch, S., Rausch, A., Gorzawski, G., Helas, G., Hoffmann, P., and Wex, H.: Complex refractive index of aerosols during LACE 98 as derived from the analysis of individual particles, Journal of Geophysical Research: Atmospheres, doi: 10.1029/2000JD000195, 2002.

Ebert, M., Weinbruch, S., Hoffmann, P., and Ortner, H. M.: Chemical Characterization of North Sea Aerosol Particles, Journal of Aerosol Science, doi: 10.1016/S0021-8502(99)00549-2, 2000.

Ebert, M., Worringen, A., Benker, N., Mertes, S., Weingartner, E., and Weinbruch, S.: Chemical composition and mixing-state of ice residuals sampled within mixed phase clouds, Atmospheric Chemistry and Physics, doi: 10.5194/acp-11-2805-2011, 2011.

Ebert, M., Weigel, R., Kandler, K., Günther, G., Molleker, S., Grooß, J. U., Vogel, B., Weinbruch, S., and Borrmann, S.: Chemical analysis of refractory stratospheric aerosol particles collected within the arctic vortex and inside polar stratospheric clouds, Atmospheric Chemistry and Physics, doi: 10.5194/acp-16-8405-2016, 2016.

Eriksen Hammer, S., Mertes, S., Schneider, J., Ebert, M., Kandler, K., and Weinbruch, S.: Composition of ice particle residuals in mixed-phase clouds at Jungfraujoch (Switzerland): enrichment and depletion of particle groups relative to total aerosol, Atmospheric Chemistry and Physics, doi: 10.5194/acp-18-13987-2018, 2018.

Eriksen Hammer, S., Ebert, M., and Weinbruch, S.: Comparison of operator- and computer-controlled scanning electron microscopy of particles from different atmospheric aerosol types, Analytical and Bioanalytical chemistry, doi: 10.1007/s00216-019-01614-7, 2019.

Fisher, G. L., Chang, D. P. Y., and Brummer, M.: Fly Ash Collected from Electrostatic Precipitators: Microcrystalline Structures and the Mystery of the Spheres, Science, doi: 10.1126/science.192.4239.553, 1976.

Freedman, M. A.: Potential Sites for Ice Nucleation on Aluminosilicate Clay Minerals and Related Materials, The Journal of Physical Chemistry Letters, doi: 10.1021/acs.jpclett.5b01326, 2015.

Froyd, K. D., Murphy, D. M., Lawson, P., Baumgardner, D., and Herman, R. L.: Aerosols that form subvisible cirrus at the tropical tropopause, Atmospheric Chemistry and Physics, doi: 10.5194/acp-10-209-2010, 2010.

Garimella, S., Kristensen, T. B., Ignatius, K., Welti, A., Voigtländer, J., Kulkarni, G. R., Sagan, F., Kok, G. L., Dorsey, J., Nichman, L., Rothenberg, D. A., Rösch, M., Kirchgäßner, A. C. R., Ladkin, R., Wex, H., Wilson, T. W., Ladino, L. A., Abbatt, J. P. D., Stetzer, O., Lohmann, U., Stratmann, F., and Cziczo, D. J.: The SPectrometer for Ice Nuclei (SPIN): an instrument to investigate ice nucleation, Atmospheric Measurement Techniques, doi: 10.5194/amt-9-2781-2016, 2016.

Grawe, S., Augustin-Bauditz, S., Hartmann, S., Hellner, L., Pettersson, J. B. C., Prager, A., Stratmann, F., and Wex, H.: The immersion freezing behavior of ash particles from wood and brown coal burning, Atmospheric Chemistry and Physics, doi: 10.5194/acp-16-13911-2016, 2016.

Grawe, S., Augustin-Bauditz, S., Clemen, H. C., Ebert, M., Eriksen Hammer, S., Lubitz, J., Reicher, N., Rudich, Y., Schneider, J., Staacke, R., Stratmann, F., Welti, A., and Wex, H.: Coal fly ash: linking immersion freezing behavior and physicochemical particle properties, Atmospheric Chemistry and Physics, doi: 10.5194/acp-18-13903-2018, 2018.

Gunsch, M. J., Kirpes, R. M., Kolesar, K. R., Barrett, T. E., China, S., Sheesley, R. J., Laskin, A., Wiedensohler, A., Tuch, T., and Pratt, K. A.: Contributions of transported Prudhoe Bay oil field emissions to the aerosol population in Utqiaġvik, Alaska, Atmospheric Chemistry and Physics, doi: 10.5194/acp-17-10879-2017, 2017.

Hartmann, S., Augustin, S., Clauss, T., Wex, H., Šantl-Temkiv, T., Voigtländer, J., Niedermeier, D., and Stratmann, F.: Immersion freezing of ice nucleation active protein complexes, Atmospheric Chemistry and Physics, doi: 10.5194/acp-13-5751-2013, 2013.

Hatch, L. E., Pratt, K. A., Huffman, J. A., Jimenez, J. L., and Prather, K. A.: Impacts of Aerosol Aging on Laser Desorption/Ionization in Single-Particle Mass Spectrometers, Aerosol Science and Technology, doi: 10.1080/02786826.2014.955907, 2014.

Havlíček, D., Přibil, R., and Školoud, O.: The chemical and mineralogical composition of the water-soluble fraction of power-plant ash and its effect on the process of crystallization of water, Atmospheric Environment. Part A. General Topics, doi: 10.1016/0960-1686(93)90183-Y, 1993.

Heintzenberg, J., Okada, K., and Ström, J.: On the composition of non-volatile material in upper tropospheric aerosols and cirrus crystals, Atmospheric Research, doi: 10.1016/0169-8095(95)00042-9, 1996.

Hiranuma, N., Hoffmann, N., Kiselev, A., Dreyer, A., Zhang, K., Kulkarni, G., Koop, T., and Möhler, O.: Influence of surface morphology on the immersion mode ice nucleation efficiency of hematite particles, Atmospheric Chemistry and Physics, doi: 10.5194/acp-14-2315-2014, 2014.

Hiranuma, N., Möhler, O., Yamashita, K., Tajiri, T., Saito, A., Kiselev, A., Hoffmann, N., Hoose, C., Jantsch, E., Koop, T., and Murakami, M.: Ice nucleation by cellulose and its potential contribution to ice formation in clouds, Nature Geoscience, doi: 10.1038/ngeo2374, 2015.

Hiranuma, N., Möhler, O., Kulkarni, G., Schnaiter, M., Vogt, S., Vochezer, P., Järvinen, E., Wagner, R., Bell, D. M., Wilson, J., Zelenyuk, A., and Cziczo, D. J.: Development and characterization of an ice-selecting pumped counterflow virtual impactor (IS-PCVI) to study ice crystal residuals, Atmospheric Measurement Techniques, doi: 10.5194/amt-9-3817-2016, 2016.

Hoose, C., and Möhler, O.: Heterogeneous ice nucleation on atmospheric aerosols: a review of results from laboratory experiments, Atmospheric Chemistry and Physics, doi: 10.5194/acp-12-9817-2012, 2012.

Kamphus, M., Ettner-Mahl, M., Klimach, T., Drewnick, F., Keller, L., Cziczo, D. J., Mertes, S., Borrmann, S., and Curtius, J.: Chemical composition of ambient aerosol, ice residues and cloud droplet residues in mixed-phase clouds: single particle analysis during the Cloud and Aerosol Characterization Experiment (CLACE 6), Atmospheric Chemistry and Physics, doi: 10.5194/acp-10-8077-2010, 2010.

Kandler, K., Benker, N., Bundke, U., Cuevas, E., Ebert, M., Knippertz, P., Rodriguez, S., Schutz, L., and Weinbruch, S.: Chemical composition and complex refractive index of Saharan Mineral Dust at Izana, Tenerife (Spain) derived by electron microscopy, Atmospheric Environment, doi: 10.1016/j.atmosenv.2007.06.047, 2007.

Kandler, K., Lieke, K., Benker, N., Emmel, C., Küpper, M., Müller-Ebert, D., Ebert, M., Scheuvens, D., Schladitz, A., Schütz, L., and Weinbruch, S.: Electron microscopy of particles collected at Praia, Cape Verde, during the Saharan Mineral Dust Experiment: particle chemistry, shape, mixing state and complex refractive index, Tellus B: Chemical and Physical Meteorology, doi: 10.1111/j.1600-0889.2011.00550.x, 2011.

Kandler, K., Schneiders, K., Ebert, M., Hartmann, M., Weinbruch, S., Prass, M., and Pöhlker, C.: Composition and mixing state of atmospheric aerosols determined by electron microscopy: method development and application to aged Saharan dust deposition in the Caribbean boundary layer, Atmospheric Chemistry and Physics, doi: 10.5194/acp-18-13429-2018, 2018.

Kanji, Z. A., Ladino, L. A., Wex, H., Boose, Y., Burkert-Kohn, M., Cziczo, D. J., and Krämer, M.: Overview of Ice Nucleating Particles, Meteorological Monographs, doi: 10.1175/AMSMONOGRAPHS-D-16-0006.1, 2017.

Kiselev, A., Bachmann, F., Pedevilla, P., Cox, S. J., Michaelides, A., Gerthsen, D., and Leisner, T.: Active sites in heterogeneous ice nucleation—the example of K-rich feldspars, Science, doi: 10.1126/science.aai8034, 2017.

Korolev, A., McFarquhar, G., Field, P. R., Franklin, C., Lawson, P., Wang, Z., Williams, E., Abel, S. J., Axisa, D., Borrmann, S., Crosier, J., Fugal, J., Krämer, M., Lohmann, U., Schlenczek, O., Schnaiter, M., and Wendisch, M.: Mixed-Phase Clouds: Progress and Challenges, Meteorological Monographs, doi: 10.1175/amsmonographs-d-17-0001.1, 2017.

Kulkarni, P., Baron, P. A., and Willeke, K.: Introduction to Aerosol Characterization, in: Aerosol Measurement, John Wiley & Sons, doi: 10.1002/9781118001684.ch1, 2011.

Kupiszewski, P., Weingartner, E., Vochezer, P., Schnaiter, M., Bigi, A., Gysel, M., Rosati, B., Toprak, E., Mertes, S., and Baltensperger, U.: The Ice Selective Inlet: a novel technique for exclusive extraction of pristine ice crystals in mixed-phase clouds, Atmospheric Measurement Techniques, doi: 10.5194/amt-8-3087-2015, 2015.

Lacher, L., Lohmann, U., Boose, Y., Zipori, A., Herrmann, E., Bukowiecki, N., Steinbacher, M., and Kanji, Z. A.: The Horizontal Ice Nucleation Chamber (HINC): INP measurements at conditions relevant for mixed-phase clouds at the High Altitude Research Station Jungfraujoch, Atmospheric Chemistry and Physics, doi: 10.5194/acp-17-15199-2017, 2017.

Laskin, A., Cowin, J. P., and Iedema, M. J.: Analysis of individual environmental particles using modern methods of electron microscopy and X-ray microanalysis, Journal of Electron Spectroscopy and Related Phenomena, doi: 10.1016/j.elspec.2005.06.008, 2006.

Marsden, N., Flynn, M. J., Taylor, J. W., Allan, J. D., and Coe, H.: Evaluating the influence of laser wavelength and detection stage geometry on optical detection efficiency in a single-particle mass spectrometer, Atmospheric Measurement Techniques, doi: 10.5194/amt-9-6051-2016, 2016.

Marsden, N. A., Flynn, M. J., Allan, J. D., and Coe, H.: Online differentiation of mineral phase in aerosol particles by ion formation mechanism using a LAAP-TOF single-particle mass spectrometer, Atmospheric Measurement Techniques, doi: 10.5194/amt-11-195-2018, 2018.

Marsden, N. A., Ullrich, R., Möhler, O., Eriksen Hammer, S., Kandler, K., Cui, Z., Williams, P. I., Flynn, M. J., Liu, D., Allan, J. D., and Coe, H.: Mineralogy and mixing state of North African mineral dust by on-line single-particle mass spectrometry, Atmospheric Chemistry and Physics, doi: 10.5194/acp-19-2259-2019, 2019.

McMurry, P. H.: A review of atmospheric aerosol measurements, Atmospheric Environment, doi: 10.1016/S1352-2310(99)00455-0, 2000.

Mertes, S., Verheggen, B., Walter, S., Connolly, P., Ebert, M., Schneider, J., Bower, K. N., Cozic, J., Weinbruch, S., Baltensperger, U., and Weingartner, E.: Counterflow Virtual Impactor Based Collection of Small Ice Particles in Mixed-Phase Clouds for the Physico-Chemical Characterization of Tropospheric Ice Nuclei: Sampler Description and First Case Study, Aerosol Science and Technology, doi: 10.1080/02786820701501881, 2007.

Möhler, O., Nink, A., Saathoff, H., Schaefers, S., Schnaiter, M., Schöck, W., and Schurath, U.: The Karlsruhe aerosol chamber facility AIDA: Technical description and first results of homogenous and heterogenous ice nucleation experiments, in: CERN Yelloe Reports: Conference Proceedings, Workshop on ion-aerosol-cloud interactions, Geneva, 2001.

Möhler, O., Stetzer, O., Schaefers, S., Linke, C., Schnaiter, M., Tiede, R., Saathoff, H., Krämer, M., Mangold, A., Budz, P., Zink, P., Schreiner, J., Mauersberger, K., Haag, W., Kärcher, B., and Schurath, U.: Experimental investigation of homogeneous freezing of sulphuric acid particles in the aerosol chamber AIDA, Atmospheric Chemistry and Physics, doi: 10.5194/acp-3-211-2003, 2003.

Murphy, D. M., Cziczo, D. J., Hudson, P. K., Thomson, D. S., Wilson, J. C., Kojima, T., and Buseck, P. R.: Particle Generation and Resuspension in Aircraft Inlets when Flying in Clouds, Aerosol Science and Technology, doi: 10.1080/02786820490443094, 2004.

Murphy, D. M.: The design of single particle laser mass spectrometers, Mass Spectrometry Reviews, doi: 10.1002/mas.20113, 2007.

Myhre, G., D. Shindell, F.-M. Bréon, W. Collins, J. Fuglestvedt, J. Huang, D. Koch, J.-F. Lamarque, D. Lee, B. Mendoza, T. Nakajima, A. Robock, G. Stephens, T. Takemura, and H. Zhang: Anthropogenic and Natural Radiative Forcing. In: Climate Change 2013: The Physical Science Basis. Contribution of Working Group I to the Fifth Assessment Report of the Intergovernmental Panel on Climate Change, Cambridge, United Kingdom and New York, NY, USA, 2013.

O'Brien, R. E., Wang, B., Laskin, A., Riemer, N., West, M., Qi, Z., Yele, S., Xiao-Ying, Y., Peter, A., A., K. D., K., G. M., and C., M. R.: Chemical imaging of ambient aerosol particles: Observational constraints on mixing state parameterization, Journal of Geophysical Research: Atmospheres, doi: 10.1002/2015JD023480, 2015.

O'Sullivan, D., Murray, B. J., Ross, J. F., Whale, T. F., Price, H. C., Atkinson, J. D., Umo, N. S., and Webb, M. E.: The relevance of nanoscale biological fragments for ice nucleation in clouds, Scientific Reports, doi: 10.1038/srep08082. 2015

Ogren, J. A., Heintzenberg, J., and Charlson, R. J.: In-situ sampling of clouds with a droplet to aerosol converter, Geophysical research letters, doi: 10.1029/GL012i003p00121, 1985.

Paton-Walsh, C., Smith, T. E. L., Young, E. L., Griffith, D. W. T., and Guérette, É. A.: New emission factors for Australian vegetation fires measured using open-path Fourier transform infrared spectroscopy – Part 1: Methods and Australian temperate forest fires, Atmos. Chem. Phys., 14, 11313-11333, doi: 10.5194/acp-14-11313-2014, 2014.

Pekour, M. S., and Cziczo, D. J.: Wake Capture, Particle Breakup, and Other Artifacts Associated with Counterflow Virtual Impaction, Aerosol Science and Technology, doi: 10.1080/02786826.2011.558942, 2011.

Pummer, B. G., Budke, C., Augustin-Bauditz, S., Niedermeier, D., Felgitsch, L., Kampf, C. J., Huber, R. G., Liedl, K. R., Loerting, T., Moschen, T., Schauperl, M., Tollinger, M., Morris, C. E., Wex, H., Grothe, H., Pöschl, U., Koop, T., and Fröhlich-Nowoisky, J.: Ice nucleation by water-soluble macromolecules, Atmospheric Chemistry and Physics, doi: 10.5194/acp-15-4077-2015, 2015.

Quesenberry, C. P., and Hurst, D. C.: Large Sample Simultaneous Confidence Intervals for Multinomial Proportions, Technometrics, doi: 10.1080/00401706.1964.10490163, 1964.

Reilly, P. T. A., Lazar, A. C., Gieray, R. A., Whitten, W. B., and Ramsey, J. M.: The Elucidation of Charge-Transfer-Induced Matrix Effects in Environmental Aerosols Via Real-Time Aerosol Mass Spectral Analysis of Individual Airborne Particles, Aerosol Science and Technology, doi: 10.1080/027868200410895, 2000.

Roth, A., Schneider, J., Klimach, T., Mertes, S., van Pinxteren, D., Herrmann, H., and Borrmann, S.: Aerosol properties, source identification, and cloud processing in orographic clouds measured by single particle mass spectrometry on a central European mountain site during HCCT-2010, Atmospheric Chemistry and Physics, doi: 10.5194/acp-16-505-2016, 2016.

Schmidt, S., Schneider, J., Klimach, T., Mertes, S., Schenk, L. P., Kupiszewski, P., Curtius, J., and Borrmann, S.: Online single particle analysis of ice particle residuals from mountain-top mixed-phase clouds using laboratory derived particle type assignment, Atmospheric Chemistry and Physics, doi: 10.5194/acp-17-575-2017, 2017.

Shen, X., Ramisetty, R., Mohr, C., Huang, W., Leisner, T., and Saathoff, H.: Laser ablation aerosol particle time-of-flight mass spectrometer (LAAPTOF): performance, reference spectra and classification of atmospheric samples, Atmospheric Measurement Techniques, doi: 10.5194/amt-11-2325-2018, 2018.

Storelvmo, T.: Aerosol Effects on Climate via Mixed-Phase and Ice Clouds, Annual Review of Earth and Planetary Sciences, doi: 10.1146/annurev-earth-060115-012240, 2017.

Stratmann, F., Kiselev, A., Wurzler, S., Wendisch, M., Heintzenberg, J., Charlson, R. J., Diehl, K., Wex, H., and Schmidt, S.: Laboratory Studies and Numerical Simulations of Cloud Droplet Formation under Realistic Supersaturation Conditions, Journal of Atmospheric and Oceanic Technology, doi: 10.1175/1520-0426(2004)021<0876:lsanso>2.0.co;2, 2004.

Subbiah, M.: CoinMinD: Simultaneous Confidence Interval for Multinomial Proportion, R package 1.1., 2013.

Sullivan, R. C., and Prather, K. A.: Recent Advances in Our Understanding of Atmospheric Chemistry and Climate Made Possible by On-Line Aerosol Analysis Instrumentation, Analytical Chemistry, doi: 10.1021/ac050716i, 2005.

Targino, A. C., Krejci, R., Noone, K. J., and Glantz, P.: Single particle analysis of ice crystal residuals observed in orographic wave clouds over Scandinavia during INTACC experiment, Atmospheric Chemistry and Physics, doi: 10.5194/acp-6-1977-2006, 2006.

Trimborn, A., Hinz, K. P., and Spengler, B.: Online Analysis of Atmospheric Particles with a Transportable Laser Mass Spectrometer, Aerosol Science and Technology, doi: 10.1080/027868200410921, 2000.

Twohy, C. H., and Poellot, M. R.: Chemical characteristics of ice residual nuclei in anvil cirrus clouds: evidence for homogeneous and heterogeneous ice formation, Atmospheric Chemistry and Physics, doi: 10.5194/acp-5-2289-2005, 2005.

Umo, N. S., Murray, B. J., Baeza-Romero, M. T., Jones, J. M., Lea-Langton, A. R., Malkin, T. L., O'Sullivan, D., Neve, L., Plane, J. M. C., and Williams, A.: Ice nucleation by combustion ash particles at conditions relevant to mixed-phase clouds, Atmospheric Chemistry and Physics, doi: 10.5194/acp-15-5195-2015, 2015.

Vali, G., DeMott, P. J., Möhler, O., and Whale, T. F.: Technical Note: A proposal for ice nucleation terminology, Atmospheric Chemistry and Physics, doi: 10.5194/acp-15-10263-2015, 2015.

Van den Boogaart, K. G., and Tolosana-Delgado, R.: Analyzing compositional data with R, Springer, 2013.

Wagner, A. C., Bergen, A., Brilke, S., Bühner, B., Ebert, M., Haunold, W., Heinritzi, M., Herzog, S., Jacobi, S., Kürten, A., Piel, F., Ramme, A., Weber, D., Weinbruch, S., and Curtius, J.: Characterization of Aerosol Particles Produced by a Skyscraper Demolition by Blasting, Journal of Aerosol Science, doi: 10.1016/j.jaerosci.2017.06.007, 2017.

Wagner, R., Kiselev, A., Möhler, O., Saathoff, H., and Steinke, I.: Pre-activation of ice-nucleating particles by the pore condensation and freezing mechanism, Atmospheric Chemistry and Physics, doi: 10.5194/acp-16-2025-2016, 2016.

Weinbruch, S., Wentzel, M., Kluckner, M., Hoffmann, P., and Ortner, H. M.: Characterization of individual atmospheric particles by element mapping in electron probe microanalysis, Microchimica Acta, doi: 10.1007/bf01246176, 1997.

Weinbruch, S., Ebert, M., Gorzawski, H., Dirsch, T., Berg, T., and Steinnes, E.: Characterisation of individual aerosol particles on moss surfaces: implications for source apportionment, Journal of Environmental Monitoring, doi: 10.1039/B926876F, 2010.

Weinbruch, S., Wiesemann, D., Ebert, M., Schütze, K., Kallenborn, R., and Ström, J.: Chemical composition and sources of aerosol particles at Zeppelin Mountain (Ny Ålesund, Svalbard): An electron microscopy study, Atmospheric Environment, doi: 10.1016/j.atmosenv.2011.12.008, 2012.

Weingartner, E., Nyeki, S., and Baltensperger, U.: Seasonal and diurnal variation of aerosol size distributions (10<D<750 nm) at a high-alpine site (Jungfraujoch 3580 m asl), Journal of Geophysical Research: Atmospheres (1984–2012), doi: 10.1029/1999JD900170, 1999.

Wilson, T. W., Ladino, L. A., Alpert, P. A., Breckels, M. N., Brooks, I. M., Burrows, S. M., Carslaw, K. S., Huffman, J. A., Judd, C., and Kilthau, W. P.: A marine biogenic source of atmospheric ice-nucleating particles, Nature, doi: 10.1038/nature14986, 2015.

Wolf, M., Coe, A., Dove, L., Zawadowicz, M. A., Dooley, K., Biller, S., Zhang, Y., Chisholm, S. W., and Cziczo, D. J.: Investigating the Heterogeneous Ice Nucleation of Sea Spray Aerosols Using Prochlorococcus as a Model Source of Marine Organic Matter, Environmental Science & Technology, doi: 10.1021/acs.est.8b05150, 2018.

Worringen, A., Kandler, K., Benker, N., Dirsch, T., Mertes, S., Schenk, L., Kästner, U., Frank, F., Nillius, B., Bundke, U., Rose, D., Curtius, J., Kupiszewski, P., Weingartner, E., Vochezer, P., Schneider, J., Schmidt, S., Weinbruch, S., and Ebert, M.: Single-particle characterization of ice-nucleating particles and ice particle residuals sampled by three different techniques, Atmospheric Chemistry and Physics, doi: 10.5194/acp-15-4161-2015, 2015.

Yao, Z. T., Ji, X. S., Sarker, P. K., Tang, J. H., Ge, L. Q., Xia, M. S., and Xi, Y. Q.: A comprehensive review on the applications of coal fly ash, Earth-Science Reviews, doi: 10.1016/j.earscirev.2014.11.016, 2015.

Zhu, Y.-J., Olson, N., and Beebe, T. P.: Surface chemical characterization of 2.5-μm particulates (PM2. 5) from air pollution in Salt Lake City using TOF-SIMS, XPS, and FTIR, Environmental science & technology, doi: 10.1021/es0019530, 2001.

Zimmermann, F., Weinbruch, S., Schütz, L., Hofmann, H., Ebert, M., Kandler, K., and Worringen, A.: Ice nucleation properties of the most abundant mineral dust phases, Journal of Geophysical Research: Atmospheres, doi: 10.1029/2008JD010655, 2008.

ABBREVIATIONS

AIDA	Aerosol interaction and dynamics in the atmosphere
ALABAMA	Aircraft-based laser ablation aerosol mass spectrometer
BSE	Backscattered electrons
CCN	Cloud condensation nuclei
ccSEM	Computer controlled scanning electron microscopy
DMA	Differential Mobility Analyser
EDX	Energy dispersive X-ray microanalysis
Ice-CVI	Ice selective counter flow impactor
ICP-MS	Inductively coupled plasma mass spectrometry
INM	Ice nucleating macromolecule
INP	Ice nucleation particle
INUIT	Ice nuclei research unit
IR	Ice particle residual
LAAPTOF	Laser ablation aerosol particles time of flight
LACIS	Leipzig Aerosol Cloud Interaction Simulator
LDI	Laser desorption ionisation
LOD	Limit of detection
MS	Mass spectrometry
n_s	Ice nucleation active surface site density
OPS	Optical particle spectrometer
opSEM	operator controlled scanning electron microscopy
SEM	Scanning electron microscopy
SE	Secondary electron
SP-MS	Single particle mass spectrometry
TEM	Transmission electron microscopy
TOF	Time of flight
TOPS-Ice	Thermostabilized Optical Particle Spectrometer for the detection of Ice
XRD	X-ray powder diffraction

List of figures

Figure 1: The Ice-CVI based on Mertes et al. (2007) 6

Figure 2: The mineral structure of a) kaolinite, b) illite and c) K-feldspar. Figure 1 in *"Mineralogy and mixing state of North African mineral dust by on-line single-particle mass spectrometry"* by Marsden et al. (2019) 9

Figure 3: Comparison between opSEM and ccSEM of an urban background sample in Mainz (n=2751 in ccSEM, and n=523 in opSEM) and rural background/marine sample from Cyprus (n=1348 in ccSEM, and n=503 in opSEM). The particles were sampled with a 50 % cut off diameter at 0.1μm. The relative number abundance of each particle group was normalised by the substrate area analysed. From figure 2 in Eriksen Hammer et al. (2019). 13

Figure 4: ccSEM (n=3751) and opSEM (n=529) analysis of a sample from the free troposphere- Swiss Alps. Particles were sampled with a (sampled with 50 % cut off diameter at 0.1μm). The relative number abundance of each particle group was normalised by the substrate area analysed. From figure 2 in Eriksen Hammer et al. (2019). 14

Figure 5: Comparison of opSEM and ccSEM of a traffic hotspot sample – Essen, Germany (n=6940 in ccSEM, and n=552 in opSEM) and a rural background sample – Odenwald, Germany (n=1103 in ccSEM, and n=501 in opSEM). Particles were sampled with 50 % cut-off diameter at 1.0 μm. The relative number abundance of each particle group was normalised by the substrate area analysed. From figure 2 in Eriksen Hammer et al. (2019). 14

Figure 6: Relative number abundance of different particle groups in total aerosol and ice particle residuals sampled during Jungfraujoch campaign 2017. The samples marked with a/b behind number are parallel sampled. Figure 4 and 6 in Eriksen Hammer et al. (2018) 16

Figure 7: Enrichment or depletion of the different particle groups within the IR fraction relative to the aluminosilicate group expressed as odds ratio. Confidence intervals (95%) are presented as error bars, and the arrows indicates undefined upper/ lower limits due to counting statistics. Figure 8 from Eriksen Hammer et al. (2018) 17

Figure 8: Secondary electron image of coal fly ash sample 1 dispersed dry and after suspension in distilled water 19

Figure 9: Secondary electron image of different coal fly ash samples dispersed dry and after suspension in distilled water 20

Figure 10: Relative number abundance of particle groups from mineral dust samples, S- in front of the sample name indicates Sahelian and M- Moroccan sample..... 22

Figure 11: Average composition of nominally pure minerals from the literature (a), SEM-EDX analysis (atomic %) of the Moroccan samples (b, c), and the Sahelian samples (d, e, f). Figure 5 in Marsden et al. (2019)..... 23

Figure 12: Histograms of the Al+Si sub-composition with respect to the alkali metals (Al+Si)/ (Al+Si+K+Na) in single particles of Moroccan (a and b) and Sahelian (c,d) samples comparing SEM-EDX and SP-MS technique. From figure 8 in Marsden et al., (2019)..... 24

List of tables

Table 1: Samples and sampler set-up..... 10

Short CV

Stine Eriksen Hammer

Born in Tønsberg, Norway the 22nd of July 1991

Education

04/2016 -	**PhD student at TU Darmstadt as a part of the INUIT project** Institute of Applied Geosciences, Environmental minerology Darmstadt, Germany
08/2013-06/2015	**Master student at the Norwegian University of life sciences** Faculty of chemistry, biotechnology and food sciences (IKBM) and faculty of environmental Sciences (IMV) Ås, Norway
01/-06/2012	**Study abroad at Lincoln University** Christchurch, New Zealand
08/2010-06/2013	**Bachelor student at the Norwegian University of life sciences** Faculty of chemistry, biotechnology and food sciences Ås, Norway
08/2007-06/2010:	**Horten High School** Horten, Norway

Work experience:

01/-03/2016	**Chemical engineer** Vitas AS, Oslo, Norway
05/-09/2015	**Project position – Ungforsk** The Norwegian University of Life Sciences, Ås, Norway
07/2012-01/2016	**Assistant - healthcare** Horten Kommune, Horten, Norway

Atmos. Chem. Phys., 18, 13987–14003, 2018
https://doi.org/10.5194/acp-18-13987-2018

Atmospheric Chemistry and Physics
Open Access
EGU

Composition of ice particle residuals in mixed-phase clouds at Jungfraujoch (Switzerland): enrichment and depletion of particle groups relative to total aerosol

Stine Eriksen Hammer[1], **Stephan Mertes**[2], **Johannes Schneider**[3], **Martin Ebert**[1], **Konrad Kandler**[1], **and Stephan Weinbruch**[1]

[1]Institute of Applied Geosciences, Darmstadt University of Technology, Schnittspahnstraße 9, 64287 Darmstadt, Germany
[2]Leibniz-Institute for Tropospheric Research, Permoserstraße 15, 04318 Leipzig, Germany
[3]Particle Chemistry Department, Max Planck Institute for Chemistry, Hahn-Meitner-Weg 1, 55128 Mainz, Germany

Correspondence: Stine Eriksen Hammer (sehammer@geo.tu-darmstadt.de)

Received: 12 May 2018 – Discussion started: 1 June 2018
Revised: 4 September 2018 – Accepted: 10 September 2018 – Published: 2 October 2018

Abstract. Ice particle residuals (IRs) and the total aerosol particle population were sampled in parallel during mixed-phase cloud events at the high-altitude research station Jungfraujoch in January–February 2017. Particles were sampled behind an ice-selective counterflow impactor (Ice-CVI) for IRs and a heated total inlet for the total aerosol particles. A dilution set-up was used to collect total particles with the same sampling duration as for IRs to prevent overloading of the substrates. About 4000 particles from 10 Ice-CVI samples (from 7 days of cloud events at temperatures at the site between −10 and −18 °C) were analysed and classified with operator-controlled scanning electron microscopy. Contamination particles (identified by their chemical composition), most likely originating from abrasion in the Ice-CVI and collection of secondary ice, were excluded from further analysis. Approximately 3000 total aerosol particles (IRs and interstitial particles) from 5 days in clouds were also analysed. Enrichment and depletion of the different particle groups (within the IR fraction relative to the total aerosol reservoir) are presented as an odds ratio relative to alumosilicate (particles only consisting of Al, Si, and O), which was chosen as reference due to the large enrichment of this group relative to total aerosol and the relatively high number concentration of this group in both total aerosol and the IR samples. Complex secondary particles and soot are the major particle groups in the total aerosol samples but are not found in the IR fraction and are hence strongly depleted. C-rich particles (most likely organic particles) showed a smaller enrichment compared to aluminosilicates by a factor of ∼ 20. The particle groups with enrichment similar to aluminosilicate are silica, Fe aluminosilicates, Ca-rich particles, Ca sulfates, sea-salt-containing particles, and metal/metal oxide. Other aluminosilicates – consisting of variable amounts of Na, K, Ca, Si, Al, O, Ti, and Fe – are somewhat more enriched (factor ∼ 2) and Pb-rich particles are more (factor ∼ 8) enriched than aluminosilicates. None of the sampled IR groups showed a temperature or size dependence in respect to ice activity, which might be due to the limited sampling temperature interval and the similar size of the particles. Footprint plots and wind roses could explain the different total aerosol composition in one sample (carbonaceous particle emission from the urban/industrial area of Po Valley), but this did not affect the IR composition. Taking into account the relative abundance of the particle groups in total aerosol and the ice nucleation ability, we found that silica, aluminosilicates, and other aluminosilicates were the most important ice particle residuals at Jungfraujoch during the mixed-phase cloud events in winter 2017.

1 Introduction

Mixed-phase clouds are important because they have an impact on the hydrological cycle and cloud electrification and because they influence the atmospheric radiation balance (Storelvmo, 2017). Ice-nucleating particles (INPs) can initiate cloud glaciation, which may cause precipitation (Myhre et al., 2013). The order of magnitude of the effect from

aerosol–cloud interaction on the "second indirect aerosol effect" and "semi-indirect effect" is still uncertain (Myhre et al., 2013; Flato et al., 2013; Korolev et al., 2017).

In nature, spontaneous freezing of supersaturated droplets occurs at temperatures below −38 °C and a relative humidity with respect to ice $> \sim 140\,\%$ (Kanji et al., 2017), termed homogeneous ice nucleation (Vali et al., 2015). At higher temperatures, a surface – like a particle surface – can lower the free energy and thereby assist the phase transition to ice when relative humidity allows for this, termed heterogeneous ice nucleation. Heterogeneous ice nucleation can occur in different hypothesized modes: (1) deposition nucleation, (2) immersion freezing, (3) contact freezing, and (4) condensation freezing. A detailed description of the different modes is found elsewhere (Vali et al., 2015; Kanji et al., 2017). Mixed-phase cloud temperature ranges between −40 and 0 °C (Storelvmo, 2017), with immersion and contact freezing as the dominating ice formation modes (Lohmann and Diehl, 2006).

Ice nucleation ability was studied offline and online in many laboratory and field experiments as well as by modelling (Hoose et al., 2010; Hoose and Möhler, 2012; Kanji et al., 2017, and references therein). Summarized from laboratory studies (Hoose and Möhler, 2012), biological particles seem to dominate the ice activity at higher temperatures above −10 °C, whereas mineral dust is found to be mostly ice active below −10 °C, and organic particles and soot nucleate ice below −30 °C close to homogenous freezing. A model study of mixed-phase clouds on a global scale by Hoose et al. (2010) shows that the main component of INPs is mineral dust particles. The findings of field experiments at different locations globally are presented by Kanji et al. (2017) as a function of nucleation temperature. In this paper only broadly defined classes are given to characterize the ice nucleation efficiency from INP concentration in different environments. To summarize, biological particles from rural areas dominate at higher temperatures (−5 to −20 °C), and marine particles from coastal areas show a lower ice activity in the higher temperature range than biological particles (−5 to −30 °C). Particles from Arctic and Antarctic locations seem to have a relatively high INP abundance between −17 and −25 °C, and particles from areas with biomass burning show high INP concentrations between −10 and −30 °C. Mineral-dust-rich regions show particles with the highest ice activity in the range of −10 to −40 °C, and these particles seem to be the most ice-active component. Exact number concentration is found in Kanji et al. (2017) and references therein. Particle groups determined based on chemical composition in cirrus clouds are reported as sulfates, organics, sea salt, mineral dust or fly ash, metal particles, soot, and biological material in the ice particle residual (IR) fraction (Heintzenberg et al., 1996; Cziczo et al., 2004, 2013). Twohy and Poellot (2005) found the highest abundance of salts and industrial particles in cirrus, followed by crustal, organic and soot particles. In mixed-phase clouds, at the high-altitude research station Jungfraujoch in Switzerland, different IR groups were reported to act as ice nuclei. With the use of electron microscopy and looking at the enrichment relative to interstitial aerosol, Ebert et al. (2011) interpreted complex secondary aerosol, Pb-bearing particles, and complex mixtures as ice nuclei. In contrast, Worringen et al. (2015) considered only particle groups as ice nuclei, which were found with three different techniques (FINCH + PCVI, Ice-CVI, and ISI). These groups included silicates, Ca-rich particles, carbonaceous particles, metal/metal oxide, and soot. Using single-particle mass spectrometry, Schmidt et al. (2017) considered all particles observed in the IR fraction as INPs (biological, soil dust, minerals, sea salt/cooking, aged material, engine exhaust, soot, lead-containing particles, industrial metals, Na- and K-dominated particles, and others). Kamphus et al. (2010) report mineral dust and fly ash (with and without some volatiles), metallic particles, and black carbon as the most ice-active particles, measured with two different mass spectrometers behind the Ice-CVI. Cozic et al. (2008a) investigated black carbon enrichment with two particle soot absorption photometers simultaneously behind the Ice-CVI and a total inlet and by aerosol mass spectrometry (AMS) and single-particle mass spectrometer (measuring particles between 200 nm and 2 µm) behind the Ice- CVI during cloud events. They concluded, based on the enrichment, that black carbon is ice active.

In situ cloud measurements of IRs can be performed with an aircraft for pure ice clouds, like for cirrus clouds, with the use of a counterflow virtual impactor (CVI) (Ogren et al., 1985; Heintzenberg et al., 1996; Ström and Ohlsson, 1998; Twohy et al., 2003; Froyd et al., 2010; Cziczo and Froyd, 2014; Cziczo et al., 2017) and references therein). In situ IR sampling in mixed-phase cloud requires an extra step to separate ice crystals from droplets and has, therefore, up to now been restricted to ground-based measurements. A dedicated inlet system (Ice-CVI) was developed by Mertes et al. (2007) to sample freshly produced ice particles in mixed-phase clouds and, after sublimating the ice, deliver the residuals (IRs) to connected sampling or analysing instruments. As described in Mertes et al. (2007), a residual particle can be interpreted as its original INP only when sampling small ice crystals. There are three reasons for this size restriction leading to sampling of rather young ice particles. The first reason is that only the small ice particles grow by water vapour diffusion; in contrast, larger ice particles could further grow by riming. Moreover, larger and older ice particles experience impaction scavenging by interstitial particles. Both processes add more aerosol particles to the ice crystal and thus the original INP cannot be identified any more after ice sublimation in the Ice-CVI. Last is the technical reason that larger ice particles would shatter and break up at the inner surfaces of the Ice-CVI sampling system.

The major aims of our paper are to improve the sampling approach and to study the variation in IRs in mixed-phase clouds. In contrast to previous work (Worringen et al., 2015;

Ebert et al., 2011; Kamphus et al., 2010; Schmidt et al., 2017), IR and total aerosol were collected in parallel. This allows us to examine the ice nucleation efficiency of the various particle groups and to investigate the dependence on temperature, particle size, and air mass history.

2 Experimental

2.1 Sampling

In January–February 2017 an extensive field campaign was conducted by INUIT (Ice Nucleation Research Unit funded by the German Research Foundation, DFG) at the high-altitude research station Jungfraujoch in Switzerland (3580 m a.s.l.). The campaign lasted for 5 weeks with the aim to investigate IRs from mixed-phase clouds, which are considered to be the original true INPs. During mixed-phase cloud events, IRs were separated from other cloud constituents like interstitial aerosol particles, supercooled droplets, and large ice aggregates by use of the Ice-CVI (Mertes et al., 2007). Total aerosol particles (interstitial particles and IRs) were sampled in parallel. Particles were sampled by the use of multi MINI cascade impactors with the same design as described in Ebert et al. (2016) and Schütze et al. (2017), but with the use of only one stage with a lower 50 % cut-off diameter of approximately 0.1 µm (aerodynamic). The multi MINI cascade impactor is equipped with purge flow and 5 min flushing of the system was always performed prior to sampling to avoid carryover of particles from previous samples. The particles were collected on boron substrates to allow detection of light elements including carbon (Choël et al., 2005; Ebert et al., 2016).

2.2 Total aerosol sampling

Total aerosol particles were sampled in parallel to IRs behind a heated inlet (Weingartner et al., 1999) to study IR enrichment and depletion, identify contaminants, and characterize the air masses present. Total aerosol samples were collected with a dilution set-up (Fig. 1) to match the longer sampling time (up to 5 h) of the Ice-CVI. The dilution unit is built up by two valves to control the air stream in and out of the system, making it possible to send air through two filters to dilute the incoming aerosol flow. Without this dilution, due to the much higher concentration of total particles, these samples would be overloaded and not suited for single-particle analysis.

2.3 Ice-CVI

The Ice-CVI is a modified counterflow virtual impactor which can separate freshly formed ice particles in mixed-phase clouds; for details see Mertes et al. (2007). The inlet consists of several components to separate: (a) large precipitating ice crystals >50 µm by the 90° inlet, (b) large ice particles >20 µm with a virtual impactor, (c) supercooled droplets

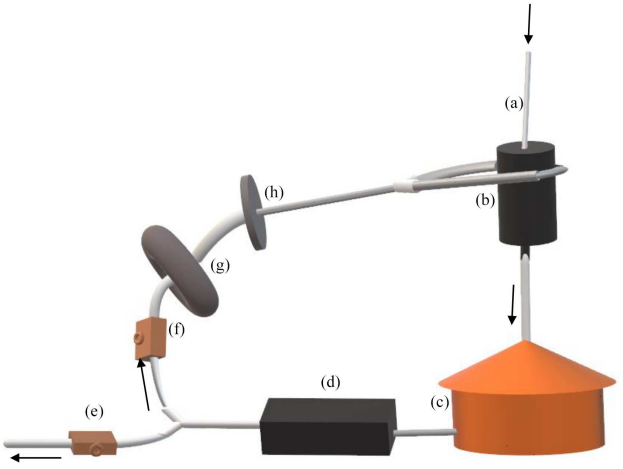

Figure 1. Illustration of the dilution unit behind the heated total inlet. **(a)** An inlet tube attached to the total inlet, **(b)** diluter, **(c)** multi MINI impactor, **(d)** pump, **(e)** valve to control outflow, **(f)** valve to control air going back in the system, **(g)** pre-filter (Whatman, Sigma-Aldrich), and **(h)** main filter (Millipore, Sigma-Aldrich). Arrows indicate the air flow direction.

>5 µm with two cold impaction plates where the droplets freeze and the ice crystals bounce off, and (d) interstitial particles <5 µm, which are removed by a counterflow virtual impactor.

2.4 Scanning electron microscopy

Size, morphology, chemical composition, and mixing state of IRs and total aerosol particles were investigated by scanning electron microscopy using a FEI Quanta 400 ESEM FEG instrument (FEI, Eindhoven, the Netherlands) equipped with an energy-dispersive X-ray detector (Oxford, Oxfordshire, UK). All analyses were carried out manually, referred to as operator-controlled scanning electron microscopy (SEM) instrument, using an acceleration voltage of 15 kV and a sample chamber pressure of around 1×10^{-5} mbar. The multi-point feature "point&ID" in the Oxford software Aztec (version 3.3 SP1) was used for the operator-controlled single-particle analysis. On each sample, about 500 particles were measured with 5 s of counting time for X-ray microanalysis. To ensure unbiased results, all particles in an image frame with an equivalent projected area diameter $\geq$ 100 nm were investigated. The particles were classified based on chemical composition, mixing state, morphology, and stability under the electron beam. Classification criteria and possible sources are given in Table 1. Particles that could not be assigned to any of the defined classes were grouped as "other". This group contains for example Mg-rich, Zn-rich, and Ag-containing particles. Four groups are interpreted as contamination particles: pure salt, alumina, and Cu-rich and Ni-rich particles.

Table 1. Classification criteria and possible sources/explanations for particle groups for both total aerosol and ice particle residuals.

Group	Major elements	Morphology/ beam stability	Source/particle explanation
Soot	C	Chain-like or more compact agglomerates of primary particles	Combustion, black carbon
C-rich particles	C	No soot morphology	Organic aerosol, biomass burning**, biological**
Complex secondary particles	No X-ray spectra or S peak	Most particles evaporating, some relatively stable	Sulfur-rich secondary organic aerosol; might also contain a substantial fraction of nitrates and other organics
Aged – sea salt	Na, S (sometimes small amount of Cl and Mg)	Relatively stable	Marine aerosol, sea spray, might contain organics
Mixed – sea salt	Na, S (sometimes small amount of Cl and Mg) + mineral composition		Marine aerosol mixed with mineral particles. Might contain organics.
Ca-rich particles	Ca, C, O		Mineral particles, calcium carbonates, e.g. calcite
Ca sulfate	Ca, S, O		Mineral particles, e.g. gypsum and anhydrite
Silica	Si, O		Mineral particles, e.g. quartz
Aluminosilicate	Al, Si, O		Mineral particles, e.g. kaolinite
Fe aluminosilicate	Al, Si, Fe, O		Mineral particles, e.g. almandine
Other aluminosilicates	Variable amounts of Na, K, Ca, Si, Al, O, Ti, and Fe		Mineral particles, e.g. feldspars, illite, and smectite (montmorillonite)
Metal/metal oxides	Fe, O or Ti, O or Fe, Cr, Mn	Fly ash was detected as spherical particles	Mineral particles like hematite, magnetite, and rutile, or steel particles (alloys)
Pb-rich particles	Pb, or Pb, Cl	Single particle or inclusions within particle	Helicopters and small aircrafts, previously reported at Jungfraujoch
Other	Particles which do not meet the classification criteria above		
Alumina*	Al, O		Artefact, Ice-CVI
Ni-rich particles*	Ni		Artefact, Ice-CVI
Cu-rich particles*	Cu		Artefact, particle substrate
Pure salt*	Na, Cl		Artefact, hypothesized from secondary ice processes, e.g. crystal break-up, marine origin**

*Most likely contamination. **Uncertain origin because the chemical characterization and/or morphology was not typical for this particle group.

2.5 Sampling days, meteorology, and footprint plots

During 7 days, 10 Ice-CVI samples were taken in clouds at site temperatures between −10 and −18 °C. Sampling day, time, and site temperatures are presented in Fig. 2 and as a table in the electronic Supplement (Table S1). Temperatures were measured at the station and can differ from the onset ice nucleation temperature of the particles depending on where in the mixed phase cloud nucleation occurred. Six parallel total aerosol samples were successfully collected. The

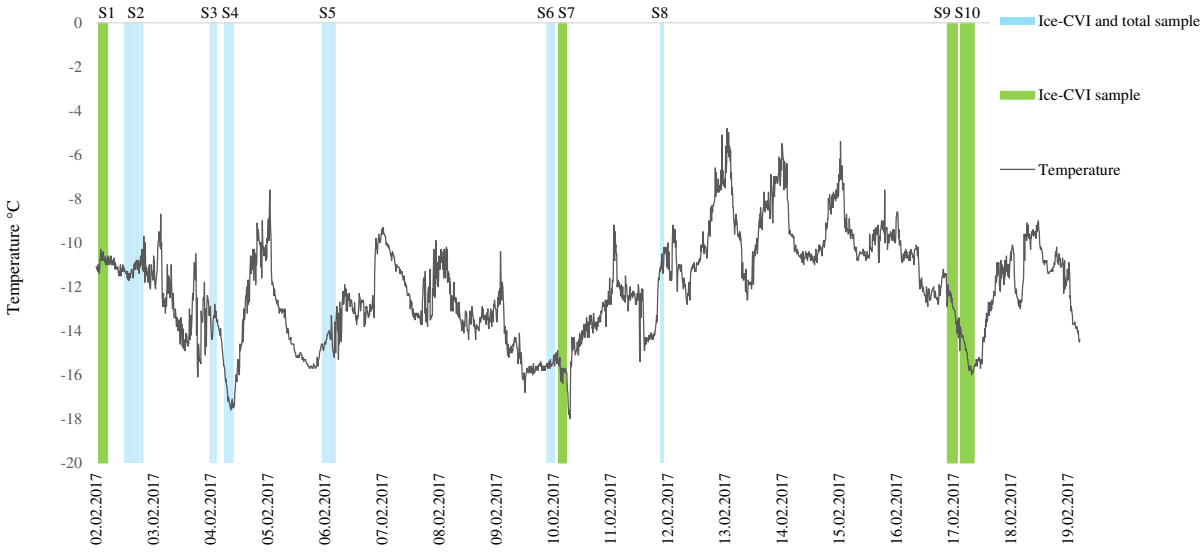

Figure 2. Temperature (°C) and sampling times in February 2017 behind Ice-CVI and total inlet. Sample numbers are given above the bars. Blue bars indicate sampling periods with parallel samples, and green bars periods for which only IR samples could be analysed. Temperature data were received from the Federal Office of Meteorology and Climatology (MeteoSwiss; https://www.meteoswiss.admin.ch, last access: 17 October 2017).

other four total samples are either overloaded or do not have enough particles on the substrate.

During the whole campaign, north-easterly and south-westerly winds were the dominating local wind directions in accordance with the topography at Jungfraujoch. Footprint plots, showing the probable air mass residence time at the surface, were calculated with the FLEXPART model (Stohl et al., 1998, 2005; Stohl and Thomson, 1999; Seibert and Frank, 2004). These plots are calculated with 10-day back trajectories and a potential emission sensitivity to determine the probable emission region of the particles arriving at Jungfraujoch. Wind roses and footprint plots are presented in Fig. 3.

2.6 Methodological problems

2.6.1 Sampling artefacts

The observed alumina, pure salt, and Ni-rich and Cu-rich particles are regarded as sampling artefacts. The IR samples are heavily loaded with artefacts (40 %–78 % of the particles – alumina, Ni-rich particles, and pure salt) easily characterized and removed in further analysis. The Cu-rich particles are a part of the substrates and can in principle be found in both IR samples and total aerosol samples. Alumina particles are found in all IR samples at relative high number abundances between 25 % and 70 %, despite the fact that the Ice-CVI was coated before the present campaign with Ni to avoid this contamination. The relative abundance of alumina particles in IR samples is higher in our campaign compared to two previous campaigns at Jungfraujoch using the same instrumentation but without the Ni coating of the Ice-CVI (Ebert et al., 2011; Worringen et al., 2015). This might be explained by the fact that we only focused on the sub-micrometer particles and/ or the difference in meteorology, sample time, and particle load all influencing the relative composition of contamination particles. In contrast to previous work, we sampled IR and total aerosol in parallel to be able to clearly distinguish instrumental artefacts from IRs. As we did not detect a single alumina particle in total aerosol samples, this particle group is regarded as contamination. Alumina particles are easily recognized and were subtracted from the real IRs. Nevertheless, their presence helped substantially to locate the impaction spot on the boron substrates.

Secondary ice processes can produce ice crystals in the critical size range selected by the Ice-CVI. The low temperature during sampling does not support the Hallett–Mossop process (Hallett and Mossop, 1974) regarding rime splintering, but other secondary processes producing ice crystals like ice-crystal break-up, blown snow, or crystal–crystal collisions in the critical size range are plausible (Mertes et al., 2007). We hypothesize that pure salt is an artefact due to sampling of the mentioned secondary ice production processes in clouds. The presence of sodium and chloride in ice crystals previously acting as cloud condensation nuclei can later form solid NaCl in line or on the substrate after evaporation of water. This hypothesis is inconclusive because pure salt is not observed in the total aerosol fraction, where only aged and mixed salt are present. This might be explained by evaporation of ice crystals in the heated inlet and the longer sampling line and the relatively low number concentration of these particles compared to the dominating groups (soot and complex

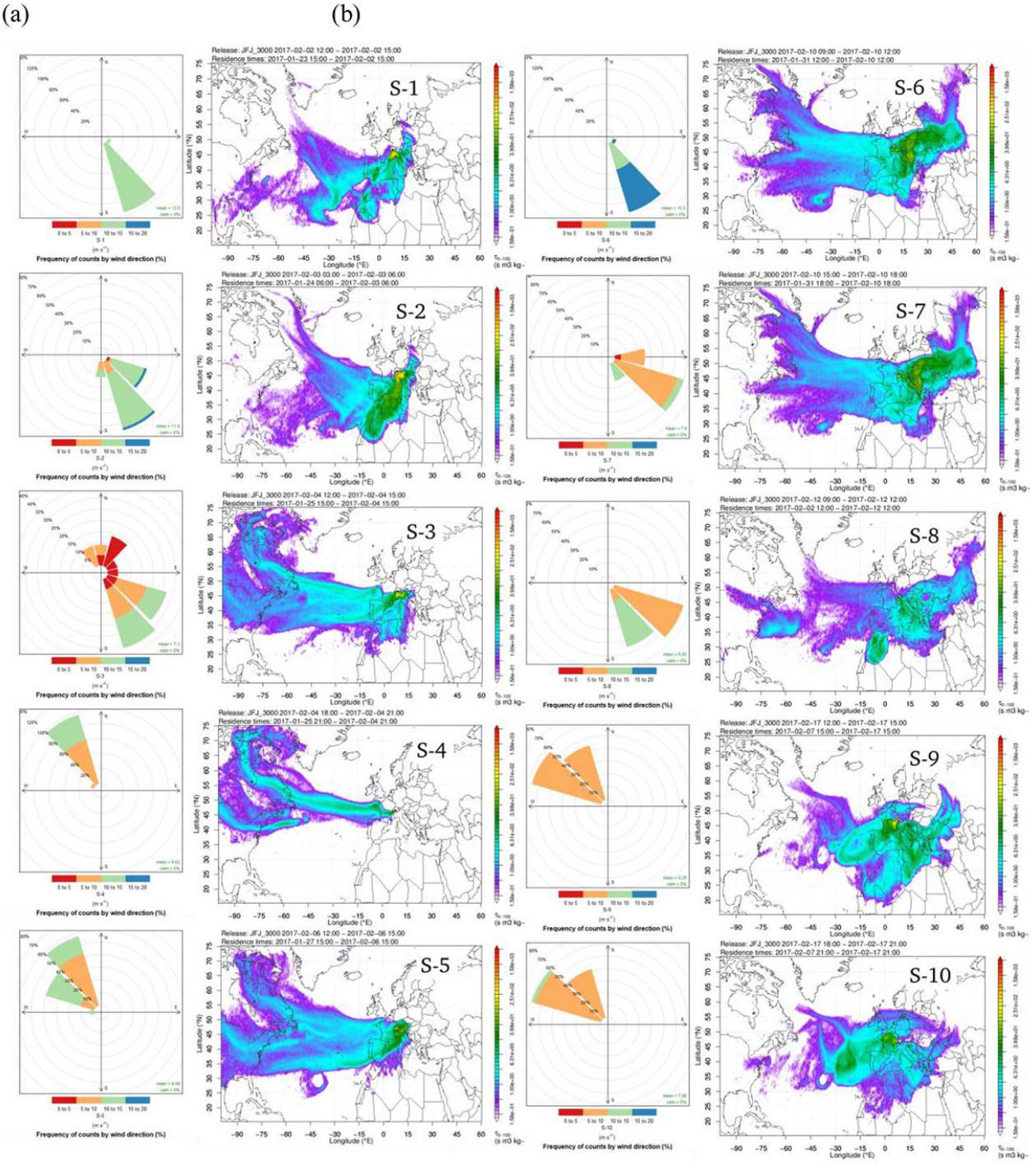

Figure 3. Wind rose **(a)** and footprint plots **(b)** calculated with the FLEXPART model, http://lagrange.empa.ch/FLEXPART_browser/ (last access: 17 January 2018) (Stohl et al., 1998, 2005; Stohl and Thomson, 1999; Seibert and Frank, 2004). Horizontal wind direction and speed were obtained from the Federal Office of Meteorology and Climatology (MeteoSwiss; https://www.meteoswiss.admin.ch, last access: 17 October 2017).

secondary particles) in the total aerosol samples. It should be mentioned here that sea salt was considered to be an artefact in the IR fraction by Worringen et al. (2015).

A few Ni-rich particles (1 %–7 % relative by number) were encountered in the IR fraction but not in the total aerosol. The Ni-rich particles most likely stem from the Ni coating of some parts of the Ice-CVI. The few Cu-rich particles found, in both total aerosol and the IR samples, are from the boron substrate in which boron is embedded in copper.

2.6.2 Accuracy of particle group abundance

Accuracy of the particle group abundance depends on three different factors: (1) separation of IR from the rest of the aerosol particles by the Ice-CVI and deposition losses behind both inlets, (2) detection of particles in SEM, and (3) the classification procedure. Sampling issues like abrasion, deposition losses, and ice crystal break-up may occur in the Ice-CVI (Mertes et al., 2007). Abrasion particles were easily recognized as discussed in the previous paragraph. Sampling of secondary ice may have led to the relatively high abundance ($\sim 2\,\%$–$28\,\%$) of pure salt particles in the IR fraction discussed in the previous paragraph. As we regard pure salt particles as an artefact, they are not included in the sea-salt-containing particle group. Deposition loss can generally not be excluded. Three of the total aerosol samples (S-3b, S-4b, and S-6b) are sampled under conditions in which the concentration (measured with condensation particle counters) of the total inlet was lower than the interstitial inlet. There are two possible explanations for this: deposition loss in the total aerosol inlet and/or a leak in the interstitial inlet. The relative abundance of the different particle groups in these samples is however comparable to previous findings at Jungfraujoch (Cozic et al., 2008b; Kamphus et al., 2010; Fröhlich et al., 2015). A possible deposition loss leading to systematic bias in the concentration measurements does not seem to change the relative abundance of the different particle groups. Our conclusions are thus not affected as we do not discuss number concentrations.

For most particle groups we do not expect to have significant detection artefacts in SEM. These particle groups are detected with high efficiency, in both the total aerosol as well as the IR fraction. However, C-rich particles and soot may be interchanged in total aerosol samples because the image quality can be reduced by evaporating complex secondary particles, leading to less efficient detection of carbonaceous species, which have a low contrast in SEM images. Usually, evaporation of complex secondary particles is not a problem because the particles are observed at the start of analysis. Nevertheless, in one sample, complex secondary particles were lost prior to observation because this sample was erroneously left in the chamber for a longer time before it was analysed. However, these effects seem to be small because we have observed an abundance of carbonaceous particles and complex secondary aerosol particles (in total aerosol) comparable to in previous work (Cozic et al., 2008b).

The classification criteria used (Table 1) may lead to problems for small (below approximately 150 nm equivalent projected area diameter) carbonaceous particles. Due to the limited lateral resolution of the instrument, the typical morphology of soot may not be recognized for small particles. In this case, soot would be misclassified as C-rich particles. Still, the sum of both particle groups should be accurate. However, this problem is only significant for the total aerosol samples because evaporating secondary aerosol in these samples leads to deterioration of the image quality. Misclassification of soot as C-rich particles would imply that soot is even more depleted in the IR fraction.

2.7 Statistical analysis

To calculate enrichment and depletion of the different particle groups in the IR fraction relative to total aerosol, all particle group abundances are normalized to the abundance of the aluminosilicate group. We have chosen this group as a reference as it has the highest relative abundance in both the IR samples and the total aerosol. We do not show a simple ratio of proportions (e.g. proportion of aluminosilicates in IRs divided by proportion of this group in total aerosol) because the proportion is constrained to values between 0 and 1. This is generally referred to as closed data (Aitchison, 2003; Van den Boogaart and Tolosana-Delgado, 2013) and implies that only ratios of two groups can be interpreted (i.e. not the proportion of one group alone). Furthermore, we do not discuss differences in proportions between IR and total aerosol as in Ebert et al. (2011), as this difference is strongly dependent on the relative abundance of a particle group. To overcome these problems, only aluminosilicate normalized particle group abundances are used to quantify enrichment/depletion of a particle group in the IR fraction. This measure is termed odds ratio in the statistical literature.

The odds ratios (OR) is calculated in the following way:

$$\mathrm{OR_i} = \frac{\left(\frac{n_\mathrm{i}}{n_\mathrm{AlSi}}\right)_\mathrm{IR}}{\left(\frac{n_\mathrm{i}}{n_\mathrm{AlSi}}\right)_\mathrm{total}}, \quad (1)$$

with n_i the absolute number of particles in particle group i, n_AlSi the absolute number of particles in the group of aluminosilicates in both IR and the total aerosol fraction. For particle groups which did not contain a single particle, one particle (which is the detection limit) was added to the respective group in order to calculate an odds ratio. For these groups the odds ratios shown in Fig. 8 represent an upper or lower limit. The odds ratios represent enrichment or depletion of a particle group normalized to aluminosilicates when the IR fraction is compared to the total aerosol. Enrichment relative to aluminosilicates is discussed for each group that is present in the IR. The two groups of complex secondary particles and soot are interpreted as depleted because these

particles are not found in the IR fraction. These two particle groups are hence depleted compared to aluminosilicates and absolutely depleted compared to total aerosol.

The Fisher test was applied to estimate confidence intervals for the odds ratio and was calculated with RStudio (RStudioTeam, 2016). Figures 5, 7, and 8 are plotted in RStudio with the package "ggplot2" (Wickham, 2009). Wind roses (Fig. 3) were plotted with the RStudio package "openair" (Carlslaw and Ropkins, 2012).

3 Results

3.1 Total aerosol

Particle groups observed in the total aerosol samples include complex secondary particles, soot, C-rich particles, Ca-rich particles, Ca sulfates, silica, aluminosilicates, Fe aluminosilicates, other aluminosilicates, metal/metal oxide, sea-salt-containing particles (aged and mixed), and other particles (Fig. 4).

A few fly ash particles were detected in the metal/metal oxides group. In addition, one group of artefact particles (Cu-rich particles) originating from the substrate was found and excluded from further analysis. Four of the six samples are dominated by secondary aerosol, which consists of sulfates and highly instable particles (under vacuum and/or electron bombardment) for which no X-ray spectrum could be obtained. Still, remains of these particles are easily seen in the secondary electron images. The highly instable particles are classified based on the fact that they evaporated during the operator-controlled X-ray analysis. In contrast to the IR fraction, we observed two groups of carbonaceous particles. Carbon-dominated particles without typical morphology are classified as C-rich particles (Fig. S1). Chain-like or more compacted agglomerates of spherical primary carbonaceous particles are interpreted as soot in accordance with previous literature, e.g. Wentzel et al. (2003), Buseck et al. (2014), and Weinbruch et al. (2018). Sample S-2b was taken during night-time and consists of two separate samples directly taken one after the other (for 3 h each). The unusually high abundance of carbonaceous particles within this sample most likely results from urban/industrial sources of the Po Valley seen in the footprint plot (Fig. 3). Sample S-5b shows a high relative abundance of mineral particles, which may be the result of having lost complex secondary particles in the instrument, as this sample was exposed to the vacuum of the electron microscope for a much longer time than the other samples.

Most of the total aerosol particles have a geometric diameter below 500 nm (Fig. 5). The mineral groups of aluminosilicates, Fe aluminosilicates, and other aluminosilicates are somewhat larger than the rest of the particle groups. The size distribution ($dNdlogD_p$ vs. particle diameter) is shown in the electronic Supplement (Fig. S3).

3.2 Ice particle residuals

The following particle groups were observed in the IR samples (Fig. 6): minerals (silica, aluminosilicates, Fe aluminosilicates, other aluminosilicates, Ca sulfates, and Ca-rich particles), sea-salt-containing particles (aged and mixed salt), C-rich particles, Pb-rich particles, metal/metal oxide, and other particles. In addition, four groups of sampling artefacts were found: pure salt, alumina, and Ni-rich and Cu-rich particles. The sampling artefacts are regarded as contamination (see Sect. 2.6.) and are thus not included in the figures. Composition including contamination particles is given in the electronic Supplement (Fig. S5).

Mineral particles are of highest relative abundance (between 60 % and 90 % by number) in all samples (Fig. 6), and mainly consist of silica, aluminosilicates, and other aluminosilicates, as well as smaller fractions of Fe aluminosilicates, Ca sulfates, and Ca-rich particles. A small percentage (≤ 7 % by number) of Pb-rich particles – PbCl or particles containing heterogeneous Pb inclusions – are found in eight of the samples. Sea-salt-containing particles are present in all samples in variable amounts of up to 12 %. The C-rich particles observed in the IR fraction can be excluded from soot because they do not show the typical morphology of chain-like or more compacted agglomerates of primary particles (see Fig. S1). Instead, these particles are most probably organic particles. The group of metal/metal oxide particles includes Fe oxides/hydroxides, Ti oxides, and steel particles (Fe, Cr, Mn alloys).

Most IRs have an equivalent projected area diameter below 500 nm (Fig. 7). The groups of Fe aluminosilicates and other aluminosilicates are somewhat larger and show a higher variation than the rest of the particle groups. The size distribution ($dNdlogD_p$ vs. particle diameter) is shown in the electronic Supplement in Fig. S4.

3.3 IR vs. total aerosol

For six sample pairs (simultaneous sampling of total aerosol and IR) the enrichment or depletion of the particle groups compared to aluminosilicates is shown in Fig. 8 as the odds ratio. Complex secondary particles and soot are always strongly depleted in the IR fraction, as not a single particle of both groups was observed as IR. An upper limit for the depletion relative to aluminosilicates can be obtained by setting the number of particles in the IR fraction for both groups equal to 1 (the detection limit). With this assumption it can be seen that soot is depleted in the IR fraction relative to aluminosilicates by at least a factor of 700 and secondary aerosol particles by a factor of at least 4200. Both particle groups are also depleted in the IR fraction relative to total aerosol. C-rich particles are less enriched in the IR fraction than aluminosilicates by a factor of approximately 20.

Pb-rich particles and other aluminosilicates are enriched (relative to aluminosilicates) within the IR fraction. However,

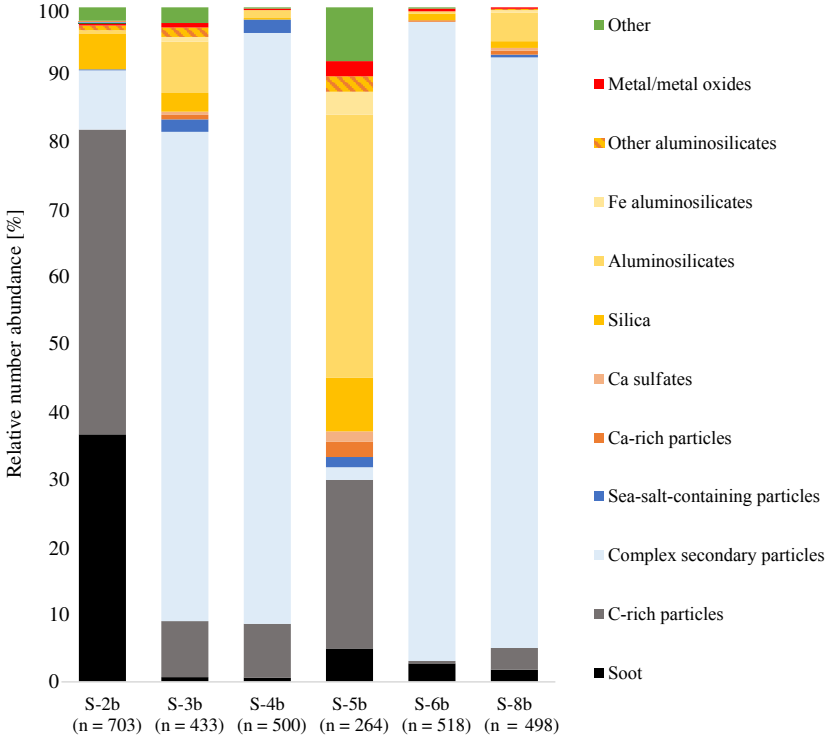

Figure 4. Relative number abundance of the different particle groups within total aerosol samples. Sample S-2b shows a combustion event with air mass history from the Po Valley, and sample S-5b is influenced by an analytical artefact from particle loss of volatile particles.

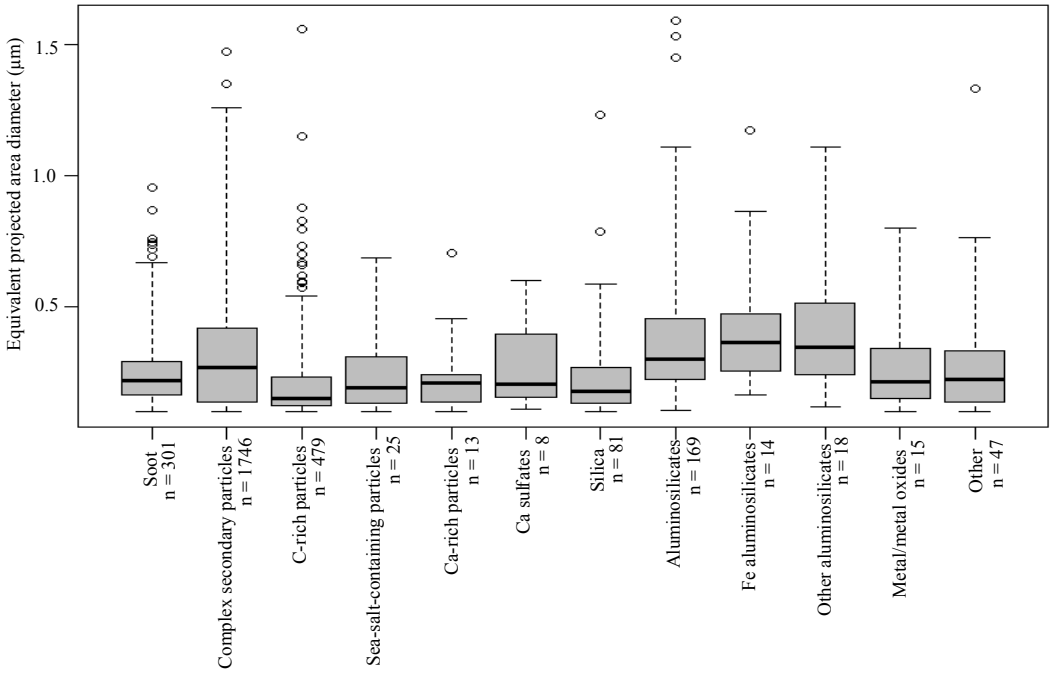

Figure 5. Size of total aerosol particles.

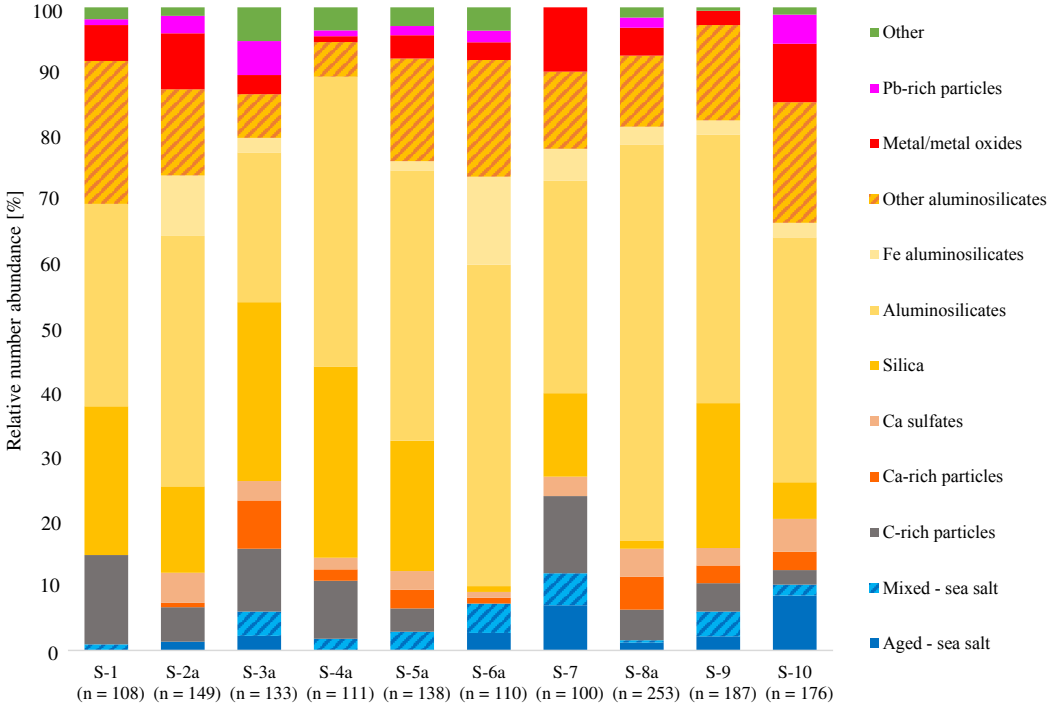

Figure 6. Relative number abundance of the different particle groups of IR sampled in mixed-phase clouds at site temperatures between −10 and −18 °C. Sampling artefacts (pure salt, alumina, and Ni-rich and Cu-rich particles) are not shown.

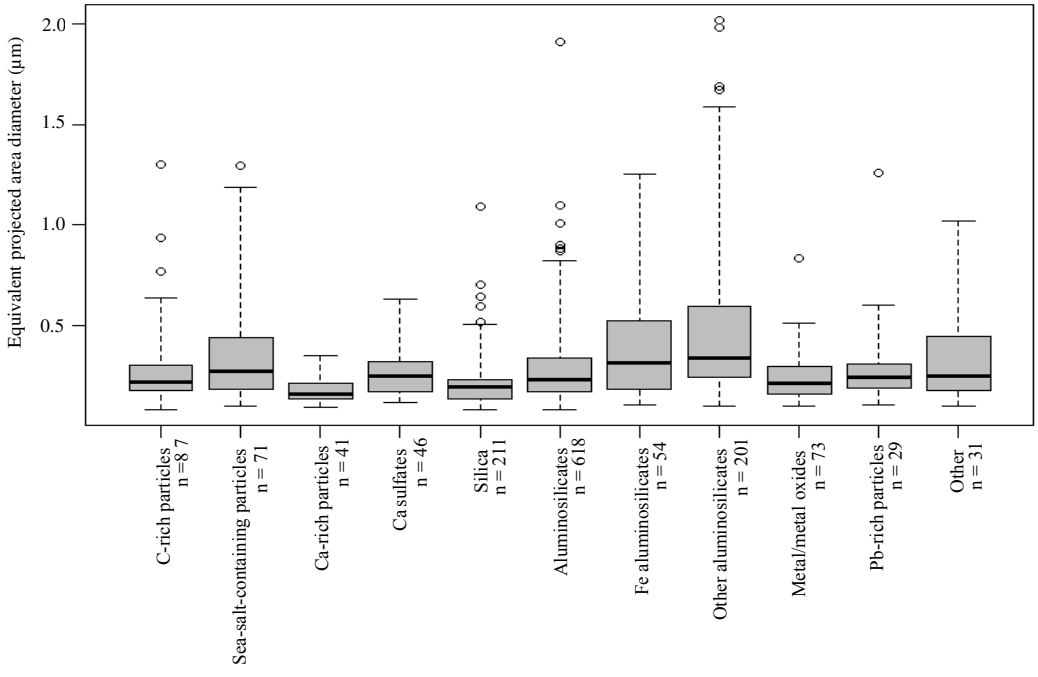

Figure 7. Size of IRs. Three outliers of other aluminosilicates are shown (2.7, 2.9, and 3.4 µm).

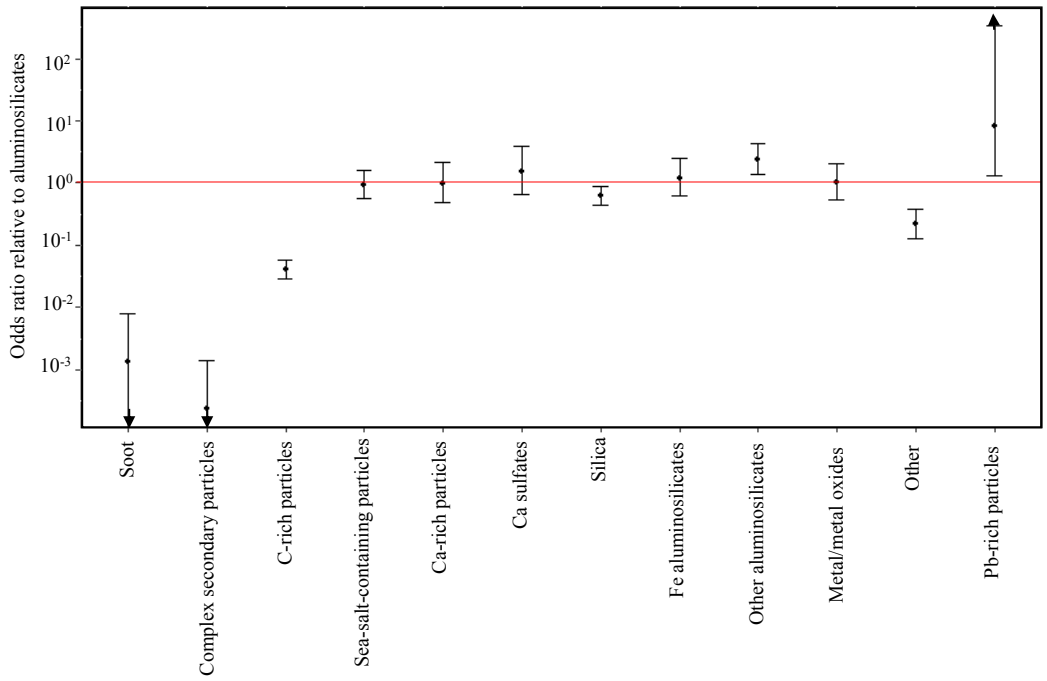

Figure 8. Enrichment or depletion of the different particle groups within the IR fraction expressed as the odds ratio (see text for details). The 95 % confidence interval (CI) of the odds ratio is shown as error bars. For soot and complex secondary particles the lower limit of the CI, and for Pb-rich particles the upper limit of the CI, cannot be defined precisely due to counting statistics. Thus they are marked by arrows.

the enrichment factor has large uncertainties due to counting statistics. The remaining particle groups are, within counting error, enriched similarly in the IR fraction to aluminosilicates (for this latter group the odd ratio is 1 per definition).

4 Discussion

The major finding of our paper is that sea-salt-containing particles, Ca-rich particles, Ca sulfates, silica, Fe aluminosilicates, and metal/metal oxides are ice active similar to aluminosilicates at Jungfraujoch in warm mixed-phase clouds (−10 to −18 °C). Other aluminosilicates and the Pb-rich particles seem to be even more ice active as aluminosilicates. In contrast, soot and complex secondary particles are strongly depleted (compared to aluminosilicates and absolutely compared to total aerosol) in the ice residuals. C-rich particles are less enriched than aluminosilicates by a factor of approximately 20. Thus, it is concluded that their ice nucleation ability under these conditions is significantly lower. The ice nucleation activities of the different particle groups are discussed in Sect. 4.2.

4.1 Composition of total aerosol

Four of the six total aerosol samples are dominated by complex secondary particles (Fig. 4), which seems to be typical for Jungfraujoch (Cozic et al., 2008b; Fröhlich et al., 2015). Two samples (S-2b and S-5b) have a different composition (Fig. 4). The first sample (S-2b) shows a higher carbonaceous fraction, and the second sample (S-5b) a higher fraction of mineral particles and C-rich particles. The high soot and C-rich particle abundance of the first sample may be explained by footprint plots showing that the air mass had a longer surface residence time over the Po Valley (Italy), which is an urban/industrial area with abundant sources of carbonaceous particles. The potential artefact in the second sample does not influence the enrichment factor for all other particle groups. The odds ratio of complex secondary particles shown in Fig. 8 will merely be somewhat lower. Our general conclusion that complex secondary particles are inefficient ice nuclei under the investigated conditions is not changed.

Most particles of the total aerosol have sizes below approximately 1 µm, which is in good agreement with Herrmann et al. (2015).

Overall, our total aerosol samples consist of complex secondary particles (60 % by number) and C-rich particles (16 %), soot (10 %), and mineral particles (14 %). This composition is similar to previous findings at Jungfraujoch during winter. According to Cozic et al. (2008b) the total aerosol is dominated by organic matter and secondary aerosol (87 % by mass), with smaller contributions of black carbon (4 %) and a non-determined mass (reported as "assumed to be composed of insoluble compounds such as silicate from mineral dust") fraction (9 %). It was also shown by Kamphus et al. (2010)

that the main components of the ambient aerosol at Jungfraujoch in winter (2007) are sulfate and organics, and only a small fraction (between 1 % and 17 %) is classified as mineral particles.

With respect to ice nucleation, mineral dust particles are of the most importance (see Sect. 4.2.). Aluminosilicates are the most abundant group of mineral particles in the total aerosol with almost twice the amount of silica. This fits well to the distribution of different minerals in soils presented by Hoose et al. (2008) in which kaolinite and illite show a higher abundance than calcite and quartz in the clay fraction worldwide. Other aluminosilicates and Ca-rich particles are present in four of the six samples at a low number concentration (1–2 %). Ca-containing particles at Jungfraujoch were also found by Cozic et al. (2008b), albeit mainly in the coarse mode.

The footprint plots (Fig. 3) were quite similar with high particle residence time over the North Atlantic Ocean. None of the samples are taken during mineral dust events, which normally occur in spring at Jungfraujoch (Coen et al., 2007). One total aerosol sample with a higher fraction of carbonaceous particles had a higher surface residence time over the Po Valley than the rest.

4.2 Ice nucleation activity of different particle groups

IRs mainly consist of mineral particles (Fig. 6). The classes of Fe aluminosilicates, Ca sulfates, Ca-rich particles, silica, sea-salt-containing particles, and metal/metal oxides are enriched similar to aluminosilicates (odds ratio ~ 1). Other aluminosilicates are more enriched than aluminosilicates by a factor of ~ 2. The mineral particles' abundance between 60 % and 85 % in the IR fraction is in good agreement with previous findings for mixed-phase clouds at Jungfraujoch (Kamphus et al., 2010; Ebert et al., 2011; Worringen et al., 2015). Mineral particles are also reported as ice active in cirrus clouds (DeMott et al., 2003; Cziczo and Froyd, 2014). Studies of IRs in cirrus clouds are mentioned sometimes in the discussion to show which kinds of IRs are found in the environment, independent on the cloud regime. It has to be emphasized here that this is not meant as a direct comparison as the temperature and freezing regimes are quite different; note that deposition nucleation dominates in cirrus clouds (Cziczo et al., 2013).

The size of IRs varies between the detection limit (100 nm) and 3.4 µm (Fig. 7). The size distribution is comparable to previous findings by Worringen et al. (2015) showing a maximum around 300 nm. We did not find a relationship between the size of the particles and the enrichment factor (odds ratio), presumably because the particle size did not differ much.

The sampling temperature at the site varied between -10 and -18 °C (Fig. 2). Temperature was measured at the station and can differ from the onset ice nucleation temperature of the particles depending on where in the mixed-phase cloud nucleation occurred. None of the particle group abundances in the IR fraction showed a systematic temperature dependence. However, based on the limited number of samples and the relatively small temperature range, no definite conclusion regarding the temperature dependence can be drawn.

The importance of a given particle group for ice nucleation in the atmosphere depends on the ice nucleation ability and the abundance of this group in the total aerosol. Both parameters will be discussed in the following. Complex secondary aerosol particles and soot were not found in the IR fraction, in contrast to previous work at Jungfraujoch (Cozic et al., 2008a; Ebert et al., 2011; Worringen et al., 2015; Schmidt et al., 2017), even though these groups dominate the total aerosol fraction. Thus, their ice-nucleating ability under the conditions of our campaign can be assumed to be very low. One explanation for this difference might be the higher site temperatures during our campaign. In the present study, complex secondary particles are defined by the presence of an S peak in the X-ray spectrum and/or the instability under electron bombardment. It must be emphasized here that this particle group most likely also consists of a substantial fraction of organics and nitrates (Vester et al., 2007), see Table 1.

C-rich particles were observed in the total aerosol and the IR fraction but are less ice active than aluminosilicates (odds ratio ~ 0.04). C-rich particles are reported in previous studies of mixed-phase clouds at Jungfraujoch (Mertes et al., 2007; Cozic et al., 2008; Kamphus et al., 2010; Ebert et al., 2011; Worringen et al., 2015; Schmidt et al., 2017). Our results are also in agreement with findings of many cirrus cloud field studies (see recent review by Knopf et al., 2018, and references therein), which show that organic aerosol is found in the IR fraction but is depleted relative to total aerosol.

Aluminosilicates are enriched in all samples and have the highest relative number abundance in the IR fraction. Aluminosilicates are also found to be efficient ice nuclei in other field experiments (Cziczo et al., 2013; Worringen et al., 2015; Iwata and Matsuki, 2018). Among aluminosilicates, kaolinite is reported as efficient ice nucleus in laboratory studies (Zimmermann et al., 2007; Murray et al., 2011; Wex et al., 2014; Freedman, 2015). As aluminosilicates often have a high abundance in the total aerosol and in the IR samples, they are the most important particle group for ice nucleation. Therefore the enrichment or depletion of the particle groups was normalized to this group.

Silica is the second most abundant mineral particle group in the IR samples and the only mineral group which seems to have a somewhat lower ice activity than aluminosilicates (upper limit of 95 % confidence interval of the odds ratio <1). However, keeping in mind the counting error for aluminosilicates, silica is statistically similarly enriched. This observation is in agreement with Atkinson et al. (2013) but in contradiction to Eastwood et al. (2008), who concluded that quartz is less ice active than kaolinite and montmorillonite. The silica fraction in the IR samples varies between 1 % and 30 %. Boose et al. (2016) point out that quartz is always present in atmospheric dust in all size ranges, even in

the smallest size fraction, which is dominated by clay minerals. They conclude that quartz is an important atmospheric INP component because it is present in the size fraction with the longest atmospheric residence time. Despite the fact that the enrichment of silica is somewhat lower than aluminosilicate, the relative high abundance in the IR fraction in our samples confirms this conclusion.

Fe aluminosilicates are similarly enriched in the IR fraction as aluminosilicates. Fe aluminosilicates were reported as cloud residual by Matsuki et al. (2010). As these authors did not differentiate between droplet and ice crystals, nothing can be said about the ice nucleation ability of Fe aluminosilicates. This mineral group is not present at high relative abundance at Jungfraujoch; thus, it will not contribute much to ice nucleation at this location.

The group of other aluminosilicates most likely consists of different minerals like feldspars, illite, and smectite. Laboratory studies (Atkinson et al., 2013; Iwata and Matsuki, 2018) showed that K feldspar and clay minerals (Zimmermann et al., 2008; Hiranuma et al., 2015; Boose et al., 2016) have a high ice nucleation ability compared to other minerals. A high ice nucleation ability of clay minerals is also reported from field experiments (Targino et al., 2006; Worringen et al., 2015). Also, our field study shows an enrichment of other aluminosilicates in the IR fraction, indicating a high ice nucleation ability. However, as feldspar is less common in the smallest dust fraction, it was concluded by Boose et al. (2016) that at least the feldspar group is generally of minor importance.

Ca-rich and Ca-sulfate particles are relatively low in number concentration, both in total aerosol and IR samples. Similar to quartz, calcium-containing particles showed different ice nucleation ability in previous laboratory studies (Zimmermann et al., 2008; Atkinson et al., 2013). In field experiments, however, Ca-rich particles and Ca sulfates were observed in the IR fraction (Ebert et al., 2011; Worringen et al., 2015; Iwata and Matsuki, 2018).

Based on chemistry, three subgroups of salt can be distinguished in the IR samples: pure salt, aged sea salt, and mixed sea salt. The pure salt is regarded as an artefact (see Sect. 2.6.1.) and thus excluded from the further analysis. Due to their low number abundance, the two other salt subgroups are combined into the sea-salt-containing particles group. Sea-salt-containing particles is enriched similar to aluminosilicates. The ice activity of salt and sea salt is still controversial due to discrepancies among different laboratory studies (Wise et al., 2012; Niehaus and Cantrell, 2015; Ladino et al., 2016). Kanji et al. (2017) assign these differences to the experimental set-up, i.e. different size, composition, and particle generation methods. In field experiments, however, salts are present in the IR fraction of both cirrus and mixed-phase clouds (Targino et al., 2006; Ebert et al., 2011; Cziczo et al., 2013; Worringen et al., 2015; Iwata and Matsuki, 2018). It is advocated by Iwata and Matsuki (2018) that pure NaCl is not ice active due to molar depression of the freezing point. Sea-salt-containing particles may act as an INP due to the presence of organics (Wilson et al., 2015; DeMott et al., 2016; Iwata and Matsuki, 2018). However, we cannot define where the ice nucleation occurs in a particle, i.e. pores or thin coating, with our measurement technique.

The enrichment of metal and metal oxides is similar to aluminosilicates. The ice activity of different metal and metal oxide particles varies with their chemical composition (Kanji et al., 2017). Our samples are dominated by FeCrMn (steel), Ti oxide, and Fe oxide. Literature regarding the metal/metal oxide group is ambiguous. Hematite was reported as ice active by Zimmermann et al. (2008). In contrast, hematite, magnetite, and rutile were found not to be very ice active in deposition mode by Yakobi-Hancock et al. (2013). Even so, metal and metal oxides are often found in IR samples from cirrus and mixed-phase clouds (Kamphus et al., 2010; DeMott et al., 2003; Ebert et al., 2011; Worringen et al., 2015; Schmidt et al., 2017).

Pb-containing particles are present in the IR fraction as already reported in previous work at Jungfraujoch (Cziczo et al., 2009; Kamphus et al., 2010; Ebert et al., 2011; Worringen et al., 2015; Schmidt et al., 2017). In the present study, Pb-rich particles are the most enriched particle group. A high enrichment of Pb-rich particles among IRs was also reported by Ebert et al. (2011). In addition, laboratory work showed that Pb can increase the ice activity of mineral particles considerably (Cziczo et al., 2009; Yakobi-Hancock et al., 2013). Helicopters and small aircrafts were discussed as local sources of Pb at Jungfraujoch by Kamphus et al. (2010) and Ebert et al. (2011). As the samples were collected during in-cloud conditions, we do not expect Pb-rich particles emitted freshly on-site from the mentioned sources. A time delay between emission and sampling results in relatively low concentrations of Pb in the ambient air in clouds at Jungfraujoch. However, Kamphus et al. (2010) and Schmidt et al. (2017) detected Pb-bearing particles with mass spectrometry in both ambient air and IRs. Keeping in mind the better counting statistics of mass spectrometry, it seems plausible that total aerosol contains a small amount of Pb-rich particles which were missed in our total samples.

To summarize, the two particle groups of complex secondary particles and soot are strongly depleted compared to aluminosilicates as well as absolutely depleted compared to the total aerosol. Despite an uncertainty due to potential misclassification, the C-rich group is less enriched compared to aluminosilicates. Other aluminosilicates and Pb-rich particles are enriched compared to aluminosilicates. A high enrichment of Pb-rich particles indicates that this group is more ice active than the rest of the groups present in the IR fraction. All other particle groups (silica, Fe aluminosilicates, Ca sulfates, Ca-rich particles, sea-salt-containing particles, and metal/metal oxides) are enriched similar to aluminosilicate. The relatively high abundance of artefacts was identified by comparing the IR and total aerosol fraction, showing how important parallel sampling is for identification of IRs. Tak-

ing into account the relative abundance of the particle groups in total aerosol and the ice nucleation ability, we conclude that silica, aluminosilicates, and other aluminosilicates were the most important ice-nucleating particles in mixed-phase clouds at site temperatures between −10 and −18 °C during the campaign at Jungfraujoch in winter 2017.

Data availability. The data set is available for the community and can be accessed by request to Stine Eriksen Hammer (sehammer@geo.tu-darmstadt.de) of the Technical University Darmstadt.

The Supplement related to this article is available online at https://doi.org/10.5194/acp-18-13987-2018-supplement.

Author contributions. SEH collected the samples, analysed the particles by electron microscopy, performed data analysis, and prepared the paper. ME contributed to electron microscopy and data analysis. KK designed the dilution unit and contributed to data analysis. SM designed, improved, and operated the Ice-CVI during the campaign. JS organized the field campaign at Jungfraujoch and contributed to data analysis. SW contributed to data analysis and paper preparation.

Competing interests. The authors declare that they have no conflict of interest.

Special issue statement. This article is part of the special issue "Results from the ice nucleation research unit (INUIT) (ACP/AMT inter-journal SI)". It is not associated with a conference.

Acknowledgements. Stine Eriksen Hammer would like to thank Annette Worringen and Nathalie Benker for discussion and support and Thomas Dirsch for building the dilution unit. We thank the whole INUIT-JFJ team for discussions and support. The authors thank MeteoSwiss for meteorological data and the International Foundation HFSJG, who made it possible to carry out the experiment at the high-altitude research station Jungfraujoch. The authors also gratefully acknowledge the German Research Foundation for financial support within the research group INUIT – INUIT (FOR 1525) and within grant KA 2280/2-1.

This project has received funding from the European Union's Horizon 2020 research and innovation programme under grant agreement no. 654109.

Edited by: Allan Bertram
Reviewed by: two anonymous referees

References

Aitchison, J.: A concise guide to compositional data analysis, Cairndow, UK, 2003.

Atkinson, J. D., Murray, B. J., Woodhouse, M. T., Whale, T. F., Baustian, K. J., Carslaw, K. S., Dobbie, S., O'Sullivan, D., and Malkin, T. L.: The importance of feldspar for ice nucleation by mineral dust in mixed-phase clouds, Nature, 498, 355–358, https://doi.org/10.1038/nature12278, 2013.

Boose, Y., Welti, A., Atkinson, J., Ramelli, F., Danielczok, A., Bingemer, H. G., Plötze, M., Sierau, B., Kanji, Z. A., and Lohmann, U.: Heterogeneous ice nucleation on dust particles sourced from nine deserts worldwide – Part 1: Immersion freezing, Atmos. Chem. Phys., 16, 15075–15095, https://doi.org/10.5194/acp-16-15075-2016, 2016.

Buseck, P. R., Adachi, K., Gelencsér, A., Tompa, É., and Pósfai, M.: Ns-Soot: A Material-Based Term for Strongly Light-Absorbing Carbonaceous Particles, Aerosol Sci. Tech., 48, 777–788, https://doi.org/10.1080/02786826.2014.919374, 2014.

Carlslaw, D. C. and Ropkins, K.: Openair – an R package for air quality data analysis, Environ. Modell. Softw., 27–28, 52–61, https://doi.org/10.1016/j.envsoft.2011.09.008, 2012.

Choël, M., Deboudt, K., Osán, J., Flament, P., and Van Grieken, R.: Quantitative Determination of Low-Z Elements in Single Atmospheric Particles on Boron Substrates by Automated Scanning Electron Microscopy-Energy-Dispersive X-ray Spectrometry, Anal. Chem., 77, 5686–5692, https://doi.org/10.1021/ac050739x, 2005.

Coen, M. C., Weingartner, E., Nyeki, S., Cozic, J., Henning, S., Verheggen, B., Gehrig, R., and Baltensperger, U.: Long-term trend analysis of aerosol variables at the high-alpine site Jungfraujoch, J. Geophys. Res.-Atmos., 112, D13213, https://doi.org/10.1029/2006JD007995, 2007.

Cozic, J., Mertes, S., Verheggen, B., Cziczo, D. J., Gallavardin, S. J., Walter, S., Baltensperger, U., and Weingartner, E.: Black carbon enrichment in atmospheric ice particle residuals observed in lower tropospheric mixed phase clouds, J. Geophys. Res.-Atmos., 113, D15209, https://doi.org/10.1029/2007JD009266, 2008a.

Cozic, J., Verheggen, B., Weingartner, E., Crosier, J., Bower, K. N., Flynn, M., Coe, H., Henning, S., Steinbacher, M., Henne, S., Collaud Coen, M., Petzold, A., and Baltensperger, U.: Chemical composition of free tropospheric aerosol for PM1 and coarse mode at the high alpine site Jungfraujoch, Atmos. Chem. Phys., 8, 407–423, https://doi.org/10.5194/acp-8-407-2008, 2008b.

Cziczo, D. J. and Froyd, K. D.: Sampling the composition of cirrus ice residuals, Atmos. Res., 142, 15–31, https://doi.org/10.1016/j.atmosres.2013.06.012, 2014.

Cziczo, D. J., DeMott, P. J., Brooks, S. D., Prenni, A. J., Thomson, D. S., Baumgardner, D., Wilson, J. C., Kreidenweis, S. M., and Murphy, D. M.: Observations of organic species and atmospheric ice formation, Geophys. Res. Lett., 31, L12116, https://doi.org/10.1029/2004GL019822, 2004.

Cziczo, D. J., Stetzer, O., Worringen, A., Ebert, M., Weinbruch, S., Kamphus, M., Gallavardin, S. J., Curtius, J., Borrmann, S., and Froyd, K. D.: Inadvertent climate modification due to anthropogenic lead, Nat. Geosci., 2, 333–336, https://doi.org/10.1038/ngeo499, 2009.

Cziczo, D. J., Froyd, K. D., Hoose, C., Jensen, E. J., Diao, M., Zondlo, M. A., Smith, J. B., Twohy, C. H., and Mur-

phy, D. M.: Clarifying the Dominant Sources and Mechanisms of Cirrus Cloud Formation, Science, 340, 1320–1324, https://doi.org/10.1126/science.1234145, 2013.

Cziczo, D. J., Ladino, L., Boose, Y., Kanji, Z. A., Kupiszewski, P., Lance, S., Mertes, S., and Wex, H.: Measurements of Ice Nucleating Particles and Ice Residuals, Meteor. Mon., 58, 8.1–8.13, https://doi.org/10.1175/amsmonographs-d-16-0008.1, 2017.

DeMott, P., Cziczo, D., Prenni, A., Murphy, D., Kreidenweis, S., Thomson, D., Borys, R., and Rogers, D.: Measurements of the concentration and composition of nuclei for cirrus formation, P. Natl. Acad. Sci. USA, 100, 14655–14660, https://doi.org/10.1073/pnas.2532677100, 2003.

DeMott, P. J., Hill, T. C. J., McCluskey, C. S., Prather, K. A., Collins, D. B., Sullivan, R. C., Ruppel, M. J., Mason, R. H., Irish, V. E., Lee, T., Hwang, C. Y., Rhee, T. S., Snider, J. R., McMeeking, G. R., Dhaniyala, S., Lewis, E. R., Wentzell, J. J. B., Abbatt, J., Lee, C., Sultana, C. M., Ault, A. P., Axson, J. L., Diaz Martinez, M., Venero, I., Santos-Figueroa, G., Stokes, M. D., Deane, G. B., Mayol-Bracero, O. L., Grassian, V. H., Bertram, T. H., Bertram, A. K., Moffett, B. F., and Franc, G. D.: Sea spray aerosol as a unique source of ice nucleating particles, P. Natl. Acad. Sci. USA, 113, 5797–5803, https://doi.org/10.1073/pnas.1514034112, 2016.

Eastwood, M. L., Cremel, S., Gehrke, C., Girard, E., and Bertram, A. K.: Ice nucleation on mineral dust particles: Onset conditions, nucleation rates and contact angles, J. Geophys. Res.-Atmos., 113, D22203, https://doi.org/10.1029/2008JD010639, 2008.

Ebert, M., Worringen, A., Benker, N., Mertes, S., Weingartner, E., and Weinbruch, S.: Chemical composition and mixing-state of ice residuals sampled within mixed phase clouds, Atmos. Chem. Phys., 11, 2805–2816, https://doi.org/10.5194/acp-11-2805-2011, 2011.

Ebert, M., Weigel, R., Kandler, K., Günther, G., Molleker, S., Grooß, J.-U., Vogel, B., Weinbruch, S., and Borrmann, S.: Chemical analysis of refractory stratospheric aerosol particles collected within the arctic vortex and inside polar stratospheric clouds, Atmos. Chem. Phys., 16, 8405–8421, https://doi.org/10.5194/acp-16-8405-2016, 2016.

Flato, G., Marotzke, J., Abiodun, B., Braconnot, P., Chou, S. C., Collins, W. J., Cox, P., Driouech, F., Emori, S., Eyring, V., Forest, C., Gleckler, P., Guilyardi, E., Jakob, C., Kattsov, V., Reason, C., and Rummukaines, M.: Evaluation of Climate Models, in: Climate Change 2013: The Physical Science Basis. Contribution of Working Group I to the Fifth Assessment Report of the Intergovernmental Panel on Climate Change, Assessment Reports of IPCC, edited by: Stocker, T. F., Qin, D., Plattner, G.-K., Tignor, M., Allen, S. K., Boschung, J., Nauels, A., Xia, Y., Bex, V., and Midgley, P. M., Cambridge University Press, Cambridge, UK and New York, NY, USA, 741–866, available at: https://www.ipcc.ch/pdf/assessment-report/ar5/wg1/WG1AR5_Chapter09_FINAL.pdf (last access: 13 March 2017), 2013.

Freedman, M. A.: Potential Sites for Ice Nucleation on Aluminosilicate Clay Minerals and Related Materials, J. Phys. Chem. Lett., 6, 3850–3858, https://doi.org/10.1021/acs.jpclett.5b01326, 2015.

Fröhlich, R., Cubison, M. J., Slowik, J. G., Bukowiecki, N., Canonaco, F., Croteau, P. L., Gysel, M., Henne, S., Herrmann, E., Jayne, J. T., Steinbacher, M., Worsnop, D. R., Baltensperger, U., and Prévôt, A. S. H.: Fourteen months of on-line measurements of the non-refractory submicron aerosol at the Jungfraujoch (3580 m a.s.l.) – chemical composition, origins and organic aerosol sources, Atmos. Chem. Phys., 15, 11373–11398, https://doi.org/10.5194/acp-15-11373-2015, 2015.

Froyd, K. D., Murphy, D. M., Lawson, P., Baumgardner, D., and Herman, R. L.: Aerosols that form subvisible cirrus at the tropical tropopause, Atmos. Chem. Phys., 10, 209–218, https://doi.org/10.5194/acp-10-209-2010, 2010.

Hallett, J. and Mossop, S. C.: Production of secondary ice particles during the riming process, Nature, 249, 26–28, https://doi.org/10.1038/249026a0, 1974.

Heintzenberg, J., Okada, K., and Ström, J.: On the composition of non-volatile material in upper tropospheric aerosols and cirrus crystals, Atmos. Res., 41, 81–88, https://doi.org/10.1016/0169-8095(95)00042-9, 1996.

Herrmann, E., Weingartner, E., Henne, S., Vuilleumier, L., Bukowiecki, N., Steinbacher, M., Conen, F., Collaud Coen, M., Hammer, E., and Jurányi, Z.: Analysis of long-term aerosol size distribution data from Jungfraujoch with emphasis on free tropospheric conditions, cloud influence, and air mass transport, J. Geophys. Res.-Atmos., 120, 9459–9480, https://doi.org/10.1002/2015JD023660, 2015.

Hiranuma, N., Augustin-Bauditz, S., Bingemer, H., Budke, C., Curtius, J., Danielczok, A., Diehl, K., Dreischmeier, K., Ebert, M., Frank, F., Hoffmann, N., Kandler, K., Kiselev, A., Koop, T., Leisner, T., Möhler, O., Nillius, B., Peckhaus, A., Rose, D., Weinbruch, S., Wex, H., Boose, Y., DeMott, P. J., Hader, J. D., Hill, T. C. J., Kanji, Z. A., Kulkarni, G., Levin, E. J. T., McCluskey, C. S., Murakami, M., Murray, B. J., Niedermeier, D., Petters, M. D., O'Sullivan, D., Saito, A., Schill, G. P., Tajiri, T., Tolbert, M. A., Welti, A., Whale, T. F., Wright, T. P., and Yamashita, K.: A comprehensive laboratory study on the immersion freezing behavior of illite NX particles: a comparison of 17 ice nucleation measurement techniques, Atmos. Chem. Phys., 15, 2489–2518, https://doi.org/10.5194/acp-15-2489-2015, 2015.

Hoose, C., Lohmann, U., Erdin, R., and Tegen, I.: The global influence of dust mineralogical composition on heterogeneous ice nucleation in mixed-phase clouds, Environ. Res. Lett., 3, 025003, https://doi.org/10.1088/1748-9326/3/2/025003, 2008.

Hoose, C., Kristjánsson, J. E., and Burrows, S. M.: How important is biological ice nucleation in clouds on a global scale?, Environ. Res. Lett., 5, 024009, https://doi.org/10.1088/1748-9326/5/2/024009, 2010.

Hoose, C. and Möhler, O.: Heterogeneous ice nucleation on atmospheric aerosols: a review of results from laboratory experiments, Atmos. Chem. Phys., 12, 9817–9854, https://doi.org/10.5194/acp-12-9817-2012, 2012.

Iwata, A. and Matsuki, A.: Characterization of individual ice residual particles by the single droplet freezing method: a case study in the Asian dust outflow region, Atmos. Chem. Phys., 18, 1785–1804, https://doi.org/10.5194/acp-18-1785-2018, 2018.

Kamphus, M., Ettner-Mahl, M., Klimach, T., Drewnick, F., Keller, L., Cziczo, D. J., Mertes, S., Borrmann, S., and Curtius, J.: Chemical composition of ambient aerosol, ice residues and cloud droplet residues in mixed-phase clouds: single particle analysis during the Cloud and Aerosol Characterization Experiment (CLACE 6), Atmos. Chem. Phys., 10, 8077–8095, https://doi.org/10.5194/acp-10-8077-2010, 2010.

Kanji, Z. A., Ladino, L. A., Wex, H., Boose, Y., Burkert-Kohn, M., Cziczo, D. J., and Krämer, M.: Overview of Ice Nucleating Particles, Meteor. Mon., 58, 1.1–1.33, https://doi.org/10.1175/AMSMONOGRAPHS-D-16-0006.1, 2017.

Knopf, D. A., Alpert, P. A., and Wang, B.: The Role of Organic Aerosol in Atmospheric Ice Nucleation: A Review, ACS Earth Space Chem., 2, 168–202, https://doi.org/10.1021/acsearthspacechem.7b00120, 2018.

Korolev, A., McFarquhar, G., Field, P. R., Franklin, C., Lawson, P., Wang, Z., Williams, E., Abel, S. J., Axisa, D., Borrmann, S., Crosier, J., Fugal, J., Krämer, M., Lohmann, U., Schlenczek, O., Schnaiter, M., and Wendisch, M.: Mixed-Phase Clouds: Progress and Challenges, Meteor. Mon., 58, 5.1–5.50, https://doi.org/10.1175/amsmonographs-d-17-0001.1, 2017.

Ladino, L. A., Yakobi-Hancock, J. D., Kilthau, W. P., Mason, R. H., Si, M., Li, J., Miller, L. A., Schiller, C. L., Huffman, J. A., Aller, J. Y., Knopf, D. A., Bertram, A. K., and Abbatt, J. P. D.: Addressing the ice nucleating abilities of marine aerosol: A combination of deposition mode laboratory and field measurements, Atmos. Environ., 132, 1–10, https://doi.org/10.1016/j.atmosenv.2016.02.028, 2016.

Lohmann, U. and Diehl, K.: Sensitivity Studies of the Importance of Dust Ice Nuclei for the Indirect Aerosol Effect on Stratiform Mixed-Phase Clouds, J. Atmos. Sci., 63, 968–982, https://doi.org/10.1175/jas3662.1, 2006.

Matsuki, A., Schwarzenboeck, A., Venzac, H., Laj, P., Crumeyrolle, S., and Gomes, L.: Cloud processing of mineral dust: direct comparison of cloud residual and clear sky particles during AMMA aircraft campaign in summer 2006, Atmos. Chem. Phys., 10, 1057–1069, https://doi.org/10.5194/acp-10-1057-2010, 2010.

Mertes, S., Verheggen, B., Walter, S., Connolly, P., Ebert, M., Schneider, J., Bower, K. N., Cozic, J., Weinbruch, S., Baltensperger, U., and Weingartner, E.: Counterflow Virtual Impactor Based Collection of Small Ice Particles in Mixed-Phase Clouds for the Physico-Chemical Characterization of Tropospheric Ice Nuclei: Sampler Description and First Case Study, Aerosol Sci. Tech., 41, 848–864, https://doi.org/10.1080/02786820701501881, 2007.

Murray, B. J., Broadley, S. L., Wilson, T. W., Atkinson, J. D., and Wills, R. H.: Heterogeneous freezing of water droplets containing kaolinite particles, Atmos. Chem. Phys., 11, 4191–4207, https://doi.org/10.5194/acp-11-4191-2011, 2011.

Myhre, G., Shindell, D., Bréon, F.-M., Collins, W., Fuglestvedt, J., Huang, J., Koch, D., Lamarque, J.-F., Lee, D., Mendoza, B., Nakajima, T., Robock, A., Stephens, G., Takemura, T., and Zhang, H.: Anthropogenic and Natural Radiative Forcing, in: Climate Change 2013: The Physical Science Basis, Contribution of Working Group I to the Fifth Assessment Report of the Intergovernmental Panel on Climate Change, edited by: Stocker, T. F., Qin, D., Plattner, G.-K., Tignor, M., Allen, S. K., Boschung, J., Nauels, A., Xia, Y., Bex, V., and Midgley, P. M., Cambridge University Press, Cambridge, UK and New York, NY, USA, 2013.

Niehaus, J. and Cantrell, W.: Contact Freezing of Water by Salts, J. Phys. Chem. Lett., 6, 3490–3495, https://doi.org/10.1021/acs.jpclett.5b01531, 2015.

Ogren, J. A., Heintzenberg, J., and Charlson, R. J.: In-situ sampling of clouds with a droplet to aerosol converter, Geophys. Res. Lett., 12, 121–124, https://doi.org/10.1029/GL012i003p00121, 1985.

Ogren, J. A., Heintzenberg, J., and Charlson, R. J.: In-Situ Sampling of Clouds with a Droplet to Aerosol Converter, Geophys. Res. Lett., 12, 121–124, https://doi.org/10.1029/GL012i003p00121, 1985.

RStudio Team: RStudio: Integrated Development for R, RStudio Inc., Boston, MA, available at: http://www.rstudio.com/ (last access: 9 March 2018), 2016.

Schmidt, S., Schneider, J., Klimach, T., Mertes, S., Schenk, L. P., Kupiszewski, P., Curtius, J., and Borrmann, S.: Online single particle analysis of ice particle residuals from mountain-top mixed-phase clouds using laboratory derived particle type assignment, Atmos. Chem. Phys., 17, 575–594, https://doi.org/10.5194/acp-17-575-2017, 2017.

Schütze, K., Wilson, J. C., Weinbruch, S., Benker, N., Ebert, M., Günther, G., Weigel, R., and Borrmann, S.: Sub-micrometer refractory carbonaceous particles in the polar stratosphere, Atmos. Chem. Phys., 17, 12475–12493, https://doi.org/10.5194/acp-17-12475-2017, 2017.

Seibert, P. and Frank, A.: Source-receptor matrix calculation with a Lagrangian particle dispersion model in backward mode, Atmos. Chem. Phys., 4, 51–63, https://doi.org/10.5194/acp-4-51-2004, 2004.

Stohl, A., Hittenberger, M., and Wotawa, G.: Validation of the lagrangian particle dispersion model FLEXPART against large-scale tracer experiment data, Atmos. Environ., 32, 4245–4264, https://doi.org/10.1016/S1352-2310(98)00184-8, 1998.

Stohl, A. and Thomson, D. J.: A Density Correction for Lagrangian Particle Dispersion Models, Bound.-Lay. Meteorol., 90, 155–167, https://doi.org/10.1023/a:1001741110696, 1999.

Stohl, A., Forster, C., Frank, A., Seibert, P., and Wotawa, G.: Technical note: The Lagrangian particle dispersion model FLEXPART version 6.2, Atmos. Chem. Phys., 5, 2461–2474, https://doi.org/10.5194/acp-5-2461-2005, 2005.

Storelvmo, T.: Aerosol Effects on Climate via Mixed-Phase and Ice Clouds, Annu. Rev. Earth Planet. Sci., 45, 199–222, https://doi.org/10.1146/annurev-earth-060115-012240, 2017.

Ström, J. and Ohlsson, S.: Real-time measurement of absorbing material in contrail ice using a counterflow virtual impactor, J. Geophys. Res.-Atmos., 103, 8737–8741, https://doi.org/10.1029/98JD00425, 1998.

Targino, A. C., Krejci, R., Noone, K. J., and Glantz, P.: Single particle analysis of ice crystal residuals observed in orographic wave clouds over Scandinavia during INTACC experiment, Atmos. Chem. Phys., 6, 1977–1990, https://doi.org/10.5194/acp-6-1977-2006, 2006.

Twohy, C. H., Strapp, J. W., and Wendisch, M.: Performance of a Counterflow Virtual Impactor in the NASA Icing Research Tunnel, J. Atmos. Ocean. Tech., 20, 781–790, https://doi.org/10.1175/1520-0426(2003)020<0781:poacvi>2.0.co;2, 2003.

Twohy, C. H. and Poellot, M. R.: Chemical characteristics of ice residual nuclei in anvil cirrus clouds: evidence for homogeneous and heterogeneous ice formation, Atmos. Chem. Phys., 5, 2289–2297, https://doi.org/10.5194/acp-5-2289-2005, 2005.

Vali, G., DeMott, P. J., Möhler, O., and Whale, T. F.: Technical Note: A proposal for ice nucleation terminology, Atmos. Chem. Phys., 15, 10263–10270, https://doi.org/10.5194/acp-15-10263-2015, 2015.

Van den Boogaart, K. G. and Tolosana-Delgado, R.: Analyzing compositional data with R, Springer, Berlin, 2013.

Vester, B. P., Ebert, M., Barnert, E. B., Schneider, J., Kandler, K., Schütz, L., and Weinbruch, S.: Composition and mixing state of the urban background aerosol in the Rhein-Main area (Germany), Atmos. Environ., 41, 6102–6115, https://doi.org/10.1016/j.atmosenv.2007.04.021, 2007.

Weinbruch, S., Benker, N., Kandler, K., Schütze, K., Kling, K., Berlinger, B., Thomassen, Y., Drotikova, T., and Kallenborn, R.: Source identification of individual soot agglomerates in Arctic air by transmission electron microscopy, Atmos. Environ., 172, 47–54, https://doi.org/10.1016/j.atmosenv.2017.10.033, 2018.

Weingartner, E., Nyeki, S., and Baltensperger, U.: Seasonal and diurnal variation of aerosol size distributions ($10<D<750$ nm) at a high-alpine site (Jungfraujoch 3580 m a.s.l.), J. Geophys. Res.-Atmos., 104, 26809–26820, https://doi.org/10.1029/1999JD900170, 1999.

Wentzel, M., Gorzawski, H., Naumann, K. H., Saathoff, H., and Weinbruch, S.: Transmission electron microscopical and aerosol dynamical characterization of soot aerosols, J. Atmos. Sci., 34, 1347–1370, https://doi.org/10.1016/S0021-8502(03)00360-4, 2003.

Wex, H., DeMott, P. J., Tobo, Y., Hartmann, S., Rösch, M., Clauss, T., Tomsche, L., Niedermeier, D., and Stratmann, F.: Kaolinite particles as ice nuclei: learning from the use of different kaolinite samples and different coatings, Atmos. Chem. Phys., 14, 5529–5546, https://doi.org/10.5194/acp-14-5529-2014, 2014.

Wickham, H.: ggplot2: Elegant Graphics for Data Analysis, Springer-Verlag New York, New York, 2009.

Wilson, T. W., Ladino, L. A., Alpert, P. A., Breckels, M. N., Brooks, I. M., Burrows, S. M., Carslaw, K. S., Huffman, J. A., Judd, C., and Kilthau, W. P.: A marine biogenic source of atmospheric ice-nucleating particles, Nature, 525, 234–238, https://doi.org/10.1038/nature14986, 2015.

Wise, M. E., Baustian, K. J., Koop, T., Freedman, M. A., Jensen, E. J., and Tolbert, M. A.: Depositional ice nucleation onto crystalline hydrated NaCl particles: a new mechanism for ice formation in the troposphere, Atmos. Chem. Phys., 12, 1121–1134, https://doi.org/10.5194/acp-12-1121-2012, 2012.

Worringen, A., Kandler, K., Benker, N., Dirsch, T., Mertes, S., Schenk, L., Kästner, U., Frank, F., Nillius, B., Bundke, U., Rose, D., Curtius, J., Kupiszewski, P., Weingartner, E., Vochezer, P., Schneider, J., Schmidt, S., Weinbruch, S., and Ebert, M.: Single-particle characterization of ice-nucleating particles and ice particle residuals sampled by three different techniques, Atmos. Chem. Phys., 15, 4161–4178, https://doi.org/10.5194/acp-15-4161-2015, 2015.

Yakobi-Hancock, J. D., Ladino, L. A., and Abbatt, J. P. D.: Feldspar minerals as efficient deposition ice nuclei, Atmos. Chem. Phys., 13, 11175–11185, https://doi.org/10.5194/acp-13-11175-2013, 2013.

Zimmermann, F., Ebert, M., Worringen, A., Schütz, L., and Weinbruch, S.: Environmental scanning electron microscopy (ESEM) as a new technique to determine the ice nucleation capability of individual atmospheric aerosol particles, Atmos. Environ., 41, 8219–8227, https://doi.org/10.1016/j.atmosenv.2007.06.023, 2007.

Zimmermann, F., Weinbruch, S., Schütz, L., Hofmann, H., Ebert, M., Kandler, K., and Worringen, A.: Ice nucleation properties of the most abundant mineral dust phases, J. Geophys. Res.-Atmos., 113, D23204, https://doi.org/10.1029/2008JD010655, 2008.

Analytical and Bioanalytical Chemistry
https://doi.org/10.1007/s00216-019-01614-7

RESEARCH PAPER

Comparison of operator- and computer-controlled scanning electron microscopy of particles from different atmospheric aerosol types

Stine Eriksen Hammer[1] · Martin Ebert[1] · Stephan Weinbruch[1]

Received: 27 October 2018 / Revised: 10 January 2019 / Accepted: 15 January 2019

Abstract

Individual aerosol particles from an urban background site in Mainz (Germany), a traffic hotspot site in Essen (Germany), the free troposphere in the Swiss Alps (high altitude research station Jungfraujoch), a rural background/marine site on Cyprus (Cyprus Atmospheric Observatory) and a rural background site in the forested area of Odenwald (Germany) were characterised with two different scanning electron microscopy techniques, operator controlled (opSEM) and computer controlled (ccSEM). For all samples, about 500 particles were investigated by opSEM, and between 1103 and 6940 particles by ccSEM. Large systematic differences (in some cases a factor up to ~ 20) in the abundance of the various particle groups are observed in the results of the two techniques. These differences are dependent on particle type and size. With ccSEM, information on the mixing state of particles (e.g., presence of heterogeneous inclusions, surface coatings or gradients in chemical composition) cannot be obtained, and particle groups which are recognised by their complex morphology (e.g., soot and fly ash particles) are classified into other particle groups. In addition, highly volatile particles (i.e., particles which evaporate under electron bombardment within seconds) will be overlooked by ccSEM. If these limitations of ccSEM are not considered, normalising the particle group abundances to 100% (a popular practise in many publications) may lead to drastic misinterpretation of the real aerosol composition. OpSEM is indispensable when detailed information of particle composition is required, although it suffers from a much higher expenditure of time. In conclusion, both techniques might be used for single particle characterisation as long as drawbacks of each are considered.

Keywords Scanning electron microscopy · Atmospheric aerosol particles · Operator-controlled SEM · Computer-controlled SEM · Particle characterisation

Introduction

Characterisation of atmospheric particles is an important analytical task in many scientific fields including climate research, atmospheric chemistry, environmental health, and environmental engineering [1]. The chemical and phase composition of particles may be used for source apportionment or for deduction of physical properties (e.g., scattering and absorption of light, ice nucleation, solubility). The chemical composition of aerosol particles is often determined by bulk techniques using amongst others inductively coupled plasma mass spectrometry (ICP-MS), X-ray fluorescence analysis (XRF), aerosol mass spectrometry (AMS) and ion chromatography (IC) [2, 3].

Beside bulk techniques, characterisation of individual particles has also found wide attention [4] as a variety of parameters (e.g., chemistry, size, morphology and mixing state) can be determined. Single particle mass spectrometry (SP-MS) and scanning electron microscopy (SEM) are the most often used techniques for characterisation of individual aerosol particles [3, 5–11]. Other single particle techniques applied to atmospheric aerosol particles include micro-Raman spectroscopy (mRS; e.g. [12]), Fourier-transform infrared spectroscopy (FT-IR; e.g. [13]), X-ray photo electron spectroscopy (XPS; [14, 15]) and transmission electron microscopy (TEM; [16, 17]).

Electronic supplementary material The online version of this article (https://doi.org/10.1007/s00216-019-01614-7) contains supplementary material, which is available to authorized users.

✉ Stine Eriksen Hammer
sehammer@geo.tu-darmstadt.de

[1] Institute for Applied Geosciences, Technical University Darmstadt, Schnittspahnstraße 9, 64287 Darmstadt, Germany

Published online: 06 February 2019

In most cases, SEM is combined with energy-dispersive X-ray microanalysis (EDX) in order to determine the chemical composition of particles [18]; in some cases, SEM is combined with wavelength-dispersive X-ray microanalysis [19, 20]. Readers not familiar with SEM are referred to Goldstein [18] and Exner, Weinbruch [21]. SEM-EDX may be performed operator controlled (opSEM) or computer controlled (ccSEM). ccSEM overcomes the limitations caused by the relatively time-consuming manual procedures of opSEM, thus enabling analysis of a much larger number of particles and respectively higher number of samples. With modern drift chamber detectors, ccSEM is even suited for monitoring applications [22]. In return, details of the particle morphology and mixing state may be lost in the ccSEM procedure. In addition, ccSEM may suffer from experimental artefacts (e.g. overlapping particles, contrast artefacts, surface imperfections confused with particles) which are usually recognised by experienced operators. Despite a large number of publications using ccSEM for characterisation of atmospheric particles, to our knowledge, the differences between the two analytical approaches was only studied in one report [23] and one publication [24] to date. Willis et al. [23] summarised different applications of op- and ccSEM and discuss different topics like details of SEM-EDX, analysis procedure and classification. Our contribution additionally contains a direct comparison for atmospheric samples emphasising differences arising when various aerosol types are investigated. Mamane et al. [24] focusses on an urban aerosol sample for particles in the $PM_{10–2.5}$ fraction [24]. In their study, they found two main errors associated with ccSEM, respectively, those resulting from the use of an automated threshold and those associated with excessive particle loading on the substrate. We will here focus on smaller particles (down to 100 nm compared to 1.5 μm) and we use a substrate with a lower average atomic number (boron compared to a polycarbonate filter) which will result in a better contrast to the background ratio for light elements.

In the present paper, advantages and disadvantages of opSEM and ccSEM are investigated in more detail. First, as different atmospheric aerosol types consist of particles with highly different properties (e.g., size distribution, volatility, mixing state), it can be expected that the advantages and disadvantages of both analytical approaches strongly depend on the sampling location. Therefore, samples of different aerosol types (urban, marine, rural, mineral dust, traffic and free troposphere) were collected in order to obtain more general results. Second, a larger number of experimental artefacts that may lead to systematic differences between opSEM and ccSEM are studied. Our contribution further elucidates the systematic differences between the two SEM techniques, and it is expected to guide future work in deciding which technique to use.

Materials and methods

Sampling locations

Ambient aerosol particles were collected in different environments: an urban background in Mainz (Germany), a traffic hotspot in Gladbecker Straße, Essen (Germany), the free troposphere in the Swiss Alps, a rural background/ marine on Cyprus and a rural background in Germany. Sampling date, time, temperature, pressure and inlet specifics are found in the Electronic Supplementary Material (ESM) Table S1.

The urban background sample was taken from an inlet ~ 1 m above the ground going directly into the laboratory of the Max-Plank Institute of Chemistry in the suburbia of Mainz, Germany (49.99 N; 8.23 E; 131 m asl). The inlet is located on the opposite side of the building from the road, thus, shielding from direct traffic emissions. The sample was collected after rush hour to avoid a dominant contribution of local traffic. Single particle analysis by SEM was previously performed at this location by Vester et al. [25].

The traffic hotspot sample was collected at a kerbside station in Gladbecker Straße, Essen, Germany (51.48 N; 7.0 E; 55 m asl), located at a major four-lane street in an urban street canyon. The daily traffic volume at the kerbside station was ~ 40,000 vehicles with ~ 5.2% heavy-duty vehicles. SEM investigations of particles from this location were reported by Weinbruch et al. [26].

The free troposphere sample was collected in February at the high altitude research station Jungfraujoch (Switzerland; 46.55 N; 7.98E; 3580 m asl). During winter, this site represents the lower free troposphere above a continental area [27–29]. Ambient total aerosol particles at Jungfraujoch were thoroughly investigated earlier [10, 29–32].

On Cyprus, particle sampling took place at the Cyprus Atmospheric Observatory (CAO; 35.04 N; 33.06 E; 535 m asl) located in the middle of the Island in the foothills of the Troodos mountains. This station is influenced by mineral dust from the Sahara and the Arabian Peninsula and pollution from the Middle East, Western/Eastern Europe and Turkey as well as sea salt from the surrounding sea [33, 34].

The rural background sample from Germany was taken in the small village of Schannenbach (~ 150 inhabitants) in the forested area of Odenwald (49.86 N; 8.72 E; 490 m asl) during spring.

Sampling

The urban background, free troposphere, and rural background/ marine samples were collected with a multi Micro Inertial Impactor (MINI) using one stage with a 50% lower cut-off diameter of 0.1 μm. The multi MINI is equipped with a purge flow, and 5 min flushing was consistently performed before each new sample to avoid carryover of

particles. Further information on the multi MINI is found in Ebert et al. [35]. For the collection of the free troposphere and rural background/marine samples, a dilution unit was applied to be able to sample for a longer time period [10]. At the traffic hotspot and rural background location in Germany, particles were collected with a single-stage MINI with a 50% lower cut-off diameter of 1 μm (for details see Kandler et al. [36]). The MINI has a volume flow of ~ 0.5 l/min (8 cm^3/s), the orifice used was 0.69 mm for a 1-μm cut-off and 0.25 mm for a 0.1-μm cut-off. Pressure and temperature during sampling are provided in Table S1 (see ESM). The upper cut-off is mostly dependent on the concentration of large atmospheric particles rather than the orifice size. For all samples, particles between approximately 0.1–10 equivalent aerodynamic diameter (micrometers) were analysed. Boron substrates (polished elemental boron embedded in copper as a conductive material) were used for all samples to enable detection of carbon [35, 37].

Scanning electron microscopy

Size, morphology, chemical composition and mixing state of the particles were investigated by scanning electron microscopy using an FEI Quanta 400 FEG instrument (FEI, Eindhoven, The Netherlands) equipped with an X-Max150 energy-dispersive silicon drift X-ray detector (Oxford, Oxfordshire, UK). The X-ray detector allows analysis of all elements with $Z > 3$ (Li). All samples were analysed under high-vacuum conditions (10^{-5} mbar sample chamber pressure), at a working distance of 10 mm with an accelerating voltage of 15 kV, spot size 4 and ~ 2–10-nA beam current. This accelerating voltage was applied to be able to detect elements of higher atomic number and is a compromise between detecting heavier elements and overlooking lighter elements. With the used instrumental parameters, we were able to detect carbonaceous particles down to ~ 100-nm geometric diameter. The Oxford software Aztec (version 3.3. SP1) was used for both ccSEM and opSEM.

Operator-controlled analysis

Both, secondary electrons (SE) and backscatter electrons (BSE) were used to image ~ 500 particles per sample manually. A magnification between ~ × 6000 and ~ × 27,000 was set depending on the particle load, with the average load of ~ 20 particles per image frame. The analysis is always performed as a circular sector of the impaction spot. First, all particles with an equivalent projected area diameter > 0.1 μm within an image frame were selected by the operator for chemical characterisation by EDX. Second, these particles were measured with 5-s live time. The particles where then classified based on chemical composition, mixing state, morphology and stability under the electron beam. Classification criteria are given in the ESM Table S2. Particles without any chemical information and without characteristic morphology are grouped in the "undefined" class. Particles that could not be assigned to any of the defined classes were grouped as "other".

Computer-controlled analysis

Samples were prepared for ccSEM directly after they were analysed as operator controlled. For all samples, except the traffic hotspot and rural background samples, a magnification of × 20,000 per frame was set. The rural background sample was set to a magnification of × 10,000 and the traffic hotspot sample to × 5000 because the particles in these samples where larger and had a higher contrast. The total number of particles per sample analysed varied between 1103 and 6940 (see sample specific in Fig. 1) with an average particle number per image of ~ 50 particles. The whole impaction spot was analysed by ccSEM. The Aztec software automation function "Feature" was used to set parameters for contrast boundary (for segmentation of particles with backscatter image), size filter (> 0.1 μm equivalent projected aerodynamic diameter), defined area of analysis, and acquisition live time (5 s per particle). The segmentation of particles from the background is set by arbitrary threshold limits empirically determined on low-contrast particles (in most cases carbonaceous particles). SE images were always taken together with the template BSE image to have the possibility to manually investigate the sample after acquisition.

Classification criteria (ESM Table S3) were set using the Aztec software. These criteria are inspired by the classes defined manually in opSEM in order to obtain comparable particle groups. The classification procedure was optimised by tuning the criteria on the typical particle of each group. The tuning includes checking the fit of the classification criteria for several randomly chosen particles within the groups. This manual intervention to classification is absolutely necessary because all samples have different background signals which influence the identification of characteristic X-ray peaks. For example, the group of carbonaceous particles had to be defined with different thresholds for C concentrations, due to different levels of bremsstrahlung on the various samples. From our experience, a universal classification scheme that can be applied to all different aerosol types would be inaccurate.

Results

There are pronounced differences in the particle group abundances when the two analytical approaches are compared (Figs. 1 and 2). The relative abundance of a particle group is strongly dependent on the detection efficiency as well as the classification procedure. The different detection efficiency is a result of the BSE image used as a template in ccSEM compared to both SE and BSE in opSEM, as well as the

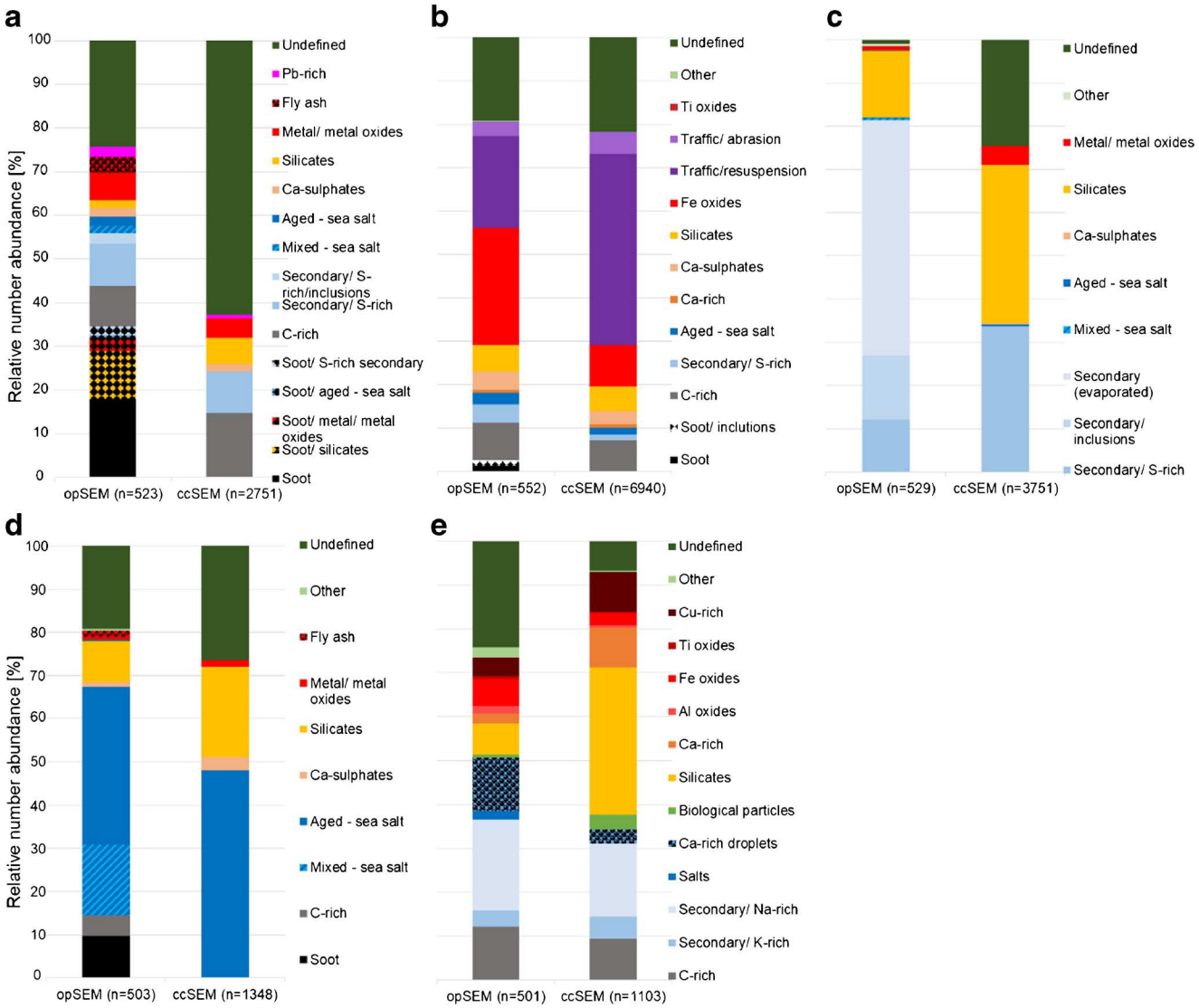

Fig. 1 Relative particle number abundance of the different samples measured with opSEM and ccSEM. **a** Urban background—Mainz. **b** Traffic hotspot—Essen. **c** Free troposphere—Swiss Alps. **d** Rural background/marine—Cyprus. **e** Rural background—Germany

possibility to observe evaporating particles in opSEM. It is noteworthy that ccSEM is carried out after opSEM; hence, some of the evaporated secondary particles are no longer present in the sample. Still, one-tenth of the substrate area was analysed by opSEM compared to ccSEM (in the applicable sample—free troposphere sample from the Swiss Alps), so this error is small.

Relative number abundance of the different particle groups

The relative number abundance of the different particle groups is presented in Fig. 1. All samples have a group of undefined particles where no characteristic X-ray spectrum or morphology was observed. Particles which failed the classification criteria in ccSEM are also included. This group is attributed to analytical artefacts (substrate irregularities and image shift) or particle properties like high volatility or small size.

According to opSEM, the urban background aerosol consists of soot, soot with inclusions of other particle groups (silicates, metal/metal oxide, aged sea salt or secondary particles; see ESM Fig. S2 a and b), C-rich particles, secondary/S-rich particles, secondary/S-rich particles with inclusions, mixed sea salt, aged sea salt, Ca-sulphates, silicates, metal/metal oxides, fly ash particles (ESM Fig. S2 e), Pb-rich particles and undefined particles. In ccSEM, the groups of soot, soot with inclusions, secondary/S-rich particles with inclusions, the sea salt groups and fly ash particles are not recognised. The relative number abundance of undefined particles is much higher in ccSEM most likely due to analytical artefacts, like substrate irregularity and image shift (see "Discussion" for details).

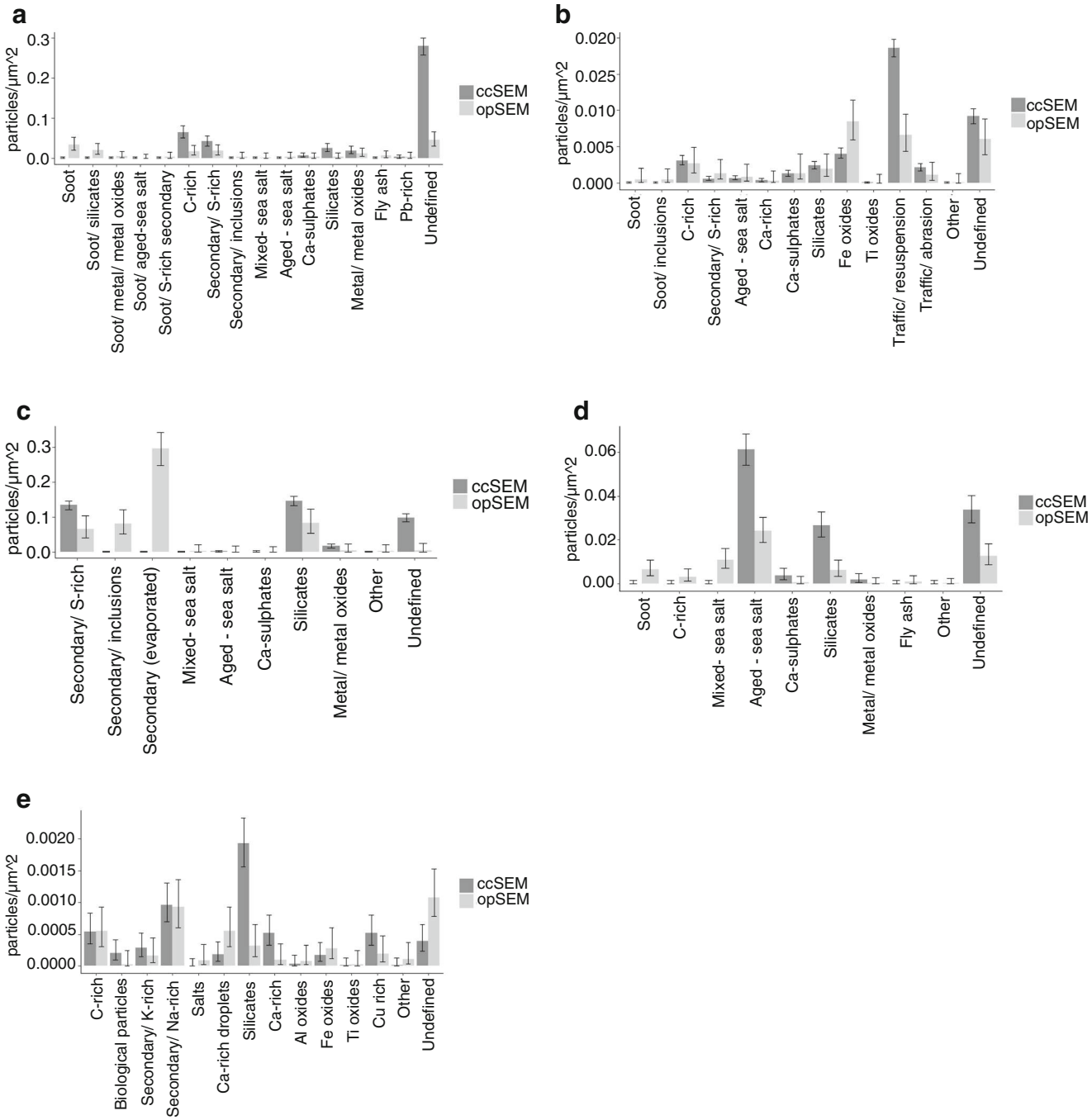

Fig. 2 Particle group abundance normalised to the substrate area analysed. Error bars are 95% confidence intervals (CIs) calculated after Quesenberry, Hurst [38] assuming a lognormal distribution. The CIs were computed with the RStudio package "CoinMinD" (M.Subbiah, 2013). **a** Urban background—Mainz. **b** Traffic hotspot—Essen. **c** Free troposphere—Swiss Alps. **d** Rural background/marine—Cyprus. **e** Rural background—Germany

At the traffic hotspot, the following particle groups were detected by opSEM: soot, soot with inclusions (ESM Fig. S2 f, g and h), C-rich particles, S-rich secondary particles, aged sea salt, Ca-rich particles, Ca-sulphates, silicates, Fe oxides, traffic/resuspension, traffic/abrasion, Ti oxides and other particles. The main difference between the two techniques is the lower abundance of Fe oxides and a higher traffic/resuspension component abundance in ccSEM. This difference most likely results from the classification procedure (see "Discussion"). Also in this sample, soot and soot with inclusions are not determined with ccSEM.

The most abundant particle groups in the free troposphere sample from the Swiss Alps are, according to opSEM, secondary aerosol particles (secondary/S-rich with inclusions and

secondary without a characteristic X-ray spectrum) and silicates. A smaller fraction of aged and mixed sea salt, minerals (Ca-sulphates and silicates), metal/metal oxides and other particles was also detected. The ccSEM procedure is clearly limited by the fact that many of the particles evaporate leaving no chemical information and thus have to be classified as undefined. Still, ccSEM shows a relatively high abundance of S-rich secondary particles because the overall analysis time is shorter than that in opSEM leaving the possibility to obtain chemical information of some volatile particles, as well as because some of the S-rich particles with inclusions are classified in this group.

The rural background/ marine sample from Cyprus consists of soot, C-rich particles, mixed sea salt, aged sea salt, Ca-sulphates, silicates, metal/metal oxides, fly ash particles and other (opSEM). Again, soot is not recognised by ccSEM due to the lack of information on morphology. The pronounced differences between both analytical approaches of the relative abundance of silicates, aged sea salt and mixed sea salt can be explained by the classification procedure (see "Discussion" for details). The general high fraction of aged sea salt in this sample, determined with both techniques, is supported by the back trajectories showing air mass travelling over the Mediterranean Sea before reaching the island of Cyprus (see ESM Fig. S1).

The rural background sample from Germany includes, according to opSEM, C-rich particles, K-rich and Na-rich secondary particles, salts (cubic morphology), Ca-rich droplets (present as particles surrounded by a halo around), biological particles (ESM Fig. S2 c and d), silicates, Ca-rich particles, Al oxides, Fe oxides, Ti oxides and some Cu-rich particles which most likely stem from the substrate. The major differences between the two SEM approaches are a much higher abundance of silicates and a lower abundance of undefined particles by ccSEM. The former can be partly explained by Ca-rich droplets containing silicate inclusions. The reason for the higher abundance of undefined particles in opSEM is probably due to the fact that only backscatter images are used for particle segmentation in ccSEM.

Area-normalised particle abundance

We additionally present the data normalised to the area analysed (Fig. 2) because the relative number abundance shown in Fig. 1 suffers from a systematic error caused by the loss of volatile components. In addition, presenting the results as area normalised has two advantages: correct assignment of the misclassified particles and quantification of the differences of the two approaches. For details, the readers are referred to the ESM.

Differences between the two SEM techniques are observed for a number of particle groups. Silicates are higher in the ccSEM by a factor of ~ 7 in the urban background sample, ~ 2 in the free troposphere, ~ 4 in the rural background/marine sample from Cyprus and ~ 6 in the rural background sample from Germany. Soot mixed with silicates is not recognised by ccSEM in the urban background. In the urban background sample, the abundance of C-rich particles is approximately four times higher in ccSEM compared to opSEM, as soot is misclassified as C-rich in the former technique. In the rural background/marine sample from Cyprus, aged sea salt is higher by a factor of ~ 2.5 by ccSEM. Mixed sea salt is not recognised at all by ccSEM. In the traffic hotspot sample, 2 times more Fe oxide particles are found by opSEM, and 3 times more traffic/ resuspension particles by ccSEM in the traffic hotspot sample. All samples, except the traffic hotpot, show a difference between the two techniques for undefined particles. By ccSEM, this particle group is higher in urban background (~ 6 times), free troposphere (~ 19 times) and rural background/marine (~ 3 times) and lower in the rural background sample from Germany (~ 1.5 times). These factors show that there are sometimes very large differences between the two methods which will addressed in the "Discussion" section.

Particle size

The equivalent projected area diameter of particles is presented in Fig. 3.

The size of particles as well as the thickness of coatings might be underestimated due to the choice of the acceleration voltage. Still, as the same accelerating voltage is used for opSEM and ccSEM, this will not influence the comparison between the two techniques.

The size (Fig. 3) of silicates in the urban background, free troposphere, rural background/marine and rural background—Germany samples is generally smaller in ccSEM than in opSEM. This can be explained by the presence of silicates as inclusions in soot (see ESM Fig. S2 f, g and h) and/or secondary particles (ESM Fig. S2 o, p and q) as well as in mixed sea salt particles (ESM Fig. S2 k and l) or Ca-rich droplets. In ccSEM, silicate inclusions will in many cases be classified as silicates. Thus, this group contains more small particles than the corresponding group in opSEM.

The size of aged sea salt in the rural background/marine sample from Cyprus is somewhat smaller in ccSEM than opSEM (seen in Fig. 3). This may be explained by the fact that these particles can be divided sometimes due to contrast settings. This is especially true for particles which dried on the substrate leading to inhomogeneous density of the crystallised material. Areas with different densities may be counted as individual particles by ccSEM.

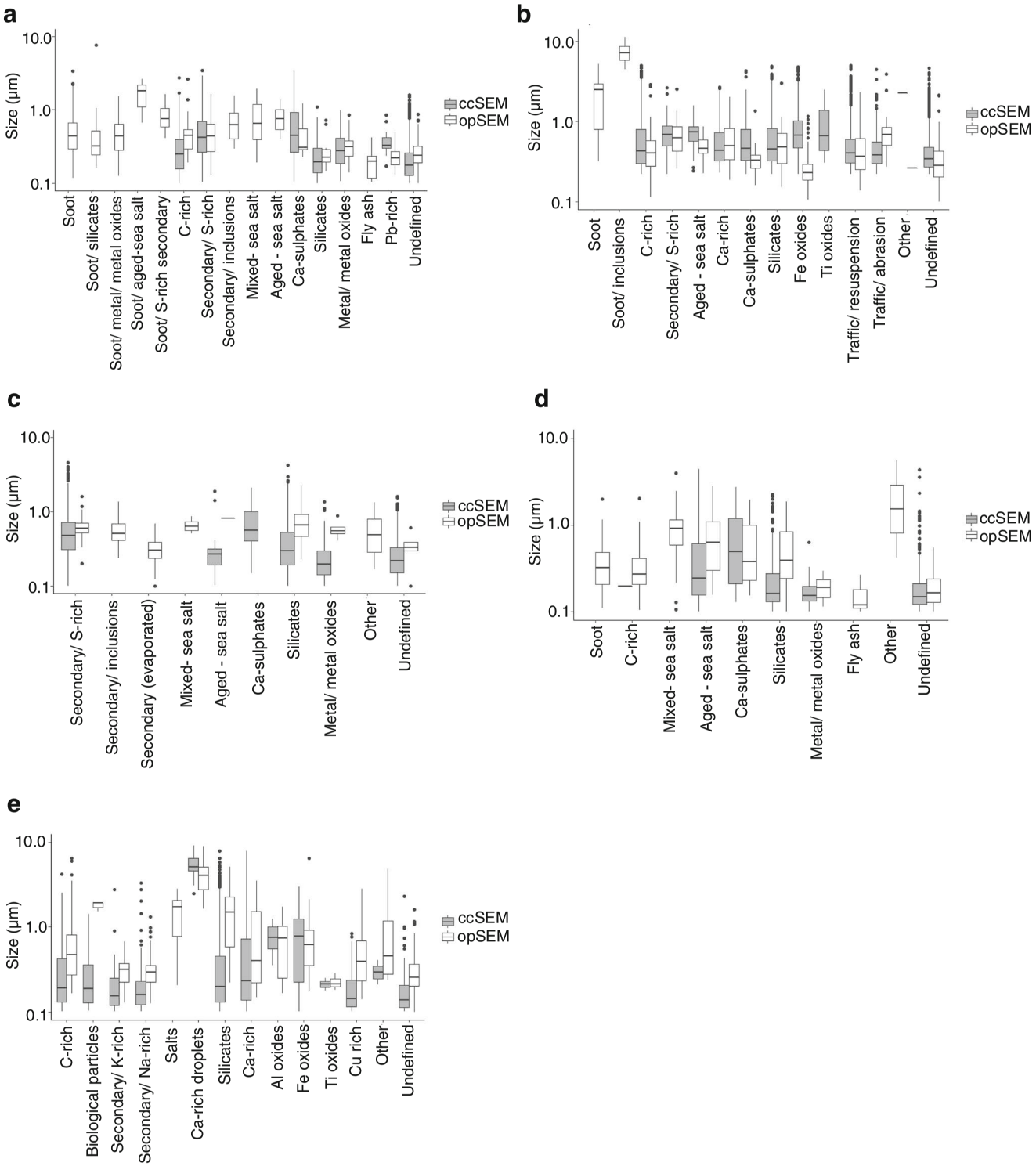

Fig. 3 Equivalent projected area diameter of particles from the urban background—Mainz (**a**), traffic hotspot—Essen (**b**), free troposphere—Swiss Alps (**c**), rural background/marine—Cyprus (**d**), and rural background—Germany (**e**). In ccSEM, the size of the particles is based on BSE images and on SE images in opSEM. Boxplots are calculated with RStudio package ggplot2 [39]. The whiskers shown extend to the most extreme data points which are no more than 1.5 times the interquartile range away from the box

Discussion

Comparison between opSEM and ccSEM

In the following discussion, opSEM is regarded as more accurate than ccSEM, i.e., the results of the former approach are closer to the real—but still to some extent unknown—composition of the atmospheric aerosol.

Measurement artefacts

Particles might be spread heterogeneously on the substrate. The impaction spot on the substrate is a circle, with a slight gradient distribution from the centre to the border region. To address this, opSEM analysis was always performed as a circular sector relative to the impaction spot, and the ccSEM analysis covered the whole spot. In this way, the relative abundance of the particle groups should be comparable. This assumption is supported by Fig. 3 showing that the size regions of most particle groups overlaps if the two techniques are compared. The only exemptions are silicates, metal/metal oxides and Pb-rich particles in one sample each (rural background—Germany, rural background/marine—Cyprus and urban background—Mainz, respectively) and aged sea salt and other particles in two samples with very low abundance leading to poor counting statistics.

With both techniques, there is a substantial fraction of unidentified particles which may amount up to ~ 25% in opSEM and ~ 60% in ccSEM (Fig. 1). In opSEM, the unidentified group includes small particles prone to a slight image shift during analysis (which can be a consequence of charging, mechanical vibration, external electromagnetic fields or specimen movement), small C-rich particles without a typical morphology and highly volatile particles which yield no characteristic X-ray peaks. In ccSEM, the unidentified particles additionally incorporate highly volatile particles without a characteristic X-ray spectrum (see "Morphology-based classification" for details about the volatile particles) and substrate irregularities. An unambiguous classification of a particle in ccSEM is only possible when a characteristic EDX spectrum is received. Small and/or film-like particles such as highly volatile particles (which in opSEM often can be classified) are therefore often misinterpreted or overlooked in ccSEM (ESM Fig. S2 i and j). For this reason, there are generally more unidentified particles by ccSEM. To address the unidentified particles, different sorting out procedures can be performed in terms of an algorithm in the software during analysis skipping particles with chemistry similar to the background and/or post-processing software to discard/ replace particles in this group [40].

Detection of the particles by ccSEM depends on the electron signal used, in most cases BSE. As boron substrates are deployed in our analysis, all elements with a higher atomic number than boron give a brighter signal than the background. The detection of all particle groups was ensured by checking the contrast of carbonaceous particles (soot and C-rich particles). The contrast was generally sufficient to detect carbonaceous particles with ccSEM. The main difference in the two techniques due to contrast setting is not the detection of the relevant particle groups but the enhancement in number concentration of some particle groups (C-rich, aged sea salt particle) and an accurate determination of particle size (Fig. 3). A particle with low contrast (relative to the background) and jagged morphology can be cut into two or more particles by the software, leading to a higher number of these particles. This is one of the reasons for the higher abundance of C-rich particles in the urban background sample as well as aged sea salt in the rural background/ marine sample from Cyprus analysed with ccSEM. The contrast/brightness is mainly increasing with increasing atomic number but also depending on the density of the particle, e.g., a thin film of sea salt will give a lower contrast than a dense sea salt particle. For this reason, the size of aged sea salt, carbonaceous particles (except in the traffic hotspot sample), secondary particles in the free troposphere and rural background samples, as well as biological particles, is often smaller when measured with ccSEM compared to opSEM. Summarised, on low-Z substrates like boron, low-Z particles may have insufficient contrast leading often to an underestimation of their size in ccSEM (see Fig. 3).

Classification

We use two different classification schemes for opSEM and ccSEM, because different information is obtained with each technique. In opSEM, the classification criteria are qualitative based on chemical, morphological and beam stability information from both BSE and SE images (ESM Table S2). In ccSEM, the classification is semi-quantitative based on chemical composition (ESM Table S3), and only in one case additional information on aspect ratio (Ca-rich droplets) was used. For example, generally fly ash particles cannot be recognised by ccSEM and are thus contained in the groups of metal oxides, C-rich, Ca-rich and silicates, at least when they are not differentiated based on aspect ratio. In addition to fly ashes, particles that could not be classified by ccSEM include soot, mixed particles and unstable particles, which are discussed in more detail in the next subchapters. These particles are hence classified into different particle groups in ccSEM (see ESM Table S4). It should be emphasised here that the different results obtained by the two techniques are generally more influenced by the different classification schemes, which are also based on the information obtained during analysis and a priori knowledge on particle sources, than by methodological differences.

The classification can be based on atomic %, weight % or net X-ray counts, and the classification schemes are in any case optimised for the research question and sample. We do not use a universal classification scheme because such a scheme would not make use of all the information one has from a given sample. For example, Weinbruch et al. [26] investigated particles from road traffic, and in their classification scheme, traffic/exhaust, traffic/ abrasion and traffic/ resuspension are defined to differentiate between these traffic components. In the present contribution, traffic abrasion and traffic/ resuspension are based on similar chemical composition as in Weinbruch et al. [26]. Our traffic/resuspension group does not contain soot mixtures which is a separate group in our contribution. The traffic/exhaust component in Weinbruch et al. [26] is similar to the soot plus soot/S-rich secondary group in the present contribution. Please note that it is not the aim of our paper to directly compare the result to Weinbruch et al. [26].

Misinterpretation due to complex mixing state

The classification of an individual ambient aerosol particle always entails a simplification with a loss of detailed information as a result. There are no perfect external mixed particles and taking a closer look will reveal small heterogeneously distributed impurities, coatings or agglomerates. OpSEM in contrast to ccSEM offers the possibility to take a closer look to study in detail the particle morphology as well as site-specific composition by spot analysis of different regions of an individual particle. This often results in a new and more detailed classification, no longer involving only the main components (as ccSEM does) but also the admixed minor components. Consistently for all samples, particles with inclusions are systematically underestimated in the ccSEM procedure. This applies to fly ash agglomerates, mixed sea salt particles, secondary particles with inclusions, soot internally mixed particles and Ca-rich droplets. In general, this discrepancy is due to less detailed information of the mixed particles rather than missed detection. If sampled close to the source, fly ash mostly exists as individual particles (i.e. not as agglomerate) which can be classified accurately based on chemistry and aspect ratio by ccSEM. When the sample is taken further away from the source, mixing processes like coating and agglomeration will preclude the use of aspect ratio in the classification procedure. As only a small fraction of fly ashes occurred as single spheres in our samples (urban background and rural background/marine), a better classification for ccSEM was not applicable.

The mixed sea salt particles (aged sea salt mixed with minerals) can have a similar chemical composition as certain minerals (e.g. silicates). The highest sea salt abundance is found in the rural background/marine sample. Here, the sea salt particles have undergone severe ageing excluding the possibility to classify the mixed sea salt group based on the presence of chlorine. The mixed sea salt particles can also not be classified based on their aspect ratio, as these are not consistently spheres. Due to the presence of inclusions, the mixed sea salt particles (ESM Fig. S2 k and l) may be misinterpreted as silicates in ccSEM. Therefore, a higher silicate abundance and a lower mixed sea salt abundance is observed by ccSEM compared to opSEM in the rural background/ marine sample from Cyprus. Similar observations, but with overlapping confidence intervals, are made in the urban background and the free troposphere sample. The same reasoning applies to the secondary particle group with inclusions found with opSEM in the free troposphere sample. By ccSEM, the silicate group is overestimated. Silicates, in this group, are also overestimated due to volatility discussed later.

The urban background sample from Mainz includes a considerable fraction of soot particles with inclusions, ESM Fig. S2 f, g and h. In case of internally mixed soot, the inclusions have a higher contrast in the BSE image and are therefore detected with a higher efficiency than the soot particle itself. This may divide a soot agglomerate with inclusions into several particles partly explaining the higher silicate (factor of 7 larger) and secondary particles abundances (factor of ~ 2—but with overlapping CIs) by ccSEM in the urban background sample.

The Ca-rich droplets in the rural background sample from Germany also frequently contained inclusions. In this case, many Ca-rich droplets could be classified based on the aspect ratio. Still, some Ca-rich droplets failed the classification and are allocated in the silicates and Ca-rich group by ccSEM.

Morphology-based classification

Usually, BSE are used in ccSEM because particles can be easier to detect based on the chemical contrast. Even for SE images, there is currently no automated classification procedure available for recognition and classification of complex morphology, as for example soot agglomerates. Thus, morphology information used for particle classification can only be obtained by opSEM. In our ccSEM analysis, we record both, SE and BSE images. In this way, the "non-classified" soot particles can be identified by manual post-processing after analysis (see ESM Fig. S2 r). Another ccSEM method [7] uses a high-angle annular dark field detector yielding a good contrast for small soot particles that are invisible in a normal BSE image using a C-substrate (TEM grids). According to these authors, even with this optimised detector, several limitations lead to a semi-quantitative analysis of low-*Z* elements and beam-sensitive particles. This also applies to opSEM if the evaporation of beam-sensitive particles is not observed.

Volatile particles

Secondary particles (sulphates, nitrates and organic particles which often form complex internal mixtures) are challenging to identify by electron microscopy due to their instability under electron bombardment (ESM Fig. S2 m and n). In our work, secondary aerosol particles are detected based on chemistry (S and or N) and beam stability. With respect to chemistry, secondary particles are detected with similar efficiency in both approaches. With respect to beam stability, we can distinguish relatively stable (i.e. not completely evaporating within a few seconds of electron bombardment) and unstable particles. Evaporation of secondary particles during analysis has the advantage that relatively stable inclusions can be detected (ESM Fig. S2 o, p and q).

In the sample from the free troposphere, secondary particles with inclusions sometimes gave a characteristic S X-ray peak and are in this case included in the secondary/S-rich group by ccSEM. More often, the particles evaporated totally leaving behind only the inclusion particle (mostly silicates). In this case, the inclusions (~ 0.1 particle/μm^2) are classified into the silicates group (e.g. in ESM Fig. S2 o, p and q) leading to a higher fraction of silicates in ccSEM. This problem also occurs in the urban background sample, but with a much lower abundance of secondary particles with inclusions.

Highly volatile particles are not detected with ccSEM as they did not yield a characteristic X-ray spectrum which can be used for classification. This problem is especially pronounced for particles smaller than ~ 300 nm (size in Fig. 3). In principle, one could combine the two groups of highly volatile particles (fully evaporated and volatile particles with inclusions) to present secondary particles. We refrained from this, because the different volatility could be caused by a different chemical composition. Additionally, only the stable particles can be observed by ccSEM. A method to stabilise beam-sensitive particles was investigated by Worobiec et al. [41] using cryogenic cooling of the sample-holder stage. They concluded that the stability of the particles depends on beam energy and the interaction with the substrate (Be substrates yield better stability than Al or Si wafers). Another way to obtain an accurate estimate of the secondary aerosol abundance is to use other measuring techniques, as for example AMS [8, 25], in addition to electron microscopy.

Implications for characterisation of aerosol particles

In the present contribution it was shown that there are large differences in the abundance of the various particle groups determined by opSEM and ccSEM. The latter technique is limited in at least three different ways. First, information on the mixing state of particles (e.g. presence of heterogeneous inclusions, surface coatings or gradients in chemical composition) cannot be obtained. Second, particle groups which are recognised by their complex morphology (e.g. soot, biological particles) are misclassified. Third, highly volatile particles (i.e., particles which evaporate under electron bombardment within a few seconds) will be overlooked. OpSEM is clearly limited by the much higher expenditure of time leading to a significantly lower number of particles/samples that can be studied. As a result, particle groups present at very low abundance may be only detected by ccSEM. In addition, opSEM is not suited for monitoring studies in contrast to ccSEM.

Several papers show that ccSEM is a useful tool in aerosol particle characterisation. One example is the investigation of long-range transport of mineral dust [36, 42]. In this case, relatively large mineral particles (diameter > 0.5 μm) can easily be detected due to their stability and high contrast in electron images. Information on the chemical composition can then reveal the source regions of the particles, leading to a better understanding of dust transport. Other examples of ccSEM which do not suffer from the limitations described above include the inorganic non-volatile fraction of particles from coal combustion [43, 44], metallic particles in subways [45] and work place particles [19], as well as investigation of coarse combustion particles [46]. In the case of our traffic hotspot sample, ccSEM could be used to distinguish the different traffic components if manual image analysis would be applied afterwards to complement with information on soot content.

However, it is often necessary to determine all particle groups present in a sample favouring the use of opSEM. This is the case in environmental studies where morphology and mixing state can for example influence the light-scattering ability [47, 48], or ice nucleation activity of the particles [10, 49–51]. Some samples are difficult to collect increasing the need to obtain as much information as possible, e.g. stratospheric samples [35, 52–54]. OpSEM is also indispensable if particle groups which cannot be characterised accurately by ccSEM are in the focus of a study. This is certainly the case for fly ash particles [55], biological aerosol particles [56–58], soot [59] and unstable secondary particles [25, 60]. Especially the urban background and the free troposphere sample represent cases where opSEM is needed to get more detailed results which can be applied in environmental and health research.

The major drawback of opSEM in particle analysis is the much higher time needed for analysis (resulting in a much smaller number of particles studied) compared to ccSEM. Thus, if a high sample throughput is needed, ccSEM is better suited. In this case, the limitations of ccSEM outlined in the present paper may be at least partly avoided by manual post-processing. For example, soot particles at a traffic hotspot and in the urban background aerosol where recognised after ccSEM by visual interpretation of more than 111,000 electron images [26]. A similar approach (ccSEM followed by manual post-processing) was applied to Saharan dust on the Cape Verde Islands [54]. Another approach is to manually

investigate a fraction of the sample by opSEM followed by ccSEM, like Engelbrecht et al. [61] carried out when characterising mineral dust and other aerosols at different locations in Asia. Similarly, coal ash particles [62] and coarse particles (50% sampling cut-off size > 1.2 μm) of internal mixtures in marine aerosol [63] were investigated using both techniques.

Finally, a combination with other analytical techniques was often applied in the past to overcome some of the limitations of SEM. Examples include bulk chemical analysis by AMS [25], XRD [64], XRF [44], ICP-MS/ICP-OES [65] or PIXE [66] as well as other single particle techniques like ATOFMS [8, 49, 67] or STXM [68]. However, as substantial differences were already observed when comparing two SEM techniques, it can be expected that applying additional techniques (e.g., single particle mass spectrometry, micro-Raman spectroscopy) will lead to even more pronounced differences. Anyway, a combination of different complementary analytical techniques will give a more complete and presumably more accurate picture of atmospheric aerosol particles. We want to emphasise here that more research is needed which systematically compares different single particle techniques and elaborates strengths and limitations of each technique with respect to the characterisation of atmospheric aerosol particles.

In this paper, we have shown the strengths and weaknesses of both, opSEM and ccSEM, applied to different types of atmospheric aerosol. The results clearly show that both techniques can be applied to particles down to approximately 100 nm. The major advantage of ccSEM is a relatively quick analysis of a large number of particles leading to a much better counting statistics—as seen in all our atmospheric samples—compared to opSEM. The major advantage of opSEM arises from the fact that information is obtained (e.g. morphology, beam stability) that enables unequivocal identification of particle groups (e.g. soot, primary biological particles, fly ashes) which are difficult or impossible to detect by ccSEM. The major drawback of opSEM is the much higher expenditure of time resulting in fewer particles being analysed leading to a higher uncertainty of the particle group number abundances seen in many of the particle groups investigated in this work. Compared to previous work, which to some extent has already addressed the difficulty to detect soot and mixed particles, our results also accentuate the possibility to identify and characterise in detail secondary aerosol particles. We could differentiate three different groups of secondary particles from which only one (relatively stable secondary/S-rich particles) can be detected by ccSEM and opSEM. The two other groups (secondary/inclusions as well as secondary/evaporated) can only be detected by opSEM because of fast evaporation during analysis. As both groups of secondary particles are dominating the sample from the free troposphere, this point is of high importance at least for this aerosol type.

Acknowledgments Thanks to Nathalie Benker for collecting the rural background sample in Germany. We would like to thank the International Foundation High Altitude Research Stations Jungfraujoch & Gornergrat (HFSJG) who made it possible to carry out the experiment at Jungfraujoch, and Jean Sciare and the Cyprus Institute for the facility and help during the campaign in Cyprus. The authors gratefully acknowledge the National Oceanic and Atmospheric Administration (NOAA) Air Resources Laboratory (ARL) for the provision of the HYSPLIT transport and dispersion model and READY website (http://www.ready.noaa.gov, last accessed: March 2018) used in this publication. This project is funded by the Deutsche Forschungsgemeinschaft (DFG, German Research Foundation) – 264907654; 264912134; 416816480 (KA 2280) and INUIT (FOR 1525 - EB383/3-1). The present work is part of a project that has received funding from the European Union's Horizon 2020 research and innovation programme under grant agreement No. 654109. Thorough reviews by three anonymous referees helped to significantly improve the manuscript and are gratefully acknowledged.

Compliance with ethical standards

Conflict of interest The authors declare that they have no conflict of interest.

References

1. Seinfeld JH, Pandis SN. Atmospheric chemistry and physics: from air pollution to climate change. Hoboken: Wiley; 2012.
2. Kulkarni P, Baron PA, Willeke K. Aerosol measurement: principles, techniques, and applications, vol. 3. 3rd ed. Hoboken: Wiley; 2011.
3. McMurry PH. A review of atmospheric aerosol measurements. Atmos Environ. 2000. https://doi.org/10.1016/S1352-2310(99)00455-0.
4. Li W, Shao L, Zhang D, Ro C-U, Hu M, Bi X, et al. A review of single aerosol particle studies in the atmosphere of East Asia: morphology, mixing state, source, and heterogeneous reactions. J Clean Prod. 2016. https://doi.org/10.1016/j.jclepro.2015.04.050.
5. Bente M, Sklorz M, Streibel T, Zimmermann R. Online laser desorption-multiphoton postionization mass spectrometry of individual aerosol particles: molecular source indicators for particles emitted from different traffic-related and wood combustion sources. Anal Chem. 2008. https://doi.org/10.1021/ac801295f.
6. Roth A, Schneider J, Klimach T, Mertes S, van Pinxteren D, Herrmann H, et al. Aerosol properties, source identification, and cloud processing in orographic clouds measured by single particle mass spectrometry on a central European mountain site during HCCT-2010. Atmos Chem Phys. 2016. https://doi.org/10.5194/acp-16-505-2016.
7. Laskin A, Cowin JP, Iedema MJ. Analysis of individual environmental particles using modern methods of electron microscopy and X-ray microanalysis. J Electron Spectrosc Relat Phenom. 2006. https://doi.org/10.1016/j.elspec.2005.06.008.
8. Gunsch MJ, Kirpes RM, Kolesar KR, Barrett TE, China S, Sheesley RJ, et al. Contributions of transported Prudhoe Bay oil field emissions to the aerosol population in Utqiaġvik, Alaska. Atmos Chem Phys. 2017. https://doi.org/10.5194/acp-17-10879-2017.
9. Kirpes RM, Bondy AL, Bonanno D, Moffet RC, Wang B, Laskin A, et al. Secondary sulfate is internally mixed with sea spray aerosol and organic aerosol in the winter Arctic. Atmos Chem Phys. 2018. https://doi.org/10.5194/acp-18-3937-2018.

10. Eriksen Hammer S, Mertes S, Schneider J, Ebert M, Kandler K, Weinbruch S. Composition of ice particle residuals in mixed-phase clouds at Jungfraujoch (Switzerland): enrichment and depletion of particle groups relative to total aerosol. Atmos Chem Phys. 2018. https://doi.org/10.5194/acp-18-13987-2018.
11. Xhoffer C, Wouters L, Artaxo P, Van Put A, Van Grieken R. Environmental particles environmental analytical and physical chemistry series. Chelsea: Lewis Publisher; 1992.
12. Craig RL, Bondy AL, Ault AP. Surface enhanced Raman spectroscopy enables observations of previously undetectable secondary organic aerosol components at the individual particle level. Anal Chem. 2015. https://doi.org/10.1021/acs.analchem.5b01507.
13. Paton-Walsh C, Smith TEL, Young EL, Griffith DWT, Guérette ÉA. New emission factors for Australian vegetation fires measured using open-path Fourier transform infrared spectroscopy – part 1: methods and Australian temperate forest fires. Atmos Chem Phys. 2014. https://doi.org/10.5194/acp-14-11313-2014.
14. Craig N, Harker A, Novakov T. Determination of the chemical states of sulfur in ambient pollution aerosols by X-ray photoelectron spectroscopy. Atmos Environ. 1967;1974. https://doi.org/10.1016/0004-6981(74)90108-5.
15. Zhu Y-J, Olson N, Beebe TP. Surface chemical characterization of 2.5-μm particulates (PM2.5) from air pollution in Salt Lake City using TOF-SIMS, XPS, and FTIR. Environ Sci Technol. 2001. https://doi.org/10.1021/es0019530.
16. Berlinger B, Benker N, Weinbruch S, L'Vov B, Ebert M, Koch W, et al. Physicochemical characterisation of different welding aerosols. Anal Bioanal Chem. 2011. https://doi.org/10.1007/s00216-010-4185-7.
17. Weinbruch S, Benker N, Kandler K, Schütze K, Kling K, Berlinger B, et al. Source identification of individual soot agglomerates in Arctic air by transmission electron microscopy. Atmos Environ. 2018. https://doi.org/10.1016/j.atmosenv.2017.10.033.
18. Goldstein J, Newbury D, Joy D, Lyman C, Echlin P, Lifshin E, et al. Scanning electron microscopy and x-ray microanalysis. 3rd ed. New York: Plenum; 2003.
19. Höflich B, Wentzel M, Ortner H, Weinbruch S, Skogstad A, Hetland S, et al. Chemical composition of individual aerosol particles from working areas in a nickel refinery. J Environ Monit. 2000. https://doi.org/10.1039/B001146K.
20. Weinbruch S, Wentzel M, Kluckner M, Hoffmann P, Ortner HM. Characterization of individual atmospheric particles by element mapping in electron probe microanalysis. Microchim Acta. 1997. https://doi.org/10.1007/bf01246176.
21. Exner HE, Weinbruch S. Scanning Electron Microscopy. In: ASM handbook volume 9: metallography and microstructures. Novelty: ASM International; 2004.
22. Kandler K, Schneiders K, Ebert M, Hartmann M, Weinbruch S, Prass M, et al. Composition and mixing state of atmospheric aerosols determined by electron microscopy: method development and application to aged Saharan dust deposition in the Caribbean boundary layer. Atmos Chem Phys. 2018. https://doi.org/10.5194/acp-18-13429-2018.
23. Willis RD, Blanchard FT, Conner TL. Guidelines for the application of SEM/EDX analytical techniques to particulate matter samples. Washington, US. EPA report. 2002.
24. Mamane Y, Willis R, Conner T. Evaluation of computer-controlled scanning electron microscopy applied to an ambient urban aerosol sample. Aerosol Sci Technol. 2001. https://doi.org/10.1080/02786820118842.
25. Vester BP, Ebert M, Barnert EB, Schneider J, Kandler K, Schütz L, et al. Composition and mixing state of the urban background aerosol in the Rhein-Main area (Germany). Atmos Environ. 2007. https://doi.org/10.1016/j.atmosenv.2007.04.021.
26. Weinbruch S, Worringen A, Ebert M, Scheuvens D, Kandler K, Pfeffer U, et al. A quantitative estimation of the exhaust, abrasion and resuspension components of particulate traffic emissions using electron microscopy. Atmos Environ. 2014. https://doi.org/10.1016/j.atmosenv.2014.09.075.
27. Weingartner E, Nyeki S, Baltensperger U. Seasonal and diurnal variation of aerosol size distributions (10<D<750 nm) at a high-alpine site (Jungfraujoch 3580 m asl). J Geophys Res Atmos (1984–2012). 1999. https://doi.org/10.1029/1999JD900170.
28. Coen MC, Weingartner E, Nyeki S, Cozic J, Henning S, Verheggen B, et al. Long-term trend analysis of aerosol variables at the high-alpine site Jungfraujoch. J Geophys Res Atmos (1984–2012). 2007. https://doi.org/10.1029/2006JD007995.
29. Cozic J, Verheggen B, Weingartner E, Crosier J, Bower K, Flynn M, et al. Chemical composition of free tropospheric aerosol for PM1 and coarse mode at the high alpine site Jungfraujoch. Atmos Chem Phys. 2008. https://doi.org/10.5194/acp-8-407-2008.
30. Hinz K-P, Trimborn A, Weingartner E, Henning S, Baltensperger U, Spengler B. Aerosol single particle composition at the Jungfraujoch. J Aerosol Sci. 2005. https://doi.org/10.1016/j.jaerosci.2004.08.001.
31. Kamphus M, Ettner-Mahl M, Klimach T, Drewnick F, Keller L, Cziczo DJ, et al. Chemical composition of ambient aerosol, ice residues and cloud droplet residues in mixed-phase clouds: single particle analysis during the Cloud and Aerosol Characterization Experiment (CLACE 6). Atmos Chem Phys. 2010. https://doi.org/10.5194/acp-10-8077-2010.
32. Schmidt S, Schneider J, Klimach T, Mertes S, Schenk LP, Kupiszewski P, et al. Online single particle analysis of ice particle residuals from mountain-top mixed-phase clouds using laboratory derived particle type assignment. Atmos Chem Phys. 2017. https://doi.org/10.5194/acp-17-575-2017.
33. Achilleos S, Evans JS, Yiallouros PK, Kleanthous S, Schwartz J, Koutrakis P. PM10 concentration levels at an urban and background site in Cyprus: the impact of urban sources and dust storms. J Air Waste Manage Assoc. 2014. https://doi.org/10.1080/10962247.2014.923061.
34. Schrod J, Weber D, Drücke J, Keleshis C, Pikridas M, Ebert M, et al. Ice nucleating particles over the Eastern Mediterranean measured by unmanned aircraft systems. Atmos Chem Phys. 2017. https://doi.org/10.5194/acp-17-4817-2017.
35. Ebert M, Weigel R, Kandler K, Günther G, Molleker S, Grooß JU, et al. Chemical analysis of refractory stratospheric aerosol particles collected within the arctic vortex and inside polar stratospheric clouds. Atmos Chem Phys. 2016. https://doi.org/10.5194/acp-16-8405-2016.
36. Kandler K, Benker N, Bundke U, Cuevas E, Ebert M, Knippertz P, et al. Chemical composition and complex refractive index of Saharan Mineral Dust at Izana, Tenerife (Spain) derived by electron microscopy. Atmos Environ. 2007. https://doi.org/10.1016/j.atmosenv.2007.06.047.
37. Choël M, Deboudt K, Osán J, Flament P, Van Grieken R. Quantitative determination of low-Z elements in single atmospheric particles on boron substrates by automated scanning electron microscopy−energy-dispersive x-ray spectrometry. Anal Chem. 2005. https://doi.org/10.1021/ac050739x.
38. Quesenberry CP, Hurst DC. Large sample simultaneous confidence intervals for multinomial proportions. Technometrics. 1964. https://doi.org/10.1080/00401706.1964.10490163.
39. Wickham H. ggplot2: elegant graphics for data analysis. New York: Springer-Verlag New York; 2009.
40. Scheuvens D, Kandler K, Küpper M, Lieke K, Zorn RS, Ebert M, et al. Individual-particle analysis of airborne dust samples collected over Morocco in 2006 during SAMUM 1. Tellus Ser B Chem Phys Meteorol. 2011. https://doi.org/10.1111/j.1600-0889.2011.00554.x.
41. Worobiec A, de Hoog J, Osán J, Szalóki I, Ro C-U, Van Grieken R. Thermal stability of beam sensitive atmospheric aerosol particles in electron probe microanalysis at liquid nitrogen temperature.

Spectrochim Acta B At Spectrosc. 2003. https://doi.org/10.1016/S0584-8547(03)00013-2.
42. Coz E, Gómez-Moreno FJ, Pujadas M, Casuccio GS, Lersch TL, Artíñano B. Individual particle characteristics of North African dust under different long-range transport scenarios. Atmos Environ. 2009. https://doi.org/10.1016/j.atmosenv.2008.12.045.
43. Chen Y, Shah N, Huggins FE, Huffman GP, Linak WP, Miller CA. Investigation of primary fine particulate matter from coal combustion by computer-controlled scanning electron microscopy. Fuel Process Technol. 2004. https://doi.org/10.1016/j.fuproc.2003.11.017.
44. Yu D, Xu M, Zhang L, Yao H, Wang Q, Ninomiya Y. Computer-controlled scanning electron microscopy (CCSEM) investigation on the heterogeneous nature of mineral matter in six typical Chinese coals. Energy Fuel. 2007. https://doi.org/10.1021/ef060419w.
45. Sitzmann B, Kendall M, Watt J, Williams I. Characterisation of airborne particles in London by computer-controlled scanning electron microscopy. Sci Total Environ. 1999. https://doi.org/10.1016/S0048-9697(99)00326-5.
46. Sawvel EJ, Willis R, West RR, Casuccio GS, Norris G, Kumar HD, et al. Passive sampling to capture the spatial variability of coarse particles by composition in Cleveland, OH. Atmos Environ. 2015. https://doi.org/10.1016/j.atmosenv.2015.01.030.
47. Mogo S, Cachorro VE, de Frutos AM. Morphological, chemical and optical absorbing characterization of aerosols in the urban atmosphere of Valladolid. Atmos Chem Phys. 2005. https://doi.org/10.5194/acp-5-2739-2005.
48. Ebert M, Weinbruch S, Hoffmann P, Ortner HM. The chemical composition and complex refractive index of rural and urban influenced aerosols determined by individual particle analysis. Atmos Environ. 2004. https://doi.org/10.1016/j.atmosenv.2004.08.048.
49. Worringen A, Kandler K, Benker N, Dirsch T, Mertes S, Schenk L, et al. Single-particle characterization of ice-nucleating particles and ice particle residuals sampled by three different techniques. Atmos Chem Phys. 2015. https://doi.org/10.5194/acp-15-4161-2015.
50. Targino AC, Krejci R, Noone KJ, Glantz P. Single particle analysis of ice crystal residuals observed in orographic wave clouds over Scandinavia during INTACC experiment. Atmos Chem Phys. 2006. https://doi.org/10.5194/acp-6-1977-2006.
51. Iwata A, Matsuki A. Characterization of individual ice residual particles by the single droplet freezing method: a case study in the Asian dust outflow region. Atmos Chem Phys. 2018. https://doi.org/10.5194/acp-18-1785-2018.
52. Schütze K, Wilson JC, Weinbruch S, Benker N, Ebert M, Günther G, et al. Sub-micrometer refractory carbonaceous particles in the polar stratosphere. Atmos Chem Phys. 2017. https://doi.org/10.5194/acp-17-12475-2017.
53. Sheridan PJ, Brock CA, Wilson JC. Aerosol particles in the upper troposphere and lower stratosphere: elemental composition and morphology of individual particles in northern midlatitudes. Geophys Res Lett. 1994. https://doi.org/10.1029/94GL01387.
54. Mackinnon IDR, McKay DS, Nace G, Isaacs AM. Classification of the Johnson Space Center stratospheric dust collection. J Geophys Res Solid Earth. 1982. https://doi.org/10.1029/JB087iS01p0A413.
55. Kutchko BG, Kim AG. Fly ash characterization by SEM–EDS. Fuel. 2006. https://doi.org/10.1016/j.fuel.2006.05.016.
56. Matthias-Maser S, Jaefnicke R. Examination of atmospheric bioaerosol particles with radii > 0.2 μm. J Aerosol Sci. 1994. https://doi.org/10.1016/0021-8502(94)90228-3.
57. Coz E, Artíñano B, Clark LM, Hernandez M, Robinson AL, Casuccio GS, et al. Characterization of fine primary biogenic organic aerosol in an urban area in the northeastern United States. Atmos Environ. 2010. https://doi.org/10.1016/j.atmosenv.2010.07.007.
58. Valsan AE, Priyamvada H, Ravikrishna R, Després VR, Biju CV, Sahu LK, et al. Morphological characteristics of bioaerosols from contrasting locations in southern tropical India – a case study. Atmos Environ. 2015. https://doi.org/10.1016/j.atmosenv.2015.09.071.
59. Popovicheva O, Kireeva E, Persiantseva N, Timofeev M, Bladt H, Ivleva NP, et al. Microscopic characterization of individual particles from multicomponent ship exhaust. J Environ Monit. 2012. https://doi.org/10.1039/C2EM30338H.
60. Hamacher-Barth E, Leck C, Jansson K. Size-resolved morphological properties of the high Arctic summer aerosol during ASCOS-2008. Atmos Chem Phys. 2016. https://doi.org/10.5194/acp-16-6577-2016.
61. Engelbrecht JP, McDonald EV, Gillies JA, Jayanty RKM, Casuccio G, Gertler AW. Characterizing mineral dusts and other aerosols from the Middle East—part 1: ambient sampling. Inhal Toxicol. 2009. https://doi.org/10.1080/08958370802464273.
62. Zhang L, Sato A, Ninomiya Y. CCSEM analysis of ash from combustion of coal added with limestone. Fuel. 2002. https://doi.org/10.1016/S0016-2361(02)00065-0.
63. Andreae MO, Charlson RJ, Brynseels F, Storms H, Van Grieken R, Maenhaut W. Internal mixture of sea salt, silicates, and excess sulfate in marine aerosols. Science. 1986. https://doi.org/10.1126/science.232.4758.1620.
64. Kandler K, Schütz L, Jäckel S, Lieke K, Emmel C, Müller-Ebert D, et al. Ground-based off-line aerosol measurements at Praia, Cape Verde, during the Saharan Mineral Dust Experiment: microphysical properties and mineralogy. Tellus Ser B Chem Phys Meteorol. 2011. https://doi.org/10.1111/j.1600-0889.2011.00546.x.
65. Suzuki K. Characterisation of airborne particulates and associated trace metals deposited on tree bark by ICP-OES, ICP-MS. SEM-EDX and laser ablation ICP-MS Atmos Environ. 2006. https://doi.org/10.1016/j.atmosenv.2005.12.022.
66. Micheletti MI, Murruni LG, Debray ME, Rosenbusch M, Graf M, Ávila Cadena G, et al. Elemental analysis of aerosols collected at the Pierre Auger Cosmic Ray Observatory with PIXE technique complemented with SEM/EDX. Nucl Instrum Methods Phys Res B. 2012. https://doi.org/10.1016/j.nimb.2012.07.022.
67. Grawe S, Augustin-Bauditz S, Clemen HC, Ebert M, Eriksen Hammer S, Lubitz J, et al. Coal fly ash: linking immersion freezing behavior and physicochemical particle properties. Atmos Chem Phys. 2018. https://doi.org/10.5194/acp-18-13903-2018.
68. O'Brien RE, Wang B, Laskin A, Riemer N, West M, Zhang Q, et al. Chemical imaging of ambient aerosol particles: observational constraints on mixing state parameterization. J Geophys Res Atmos. 2015. https://doi.org/10.1002/2015JD023480.

Atmos. Chem. Phys., 18, 13903–13923, 2018
https://doi.org/10.5194/acp-18-13903-2018

Atmospheric Chemistry and Physics
Open Access
EGU

Coal fly ash: linking immersion freezing behavior and physicochemical particle properties

Sarah Grawe[1], Stefanie Augustin-Bauditz[1,a], Hans-Christian Clemen[2], Martin Ebert[3], Stine Eriksen Hammer[3], Jasmin Lubitz[1], Naama Reicher[4], Yinon Rudich[4], Johannes Schneider[2], Robert Staacke[5], Frank Stratmann[1], André Welti[1,b], and Heike Wex[1]

[1]Leibniz Institute for Tropospheric Research, Experimental Aerosol and Cloud Microphysics Department, Leipzig, Germany
[2]Max Planck Institute for Chemistry, Particle Chemistry Department, Mainz, Germany
[3]Darmstadt University of Technology, Institute of Applied Geosciences, Darmstadt, Germany
[4]Weizmann Institute of Science, Department of Earth and Planetary Sciences, Rehovot, Israel
[5]University of Leipzig, Felix Bloch Institute for Solid State Physics,
Division of Nuclear Solid State Physics, Leipzig, Germany
[a]now at: Deutscher Wetterdienst, Hamburg, Germany
[b]now at: Finnish Meteorological Institute, Helsinki, Finland

Correspondence: Sarah Grawe (grawe@tropos.de)

Received: 11 June 2018 – Discussion started: 3 July 2018
Revised: 29 August 2018 – Accepted: 7 September 2018 – Published: 2 October 2018

Abstract. To date, only a few studies have investigated the potential of coal fly ash particles to trigger heterogeneous ice nucleation in cloud droplets. The presented measurements aim at expanding the sparse dataset and improving process understanding of how physicochemical particle properties can influence the freezing behavior of coal fly ash particles immersed in water.

Firstly, immersion freezing measurements were performed with two single particle techniques, i.e., the Leipzig Aerosol Cloud Interaction Simulator (LACIS) and the SPectrometer for Ice Nuclei (SPIN). The effect of suspension time on the efficiency of the coal fly ash particles when immersed in a cloud droplet is analyzed based on the different residence times of the two instruments and employing both dry and wet particle generation. Secondly, two cold-stage setups, one using microliter sized droplets (Leipzig Ice Nucleation Array) and one using nanoliter sized droplets (WeIzmann Supercooled Droplets Observation on Microarray setup) were applied.

We found that coal fly ash particles are comparable to mineral dust in their immersion freezing behavior when being dry generated. However, a significant decrease in immersion freezing efficiency was observed during experiments with wet-generated particles in LACIS and SPIN. The efficiency of wet-generated particles is in agreement with the cold-stage measurements. In order to understand the reason behind the deactivation, a series of chemical composition, morphology, and crystallography analyses (single particle mass spectrometry, scanning electron microscopy coupled with energy dispersive X-ray microanalysis, X-ray diffraction analysis) were performed with dry- and wet-generated particles. From these investigations, we conclude that anhydrous $CaSO_4$ and CaO – which, if investigated in pure form, show the same qualitative immersion freezing behavior as observed for dry-generated coal fly ash particles – contribute to triggering heterogeneous ice nucleation at the particle–water interface. The observed deactivation in contact with water is related to changes in the particle surface properties which are potentially caused by hydration of $CaSO_4$ and CaO. The contribution of coal fly ash to the ambient population of ice-nucleating particles therefore depends on whether and for how long particles are immersed in cloud droplets.

Published by Copernicus Publications on behalf of the European Geosciences Union.

1 Introduction

It is known that naturally occurring aerosol such as biological particles (e.g., bacteria, pollen, spores) and mineral dust are acting as ice-nucleating particles (INPs; Hoose and Möhler, 2012 and references therein). In contrast, there is an ongoing discussion about the impact of anthropogenic aerosol emissions on the concentration of atmospheric INPs (e.g., Szyrmer and Zawadzki, 1997; Chen et al., 2018). The strongest source of anthropogenic aerosol is the combustion of fossil fuels, where primary particles such as carbonaceous aerosol and ash, as well as secondary particles from gaseous precursors, are generated.

Carbonaceous aerosol, such as soot, which is a product of incomplete combustion of organic material, has been shown to act as INPs (e.g., DeMott, 1990; Diehl and Mitra, 1998; Fornea et al., 2009). However, there are large discrepancies between studies investigating the ice nucleation ability of soot, which might be related to the source and/or mixing state of the particles (Kanji et al., 2017). Hoose and Möhler (2012) summarize that "soot is a generally worse ice nucleus than mineral dust". In contrast to soot and other carbonaceous aerosol types, ash only contains a limited amount of carbon. Defined as the solid remains from the combustion of organic substances, e.g., wood or fossil fuels, it mostly consists of the noncombustible constituents in the fuel, i.e., mineral inclusions and atoms other than C and H, e.g., K, Ca, Mn, Fe, etc. (Flagan and Seinfeld, 1988a). A distinction is made between the fine ash fraction, i.e., fly ash, that is emitted during combustion together with flue gases, and the coarse ash fraction, i.e., bottom ash. The latter is defined as the fraction that remains in the power plant, fireplace, or on the ground after a wildfire and can be emitted due to wind erosion.

Coal is difficult to substitute in the energy mix of most industrial countries and hence it is only slowly replaced by renewable energy sources (U. S. Energy Information Administration, 2017). In total, 6711 coal-fired power plants (30 MW and larger; endcoal.org, 2017; status: July 2017) are in operation worldwide, producing 600 Mt a^{-1} of coal ash (Ahmaruzzaman, 2010). The vast majority of this mass is not emitted into the atmosphere, as coal-fired power plants are equipped with different types of particle removal technology to clean flue gases of coal fly ash (CFA). Estimating CFA emissions is not trivial, because filtering systems show varying efficiencies and part of the collected CFA is emitted during disposal (Mueller et al., 2013). A rough assessment was given by Smil (2008), estimating that 30 Mt a^{-1} of CFA are released into the atmosphere worldwide. Reff et al. (2009) state that coal combustion causes $PM_{2.5}$ emissions of ~ 0.5 Mt a^{-1} in the USA. In addition to a large uncertainty in these estimates, there is no detailed information about temporal and spatial variability in CFA emission and dispersion, which is important for assessing the effect of CFA particles on cloud formation and glaciation.

A lot of research has already been conducted in the field of CFA sample characterization for identifying CFA particles in the atmosphere. This was mainly driven by concerns about the negative effects of CFA particles on human health (e.g., Davison et al., 1974; Damle et al., 1982; Yi et al., 2006; and references therein). These studies show that CFA has a complex and highly variable composition. Except for some trace elements whose contents are heterogeneously distributed among different size fractions, CFA composition is comparable to mineral dust, making it difficult to identify via single particle mass spectrometry (Cziczo et al., 2004, 2006; Kamphus et al., 2010). CFA particles are, in contrast to irregularly shaped mineral dust particles, often spherical because of their generation process, where minerals melt and form spherical droplets that retain their shape upon solidification (Damle et al., 1982; Flagan and Seinfeld, 1988a). However, shape is not a perfect criterion for identifying CFA, as other high-temperature processes such as fuel-oil combustion or metal processing also emit spherical fly ash particles. In addition, there are various aerosol types which occur in spherical shapes, e.g., biological particles (Huffman et al., 2012), tar balls (Laskin et al., 2006; Sedlacek III et al., 2018), or deliquesced salt particles (Freney et al., 2009). In conclusion, a reliable identification of CFA particles is not trivial and requires a combination of chemical composition and morphology analyses (e.g., DeMott et al., 2003; Weinbruch et al., 2010, 2012).

Concerning the ice nucleation activity of ash particles, only few studies have been published so far. Early investigations of aerosol from coal-fired power plant plumes were contradictory as to whether the particles are able to act as INPs (Parungo et al., 1978) or not (Schnell et al., 1976). More recent studies (Havlíček et al., 1993; Umo et al., 2015; Garimella, 2016; Grawe et al., 2016) agreed that ash particles indeed trigger heterogeneous ice nucleation. Havlíček et al. (1993) investigated chemical composition and ice nucleation characteristics of CFA from nine different power plants in the former Czechoslovakia focusing on the effect of water-soluble material in the samples. The chemical composition analysis showed that the water-soluble fraction of the samples varied between 0.43 and 1.34 wt % and mainly consisted of anhydrite (anhydrous $CaSO_4$). Ice nucleation experiments were carried out with two methods. Firstly, polydisperse CFA particles were aerosolized in a thermodiffusion chamber subsaturated with respect to liquid water at -15 °C, i.e., only deposition nucleation was investigated. Secondly, suspensions of CFA in distilled water were used to produce droplets onto a cooled plate (cold stage), i.e., immersion freezing was investigated. The water-soluble components were separated from all samples and ice nucleation experiments were carried out with the original samples, the water-insoluble components, and the water-soluble components. Immersion freezing was found to be less efficient than deposition nucleation in all cases. The water-insoluble components were up to 3 orders of magnitude less efficient in the

deposition mode than the untreated samples. However, when the water-soluble components alone were investigated, they showed surprisingly low efficiency. This finding illustrates the complex interplay of physicochemical particle properties and freezing behavior, as the water-soluble components increased the ice nucleation efficiency only when associated with the CFA particles.

Four ash samples including CFA, coal bottom ash, wood bottom ash, and bottom ash from a domestic oven were investigated by Umo et al. (2015). The immersion freezing behavior was quantified using a cold-stage setup (Whale et al., 2015). In comparison to the bottom ashes, CFA was more efficient at nucleating ice between −17 and −27 °C, showing a strong increase starting at −16 °C and an apparent plateau below roughly −24 °C. The bottom ashes behaved similar to one another, with a slight trend of coal bottom ash being less efficient and wood bottom ash being more efficient.

Garimella (2016) investigated the freezing behavior of four different CFA samples from the USA using the SPectrometer for Ice Nuclei (SPIN; Droplet Measurement Technologies Inc., Boulder, CO, USA). In this study, particles were dry-generated and size selected. Activated fractions of 1 % were observed at $T < -30$ °C ($1.25 < S_{ice} < 1.4$) for deposition nucleation and at $T < -20$ °C for immersion freezing. This is contradictory to the measurements by Havlíček et al. (1993) who found deposition nucleation to be more efficient than immersion freezing. When comparing measurements of CFA by Garimella (2016) and Umo et al. (2015), a discrepancy of more than 1 order of magnitude was found, with the cold-stage measurements being below the immersion freezing measurements with SPIN. In addition, Garimella (2016) showed that 300 nm particles are more efficient per unit surface area than 700 nm particles, possibly indicating that trace metals, which are enriched in smaller particles due to size-dependent cooling rates, could contribute to the immersion freezing efficiency. This could explain why the results by Umo et al. (2015), where the size distribution of immersed particles had a mode diameter of ∼ 10 µm, were much lower.

Previously (Grawe et al., 2016), we investigated the freezing behavior of wood bottom ash, coal bottom ash, and CFA. Experiments were performed with the Leipzig Aerosol Cloud Interaction Simulator (LACIS; Hartmann et al., 2011), a laminar flow tube in which single, size-selected particles are activated to droplets and cooled down to investigate immersion freezing (see Sect. 2.3.1). It was found that dry-generated CFA particles showed the highest immersion freezing efficiency of the examined samples, being only slightly less efficient below −27 °C than a K-feldspar sample (Augustin-Bauditz et al., 2014). Interestingly, a change in immersion freezing efficiency could be seen in the transition to wet particle generation, i.e., producing ash suspensions which were sprayed with an atomizer and sent through a dryer. In this case, a decrease towards the limit of detection was observed. As the size of dry- and wet-generated particles was identical, the deactivation contradicts the proposed hypothesis of Garimella (2016) that the size dependent enrichment of trace elements causes the discrepancy between measurements with single particle instruments and cold stages.

The presented study intends to function as a follow-up to our previous paper and aims at answering the following questions:

- Do CFA samples from different power plants feature a similar immersion freezing behavior?
- Is the deactivation of the ice nucleation properties in the transition from dry to wet particle generation observable for different CFA samples?
- Is it possible to find a connection between physicochemical sample properties and the observed immersion freezing behavior?
- Which particle generation technique (dry or wet particle generation) or measurement method (single particle or cold stage) is appropriate for representing atmospheric processes after CFA emission?

Four CFA samples from German power plants were investigated as immersion freezing INPs in an attempt to answer these questions. Additional sample characterization with respect to chemical composition, morphology, and crystallography, was performed and used for interpretation of the immersion freezing results.

2 Materials and methods

The immersion freezing and particle characterization measurements of CFA particles were performed during a campaign at TROPOS in November 2016 together with collaborators from the Ice Nuclei research UnIT (INUIT). The main setup (see Fig. 1) consists of particle generation, size selection, and distribution of the size-selected aerosol to the following instruments: (1) LACIS, (2) SPIN, (3) the Aircraft-based Laser ABlation Aerosol MAss spectrometer (ALABAMA), and (4) the multi-Micro INertial Impactor (multi-MINI) sampling particles onto substrates for environmental scanning electron microscopy coupled with energy dispersive X-ray spectroscopy (ESEM/EDX). In addition to LACIS and SPIN, immersion freezing measurements were performed with two cold-stage setups: (1) the Leipzig Ice Nucleation Array (LINA) and (2) the WeIzmann Supercooled Droplets Observation on Microarray (WISDOM) setup. For this, suspensions of CFA in water were prepared using the bulk material, which is why further bulk analyses regarding chemical composition and crystallography were performed.

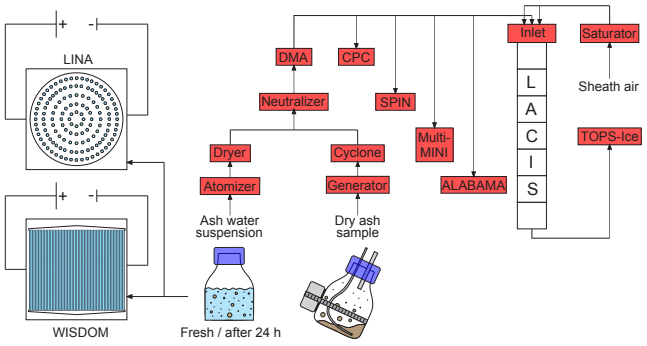

Figure 1. Instrumental setup during the INUIT campaign.

2.1 Origin of the samples

The CFA samples were taken from the electrostatic precipitators[1] of four coal-fired power plants in Germany. It is unknown which flue gas desulfurization technique is applied in the power plants or whether the electrostatic precipitators are installed up- or downstream of the flue gas desulfurization systems. This technical information could either not be obtained, or is unknown to us because the sample origin must remain anonymous. CFA1 is identical to the CFA sample from Grawe et al. (2016) and originates from the Lippendorf power plant situated 15 km south of Leipzig, Germany. CFA1, CFA2, and CFA4 are from brown (sub-bituminous) coal combustion, CFA3 is from black (bituminous) coal combustion.

Quicklime (CaO), anhydrite ($CaSO_4$), and gypsum ($CaSO_4 \cdot 2H_2O$) from Merck KGaA (Darmstadt, Germany) were used for additional investigations.

2.2 Sample preparation and particle generation

Two different kinds of particle generation were used in connection with the LACIS and SPIN immersion freezing experiments: dry particle generation, i.e., aerosolization of particles from dry ash powder, and wet particle generation, i.e., atomization of a CFA–water suspension. Suspensions were also used for the experiments with LINA and WISDOM.

[1]Electrostatic precipitators work on the principle of charging the particles and subsequently sending the flow through an electric field. Particles then migrate to the oppositely charged electrode and hence particulate matter is removed from the flue gas (Flagan and Seinfeld, 1988b). The precipitator itself does not alter particle properties like morphology or chemical composition, only number and mass size distributions are changed (Yi et al., 2006). However, it has been argued that particles which are not captured potentially contain a larger amount of species condensing from the gas phase onto the CFA surface upon cooling (Parungo et al., 1978).

2.2.1 Dry particle generation

The dry CFA samples were placed into an aerosol generator operating via pressurized air and an electric imbalance motor (Grawe et al., 2016). The samples were not sieved prior to aerosol generation. The aerosol was sent through a mixing bottle and a cyclone ($D_{50} = 500$ nm) to reduce the amount of large particles in the flow. Further downstream, a neutralizer was passed, before a differential mobility analyzer (DMA, Vienna type, medium) was used for size selection. A mobility diameter of 300 nm was chosen for the immersion freezing experiments with LACIS and SPIN for two reasons. Firstly, electrostatic precipitators have a minimum collection efficiency for particle sizes between 0.1 and 1 µm (Flagan and Seinfeld, 1988b; Nóbrega et al., 2004; Kim et al., 2012), meaning that CFA particles in this size range are more likely to be emitted compared to smaller or larger particles. Secondly, 300 nm particles will experience relevant atmospheric residence times once emitted (Jaenicke, 1978).

Afterwards, the quasi-monodisperse aerosol was distributed to a condensation particle counter (CPC, model 3010, TSI Inc., St. Paul, MN, USA), LACIS, SPIN, multi-MINI, and ALABAMA. ALABAMA measurements of vacuum aerodynamic diameter were used for multiply charged fraction determination. The multiple charge correction was made using frozen fraction values (f_{ice}, number of frozen hydrometeors divided by total number of hydrometeors). The method and results are described in Sect. S7 in the Supplement. Unfortunately, only data acquired in parallel to ALABAMA measurements could be corrected. Data without multiple charge correction are indicated.

2.2.2 Preparation of CFA suspensions for cold stages and wet particle generation

The CFA–water suspensions for LACIS, SPIN, and LINA measurements were prepared following the description in Umo et al. (2015). Briefly, a certain amount of CFA was mixed with distilled water (LINA: 0.1 g CFA in 100 mL water, LACIS and SPIN: 0.5 g CFA in 100 mL water) and ultrasonicated (RK100H Sonorex Super, BANDELIN electronic GmbH & Co. KG, Berlin, Germany) for 10 min. Afterwards, the suspension was stirred with a magnetic stirrer for 24 h. This approach was chosen to allow comparability to results by Umo et al. (2015) and Grawe et al. (2016). The procedure helps with breaking up large aggregates and hence prevents fast sedimentation that would lead to an uneven distribution of material in the droplets on LINA. As sedimentation is not a limiting factor for wet particle generation (a flask shaker was used), LACIS measurements were performed with both the standard suspensions (ultrasonification and 24 h stirring) and suspensions that were prepared right before the experiment by simply mixing 0.5 g CFA with 100 mL distilled water. In this way, particles were in suspension for no more than 5 min before being used for LACIS measurements. Due to in-

strument availability, SPIN measurements could only be performed with the standard suspensions. The suspensions, either fresh or standard, were sprayed with an atomizer (similar to Model 3076, TSI Inc., St. Paul, MN, USA) and resulting droplets were sent through a diffusion dryer. Then, size selection of the particles by the DMA and distribution to LACIS, SPIN, CPC, multi-MINI, and ALABAMA took place.

In contrast to LINA measurements, size selection of the CFA samples was necessary for WISDOM because large particles that are present in the original sample would clog the microfluidic device which is used for droplet production (see Sect. 2.3.4). Size selection took place by running dry particle generation (aerosol generator, mixing bottle, cyclone) for several hours and collecting the accumulated material from the cyclone ($D_{50} = 450$ nm). During this procedure, coarse material was deposited inside the mixing bottle and a subfraction of the bulk, hereafter referred to as fine CFA, remained in the cyclone. Suspensions of 0.1 g fine CFA in 100 mL distilled water were mixed for three cycles of 30 s each with 10 s break in a small-volume sonicator (UP200St, Hielscher Ultrasonics GmbH, Teltow, Germany) and were used for droplet production and immersion freezing experiments within 2 min.

2.3 Immersion freezing instrumentation

2.3.1 LACIS

LACIS is a laminar flow tube consisting of seven 1 m long sections, each temperature controlled by individual thermostats. At the inlet, the aerosol flow is enclosed by a humidified sheath flow. As a result, a stable 2 mm wide particle beam is created along the LACIS centerline, ensuring that all particles experience identical thermodynamic conditions. Supersaturation is created by adjusting the dew point of the sheath air and the wall temperature. Like this, each particle is activated to a droplet before being cooled down for immersion freezing investigation. The ice nucleation time in LACIS is 1.6 s.

Supercooled liquid droplets and ice particles coexist at the outlet of the tube in a certain temperature range above the homogeneous freezing limit. The thermo-stabilized Optical Particle Spectrometer for the detection of Ice (TOPS-Ice; Clauß et al., 2013) is used to determine the phase state of the hydrometeors and from this f_{ice}. The measurement principle exploits the difference in scattering properties, i.e., depolarization, between nonspherical ice particles and spherical liquid droplets.

At least 2000 hydrometeors were classified for each LACIS data point presented in this study. The only exception to this is the measurement with the fresh CFA3 suspension where, due to low particle number concentrations, only ~ 500 hydrometeors were considered (see Fig. 5). Occasionally, three or more data points of separate measurements under the same conditions were averaged. In these cases, the f_{ice} error is indicated by the standard deviation of the separate measurements. Otherwise, a Poisson error is given depending on the total number of classified hydrometeors in a single measurement. The temperature error of ± 0.3 K is defined by the temperature stability of the thermostats. The ice nucleation active surface site density n_{s} was calculated from Eq. (1) assuming the particle surface area A_{p} to be equal to the surface area of a sphere with a diameter of 300 nm.

$$n_{\mathrm{s}}(T) = -\frac{\ln(1 - f_{\mathrm{ice}}(T))}{A_{\mathrm{p}}} \quad (1)$$

2.3.2 SPIN

SPIN is a continuous flow diffusion chamber (CFDC) that has been described in detail by Garimella et al. (2016). In contrast to LACIS, the fraction of particles active as INPs (activated fraction, AF) is calculated by dividing the number of ice crystals detected with an optical particle counter (OPC) by the total number of aerosol particles measured with a CPC (model 3772, TSI Inc., St. Paul, MN, USA). A threshold size of 3 µm was used to identify ice crystals in the OPC signals. The uncertainty in AF is 14 % due to 10 % uncertainty in both CPC and OPC. The temperature uncertainties represent the highest and lowest deviations from the average lamina temperature in the chamber. When compared to LACIS measurements, SPIN data provide information on how immersion freezing results are affected by the different residence times in the two instruments. Ice nucleation times in SPIN depend on thermodynamic conditions and are between 8 and 12 s. In addition to the cyclone, an impactor (0.071 cm orifice, TSI Inc., St. Paul, MN, USA) with D_{50} = 500 nm was used upstream of the SPIN inlet to reduce the amount of multiply charged particles in the CFA aerosol. Hence, no multiple charge correction was applied to the SPIN data.

2.3.3 LINA

Based on the Bielefeld Ice Nucleation ARraY (BINARY; Budke and Koop, 2015), the newly developed LINA is a cold-stage setup for investigating immersion freezing. Ninety suspension droplets, each 1 µL in volume, were placed into separate compartments onto a hydrophobic glass slide. The compartments, formed by a perforated aluminum plate covered with a second glass slide, prevent interaction between the droplets, e.g., via the Wegener–Bergeron–Findeisen process or splintering while freezing. Also, the compartments suppress evaporation of the droplets. A cooling stage (LTS120, Linkam Scientific Instruments, Waterfield, UK) with a 40 mm × 40 mm Peltier element is used for cooling the sample array at a rate of 1 K min^{-1}. A thin layer of squalene oil on top of the Peltier element guarantees direct contact to the glass slide and improves heat transfer away from the droplets. The setup is situated in an aluminum housing that is purged with particle-free, dry air during the exper-

iment. See Chen et al. (2018) for details on the temperature calibration routine.

The determination of f_{ice} is almost fully automated. A digital camera coupled with an LED dome light takes images every 6 s, which is equal to a temperature resolution of 0.1 K at a cooling rate of 1 K min^{-1}. Parts of the LED light are shielded with a cardboard ring to cause ring-shaped structures to be reflected from the liquid droplets. As the reflective properties of a droplet change upon freezing, the reflection of the ring vanishes directly after the phase change. The images, each relating to a certain temperature, are later imported into a computer program that detects the number of rings. From this, $f_{ice}(T)$ can be derived. See Appendix A for details on the correction of LINA data with respect to background INPs, calculation of n_s, and error estimation.

2.3.4 WISDOM

The WISDOM setup (Reicher et al., 2018) was used to study the immersion freezing of the fine CFA fraction. WISDOM is a freezing array of monodisperse nanoliter droplets that are produced by a microfluidic device and subsequently arranged into an array of chambers based on Schmitz et al. (2009). Droplets are suspended in an oil mixture, consisting of mineral oil (Sigma Aldrich, St. Louis, MO, USA) stabilized with 2 wt % non-ionic surfactant (span80®, Sigma Aldrich, St. Louis, MO, USA). Pure water droplets within the device can be supercooled to below −35 °C, where first freezing occurs, i.e., above this temperature no correction regarding background INPs is necessary. The temperature accuracy of WISDOM is 0.34 °C. Freezing is observed by a microscope (BX51 with 10× objective and transmission mode, Olympus Optical, Tokyo, Japan) and detected for each droplet individually when the optical brightness of the droplet decreases due to the formation of ice crystals. The microfluidic devices are fabricated in the laboratory from polydimethylsiloxane and attached to a 1 mm microscope slide using oxygen plasma treatment. Freezing experiments are conducted in a commercial cryostage (THMS600, Linkam Scientific Instruments, Waterfield, UK) at a cooling rate of 1 K min^{-1}.

n_s was determined according to Eq. (2), with the droplet volume $V_{drop} = 478 \pm 78$ pL, the Brunauer–Emmett–Teller (BET; Brunauer et al., 1938) specific surface area of the fine CFA fraction A_{BET} (see Sect. S8), and the concentration of CFA in suspension C. The n_s error was estimated by propagating the uncertainties in the measurements of V_{drop} and A_{BET}, and the Poisson distribution of particles in suspension.

$$n_s(T) = -\frac{\ln(1 - f_{ice}(T))}{V_{drop} \cdot A_{BET} \cdot C} \quad (2)$$

2.4 Sample characterization

In the following sections, we describe the instrumentation used for the analyses of chemical composition, morphology, and crystallography of the CFA samples. The most important findings, which will be referred to in the discussion of the immersion freezing results (see Sect. 3), are summarized. For more details concerning sample characterization, see the Supplement.

2.4.1 Size-selected CFA

ALABAMA

ALABAMA, which was originally developed for aircraft operation (Brands et al., 2011) but is also used in ground-based campaigns (Roth et al., 2016; Schmidt et al., 2017), is a single particle laser ablation instrument using a Z-shaped time-of-flight mass spectrometer. After entering the instrument, aerosol particles are focused to a narrow particle beam by an aerodynamic lens. In the following, the particles pass two subsequent detection lasers (wavelength of 405 nm). Information about the time-of-flight between the detection lasers is needed to trigger the ablation laser. In addition, the time-of-flight can be used to calculate the particle vacuum aerodynamic diameter for particles in a size range between ∼ 200 and 2500 nm. The ablation laser, a Nd:YAG operating at a wavelength of 266 nm, evaporates the particles and ionizes the molecule fragments. The resulting ions are analyzed in the bipolar mass spectrometer such that one anion and one cation spectrum is obtained for each single particle, yielding information about their chemical composition. Single particle mass spectra were averaged, resulting in a mean chemical composition of each CFA sample for both dry and wet particle generation.

The overall composition of the CFA samples is comparable to mineral dust, as elements like Al, Ca, K, Fe, Si, S, P, Na, and Mg frequently occur. Some trace elements seem to be characteristic for the sampled CFA particles. Especially Ti-, Sr-, and Ba-related mass-to-charge ratios occur in more than 50 % of all dry-sampled particles (see Figs. S1 and S2) and could potentially be used as indicators for CFA particles in the atmosphere, together with the overall fingerprint of their mass spectra. There are some features that could explain differences in immersion freezing behavior between the different samples (see Fig. S4). For example, CFA1 has the highest concentration of Ca and S in 300 nm particles and CFA3 has the lowest concentration of Ca and S in 300 nm particles, whereas CFA3 has the highest concentration of Si in 300 nm particles and CFA1 has the lowest concentration of Si in 300 nm particles. Furthermore, CFA1 is the sample with the highest concentration of Pb in 300 nm particles. The comparison of averaged mass spectra of dry- and wet-generated CFA particles indicates the hydration of oxides, e.g., CaO, SrO, and BaO, in suspension (see Fig. S3). S-containing substances are present to a lower extent in wet-generated CFA compared to dry-generated particles. A more detailed description of the ALABAMA results is given in Sect. S1.

Multi-MINI – ESEM/EDX

Particles were collected on boron substrates behind the DMA with the multi-MINI (Ebert et al., 2016), using one stage with $D_{50} = 1\,\mu m$. Sampling durations ranged from 30 s to 6 min, depending on average particle number concentrations of the different samples (80 to 300 cm^{-3}). Chemical composition, size, and morphology were investigated with a Quanta 400 FEG ESEM (FEI Company, Hillsboro, OR, USA). No coating was applied to the substrates prior to the ESEM/EDX investigations. Particles impacted on the substrate located in the impaction spot were randomly selected for analysis. Chemical elements with an atomic number larger than 5 were detected with an EDX detector and analyzed with the AZtec software (version 3.3 SP1, Oxford Instruments, Abingdon, UK). All measurements were carried out with 12.5 keV, 10 mm working distance, and 20 s acquisition time per particle.

The ESEM images (see Figs. S5 and S6) show that CFA1 is special in terms of particle morphology. Dry-generated CFA1 particles consist of irregularly shaped agglomerates of small spherules, which were not observed to this extent for the other samples. Wet-generated CFA1 particles appear to be an external mixture of spherules and needle-shaped particles. CFA1 is the only sample for which needle-shaped particles were observed in connection with wet particle generation, and also the only sample for which a clear difference in morphology was observed between the dry and wet particle generation methods. The major elements detected by EDX agree with the ones identified in the ALABAMA mass spectra (see Table S1). However, trace elements, e.g., Ti, Sr, and Ba, could not be found, presumably for statistical reasons. A more detailed description of the ESEM/EDX results is given in Sect. S2.

2.4.2 Bulk CFA

XRD

For the crystallographic characterization of the CFA samples, X-ray diffraction (XRD) analyses were performed with both dry particles and suspension particles. Dry particles were ground using a mortar and pestle before being pressed into a sample holder as densely as possible. CFA suspensions were prepared as for the LACIS measurements (see Sect. 2.2.2) and then left in a desiccator (steady flow of particle-free, dry air) until all water was evaporated. The remaining dry powder was pressed into a sample holder. Both procedures were applied to all four samples, resulting in eight measurements. A Bragg–Brentano diffractometer with a Cu anode (Philips X'Pert, PANalytical, Almelo, the Netherlands) was used to perform 2Theta-Omega scans from 10 to 70° with a step size of 0.03° and an integration time of 20 s. Quantitative phase identification was done by Rietveld refinement using reference patterns from the Crystallography Open Database (Gražulis et al., 2009).

The XRD patterns indicate quartz (SiO_2) as the major crystalline phase in all CFA samples (see Figs. S7 to S10). Furthermore, anhydrite and quicklime occur in all samples, but to the largest extent in CFA1. CFA1 is also the only sample where a definite change can be seen between the original dry sample and the sample that was produced by evaporating all water from the suspension. Here, the conversion of anhydrite ($CaSO_4$) to gypsum ($CaSO_4 \cdot 2H_2O$, see R1) and the conversion of quicklime (CaO) to calcite ($CaCO_3$, see R2 and R3) can be observed. CFA3 is the sample with the highest amorphous, i.e., noncrystalline, fraction in bulk, and likely also in 300 nm particles, as an increase in the amorphous fraction in CFA towards smaller particle sizes has been reported in a previous study (Matsunaga et al., 2002). A more detailed description of the XRD results is given in Sect. S3.

$$CaSO_4(s) + 2H_2O(l) \rightarrow CaSO_4 \cdot 2H_2O(s) \quad \text{(R1)}$$

$$CaO(s) + H_2O(l) \rightarrow Ca(OH)_2(s) \quad \text{(R2)}$$

$$Ca(OH)_2(s) + CO_2(aq) \rightarrow CaCO_3(s) + H_2O(l) \quad \text{(R3)}$$

Chemical composition

The bulk chemical composition analysis was performed using inductively coupled plasma-sector field mass spectrometry (ICP-SFMS) at ALS Scandinavia AB (Luleå, Sweden). Measured mass fractions of major ions were recalculated into their most common oxide forms (see Fig. S11). Because of its high CaO content of 26 wt %, CFA1 is classified as class C CFA according to the American Society for Testing Materials (ASTM, 2015, standard C618). Class C CFA is cementitious, i.e., self-hardening in contact with water. The occurrence of needle-shaped particles in wet-generated CFA1 could cause this cementitious property. CFA2, CFA3, and CFA4 are class F CFA, meaning that additives are needed to induce hardening of a CFA–water mixture. Loss on ignition (LOI) values were determined by heating a defined amount of the CFA samples to 1000 °C and comparing pre- and post-ignition weights. LOI values are proportional to the amount of unburnt fuel resulting from incomplete combustion in the power plants. No weight change within measurement uncertainty was registered for CFA1, CFA2, or CFA3. CFA4 still contains a relevant amount of unburnt fuel (LOI = 8.1 ± 5 %). A more detailed description of the bulk chemical composition results is given in Sect. S4.

In addition to the ICP-SFMS and LOI measurements, water activity and pH values of CFA suspensions were determined. The water activity of the CFA samples was ∼ 1, i.e., no difference to pure water could be detected. The CFA2, CFA3, and CFA4 suspensions were neutral to slightly alkaline (pH ∼ 7–8). The CFA1 suspension was strongly alkaline (pH ∼ 11), likely due to the high CaO content and the for-

mation of portlandite ($Ca(OH)_2$, see R2) which dissociates into Ca^{2+} and OH^- ions.

3 Results and discussion

In the following, refer to Fig. 2 for comparing LACIS measurements of individual CFA samples with measurements of different substances contained in CFA. Figure 3 shows SPIN results of measurements with our German CFA samples and four CFA samples from the USA (Garimella, 2016). Figure 4 shows the comparison of CFA results from LACIS, LINA, and WISDOM and the intercomparison between samples.

3.1 Dry particle generation

3.1.1 CFA

LACIS measurements with dry-generated CFA particles are reported between −26 °C, where the first signal above the limit of detection could be observed, and −37 °C, where homogeneous ice nucleation starts to contribute. Data showing measurements with dry-generated particles from CFA1 have previously been published in Grawe et al. (2016). Comparing the n_s spectra of all four CFA samples (see full circles in Fig. 4) shows variation within a factor of 37 (difference between CFA2 and CFA3 at −28 °C). CFA1 has the highest n_s, followed by CFA2, CFA4, and CFA3. This order is valid throughout the whole examined temperature range, except for $T > -29$ °C, where n_s decreases rapidly in case of CFA1. The curve shape for $T < -29$ °C with the relatively shallow increase is comparable for all samples. The broad temperature range, in which the increase in n_s is observed, hints at a variety of different types of ice nucleation active sites at the surface of the CFA particles. In case of uniform ice nucleation properties, a steep increase would be observed.

To put the efficiency of the CFA particles into perspective, Fig. 2 includes fits to LACIS measurements with a K-feldspar sample (76 % microcline, 24 % albite) and different kinds of mineral dust that featured a similar immersion freezing behavior after coating with sulfuric acid (clay mineral baseline) by Augustin-Bauditz et al. (2014). Dry-generated CFA particles are not as efficient as the K-feldspar sample, which is also the most efficient mineral dust sample investigated with LACIS so far, but CFA1 is only 1 order of magnitude below. All of our dry-generated CFA samples are at least 1 order of magnitude above the clay mineral baseline for $T < -29$ °C. In conclusion, the dry-generated CFA particles are comparable to mineral dust in their immersion freezing behavior.

Figure 3 shows a comparison of SPIN measurements with 300 nm CFA particles between this study and Garimella (2016), who performed immersion freezing measurements with four CFA samples from the USA, two class C and two class F samples. Note that horizontal error bars indicating the temperature uncertainty are only included for CFA2 and CFA4. This was done for greater clarity in the case of CFA1 and CFA3, for which more data are available and temperature uncertainties are comparable to the values shown in the CFA2 and CFA4 panels. Only towards the warmer end of the examined temperature range, n_s of the samples from the USA is comparable to what we found for the German ones. At −36.5 °C, the lowest temperature at which both instruments have been operated, n_s of the samples from the USA is up to 2 orders of magnitude lower than n_s of the German samples. In general, the n_s spectra of the samples from the USA have a much shallower slope than the German CFA n_s spectra. As the same type of instrument was used for both investigations, we conclude that differences between the German samples and the samples from the USA originate from differences in physicochemical particle properties, and not from differences in methodology. Both SPIN experiments, ours and that of Garimella (2016), have in common that no large inter-sample variability was observed. This is in contrast to LACIS, where the class C CFA (CFA1) clearly has the highest efficiency. SPIN results have earlier been shown to differ from results obtained with instruments specially developed to measure immersion freezing (DeMott et al., 2015; Burkert-Kohn et al., 2017). See Sect. 4 for details on the intercomparison between SPIN and LACIS in the framework of the present study.

3.1.2 Comparison of CFA with anhydrite, quicklime, and quartz

From the comparison of n_s to chemical information from ALABAMA measurements, it was concluded that components containing Ca and S could contribute to the observed differences in immersion freezing behavior between the CFA samples (see Fig. S4a). The occurrence of the Ca cation cluster series ($(CaO)_n$, $(CaO)_nH$, and partially $Ca(CaO)_n$) together with the S anion cluster series (SO_n, see Fig. S1) could be an indication for the presence of anhydrite, as suggested by Gallavardin et al. (2008). Therefore, anhydrite and also quicklime were chosen as test substances for additional LACIS measurements. To our knowledge, these are the first immersion freezing measurements using dry-generated anhydrite and quicklime particles. Both substances are known to occur in CFA and are enriched in submicron CFA particles (Enders, 1996; Querol et al., 1996). Anhydrite is of special interest because Havlíček et al. (1993) found that water-soluble material on the CFA particle surface is mainly anhydrite and suggested that it is responsible for initiating heterogeneous freezing on the particles.

Both anhydrite and quicklime are efficient INPs in the immersion mode when being dry generated (see Fig. 2). Note that multiple charge correction was not possible for LACIS measurements with anhydrite and quicklime (in contrast to CFA). The correction would shift the n_s spectra of anhydrite and quicklime towards lower n_s values but the slope would stay the same. Generally, multiple charge correction lowers

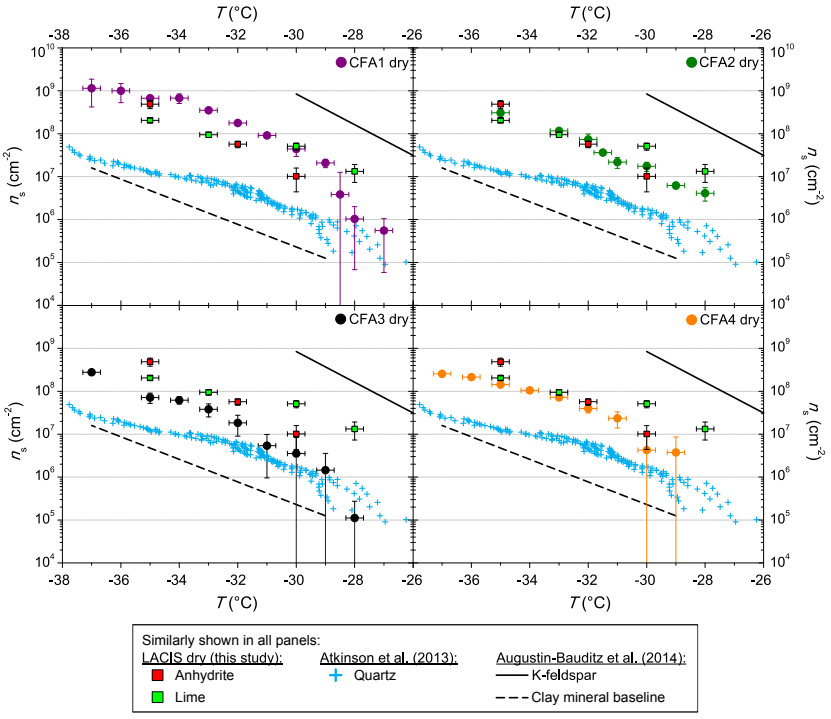

Figure 2. n_s from LACIS measurements with dry-generated CFA particles. Measurements with dry-generated anhydrite and quicklime are included for comparison in all panels but are (in contrast to CFA) not corrected with respect to multiple charges. Measurements with quartz shown in all panels are taken from Atkinson et al. (2013). Fit lines to LACIS measurements with a K-feldspar sample and different kinds of mineral dust coated with sulfuric acid (clay mineral baseline) are taken from Augustin-Bauditz et al. (2014).

n_s values for the dry-generated CFA particles by less than a factor of 3.5 and we expect that it would be comparable for the anhydrite and quicklime particles. Anhydrite is more efficient than quicklime at $T = -35\,°C$ (a factor of 2) and less efficient at $T = -30\,°C$ (a factor of 5), i.e., there is a slightly steeper slope of the anhydrite n_s spectrum. The shape and magnitude of the anhydrite n_s spectrum are comparable within measurement uncertainty to what was found for CFA2 and CFA4. CFA3, which contains the lowest concentration of Ca and S, and presumably the lowest concentration of anhydrite in 300 nm particles, is less efficient than pure anhydrite. CFA1 is more efficient than pure anhydrite, indicating that other compounds might influence the immersion freezing efficiency of this sample. A possible component contributing to n_s of CFA1 might be Pb, which occurs in 20 % of 300 nm particles from CFA1 (in $\leq$10 % of particles from CFA2, CFA3, and CFA4, see Fig. S2) and has been discussed previously as a potential INP, or as amplifying the ice nucleation efficiency of other compounds (Cziczo et al., 2009; Kamphus et al., 2010).

Quartz – which is the main crystalline phase of all our CFA samples according to XRD measurements and likely also occurs in 300 nm CFA particles (Si was identified by both ALABAMA and ESEM/EDX) – is at least 1 order of magnitude less efficient than CFA1, CFA2, and CFA4. We compared the CFA results to cold-stage measurements of quartz by Atkinson et al. (2013) here because this dataset spans the relevant temperature range and because there is a lack of immersion freezing results of dry-generated quartz in the literature. The n_s spectrum of CFA3, which contains the highest concentration of Si (presumably quartz) in 300 nm particles is higher by a factor of 2 to 10 compared to the quartz n_s spectrum. This indicates that quartz might contribute to some of the observed immersion freezing behavior, especially in the case of CFA3, but it is not the most active component in CFA1, CFA2, and CFA4; ALABAMA results showing that 300 nm particles in CFA1 contain the lowest concentration of Si compounds, followed by CFA2 and CFA4, support this hypothesis (see Fig. S4b).

The hypothesis that the amorphous material in CFA has a promoting effect on its immersion freezing efficiency (Umo et al., 2015) cannot be confirmed for our samples. XRD investigations show that CFA3, which was the least efficient of the four dry-dispersed samples, contains the highest amorphous fraction.

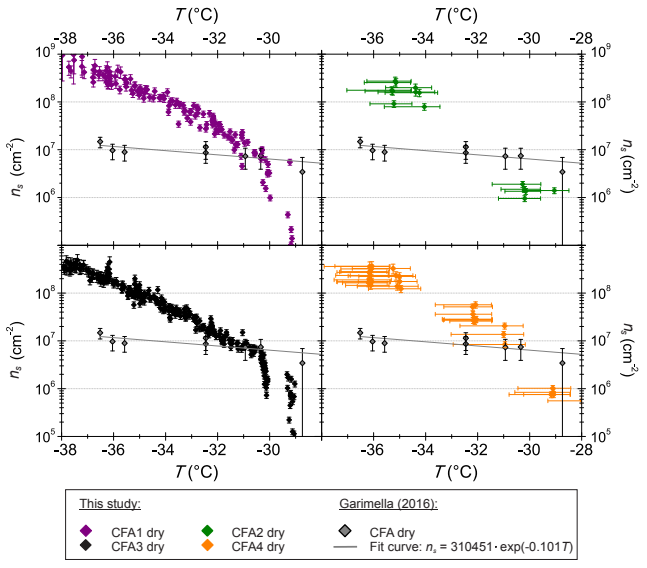

Figure 3. n_s from SPIN measurements with dry-generated 300 nm CFA particles. Horizontal error bars are omitted in the CFA1 and CFA3 panels for greater clarity but are comparable to the values shown in the CFA2 and CFA4 panels. Measurements with CFA samples from the USA (Garimella, 2016) are included for comparison.

3.2 Suspension methods

3.2.1 CFA

Figure 4 summarizes n_s derived from LACIS measurements with dry- and wet-generated CFA particles (full and open circles), n_s from WISDOM measurements with the fine CFA fraction (squares), and n_s from LINA measurements with the bulk CFA (triangles). Firstly, LACIS results will be described and then compared to those of the other two instruments. Secondly, we will compare these to measurements with the hydration products of anhydrite and quicklime by Zolles et al. (2015), and finally to measurements with a CFA sample of different origin by Umo et al. (2015). A comparison to measurements by Havlíček et al. (1993) is unfeasible because no specific surface area values of the samples are given in this publication.

LACIS

When comparing n_s from LACIS measurements with dry-generated particles (full circles in Fig. 4) to measurements with wet-generated particles (open circles), a significant decrease can be seen. The n_s values at −35 °C were lowered by between 1 (CFA3) and 4 (CFA2) orders of magnitude. The n_s values of wet-generated particles vary by up to 2 orders of magnitude between the four CFA samples. This can possibly be attributed to low values of f_{ice} that are only slightly above values usually measured for homogeneous nucleation (see Fig. B1), i.e., close to the limit of detection. As a result, the error in f_{ice} and n_s is larger than for the dry-generated particles at the same temperature.

Note that data for wet-generated CFA1 particles differ from those published in Grawe et al. (2016), which needed to be corrected due to the identification of a sample-specific artifact (see Appendix B). ESEM images from both Grawe et al. (2016) and the present study show two different particle types sampled after wet particle generation and size selection of CFA1, i.e., spheroidal particles and needle-shaped particles (see Figs. S5 and S6).

The occurrence of needle-shaped particles suggests that compounds are dissolved from the particles in suspension. During LACIS measurements, purely water-soluble particles, i.e., particles which do not contain water-insoluble material, would activate to droplets that then would only freeze homogeneously, causing an underestimation of f_{ice}. To make sure that no purely water-soluble particles with a size of 300 nm were produced when spraying the suspensions, size distributions of particles from all CFA suspensions were measured before LACIS experiments took place. From the size distribution measurements (see Sect. S5), we conclude that a negligibly small number of purely water-soluble particles with a size of 300 nm was produced from CFA2, CFA3, and CFA4, i.e., the decrease we observe in the transition from dry to wet particle generation is not caused by a measurement artifact. The evaluation of the CFA1 size distribution is not unambiguous because of the superimposition of size distributions of spheroidal and needle-shaped particles.

A decrease in immersion freezing efficiency from dry to wet particle generation was already reported for CFA and coal bottom ash in Grawe et al. (2016). A possible explanation for the observed discrepancy was presented following previous investigations of Hiranuma et al. (2015), who conducted immersion freezing measurements with both dry-dispersed mineral dust and mineral dust suspensions. There it was hypothesized that the increased time that the particles spend in contact with water leads to a change in chemical particle properties. For our previous study (Grawe et al., 2016), it was not possible to identify relevant processes because information on the chemical composition of 300 nm particles was missing. In the framework of the present study, differences in chemical composition of dry- and wet-generated CFA particles were identified (see Sects. 2.4 and S1), and will be discussed in relation with the immersion freezing results in Sect. 3.2.2.

Comparison of LACIS, LINA, and WISDOM results

LINA measurements (triangles in Fig. 4) were performed between 0 and −26 °C. In the temperature range from −8 to −23 °C, CFA3 has the highest, and CFA4 the lowest n_s values of all samples, with those being 2 orders of magnitude apart. According to LOI measurements (see Sect. S4), CFA4 contains the highest amount of unburnt fuel, which is

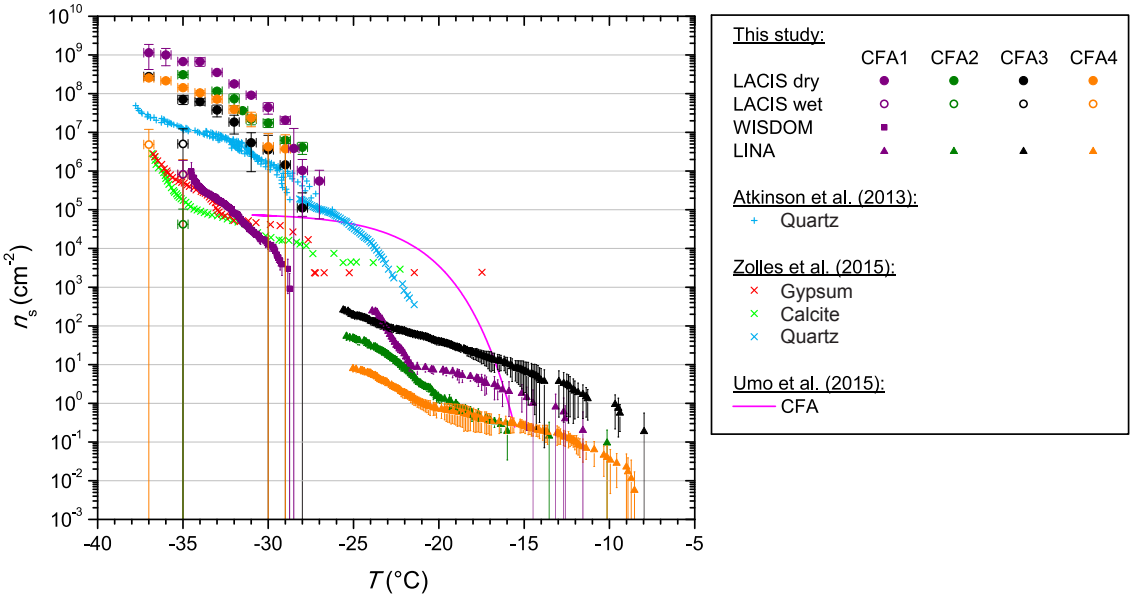

Figure 4. n_S from LACIS measurements with dry- and wet-generated 300 nm particles. n_S from WISDOM measurements with the fine CFA fraction and n_S from LINA measurements with bulk material are included for comparison. Measurements with gypsum, calcite, and quartz are taken from Zolles et al. (2015) and Atkinson et al. (2013), measurements with a CFA sample of different origin from Umo et al. (2015).

presumably made up of carbonaceous particles. The low immersion freezing efficiency of CFA4 in the investigated temperature range could hence be related to the occurrence of carbonaceous particles, which have previously been found to be inefficient at nucleating ice in the immersion mode (e.g., Chen et al., 2018). CFA1 shows a steep increase in n_S between −21 and −24 °C, below which all droplets were frozen. In contrast, the last droplets of CFA2, CFA3, and CFA4 suspensions froze below −25 °C. Note that coagulation of particles in the suspensions, which was observed to some extent for CFA suspensions with higher concentrations (see Fig. S13), might have a reducing effect on the surface area available for ice nucleation in the cold-stage measurements (Emersic et al., 2015).

WISDOM measurements (squares in Fig. 4) were performed as an attempt to close the temperature gap between LACIS measurements with wet-generated particles ($T \leq -35$ °C) and LINA measurements ($T \geq -26$ °C). This could not be realized for two reasons. Firstly, WISDOM measurements with suspensions of 0.1 g CFA in 100 mL distilled water were only possible with CFA1, because the other samples showed no immersion freezing activity. Increasing the concentration to a level, for which signals above the homogeneous freezing limit could be expected, led to strong settling of particles in the CFA2, CFA3, and CFA4 suspensions. Secondly, freezing was only observed for $T \leq -29$ °C for CFA1, i.e., there is no temperature overlap between LINA and WISDOM. However, extrapolation suggests that both instruments could yield similar results.

Good agreement can be observed for WISDOM and LACIS at $T \approx -35$ °C with CFA1. At this temperature, the contribution of homogeneous nucleation is still minor in WISDOM measurements and hence we conclude that the major contribution to the observed freezing behavior is due to immersion freezing triggered by CFA particles. The good agreement between WISDOM and LACIS firstly implies that there is no pronounced effect of size-dependent composition on the immersion freezing behavior of CFA1. This finding could be specific to CFA1, as it is in contrast to Garimella (2016), who found that n_S increases with decreasing particle size. Secondly, the successful instrument intercomparison indicates that drying of the CFA1 suspension droplets after atomization (which does not take place in WISDOM experiments) does not have a strong effect on the immersion freezing efficiency of the CFA1 particles.

Comparison to Umo et al. (2015)

Cold-stage measurements with a CFA sample of different origin by Umo et al. (2015, see Fig. 4) yielded results that differ substantially from what we measured in the framework of the present study. The efficiency of the sample investigated by Umo et al. (2015) increases strongly for $-20\,°C < T < -15\,°C$ and levels off from $T < -25\,°C$. This is in contrast to the gradual increase over a broad temperature range that we observed for our samples. Our suspensions were prepared in the same way as described by Umo et al. (2015), and LINA and the microliter Nucleation by Immersed Particles Instrument (µL-NIPI; Whale et al., 2015)

used by Umo et al. (2015) have successfully been intercompared with a different ash sample (not shown). Therefore, we infer that the CFA samples are really different in their immersion freezing behavior and we do not observe artifacts related to methodology. The comparison to Umo et al. (2015), and the results by Garimella (2016) shown in Figs. 3 and 4, suggest that CFA samples from different geographical origin show a highly variable immersion freezing behavior.

3.2.2 Comparison of CFA with gypsum and calcite

A comparison of ALABAMA measurements of dry- and wet-generated CFA particles hints at hydration of several oxides (see Fig. S3). It is difficult to say which hydration reactions in the complex mixture cause the decrease in immersion freezing behavior in measurements with the suspension methods. However, for bulk CFA1 there is clear evidence from XRD measurements that anhydrite and quicklime, which were already identified as species potentially influencing immersion freezing of the dry-generated particles, are hydrated in suspension, resulting in the formation of gypsum and calcite (see Fig. S7). In the following, we compare immersion freezing results of CFA suspension particles to measurements presented in Zolles et al. (2015) of gypsum and calcite (see Fig. 4).

Both hydration products, i.e., gypsum and calcite, are lower in their immersion freezing efficiency by 3 orders of magnitude compared to anhydrite and quicklime, i.e., as for CFA there is a significant decrease in efficiency of the hydration products compared to their anhydrous precursors. In general, gypsum and calcite are similar in their immersion freezing efficiency. LACIS measurements with wet-generated CFA and WISDOM measurements agree with the gypsum and calcite results within 1 order of magnitude. The only exception to this is CFA3 which will be discussed below in relation to quartz.

The hydration of anhydrite inevitably takes place once CFA comes into contact with water, because anhydrite is present at the particle surface (Enders, 1996). Sievert et al. (2005) described the hydration of pure anhydrite particles in the following way. Firstly, anhydrite is dissolved from the particles and Ca^{2+} and SO_4^{2-} ions are hydrated in the solution. The hydrated ions are then adsorbed to the surface of the anhydrite particles due to electrostatic attraction. From this point on, further dissolution and interaction of water molecules with the anhydrite surface is reduced because of the adsorbed layer of hydrated ions. Secondly, as the thickness of the adsorbed layer increases, cracks are formed through which water molecules migrate to the anhydrite surface. Only then, nuclei of gypsum are formed and crystallization takes place. The first process (formation of the adsorbed layer of hydrated ions) is thought to happen rather quickly; the second process (formation of gypsum) can take several hours up to days. See Sects. 3.3 and 4 for details on the duration of hydration.

The formation of calcite occurs via the hydration of quicklime to portlandite ($Ca(OH)_2$) which is then carbonated (see R2 and R3). It is possible that this process causes the precipitation of needle-shaped particles in suspension, but only if the quicklime content is sufficiently high (as for CFA1). It cannot be ruled out that calcite is also formed in the other CFA suspensions; however, in contrast to CFA1, calcite could not be clearly identified in the other samples by XRD.

Possibly, both above-described mechanisms, and potentially even more hydration reactions, cause the observed decrease in immersion freezing efficiency in the transition from dry to wet particle generation. Additional LACIS measurements with different sample treatments were performed to verify this hypothesis (see Sect. 3.3).

3.2.3 Comparison of CFA with quartz

In addition to quartz measurements by Atkinson et al. (2013), we now include quartz measurements by Zolles et al. (2015) in our discussion because they cover $T > -28\,^{\circ}\mathrm{C}$, which is the more relevant temperature range for our cold-stage measurements with CFA. We compare these to the most efficient of the quartz samples investigated by Zolles et al. (2015). The n_s spectra of the quartz samples used by Zolles et al. (2015) and Atkinson et al. (2013) agree in the narrow temperature overlap ($-26\,^{\circ}\mathrm{C} < T < -28\,^{\circ}\mathrm{C}$). It is obvious that quartz is significantly more efficient in the immersion mode than suspended particles of CFA1, CFA2, and CFA4, with n_s being at least 1 order of magnitude higher over the complete investigated temperature range. The deviation is smallest for CFA3 which contains the highest concentration of Si species (quartz) and lowest concentration of Ca and S species in 300 nm particles. For this sample, we assume the smallest effect of the hydration reactions and a larger influence of quartz on the immersion freezing behavior compared to the other samples. The fact that the other samples also contain significant amounts of quartz – both in 300 nm particles and in bulk, and, nevertheless, feature a much lower efficiency – supports the hypothesis of the particles being covered by a layer which suppresses the ice nucleation efficiency of the quartz. In the case of the dry particle generation method, the layer is more efficient at initiating immersion freezing than quartz. In the case of the suspension methods, the layer is less efficient than quartz, with this change brought on by the above-described hydration reactions.

3.3 Effect of sample treatment on the immersion freezing efficiency of CFA

Additional LACIS measurements with differently treated CFA and anhydrite samples, as well as pure gypsum, were performed in order to test the hypothesis that the hydration of anhydrite leads to a decrease in immersion freezing efficiency in suspension (see Fig. 5). All measurements

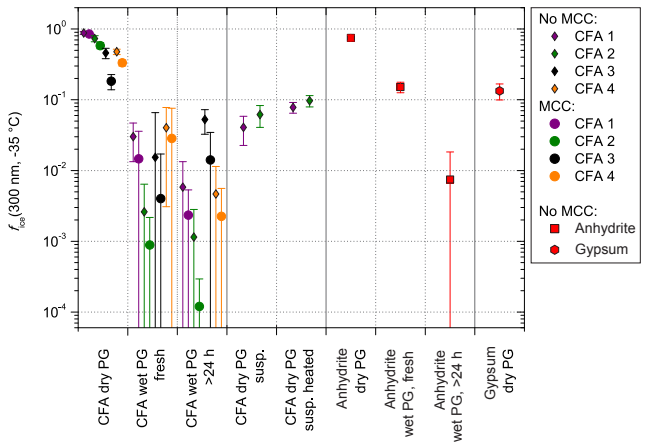

Figure 5. f_{ice} (−35 °C) from LACIS measurements with 300 nm particles. Multiple charge correction (MCC) was not performed, except for the measurements indicated by the circles in the first three columns. "Dry PG susp." means dry particle generation (PG) with a sample resulting from the evaporation of a suspension and "dry PG susp. heated" means additional heating of this sample to 250 °C prior to particle generation.

were performed at −35 °C with 300 nm particles. Here, we forewent the multiple charge correction for better comparability to measurements that took place after the campaign, where no correction was possible. The corrected values for CFA (used for the n_s calculations in Fig. 4) are shown as circles.

When comparing dry-generated CFA particles with wet-generated particles, either from a fresh suspension (i.e., measured within 5 min after preparation) or from the standard suspension (10 min of ultrasonification and 24 h stirring), a decrease in f_{ice} (−35 °C) can be observed. However, the particles from the freshly prepared suspension seem to be slightly more efficient than the ones from the standard suspension. The only exception is CFA3, where it was extremely difficult to generate a sufficiently high particle number concentration from the fresh suspension, resulting in a large error due to the small amount of classified hydrometeors (∼ 500). Dry- and wet-generated anhydrite particles show the same trend as observed for CFA, i.e., the wet-generated particles are significantly less efficient than the dry-generated particles, and the longer the particles stay in suspension, the stronger the decrease in f_{ice}.

Sullivan et al. (2010) described an increase in hygroscopicity of wet-generated anhydrite particles in comparison to dry particle generation. Also, the hygroscopicity of the wet-generated particles increased with the time that the particles spent in the suspension. Sullivan et al. (2010) attributed this behavior to the formation of hydrates and hypothesized that this process could have an effect not only on hygroscopicity but also on the ice nucleation efficiency of the particles. In our case, the dependency of immersion freezing efficiency on suspension time could result from the two stages of anhydrite hydration described in Sect. 3.2.2. Firstly, on the timescale of minutes, anhydrite is dissolved and hydrated ions form a layer on top of the CFA particles causing a sudden decrease in immersion freezing efficiency. It seems that the limited suspension time of 1.6 s in the case of dry particle generation is not sufficient to cause hydration. Secondly, on the timescale of several hours up to days, anhydrite is converted into gypsum which decreases f_{ice} further. Gypsum, like anhydrite, consists of molecules which are strong electrical dipoles (Klimchouk, 1996) and hence will also be surrounded by hydrated ions in suspension.

The ultrasonicated and stirred suspensions of CFA1 and CFA2 were left in a desiccator (steady flow of particle-free, dry air) until all water was evaporated. XRD measurements of the resulting powder show that the anhydrite–gypsum conversion had taken place and we assume that gypsum was already present in the stirred suspensions. The powder was then dry-dispersed and f_{ice} (−35 °C) of 300 nm particles was measured. An increase of almost 1 order of magnitude for CFA1 and almost 2 orders of magnitude for CFA2 in comparison to the wet-generated particles was registered. We attribute this increase to the difference in particle generation. For wet particle generation, possibly only the bulk water is removed in the diffusion dryer downstream of the atomizer, whereas the water molecules in the layer of hydrated ions remain. Drying in a desiccator, which takes several days, could lead to partial dehydration, i.e., removal of the hydrated layer surrounding the CFA particles. For dry particle generation, the limited suspension time of 1.6 s in LACIS is apparently not long enough for rehydration.

Additionally, the powder from the evaporated suspensions of CFA1 and CFA2 was heated to 250 °C for 15 min. According to Deer et al. (1992), this temperature is sufficient to dehydrate gypsum and form anhydrite. f_{ice} (−35 °C) of 300 nm particles slightly increased by a factor of 2 after the heat treatment, but it did not restore the immersion freezing efficiency of the original dry-dispersed particles. It is known that other hydrated species are present in the suspension particles that are only dehydrating at much higher temperatures (e.g., dehydration temperature of portlandite: 510 °C; Bai et al., 1994) and hence it is not surprising that only a small increase in f_{ice} could be achieved. In general, there is good agreement between measurements with dry-generated gypsum particles (see Fig. 5) and particles from the dried and heated CFA suspensions, indicating that gypsum is present in the investigated 300 nm CFA particles after they have spent a sufficiently long time in water.

It is beyond the scope of this paper to examine why hydration leads to a lower immersion freezing efficiency. Hence, we only offer some possible explanations here without further discussing their likelihood. A simple explanation would be that the adsorbed layer of hydrated ions on the particle surface blocks the interaction with the surrounding water molecules. Consequently, freezing would not be triggered as

efficiently as for the dry-generated particles, where the contact with water is too short to dissolve a sufficient amount of anhydrite. Another hypothesis (Sihvonen et al., 2014) describes a change in lattice parameters upon forced hydration of mineral dust particles towards a greater mismatch with ice.

4 Atmospheric implications

In view of the atmospheric relevance of the above-described findings, it is important to discuss whether the observed decrease in immersion freezing efficiency of CFA associated with switching from dry to wet particle generation would also occur in the atmosphere. From LACIS measurements with the freshly prepared CFA suspensions, we know that particles in the bulk suspension are deactivated within ~ 5 min but it is not clear if this would also be observed when a single particle is immersed in a cloud droplet. As already mentioned, it seems that 1.6 s, which is the residence time of CFA particles in water for LACIS measurements with dry-generated CFA, is not enough to cause hydration of anhydrite and quicklime.

Unfortunately, an increase in nucleation time by more than a factor of 2 is not possible with LACIS. However, during the campaign, SPIN measurements with dry-generated CFA particles were performed above water saturation (see Appendix C). From the results, which agree with LACIS for CFA3 and CFA4 but are below LACIS for CFA1 and CFA2, it can be speculated that the longer residence time in SPIN (~ 10 s) already leads to some deactivation by the formation of a hydrated layer on top of those particles which contain the highest concentration of water-soluble anhydrite. However, the effect is much more pronounced for longer hydration times, as can be seen in the results of SPIN measurements with wet-generated particles. It would be necessary to increase nucleation time further to evaluate the time needed to decrease the immersion freezing efficiency of single particles immersed in droplets to the efficiency of particles hydrated in the bulk suspension. Within the framework of the present study, it was not possible to keep cloud droplets with a single immersed CFA particle stable for longer than a few seconds before investigating immersion freezing. Hence, we can only give a range of how efficiently CFA induces immersion freezing in the atmosphere, because, for CFA containing a certain amount of anhydrite, this will depend on the time between activation to cloud droplets and triggering of freezing.

Figure 6 shows INP concentrations estimated from our CFA measurements in combination with size distributions measured ~ 80 km downstream of a coal-fired power plant (Parungo et al., 1978). For this, the ambient size distribution was subtracted from the size distribution in the plume to only consider particles emitted from the power plant. The procedure is explained in detail in Grawe et al. (2016), where we already estimated the INP concentration due to

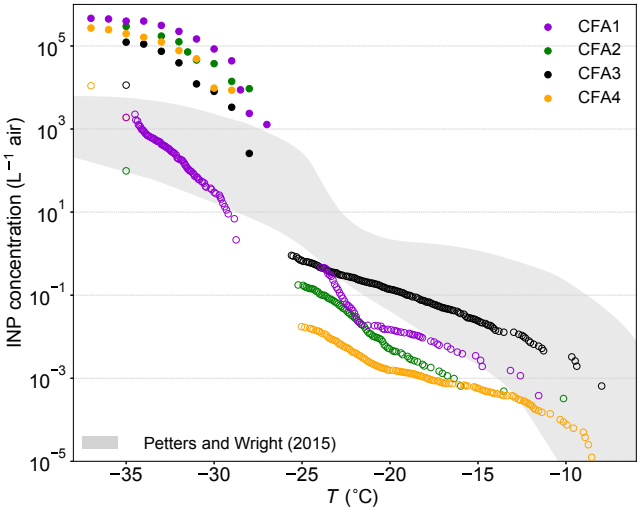

Figure 6. Estimated INP concentrations ~ 80 km downstream of a coal-fired power plant based on size distributions measured in a plume by Parungo et al. (1978). Full circles represent dry particle generation, open circles wet particle generation and cold-stage measurements. The shaded area indicates typical atmospheric INP concentrations derived from precipitation samples (Petters and Wright, 2015).

the emission of CFA1 to be higher than typical atmospheric INP concentrations, assuming n_s of dry-generated particles. This is equally true for the other dry-generated CFA samples, with estimated INP concentrations being roughly 2 orders of magnitude above the upper boundary given by Petters and Wright (2015) at -37 °C. In light of our new findings, and assuming that atmospheric processing will lead to a decrease in immersion freezing efficiency, we also estimated the INP concentrations using n_s from LACIS measurements with wet-generated CFA and cold-stage measurements. Above -30 °C, INP concentrations derived from measurements with CFA suspensions are close to or below the lower boundary given by Petters and Wright (2015), except for CFA3, which is within the boundaries given by Petters and Wright (2015) for $T > -23$ °C. This indicates that the majority of our CFA samples only contribute very little to atmospheric INP concentrations above -30 °C, when we assume that the suspension results are representative for processes occurring in the atmosphere. Our estimate suggests that particles from CFA1, CFA2, and CFA4 only become relevant for atmospheric immersion freezing at temperatures below -30 °C. Note that in close proximity to the source, i.e., in an undiluted plume directly after emission, INP concentrations will be much higher than estimated above. At greater distances from the power plant, INP concentrations will be significantly lower due to dilution. Garimella (2016) estimated that CFA particles are present at cirrus level in concentrations of ~ 0.1 to 1 L^{-1}.

5 Summary and conclusions

In the framework of this study, four CFA samples from German power plants were investigated concerning their immersion freezing behavior, chemical composition, morphology, and crystallography. In light of our new findings, we now revisit the questions from the introduction.

- Do CFA samples from different power plants feature a similar immersion freezing behavior? and
- Is the deactivation in the transition from dry to wet particle generation observable for different CFA samples?

All four samples were found to be efficient INPs in the immersion mode below −28 °C when dry particle generation was used. The n_s spectra of dry-generated particles differed by approximately 1 order of magnitude, with the curve shapes being very similar. A decrease in immersion freezing efficiency was observed for all of our samples when particles were generated from a suspension. However, the dataset is still too small to make a conclusive statement about the variability in immersion freezing results caused by different samples and differences in methodology. Comparisons to samples of different geographical origin (Umo et al., 2015; Garimella, 2016) suggest that the spread is indeed larger than what we found for the German CFA samples. Further immersion freezing measurements with more CFA samples from different sources, which should also focus on the effect of hydration, would be needed to provide a suitable parameterization.

- Is it possible to find a connection between physicochemical sample properties and the observed immersion freezing behavior?

From ALABAMA measurements, it was derived that the amount of molecular species containing Ca and S correlates with the immersion freezing efficiency of the dry-generated samples. Additional LACIS measurements with anhydrite and quicklime yielded similar results as for CFA, suggesting that both substances contribute to the observed freezing behavior. Both anhydrite and quicklime are hydrated (quicklime also carbonated) in contact with water which might cause a decrease in immersion freezing efficiency. Cold-stage measurements with the hydration products gypsum and calcite (Zolles et al., 2015) are comparable to LACIS measurements with wet-generated CFA particles and to WISDOM measurements. An exception is CFA3, which has the lowest concentration of Ca and the highest concentration of Si in both 300 nm particles and bulk. Here, the decrease in immersion freezing efficiency in the transition from dry to wet particle generation is smallest, and LACIS measurements are relatively close to cold-stage measurements with quartz (Atkinson et al., 2013). Quartz was detected as the major crystalline phase in all of the bulk samples. From this, we conclude that an influence of quartz on the immersion freezing behavior of CFA can only be seen in the case when the amount of anhydrite and quicklime is below a certain, not clearly definable, threshold.

- Which particle generation technique (dry or wet particle generation) or measurement method (single particle or cold stage) is appropriate for representing atmospheric processes after CFA emission?

It is important to know that for CFA, it is necessary to consider dissolution effects in suspension and changes in immersion freezing behavior on short timescales. We observed that dry-generated particles, which were immersed in droplets in LACIS for 1.6 s before freezing, are efficient INPs and can potentially contribute to the atmospheric INP spectrum if concentrations are high. However, for two of the samples, a decrease in freezing efficiency could already be seen when particles were immersed for ∼ 10 s in SPIN, suggesting that the ability of CFA to act as INP can decrease quickly in contact with water. Estimating atmospheric INP concentrations due to CFA emission, and assuming atmospheric processing of the particles, indicates that CFA is relevant at $T < -30$ °C, i.e., an effect on cirrus formation could be possible. Concerning this, it could also be worthwhile to further investigate deposition nucleation on CFA particles.

An approach to improve process understanding of CFA ageing in the atmosphere is to either sample particles in a coal-fired power plant plume on filters or perform in situ INP measurements, preferably at several distances downstream of the stack. In the case that it should turn out that the lower limit given by LACIS measurements with wet-generated particles and cold-stage measurements is reproducible, one might be able to provide sample-specific parameterizations and, once more samples have been investigated, boundaries for the immersion freezing efficiency of CFA.

Future research should also focus on quantifying CFA emissions and temporal and spacial variability of CFA particle concentrations. Mass spectrometry measurements of CFA, as performed in the framework of this study, can help to identify CFA in the atmosphere. However, the classification of single particles still remains difficult because CFA particles are heterogeneous in their composition and not all of them contain a characteristic marker. More composition measurements of atmospheric aerosol and ice crystal residues are needed to better assess the effect of CFA emission on weather and climate.

Data availability. The datasets are available upon request to the contact author (grawe@tropos.de) and will be stored in a publicly accessible database in the near future.

Sample availability. In consultation with the power plant operators, sample origin shall not be disclosed and distribution is not possible.

Appendix A: LINA water background correction, n_s calculation, and error estimation

For each CFA sample, $f_{\mathrm{ice,\,H_2O}}(T)$ was determined from LINA measurements with the distilled water that was used to prepare the CFA suspension. Freezing caused by impurities in the distilled water and on the glass slide was accounted for in the following way. Firstly, the number of sites active at a given temperature T per droplet volume V_{drop}, $K_{\mathrm{H_2O}}(T)$ was calculated for distilled water (Eq. A1; Vali, 1971). Secondly, this value was subtracted from $K_{\mathrm{CFA}}(T)$ (Eq. A2; Umo et al., 2015). Finally, the difference was used to calculate a corrected n_{s} value (Eq. A3), with C the mass concentration of CFA in suspension and A_{BET} the BET specific surface area (see Sect. S8).

$$K_{\mathrm{H_2O}}(T) = -\frac{\ln(1 - f_{\mathrm{ice,\,H_2O}}(T))}{V_{\mathrm{drop}}} \quad \text{(A1)}$$

$$K_{\mathrm{CFA}}(T) = -\frac{\ln(1 - f_{\mathrm{ice,\,CFA}}(T))}{V_{\mathrm{drop}}} \quad \text{(A2)}$$

$$n_{\mathrm{s,\,corr}}(T) = \frac{K_{\mathrm{CFA}}(T) - K_{\mathrm{H_2O}}(T)}{C \cdot A_{\mathrm{BET}}} \quad \text{(A3)}$$

The $n_{\mathrm{s,\,corr}}$ values from four measurements were averaged for a mean n_{s} value, i.e., a total number of 360 droplets was investigated for each sample. The uncertainty in the mean n_{s}, given as vertical error bars in Fig. 4, is equal to the standard deviation of the four $n_{\mathrm{s,\,corr}}$ values. The largest possible n_{s} error of the LINA measurements is illustrated in Fig. A1. For this, the uncertainties in concentration from weighing of the CFA sample and pipetting distilled water, as well as BET specific surface area, and volume of the droplets were propagated. Here, the error in f_{ice} was assumed to be related to the standard deviation of the Poisson distribution of particles in the suspension.

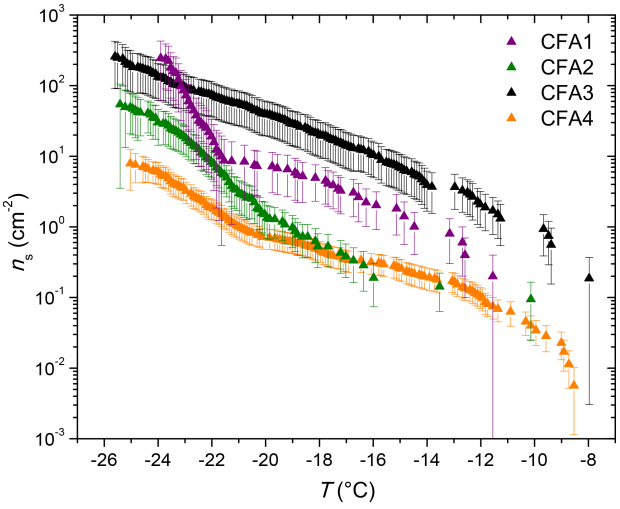

Figure A1. n_{s} (T) from LINA measurements. Vertical error bars are the result of propagating uncertainties in weighing, BET surface area, pipette volumes, and distribution of particles in the suspension.

Appendix B: Comment on misinterpreted LACIS measurements with wet-generated CFA1 particles published in Grawe et al. (2016) and correction of those

Data shown in Fig. B1 is taken from Grawe et al. (2016, similar to Fig. 4d) and shows $f_{\mathrm{ice}}(T)$ for dry- and wet-generated CFA1 particles. Measurements with dry-generated particles are identical to those shown in Fig. 2. Measurements with wet-generated particles from a suspension, prepared as described by Umo et al. (2015), i.e., 10 min of ultrasonification and 24 h of stirring, suggest that CFA1 retains some activity even when being wet generated. f_{ice} was found to be around 5 % between −24 and −35 °C, indicating no strong temperature dependence.

At this point it was already known that needle-shaped particles are present among wet-generated CFA1 particles. However, it was assumed that the needle-shaped particles are composed of water-soluble material which will dissolve once a needle-shaped particle is immersed in a droplet. f_{ice} would be underestimated due to the occurrence of purely water-soluble particles, and according to this hypothesis, f_{ice} was multiplied by a scaling factor of 4.54 (= 1/0.22, assuming that only 22 % of the droplets contained a water-insoluble particle).

Additional measurements were performed with modified suspensions. When the suspension was prepared without ultrasonification, just stirring, lower f_{ice} values around 1 % at −35 °C were observed. When filtering the suspension through a 200 nm syringe filter, f_{ice} was only slightly above values measured for highly diluted ammonium sulphate droplets, i.e., homogeneous nucleation.

ESEM images (see Figs. S5 and S6) show that CFA1 is indeed the only one of the four CFA samples for which needle-shaped particles form during wet particle generation. Optical microscope images of liquid suspension droplets (see Fig. S13a) show that the needle-shaped particles are even present in the aqueous environment, disproving the earlier hypothesis of water-soluble needle-shaped particles. Even though the substrates were loaded after size selection, needle-shaped particles which are much longer than the selected 300 nm can be seen on the ESEM images and could be introduced into LACIS. This is due to the fact that the dynamic shape factor of the needle-shaped particles differs significantly from unity. The ESEM images suggest that some of the needle-shaped particles are even longer than the usual droplet diameter at the LACIS outlet (which is 5 µm). This represents a challenge for the optical detection with TOPS-Ice, because the determination of f_{ice} is based on depolarization, and hence largely on the shape of the hydrometeors. In usual LACIS immersion freezing experiments with 300 nm particles, the supercooled liquid droplets are spher-

ical because a sufficient amount of water vapor is provided to form a thick (with respect to the particle diameter) layer of water on top of the particle upon activation. However, if we imagine an experiment with particles from the CFA1 suspension, the long needle-shaped particles have a much larger surface area that will be covered by water molecules when exposed to same supersaturation with respect to liquid water. As a result, a much thinner water layer is formed which will not be able to "hide" the irregular particle shape. Due to this, there is a fraction of needle-shaped particles longer than 5 µm causing droplets being non-spherical, yet unfrozen. Consequently, depolarization signals are produced, which are associated with ice particles. This artifact can also be observed at $T > 0\,°C$ and thus we falsely interpreted signals caused by long needle-shaped particles as frozen droplets in Grawe et al. (2016), overestimating the immersion freezing efficiency of wet-generated CFA1 particles.

To determine the realistic freezing potential of wet-generated CFA1 particles, the suspension was put through a filter (4–7 µm particle retention, grade 595, Whatman International, Ltd., Maidstone, UK) prior to wet particle generation to remove large needle-shaped particles. As a result, experiments could be conducted with 5 µm sized droplets, which were then spherical when unfrozen. f_{ice} was found to be below 0.1 % at −35 °C, i.e., the wet-generated CFA1 particles are roughly 3 orders of magnitude less efficient than the dry-generated ones.

Concerning the lower f_{ice} values for particles from the CFA1 suspension without ultrasonification from Grawe et al. (2016), it can be hypothesized that, due to the lack of agitation, less of the material responsible for the formation of needle-shaped particles was dissolved from the CFA particles. Consequently, less and/or shorter needle-shaped particles might have formed which would not disturb the spherical shape of the droplets.

Appendix C: Potential influence of residence time on immersion freezing efficiency of dry-generated CFA

SPIN measurements above water saturation ($1.03 \leq S_w <$ droplet breakthrough) were performed with dry-generated 300 nm particles from all four CFA samples and wet-generated 300 nm particles from CFA1 (see Fig. C1). Measurements with wet-generated particles could only be done for CFA1 due to instrument availability. For comparison to LACIS results, SPIN AF data are shown as measured and additionally multiplied by a factor of 3, based on results from a previous intercomparison campaign including LACIS and SPIN (Burkert-Kohn et al., 2017) and a comparison between a different CFDC and a cloud chamber (DeMott et al., 2015). Corrected data were interpolated for better clarity and are represented by the dashed lines.

The decrease in the transition from dry to wet particle generation, which was observed in LACIS, was also measured with SPIN. Concerning dry-generated CFA particles, there is nearly perfect agreement between LACIS and SPIN for CFA3 and CFA4 after correction. In the case of CFA2, SPIN results are lower than LACIS results, especially for $T \geq -30\,°C$. The biggest difference is observed for dry-generated particles of CFA1, where SPIN data are significantly below LACIS for $T \geq -35\,°C$. A possible explanation could be that CFA1 is the sample with the highest amount of Ca, and presumably anhydrite, that will be dissolved once the particles are activated. The LACIS measurements indicate that an activation time of 1.6 s is too short to cause the formation of an adsorbed layer of hydrated ions (as described in Sect. 3.2.2). The residence time of the particles in SPIN is a factor of 6 higher and this could be enough time to dissolve a sufficient amount of anhydrite. The dependency of residence time in SPIN on the thermodynamic conditions in the chamber (9.2 s at $T = -30\,°C$ and 8.2 s at $T = -40\,°C$) could explain why the discrepancy between SPIN and LACIS is higher at higher temperatures. An increase in residence time allows for more ions to dissolve from the CFA particle surface at higher temperatures, which consequently leads to a stronger decrease in AF at higher temperatures. This effect is also visible for CFA2. Following this hypothesis, CFA3 and CFA4 do not contain a sufficient amount of anhydrite to form a hydrated shell around the particles within ∼ 10 s.

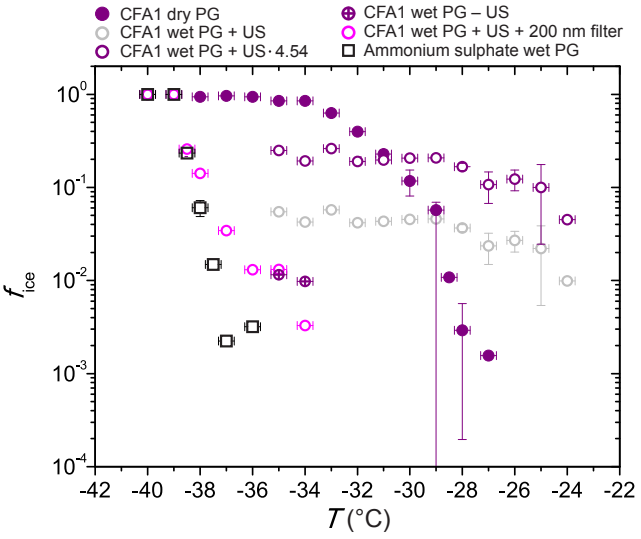

Figure B1. Data taken from Fig. 4d of Grawe et al. (2016) showing f_{ice} measured with 300 nm dry- and wet-generated CFA1 particles. US: ultrasonification, PG: particle generation.

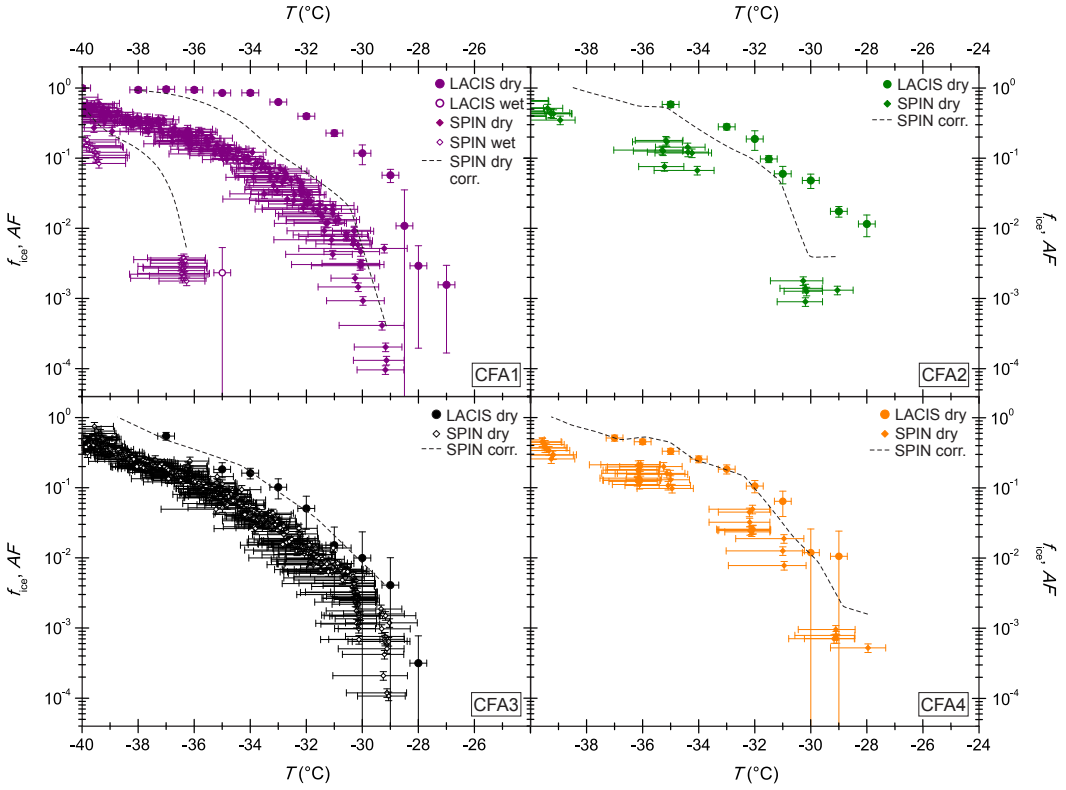

Figure C1. Comparison of CFA immersion freezing measurements with SPIN and LACIS (300 nm particles). Dashed lines indicate interpolated SPIN data after a correction factor of 3 is applied.

The Supplement related to this article is available online at https://doi.org/10.5194/acp-18-13903-2018-supplement.

Author contributions. SG wrote the manuscript with contributions from HCC, SEH, NR, and HW. LACIS measurements and data evaluation were performed by SG, SAB, and JL. LINA measurements and data evaluation were performed by JL and SG. HCC performed ALABAMA measurements and data analysis with the support of JS. SEH sampled particles with the impactor and performed the ESEM/EDX particle analysis together with ME. NR measured with WISDOM and provided BET results. AW performed SPIN measurements and data evaluation. RS performed XRD measurements. SG, SAB, FS, and HW discussed the immersion freezing results and further experiments after the campaign. HW procured the CFA samples and coordinated the campaign. All co-authors proofread and commented on the manuscript.

Competing interests. The authors declare that they have no conflict of interests.

Special issue statement. This article is part of the special issue "Results from the ice nucleation research unit (INUIT) (ACP/AMT inter-journal SI)". It is not associated with a conference.

Acknowledgements. This research was conducted in the framework of the DFG funded Ice Nuclei research UnIT (INUIT, FOR1525), WE 4722/1-2, SCHN1138/2-2. We thank the anonymous suppliers of the CFA samples, the Lippendorf power plant, Mette Sidelmann and Merete Bilde (Department of Chemistry, Aarhus University, Denmark) for water-activity measurements, Michael Lorenz (Semiconductor Physics Group, University of Leipzig, Germany) for providing access to the XRD instrument, Anke Rödger, Khanneh W. Fomba, Anett Dietze, Susanne Fuchs, and Dominik van Pinxteren (TROPOS, Leipzig, Germany) for bulk chemical composition analysis, Xianda Gong (TROPOS, Leipzig, Germany) for helpful discussions, Roswitha Heller (Leibniz Institute of Surface Modification, Leipzig, Germany) and Jens Voigtländer (TROPOS, Leipzig, Germany) for introduction to the optical microscopes, and Thomas Conrath (TROPOS, Leipzig, Germany) for technical support.

Edited by: Allan Bertram
Reviewed by: two anonymous referees

References

Ahmaruzzaman, M.: A review on the utilization of fly ash, Prog. Energ. Combust., 36, 327–363, 2010.

ASTM: C618 - 17a. Standard specification for coal fly ash and raw or calcined natural pozzolan for use in concrete, Tech. rep., Am. Soc. Test. Mater., West Conshohocken, PA, USA, 2017.

Atkinson, J. D., Murray, B. J., Woodhouse, M. T., Whale, T. F., Baustian, K. J., Carslaw, K. S., Dobbie, S., O'Sullivan, D., and Malkin, T. L.: The importance of feldspar for ice nucleation by mineral dust in mixed-phase clouds, Nature, 498, 355–358, 2013.

Augustin-Bauditz, S., Wex, H., Kanter, S., Ebert, M., Niedermeier, D., Stolz, F., Prager, A., and Stratmann, F.: The immersion mode ice nucleation behavior of mineral dusts: A comparison of different pure and surface modified dusts, Geophys. Res. Lett., 41, 7375–7382, 2014.

Bai, T. B., Koster van Groos, A. F., and Guggenheim, S.: Phase transition, dehydration, and melting relationships of portlandite, Am. Mineral., 79, 1223–1226, 1994.

Brands, M., Kamphus, M., Böttger, T., Schneider, J., Drewnick, F., Roth, A., Curtius, J., Voigt, C., Borbon, A., Beekmann, M., Bourdon, A., Perrin, T., and Borrmann, S.: Characterization of a newly developed aircraft-based laser ablation aerosol mass spectrometer (ALABAMA) and first field deployment in urban pollution plumes over Paris during MEGAPOLI 2009, Aerosol Sci. Tech., 45, 46–64, 2011.

Brunauer, S., Emmett, P. H., and Teller, E.: Adsorption of gases in multimolecular layers, J. Am. Chem. Soc., 60, 309–319, 1938.

Budke, C. and Koop, T.: BINARY: an optical freezing array for assessing temperature and time dependence of heterogeneous ice nucleation, Atmos. Meas. Tech., 8, 689–703, https://doi.org/10.5194/amt-8-689-2015, 2015.

Burkert-Kohn, M., Wex, H., Welti, A., Hartmann, S., Grawe, S., Hellner, L., Herenz, P., Atkinson, J. D., Stratmann, F., and Kanji, Z. A.: Leipzig Ice Nucleation chamber Comparison (LINC): intercomparison of four online ice nucleation counters, Atmos. Chem. Phys., 17, 11683–11705, https://doi.org/10.5194/acp-17-11683-2017, 2017.

Chen, J., Wu, Z., Augustin-Bauditz, S., Grawe, S., Hartmann, M., Pei, X., Liu, Z., Ji, D., and Wex, H.: Ice-nucleating particle concentrations unaffected by urban air pollution in Beijing, China, Atmos. Chem. Phys., 18, 3523–3539, https://doi.org/10.5194/acp-18-3523-2018, 2018.

Clauß, T., Kiselev, A., Hartmann, S., Augustin, S., Pfeifer, S., Niedermeier, D., Wex, H., and Stratmann, F.: Application of linear polarized light for the discrimination of frozen and liquid droplets in ice nucleation experiments, Atmos. Meas. Tech., 6, 1041–1052, https://doi.org/10.5194/amt-6-1041-2013, 2013.

Cziczo, D., Stetzer, O., Worringen, A., Ebert, M., Weinbruch, S., Kamphus, M., Gallavardin, S. J., Curtius, J., Borrmann, S., Froyd, K. D., Mertes, S., Möhler, O., and Lohmann, U.: Inadvertent climate modification due to anthropogenic lead, Nat. Geosci., 2, 333–336, 2009.

Cziczo, D. J., Murphy, D. M., Hudson, P. K., and Thomson, D. S.: Single particle measurements of the chemical composition of cirrus ice residue during CRYSTAL-FACE, J. Geophys. Res., 109, D4, https://doi.org/10.1029/2003JD004032, 2004.

Cziczo, D. J., Thomson, D. S., Thompson, T. L., DeMott, P. J., and Murphy, D. M.: Particle analysis by laser mass spectrometry (PALMS) studies of ice nuclei and other low number density particles, Int. J. Mass Spectrom., 258, 21–29, 2006.

Damle, A. S., Ensor, D. S., and Ranade, M. B.: Coal combustion mechanisms: A review, Aerosol Sci. Tech., 1, 119–133, 1982.

Davison, R. L., Natusch, D. F. S., Wallace, J. R., and Evans Jr., C. A.: Trace elements in fly ash: dependence of concen-

tration on particle size, Environ. Sci. Technol., 8, 1107–1113, https://doi.org/10.1021/es60098a003, 1974.

Deer, W. A., Howie, R. A., and Zussman, J.: An Introduction to the Rock Forming Minerals, 2nd edn., Longman Scientific and Technical, Essex, UK, 1992.

DeMott, P. J.: An exploratory study of ice nucleation by soot aerosols, J. Appl. Meteorol., 29, 1072–1079, 1990.

DeMott, P. J., Cziczo, D. J., Prenni, A. J., Murphy, D. M., Kreidenweis, S. M., Thomson, D. S., Borys, R., and Rogers, D. C.: Measurements of the concentration and composition of nuclei for cirrus formation, P. Natl. Acad. Sci. USA, 100, 14 655–14 660, 2003.

DeMott, P. J., Prenni, A. J., McMeeking, G. R., Sullivan, R. C., Petters, M. D., Tobo, Y., Niemand, M., Möhler, O., Snider, J. R., Wang, Z., and Kreidenweis, S. M.: Integrating laboratory and field data to quantify the immersion freezing ice nucleation activity of mineral dust particles, Atmos. Chem. Phys., 15, 393–409, https://doi.org/10.5194/acp-15-393-2015, 2015.

Diehl, K. and Mitra, S. K.: A laboratory study of the effects of a kerosene-burner exhaust on ice nucleation and the evaporation rate of ice crystals, Atmos. Environ., 32, 3145–3151, 1998.

Ebert, M., Weigel, R., Kandler, K., Günther, G., Molleker, S., Grooß, J.-U., Vogel, B., Weinbruch, S., and Borrmann, S.: Chemical analysis of refractory stratospheric aerosol particles collected within the arctic vortex and inside polar stratospheric clouds, Atmos. Chem. Phys., 16, 8405–8421, https://doi.org/10.5194/acp-16-8405-2016, 2016.

Emersic, C., Connolly, P. J., Boult, S., Campana, M., and Li, Z.: Investigating the discrepancy between wet-suspension- and dry-dispersion-derived ice nucleation efficiency of mineral particles, Atmos. Chem. Phys., 15, 11311–11326, https://doi.org/10.5194/acp-15-11311-2015, 2015.

endcoal.org: Coal plants by country (Units) – July 2017, available at: https://endcoal.org/wp-content/uploads/2017/07/PDFs-for-GCPT-July-2017-Countries-Units.pdf, last access: 25 October 2017.

Enders, M.: The CaO distribution to mineral phases in a high calcium fly ash from Eastern Germany, Cement Concrete Res., 26, 243–251, 1996.

Flagan, R. C. and Seinfeld, J. H.: Fundamentals of Air Pollution Engineering, chap. Particle formation in combustion, 358–390, Prentice-Hall, Inc., Englewood Cliffs, New Jersey, 1988a.

Flagan, R. C. and Seinfeld, J. H.: Fundamentals of Air Pollution Engineering, chap. Removal of Particles from Gas Streams, 391–478, Prentice-Hall, Inc., Englewood Cliffs, New Jersey, 1988b.

Fornea, A. P., Brooks, S. D., Dooley, J. B., and Saha, A.: Heterogeneous freezing of ice on atmospheric aerosols containing ash, soot and soil, J. Geophys. Res., 114, D13201, https://doi.org/10.1029/2009JD011958, 2009.

Freney, E. J., Martin, S. T., and Buseck, P. R.: Deliquescence and efflorescence of potassium salts relevant to biomass-burning aerosol particles, Aerosol Sci. Tech., 43, 799–807, 2009.

Gallavardin, S. J., Lohmann, U., and Cziczo, D. J.: Analysis and differentiation of mineral dust by single particle laser mass spectrometry, Int. J. Mass Spectrom., 274, 56–63, 2008.

Garimella, S.: A vertically-integrated approach to climate science: From measurements and machine learning to models and policy, PhD thesis, Massachusetts Institute of Technology, Cambridge, MA, USA, 2016.

Garimella, S., Kristensen, T. B., Ignatius, K., Welti, A., Voigtländer, J., Kulkarni, G. R., Sagan, F., Kok, G. L., Dorsey, J., Nichman, L., Rothenberg, D. A., Rösch, M., Kirchgäßner, A. C. R., Ladkin, R., Wex, H., Wilson, T. W., Ladino, L. A., Abbatt, J. P. D., Stetzer, O., Lohmann, U., Stratmann, F., and Cziczo, D. J.: The SPectrometer for Ice Nuclei (SPIN): an instrument to investigate ice nucleation, Atmos. Meas. Tech., 9, 2781–2795, https://doi.org/10.5194/amt-9-2781-2016, 2016.

Grawe, S., Augustin-Bauditz, S., Hartmann, S., Hellner, L., Pettersson, J. B. C., Prager, A., Stratmann, F., and Wex, H.: The immersion freezing behavior of ash particles from wood and brown coal burning, Atmos. Chem. Phys., 16, 13911–13928, https://doi.org/10.5194/acp-16-13911-2016, 2016.

Gražulis, S., Chateigner, D., Downs, R. T., Yokochi, A. F. T., Quirós, M., Lutterotti, L., Manakova, E., Butkus, J., Moeck, P., and Le Bail, A.: Crystallography Open Database – an open-access collection of crystal structures, J. Appl. Crystallogr., 42, 726–729, 2009.

Hartmann, S., Niedermeier, D., Voigtländer, J., Clauss, T., Shaw, R. A., Wex, H., Kiselev, A., and Stratmann, F.: Homogeneous and heterogeneous ice nucleation at LACIS: operating principle and theoretical studies, Atmos. Chem. Phys., 11, 1753–1767, https://doi.org/10.5194/acp-11-1753-2011, 2011.

Havlíček, D., Přibil, R., and Školoud, O.: The chemical and mineralogical composition of the water-soluble fraction of power-plant ash and its effect on the process of crystallization of water, Atmos. Environ., 27A, 655–660, 1993.

Hiranuma, N., Augustin-Bauditz, S., Bingemer, H., Budke, C., Curtius, J., Danielczok, A., Diehl, K., Dreischmeier, K., Ebert, M., Frank, F., Hoffmann, N., Kandler, K., Kiselev, A., Koop, T., Leisner, T., Möhler, O., Nillius, B., Peckhaus, A., Rose, D., Weinbruch, S., Wex, H., Boose, Y., DeMott, P. J., Hader, J. D., Hill, T. C. J., Kanji, Z. A., Kulkarni, G., Levin, E. J. T., McCluskey, C. S., Murakami, M., Murray, B. J., Niedermeier, D., Petters, M. D., O'Sullivan, D., Saito, A., Schill, G. P., Tajiri, T., Tolbert, M. A., Welti, A., Whale, T. F., Wright, T. P., and Yamashita, K.: A comprehensive laboratory study on the immersion freezing behavior of illite NX particles: a comparison of 17 ice nucleation measurement techniques, Atmos. Chem. Phys., 15, 2489–2518, https://doi.org/10.5194/acp-15-2489-2015, 2015.

Hoose, C. and Möhler, O.: Heterogeneous ice nucleation on atmospheric aerosols: a review of results from laboratory experiments, Atmos. Chem. Phys., 12, 9817–9854, https://doi.org/10.5194/acp-12-9817-2012, 2012.

Huffman, J. A., Sinha, B., Garland, R. M., Snee-Pollmann, A., Gunthe, S. S., Artaxo, P., Martin, S. T., Andreae, M. O., and Pöschl, U.: Size distributions and temporal variations of biological aerosol particles in the Amazon rainforest characterized by microscopy and real-time UV-APS fluorescence techniques during AMAZE-08, Atmos. Chem. Phys., 12, 11997–12019, https://doi.org/10.5194/acp-12-11997-2012, 2012.

Jaenicke, R.: Über die Dynamik atmosphärischer Aitkenteilchen, Berich. Bunsen Gesell., 82, 1198–1202, https://doi.org/10.1002/bbpc.19780821126, 1978.

Kamphus, M., Ettner-Mahl, M., Klimach, T., Drewnick, F., Keller, L., Cziczo, D. J., Mertes, S., Borrmann, S., and Curtius, J.: Chemical composition of ambient aerosol, ice residues and cloud droplet residues in mixed-phase clouds: single particle analysis during the Cloud and Aerosol Characterization Ex-

periment (CLACE 6), Atmos. Chem. Phys., 10, 8077–8095, https://doi.org/10.5194/acp-10-8077-2010, 2010.

Kanji, Z. A., Ladino, L. A., Wex, H., Boose, Y., Burkert-Kohn, M., Cziczo, D. J., and Krämer, M.: Overview of Ice Nucleating Particles, Meteor. Mon., 58, 1.1–1.33, https://doi.org/10.1175/AMSMONOGRAPHS-D-16-0006.1, 2017.

Kim, J.-H., Yoo, H.-J., Hwang, Y.-S., and Kim, H.-G.: Removal of particulate matter in a tubular wet electrostatic precipitator using a water collection electrode, Sci. World J., ID 532354, https://doi.org/10.1100/2012/532354, 2012.

Klimchouk, A.: The dissolution and conversion of gypsum and anhydrite, Int. J. Speleol., 25, 21–36, 1996.

Laskin, A., Cowin, J. P., and Iedema, M. J.: Analysis of individual environmental particles using modern methods of electron microscopy and X-ray microanalysis, J. Electron. Spectrosc., 150, 260–274, 2006.

Matsunaga, T., Kim, J. K., Hardcastle, S., and Rohatgi, P. K.: Crystallinity and selected properties of fly ash particles, Adv. Mater Res.-Switz., 325, 333–343, https://doi.org/10.1016/S0921-5093(01)01466-6, 2002.

Mueller, S. F., Mallard, J. W., Mao, Q., and Shaw, S. L.: Fugitive particulate emission factors for dry fly ash disposal, Japca J. Air Waste Ma., 63, 806–818, 2013.

Nóbrega, S. W., Falaguasta, M. C. R., and Coury, J. R.: A study of a wire-plate electrostatic precipitator operating in the removal of polydispersed particles, Braz. J. Chem. Eng., 21, 275–284, 2004.

Parungo, F. P., Ackerman, E., Proulx, H., and Pueschel, R. F.: Nucleation properties of fly ash in a coal-fired power-plant plume, Atmos. Environ., 12, 929–935, 1978.

Petters, M. D. and Wright, T. P.: Revisiting ice nucleation from precipitation samples, Geophys. Res. Lett., 42, 8758–8766, 2015.

Querol, X., Alastuey, A., Lopez-Soler, A., Mantilla, E., and Plana, F.: Mineral composition of atmospheric particulates around a large coal-fired power station, Atmos. Environ., 30, 3557–3572, 1996.

Reff, A., Bhave, P. V., Simon, H., Pace, T. G., Pouliot, G. A., Mobley, J. D., and Houyoux, M.: Emissions inventory of $PM_{2.5}$ trace elements across the United States, Environ. Sci. Technol., 43, 5790–5796, https://doi.org/10.1021/es802930x, 2009.

Reicher, N., Segev, L., and Rudich, Y.: The WeIzmann Supercooled Droplets Observation on a Microarray (WISDOM) and application for ambient dust, Atmos. Meas. Tech., 11, 233–248, https://doi.org/10.5194/amt-11-233-2018, 2018.

Roth, A., Schneider, J., Klimach, T., Mertes, S., van Pinxteren, D., Herrmann, H., and Borrmann, S.: Aerosol properties, source identification, and cloud processing in orographic clouds measured by single particle mass spectrometry on a central European mountain site during HCCT-2010, Atmos. Chem. Phys., 16, 505–524, https://doi.org/10.5194/acp-16-505-2016, 2016.

Schmidt, S., Schneider, J., Klimach, T., Mertes, S., Schenk, L. P., Kupiszewski, P., Curtius, J., and Borrmann, S.: Online single particle analysis of ice particle residuals from mountain-top mixed-phase clouds using laboratory derived particle type assignment, Atmos. Chem. Phys., 17, 575–594, https://doi.org/10.5194/acp-17-575-2017, 2017.

Schmitz, C. H. J., Rowat, A. C., Köster, S., and Weitz, D. A.: Dropspots: a picoliter array in a microfluidic device, Lab Chip, 9, 44–49, 2009.

Schnell, R. C., Valin, C. C. V., and Pueschel, R. F.: Atmospheric ice nuclei: No detectable effect from a coal-fired powerpower plume, Geophys. Res. Lett., 3, 657–660, 1976.

Sedlacek III, A. J., Buseck, P. R., Adachi, K., Onasch, T. B., Springston, S. R., and Kleinman, L.: Formation and evolution of tar balls from northwestern US wildfires, Atmos. Chem. Phys., 18, 11289–11301, https://doi.org/10.5194/acp-18-11289-2018, 2018.

Sievert, T., Wolter, A., and Singh, N. B.: Hydration of anhydrite of gypsum ($CaSO_4$. II) in a ball mill, Cement Concrete Res., 35, 623–630, 2005.

Sihvonen, S. K., Schill, G. P., Lyktey, N. A., Veghte, D. P., Tolbert, M. A., and Freedman, M. A.: Chemical and physical transformations of aluminosilicate clay minerals due to acid treatment and consequences for heterogeneous ice nucleation, J. Phys. Chem. A, 118, 8787–8796, https://doi.org/10.1021/jp504846g, 2014.

Smil, V.: Energy in Nature and Society: General Energetics of Complex Systems, MIT Press, Cambridge, MA, USA, 2008.

Sullivan, R. C., Moore, M. J. K., Petters, M. D., Kreidenweis, S. M., Qafoku, O., Laskin, A., Roberts, G. C., and Prather, K. A.: Impact of particle generation method on the apparent hygroscopicity of insoluble mineral particles, Aerosol Sci. Tech., 44, 830–846, 2010.

Szyrmer, W. and Zawadzki, I.: Biogenic and anthropogenic sources of ice-forming nuclei: A review, B. Am. Meteorol. Soc., 78, 209–228, 1997.

U. S. Energy Information Administration: International Energy Outlook 2017, available at: https://www.eia.gov/outlooks/ieo/pdf/0484(2017).pdf, last access: 24 October 2017.

Umo, N. S., Murray, B. J., Baeza-Romero, M. T., Jones, J. M., Lea-Langton, A. R., Malkin, T. L., O'Sullivan, D., Neve, L., Plane, J. M. C., and Williams, A.: Ice nucleation by combustion ash particles at conditions relevant to mixed-phase clouds, Atmos. Chem. Phys., 15, 5195–5210, https://doi.org/10.5194/acp-15-5195-2015, 2015.

Vali, G.: Quantitative evaluation of experimental results on the heterogeneous freezing nucleation of supercooled liquids, J. Atmos. Sci., 28, 402–409, 1971.

Weinbruch, S., Ebert, M., Gorzawski, H., Dirsch, T., Berg, T., and Steinnes, E.: Characterisation of individual aerosol particles on moss surfaces: implications for source apportionment, J. Environ. Monitor., 12, 1064–1071, 2010.

Weinbruch, S., Wiesemann, D., Ebert, M., Schütze, K., Kallenborn, R., and Ström, J.: Chemical composition and sources of aerosol particles at Zeppelin Mountain (Ny Ålesund, Svalbard): An electron microscopy study, Atmos. Environ., 49, 142–150, 2012.

Whale, T. F., Murray, B. J., O'Sullivan, D., Wilson, T. W., Umo, N. S., Baustian, K. J., Atkinson, J. D., Workneh, D. A., and Morris, G. J.: A technique for quantifying heterogeneous ice nucleation in microlitre supercooled water droplets, Atmos. Meas. Tech., 8, 2437–2447, https://doi.org/10.5194/amt-8-2437-2015, 2015.

Yi, H., Guo, X., Hao, J., Duan, L., and Li, X.: Characteristics of inhalable particulate matter concentration and size distribution from power plants in China, Japca J. Air Waste Ma., 56, 1243–1251, 2006.

Zolles, T., Burkart, J., Häusler, T., Pummer, B., Hitzenberger, R., and Grothe, H.: Identification of ice nucleation active sites on feldspar dust particles, J. Phys. Chem. A, 119, 2692–2700, 2015.

Atmos. Chem. Phys., 19, 2259–2281, 2019
https://doi.org/10.5194/acp-19-2259-2019

Atmospheric Chemistry and Physics
Open Access
EGU

Mineralogy and mixing state of north African mineral dust by online single-particle mass spectrometry

Nicholas A. Marsden[1], Romy Ullrich[2], Ottmar Möhler[2], Stine Eriksen Hammer[3], Konrad Kandler[3], Zhiqiang Cui[4], Paul I. Williams[1,5], Michael J. Flynn[1], Dantong Liu[1], James D. Allan[1,5], and Hugh Coe[1]

[1]School of Earth and Environmental Sciences, University of Manchester, Manchester, UK
[2]Institute of Meteorology and Climate Research, Karlsruhe Institute of Technology, Karlsruhe, Germany
[3]Institute of Applied Geosciences, Technische Universitat Darmstadt, Darmstadt, Germany
[4]School of Earth and Environment, University of Leeds, Leeds, UK
[5]National Centre for Atmospheric Science, Manchester, UK

Correspondence: Hugh Coe (hugh.coe@manchester.ac.uk)

Received: 16 July 2018 – Discussion started: 15 August 2018
Revised: 4 February 2019 – Accepted: 5 February 2019 – Published: 21 February 2019

Abstract. The mineralogy and mixing state of dust particles originating from the African continent influences climate and marine ecosystems in the North Atlantic due to its effect on radiation, cloud properties and biogeochemical cycling. However, these processes are difficult to constrain because of large temporal and spatial variability, and the lack of in situ measurements of dust properties at all stages of the dust cycle. This lack of measurements is in part due to the remoteness of potential source areas (PSAs) and transport pathways but also because of the lack of an efficient method to report the mineralogy and mixing state of single particles with a time resolution comparable to atmospheric processes, which may last a few hours or less. Measurements are equally challenging in laboratory simulations where dust particles need to be isolated and characterised in low numbers whilst conditions are dynamically controlled and monitored in real time. This is particularly important in controlled expansion cloud chambers (CECCs) where ice-nucleating properties of suspended dust samples are studied in cold and mixed phase cloud conditions.

In this work, the mineralogy and mixing state of the fine fraction ($< 2.5\,\mu m$) in laboratory-suspended dust from PSAs in north Africa were made using novel techniques with online single-particle mass spectrometry (SPMS) and traditional offline scanning electron microscopy (SEM). A regional difference in mineralogy was detected, with material sourced from Morocco containing a high number fraction of illite-like particles in contrast to Sahelian material which contains potassium- and sodium-depleted clay minerals like kaolinite. Single-particle mixing state had a much greater local variation than mineralogy, particularly with respect to organic–biological content. Applying the same methods to ambient measurement of transported dust in the marine boundary layer at Cabo Verde in the remote North Atlantic enabled the number fractions of illite/smectite clay mineral (ISCM), non-ISCM and calcium-containing particles to be reported at a 1 h time resolution over a 20-day period. Internal mixing of silicate particles with nitrate, chlorine and organic–biological material was also measured and compared to that in the suspended soils.

The results show SPMS and SEM techniques are complementary and demonstrate that SPMS can provide a meaningful high-resolution measurement of single-particle mineralogy and mixing state in laboratory and ambient conditions. In most cases, the differences in the mineralogical composition between particles within a soil sample were small. Thus, particles were not composed of discrete mineral phases. In ambient measurements, the ISCM and nitrate content was found to change significantly between distinct dust events, indicating a shift in source and transport pathways which may not be captured in offline composition analysis or remote sensing techniques.

Published by Copernicus Publications on behalf of the European Geosciences Union.

1 Introduction

Aeolian dust derived from sources in north Africa has a substantial impact on the climate and ecosystems in the North Atlantic, but our ability to simulate climate response is poor (Evan et al., 2014; Kok et al., 2018). During aeolian transport, mineral dust influences many atmospheric processes, many of which are a function of mineralogy as well as particle size and elemental composition (Formenti et al., 2011). In addition, deposition of terrestrial material into the North Atlantic ocean is important to the biogeochemical cycle of marine ecosystems as it represents a major source of iron, nitrogen and phosphorous (Baker et al., 2003; Jickells et al., 2005).

In recent years, the composition of dust has attracted extra attention because the mineral phase is thought to influence the ice-nucleating (IN) ability of single particles (Zimmermann et al., 2008; Connolly et al., 2009; Möhler et al., 2008; Cziczo et al., 2009; Niedermeier et al., 2011; Augustin-Bauditz et al., 2016) and therefore influences climate by changing the radiative properties of ice and mixed phase clouds (Rosenfeld et al., 2001; DeMott, 2003), which represent some of the biggest uncertainties in weather and climate change prediction (DeMott et al., 2010; Carslaw et al., 2013). The mechanisms involved are not well understood, and many analytical techniques have been developed to help further our understanding of this important single-particle process (Hoose and Möhler, 2012; Hiranuma et al., 2015). Recently, it has been demonstrated that the mineral phase has an influence on heterogeneous freezing temperature, with some feldspar group minerals proving to be particularly efficient ice-nucleating particles (INPs) in droplet freezing experiments with nominally pure laboratory-prepared mineral samples (Atkinson et al., 2013; Harrison et al., 2016; Peckhaus et al., 2016).

To complicate things further, cloud chamber studies of silicate mineral dust coated with secondary sulfate and organics have demonstrated that this mixing can alter hygroscopicity and change the ice-nucleation efficiency of a particle but is dependent on the ice-forming mechanism (Möhler et al., 2008; Sullivan et al., 2010a, b; Niedermeier et al., 2011; Reitz et al., 2011). In addition, laboratory studies have suggested that the internal mixing state, particularly metal oxide–clay mineral assemblages, has an important influence on direct radiative properties of dust (Nousiainen et al., 2009; Jeong and Nousiainen, 2014; Kemppinen et al., 2015; Di Biagio et al., 2017; Caponi et al., 2017). This highlights the need for measurement of single-particle composition, including both mineralogy and internal mixing state, but is extremely challenging in natural dust particles due to complex mineralogy and mixing state that is a product of the source area, emission mechanism and atmospheric processing.

Major dust emission occurs in sparsely vegetated arid areas but only when the surface properties and meteorological conditions are favourable (Knippertz and Todd, 2012), which can be difficult to predict in dust emission models (Heinold et al., 2013). During the summer months in north Africa, the process of dust advection is associated with moist convection (Schepanski et al., 2009b) and results in a complex structure of stratified layers of warm dry air with very high dust concentrations (Dunion and Marron, 2008). Satellite observations show that these layers can be transported westward in discrete plumes over the Atlantic Ocean towards the Caribbean basin (Kaufman et al., 2005; Zhu et al., 2007; Doherty et al., 2008; Tsamalis et al., 2013).

The source of these dust plumes is arid soils that consist of a complex mixture of organic and inorganic material. The inorganic material largely consists of silicate minerals (quartz, feldspars, clay minerals), carbonate and metal oxides that occur as whole grains or mixed mineral phases. The abundance of the mineral phase has a strong grain size dependence, with quartz occurring in the coarse fraction and clay minerals dominating the fine fraction, but the size distribution is modified during emission (Perlwitz et al., 2015a), so that ratios of mineral phases in the lofted mineral dust aerosol may not be completely representative of that of the source soil. Aircraft observations have demonstrated that the size distribution of dust plumes also evolves during transport, which affects optical properties (Ryder et al., 2013), but the contributions from associated changes in composition are not understood.

Measurements of ambient dust properties are needed to inform simulations of dust emission, transport and deposition processes in present-day climate and paleoclimate models. For example, the provenance of mineral dust has been determined by comparing mass fraction ratios of certain mineral phases to the bulk analysis of soils in potential source areas (PSAs) (Caquineau et al., 2002; Scheuvens et al., 2013). Although improved soil maps are available for north Africa (Claquin et al., 1999; Nickovic et al., 2012; Journet et al., 2014), they still lack the spatial resolution required to represent the heterogeneity of soil within a PSA, and this results in an oversimplification of the mineralogical relationships in a given soil type (Scanza et al., 2015). Improvements to emission simulations require validation measurements of size-resolved dust mineralogy and mixing state at varying distances from the source (Perlwitz et al., 2015b).

Identification of the source of transported dust is problematic due to the inhomogeneity of source sediments and the mixing of material during transport. Nevertheless, analysis of bulk mineralogical composition of source sediments can provide markers, with illite/kaolinite ratios being particularly useful (Caquineau et al., 2002). At the Cabo Verde islands, Glaccum and Prospero (1980) analysed day-long exposures of filters collected during the summer of 1974 and concluded that illite and mica were the dominant mineral types deposited in the tropical North Atlantic. In contrast, Kandler et al. (2011a) reported kaolinite as the dominant mineral type and attributed this to the dominance of sources in the Sahel during the summer.

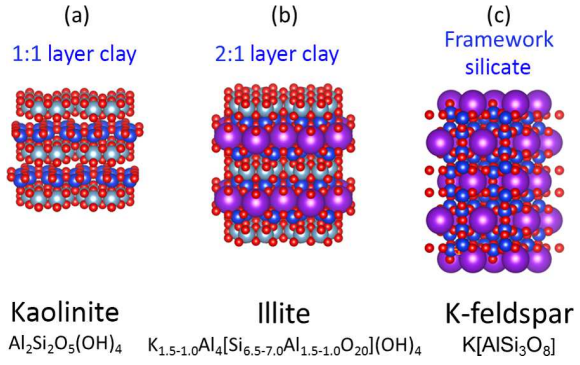

Figure 1. The crystal structures of common aluminosilicate minerals **(a)** 1 : 1 clay mineral structure of kaolinite, **(b)** the 2 : 1 clay mineral structure of illite and **(c)** the framework structure of K-feldspar. Colour code is as follows; red: anions (O, OH), grey: octahedral coordination (Al, Mg), blue: tetrahedral coordination (Si, Al), purple: interstitial complex (K, Na, Ca).

Silicates are the most important group of rock-forming minerals and comprise a huge spectrum of compositions and crystal structures. However, the fine fraction of continental soil largely consists of clay minerals with minor amounts of feldspar and quartz (Perlwitz et al., 2015b). Clay minerals are phyllosilicates which consist of 2-D layers of silicon tetrahedrally coordinated with oxygen and aluminum octahedrally coordinated with oxygen and/or hydroxyl. A simple example is that of the mineral kaolinite ($Al_2Si_2O_5(OH_4)$), in which these two layer types are repeated to form a 3-D structure referred to as a 1 : 1 layer structure (Fig. 1a).

A more complicated structure results in the presence of large cations of potassium, sodium and calcium. The charge and ionic radius of these cations are accommodated in a separate sheet of interstitial cations that must be charge balanced by the tetrahedral and octahedral layers. In the case of potassium, charge balance is achieved with the common 2 : 1 layer structure of illite ($K_{1.5-1.0}Al_4[Si_{6.5-7.0}Al_{1.5-1.0}O_{20}](OH_4)$) in which there are two tetrahedral layers for each octahedral layer (Fig. 1b). These types of clay minerals are expected to be abundant in Saharan dust. For example, in a previous study using transmission electron microscopy (TEM) of sliced dust particles collected on the island of Tenerife in the North Atlantic, the majority of particles of transported Saharan dust were clay-rich agglomerates primarily composed of a matrix of illite/smectite clay minerals (ISCMs) with inclusion of kaolinite and hematite (Jeong et al., 2016).

The feldspar group of minerals is chemically similar to the clay minerals but has a higher atomic content of alkali and alkaline Earth metals which demands a different crystal structure to achieve charge balance. In K-feldspars ($K[AlSi_3O_8]$), such as microcline and orthoclase, interstitial cations of potassium are fixed in a cavity where they are charge balanced by a 3-D network of tetrahedrally coordinated silicon and aluminum (Fig. 1c). Whilst these minerals are expected to be less common than clay minerals in fine mineral dust, they may be particularly important in ice nucleation in the atmosphere.

The analytical challenge arises from the fact that common mineral phases are very similar in composition and undergo significant alteration and weathering in the soil, making pure minerals difficult to identify (Formenti et al., 2014). For example, in clay minerals, potassium, sodium and calcium are interchangeable during the weathering process so that composition is not necessarily uniform throughout the crystal lattice. Indeed, the illite structure in Fig. 1b is the idealised version of the pure mineral, which is often referred to as an end-member of the illite series. Complete uniformity of clay mineral composition is unlikely on the scale of a single particle or between particles from the same soil sample.

In order to identify the mineral phases present, one must either make an accurate quantitative measurement of the elemental composition or make an analysis of crystal structure. An established approach to both ambient and laboratory measurements is to collect particles on filters and impactors for subsequent offline analysis. Bulk mineralogy can be obtained with crystal structure analysis by X-ray diffraction (XRD), and the composition of individual particles is assessed by advanced microscopy. Scanning electron microscopy (SEM), often combined with energy-dispersive X-ray spectrometry (EDX), is a powerful method for elucidating composition because of the ability to probe the composition of individual dust particles. The application of these techniques can differentiate silicate from calcium-rich particles and shows evidence of heterogeneous reactions in the atmosphere (Ro et al., 2005; Jeong and Chun, 2006; Sobanska et al., 2012).

However, further differentiation of the silicate mineral phase in single particles is hampered by the difficulty in leveraging the full quantitative capability of SEM due to particle morphology effects. Consequently, silicate particles are often reported in compositional groups, which describe the dominant elemental features but not the actual mineral phase (Kandler et al., 2009; Eriksen Hammer et al., 2018). In addition, there are a number of drawbacks to this offline approach including labour-intensive post-sampling analysis and loss of temporal resolution in dynamic situations.

Another, but less common, approach is to use single-particle mass spectrometry (SPMS) to provide an online assessment of aerosol composition. An advantage of this technique is that the high temporal resolution allows the evolution of the particle composition to be measured in a dynamic setting (Cziczo et al., 2006; Zelenyuk et al., 2009; Gaston et al., 2013), and the instruments can be deployed in line with other techniques such as counterflow virtual impactor (CVI) to measure ice residuals (Cziczo et al., 2003; Gallavardin et al., 2008; Baustian et al., 2012; Zelenyuk et al., 2015; Worringen et al., 2015; Schmidt et al., 2017). However, compositional analysis with SPMS is fraught with difficulties relating to poor reproducibility and the non-quantitative nature of the measurement associated with instrument function and parti-

cle matrix effects (Reilly et al., 2000; Sullivan and Prather, 2005; Murphy, 2007; Hatch et al., 2014).

The matrix effects arise from the incomplete desorption of the particle and the subsequent competitive ionisation of atoms and molecular fragments, so that covariance of analyte signals is relative to ionisation energy and electron affinity of the surrounding matrix (Reinard and Johnston, 2008). In circumstances where the composition of the matrix is known a priori, careful calibration with a suitable proxy can produce quantitative or semi-quantitative measurements of an analyte within a single particle (Gross et al., 2000; Bhave et al., 2002). However, if the particle matrix is complex, such as in soils and transported dust, this type of calibration cannot be made due to the lack of a suitable proxy.

Despite these limitations, SPMS can characterise a particle population by classifying particle types and measuring temporal trends in particle number concentrations using cluster analysis (Hinz et al., 2006; Rebotier and Prather, 2007; Gross et al., 2010). Although the reported number concentrations are not fully quantitative (Murphy, 2007), a relative trend in certain particle types can be realised. This technique has been used to discriminate mineral dust particles from other refractory aerosol types, such as sea salt (Sullivan et al., 2007a; Dall'Osto et al., 2010; Fitzgerald et al., 2015; Schmidt et al., 2017), but cannot differentiate the actual mineral phase of silicates within dust particles. More recently, a machine learning technique has shown promise for the classification of mineral dusts of similar composition (Christopoulos et al., 2018), but this technique also requires suitable mineral dust proxies for training data.

In a previous study using a single-particle laser ablation aerosol particle time-of-flight mass spectrometer (LAAPTOF, AeroMegt GmbH), Marsden et al. (2018) presented a novel method for the assessment of single-crystal structure that, when used in tandem with the more typical elemental composition measurement, performed an online differentiation of single particles of kaolinite, illite and K-feldspar mineral phases. In the present study, we applied a refined version of these techniques to suspended natural soils sampled at the Aerosol Interactions and Dynamics in the Atmosphere (AIDA) facility at the Karlsruhe Institute of Technology (KIT), as part of the Ice-Nuclei Research Unit (INUIT) programme studying heterogeneous ice formation in the atmosphere (https://www.ice-nuclei.de/the-inuit-project/, last access: 15 February 2019). The results of analysing soil from PSAs in north Africa were used to interpret ground-based ambient measurements of transported dust at Praia, Cabo Verde, in the tropical North Atlantic during the summer of 2015 as part of the Ice in Clouds Experiment – Dust (ICE-D) campaign.

2 Methods

A limited number of mineral phases were chosen to create fingerprints to which the more varied mineralogy of naturally occurring sediments could be compared. Nominally pure samples of illite, Na-montmorillonite and kaolinite, along with orthoclase (K-feldspar) and plagioclase (Na-feldspar), were used to represent the endmembers of the clay minerals and feldspar groups, respectively. This is based on the assumption that the fine fraction ($< 2.5\,\mu m$) continental sediment is primarily composed of aluminosilicate clays and feldspars. Quartz and carbonate minerals are not considered with subcompositional analysis due to the inability of the LAAPTOF to efficiently ablate pure quartz and the apparent lack of a clear carbonate signal, respectively. In ambient dust, calcium-rich particles are considered separately to aluminosilicate particles after being separated using traditional cluster analysis techniques.

The LAAPTOF instrument and data analysis methods are described below, along with SEM-EDX methods used to obtain elemental composition of the laboratory-suspended dust for method validation. The experimental setups of the INUIT09 laboratory campaign and ICE-D ambient measurement are also described in this method section.

2.1 LAAPTOF single-particle mass spectrometry

In a previous study, Shen et al. (2018) showed that the LAAPTOF single-particle mass spectrometer is capable of distinguishing the composition of particles in the ambient environment using a combination of fuzzy clustering and reference-based spectra classification, whilst Ahern et al. (2016) demonstrated a positive correlation between ion signals of organic markers and the quantity of condensed organic coating, despite inhomogeneity in the soot core of the particles. These studies show that the LAAPTOF is an appropriate platform for studying the composition and internal mixing state of refractory aerosol.

In SPMS, aerosol is directly introduced into the instrument via a pumped inlet so that sample collection and preparation are not required. Particle composition is analysed by time-of-flight mass spectrometry (TOFMS) after laser desorption ionisation (LDI) of individual particles using a high-powered UV laser. The LAAPTOF instrument features an aerodynamic lens inlet, optical particle detection, LDI ion source and bipolar TOFMS as previously described by Gemayel et al. (2016). Within the instrument, LDI is performed by ArF excimer laser (model EX5, GAM Laser Inc.), set to deliver 3–5 mJ per pulse of 193 nm radiation with a pulse width of 8 ns.

Like all single-particle mass spectrometers, the LAAPTOF measurements are subject to a number of biases that result in preferential transmission, detection and ablation efficiencies of certain particles (Murphy, 2007). The instrument used in this investigation features a modified

particle detection system based on a fibre-coupled laser delivery that allows the simple interchange of laser systems of different wavelengths. The instrument is capable of providing size-resolved composition measurements for up to 200 particles per second in the size range of approximately 0.4–2.5 µm, but the actual detection efficiency of particles within this range depends on the size, shape and composition, as well as the wavelength of the optical detection system. Differences in instrument setup between the laboratory and ambient measurements that may impact the comparison of the two data sets are presented in Sect. S1 in the Supplement.

Laboratory evaluation of the fiber-coupled laser system indicated that the peak detection efficiency is 0.25 with spherical particles (Marsden et al., 2016), but the overall efficiency of the instrument also depends on ablation efficiency with respect to particle composition. In a study of nominally pure mineral samples, Marsden et al. (2018) reported the number of optically detected particles that produced mass spectra (i.e. ablation efficiency or hit rate) was 0.29 and 0.14 for illite and kaolinite, respectively, but was also dependent on the amount of impurities such as titanium. Furthermore, from the authors' own experience, pure quartz has an ablation efficiency close to zero and is not considered in our analysis but is unlikely to be a major component in the fine fraction in any case. The potential maximum overall efficiency (detection efficiency multiplied by ablation efficiency) of the LAAPTOF measurement of clay mineral ranges from 0.0725 for pure spherical particles of illite to 0.035 for pure spherical particles of kaolinite. The exact efficiency of the instrument is not known in most situations because the size, shape and composition of the particles would have to be known a priori for accurate calibration.

2.1.1 Crystal structure analysis of silicates

In a study of ion formation mechanism, Marsden et al. (2018) showed that the ionisation potential and coordination of interstitial cations has a strong influence on how the crystal structure breaks apart during LDI process of silicate particles. This is exploited for the differentiation of the mineral phase by the measurement of average ion arrival of the O^- and SiO_3^- ion species, which is thought to record the initial kinetic energy of the ionic fragments during ablation.

With this technique, we can compare the structure of soil dust samples to nominally pure mineral samples on a particle-by-particle basis. Laboratory calibrations have demonstrated that for ISCM the abundance of exchangeable sodium and potassium cations results in a unique range of τ values between 0.2 and 0.58. Feldspars typically produce τ values > 0.58 (Fig. 2) due to the interlocking nature of the interstitial cation in their crystal structure. Kaolinite and amorphous glass produces τ values close to 1 due to the complete absence of interstitial cations and lack of crystal structure, respectively.

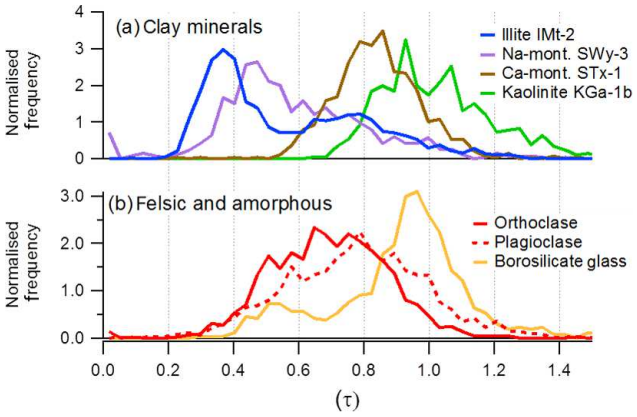

Figure 2. The differentiation of reference minerals using crystal structure analysis described by Marsden et al. (2018). The peak shift ratios (τ) were calculated from ion arrival times from individual particles in the mass spectrometer, rather than conventional peak area analysis for elemental composition. Nominally pure mineral dust was sampled after dispersion in a dust tower: **(a)** nominally pure clay minerals from the clay mineral society and **(b)** orthoclase (K-feldspar), plagioclase (Na-feldspar) and borosilicate glass.

2.1.2 Subcompositional analysis of silicates

Subcompositional analysis is a technique that is commonly used for the analysis of complex chemical relationships in circumstances in which the full composition of a substance is impossible to obtain, such as in whole-rock geochemical analysis (Pawlowsky-Glahn and Egozcue, 2006), where it is convenient to describe the composition in terms of a relative measurement of carefully chosen components. The ternary diagram provides an intuitive way of displaying relative information whilst avoiding some of the subcompositional incoherence associated with two component systems. The technique has been applied to the single-particle analysis of natural Asian mineral dust using SEM (Yuan et al., 2004) and transported Asian dust using SPMS (Sullivan et al., 2007a). It is particularly well suited to SPMS because the composition obtained from the mass spectra is inherently subcompositional due to the matrix effect.

Subcompositional analysis was used to produce fingerprints of pure mineral phases using the ternary system $Al^+ + Si^+$, K^+ and Na^+ cations readily observed in the SPMS of mineral dust (m/z 27, 28, 39 and 23, respectively). Source clay material from the clay mineral society and crushed feldspar crystals were suspended in a homemade dust tower in the experiment described in Marsden et al. (2018). Elemental composition and mineralogy of these samples have been previously characterised and can therefore be used as reference fingerprints for comparison with natural soil. Ternary diagrams of the clay minerals and feldspar standards are displayed separately in Fig. 3.

The 2-D space in these diagrams is non-linear and, due to the matrix effect, a fully quantitative composition cannot be

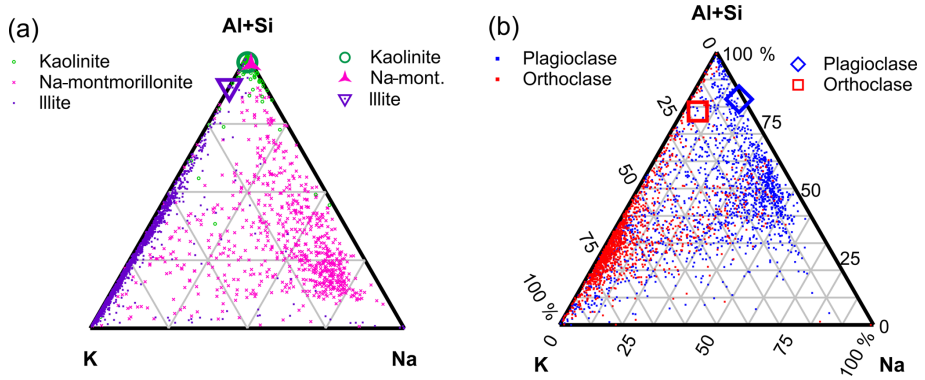

Figure 3. The differentiation of reference minerals using subcompositional analysis. Each dot in the ternary plots represents the composition of a single particle calculated from Al + Si, K and Na peak areas in the mass spectra. Larger icons represent bulk composition by X-ray fluorescence (XRF) analysis. Nominally pure mineral dust was sampled after dispersion in a dust tower: **(a)** nominally pure clay minerals illite (1806 particles), kaolinite (1388 particles) and Na-montmorillonite (800 particles) from the clay mineral society and **(b)** orthoclase (K-feldspar, 1318 particles) and plagioclase (Na-feldspar, 1568 particles).

deduced from these plots alone, but it is interesting to note that K-feldspar appears less K- and Na-rich than illite clay despite the structural formula and X-ray fluorescence (XRF) analysis of the bulk sample indicating the contrary. This is because the tetrahedral framework of the feldspar makes the release of interstitial K^+ and Na^+ without also releasing Al^+ improbable, whereas they can be released independently of Al^+ from the weakly bonded interlayer in 2 : 1 clay structure.

Although the elemental subcomposition measurement is clearly non-quantitative with respect to bulk XRF analysis, the measurement is semi-quantitative (relative) with respect to samples of minerals with the same crystal structure. For example, a clear separation between K- and Na-rich feldspar is apparent in Fig. 3, which is relative to their actual elemental ratios. This is not true if comparing the clay mineral illite with the framework silicate K-feldspar, which would not be easily distinguishable from each other if plotted in the same space, despite the clear differences in elemental composition. It is therefore necessary to apply crystal structure analysis to achieve semi-quantitative composition and distinguish clay minerals from feldspar when analysing natural soils with SPMS.

2.1.3 Subcomposition analysis of internal mixing state

Internal mixing of non-mineral species can occur during soil formation or during transport in the atmosphere where heterogeneous reactions take place on the surface of the particle (Usher et al., 2003). Reactions with nitric, sulfuric and organic acids can produce nitrate, sulfate and organics on the particle surface, respectively. Reference spectra obtained with the LAAPTOF during the FIN-1 campaign show the presence of sulfate marker HSO_4 (m/z 97) on particles after mixing suspended feldspar with ozone and sulfuric acid in the AIDA chamber (Fig. 4b). Similarly, organic markers C_2, C_2H and C_2H_2 (m/z 24, 25, 26) appear on particles after mixing suspended feldspar with ozone and α-pinene (Fig. 4c). Only small organic fragments are observed due to the extensive fragmentation of organic molecules. These ion combinations have also been observed on ambient mineral dust using SPMS instruments (Silva and Prather, 2000; Sullivan et al., 2007a; Fitzgerald et al., 2015) but may also be derived from black carbon mixed with the particle as well as charred organics.

In ambient dust, organic or biological material may have been mixed with a dust particle in the soil before emission. Indeed, the transport of microorganisms in dust storms is a human health concern (Griffin, 2007). Recently, Yamaguchi et al. (2012) provided direct evidence of bacterial cells on Asian dust particles and demonstrated a global dispersion pathway through dust transport. The internal mixing of biological material with dust particles is therefore of interest. LAAPTOF reference spectra of bacteria, also from the FIN-1 campaign, show strong signals of CN and CNO (m/z 26, 42) (Fig. 4d) representing fragments of nitrogen-containing organic compounds. These markers have been attributed to compounds of biological origin (Pratt et al., 2009; Cahill et al., 2012; Creamean et al., 2013), although other studies have found these markers in aerosol where biological components were not expected (Sodeman et al., 2005; Zawadowicz et al., 2017; Wonaschuetz et al., 2017). Consequently, we describe these markers as organic–biological (org–bio hereafter).

Internal mixing of natural soil samples with non-minerals in this work are considered with the ternary subcomposition Cl^-, $CN^- + CNO^-$, SO_4^-. These markers represent compounds that could be present in soils and ambient dust but are not present in silicate mineral structure. Phosphate marker PO_3^- is not considered because it could be derived from the calcium phosphate mineral apatite as well as biological material; therefore, it is not a reliable indicator of biological mix-

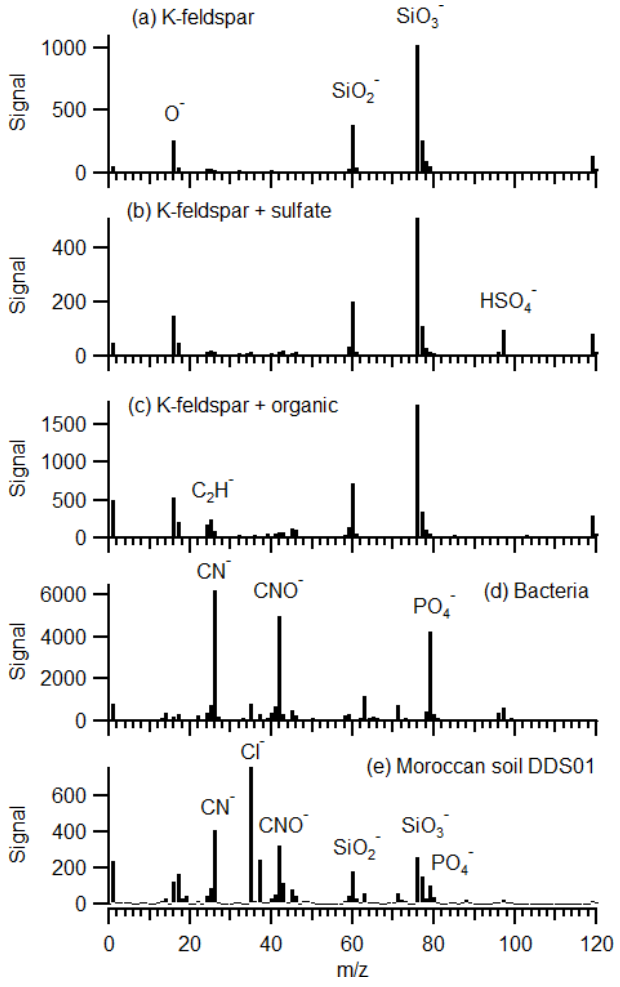

Figure 4. Average negative ion mass spectra (200 particles) of resuspended material in the AIDA chamber during the FIN-1 campaign: **(a)** pure K-feldspar, **(b)** K-feldspar with sulfate coating, **(c)** K-feldspar with organic coating, **(d)** bacteria and **(e)** Moroccan soil dust DDS01 during INUIT09.

ing state. The Cl^- elemental ion is included despite it also having mixed provenance such as primary chlorides or secondary uptake of HCl (Sullivan et al., 2007b), because it is preferentially ionised due to very high electron affinity and therefore is included as a reference that would otherwise perturb the measurement. It is also an indication of the purity of silicate particles, as pure fresh silicate should not contain chlorine.

2.2 Scanning electron microscopy

Particles were sampled from the AIDA chamber with a single-stage nozzle impactor (50 % low cut-off diameter at approximately 0.1 µm aerodynamic diameter; for specifications, see Kandler et al., 2007) on nickel grids (TEM grids type S162N9, Plano, Wetzlar, Germany). The inlet was connected to a sampling line on the AIDA chamber and the sample time varied between 12 and 16 min.

All samples were analysed with computer-controlled scanning electron microscopy (ccSEM) using a FEI Quanta 400 FEG instrument (FEI, Eindhoven, the Netherlands) equipped with an energy-dispersive X-ray detector, X-Max150 (Oxford, Oxfordshire, United Kingdom) and the Oxford software Aztec (version 3.3 SP1). An acceleration voltage of 12.5 keV, spot size 5, a working distance of 10 mm and high vacuum conditions (10^{-5} hPa) were used for all samples. Backscatter electron images were used to segment particles from substrate. The particles of interest were measured with a 4 s counting time for X-ray microanalysis. The TEM grids were mounted in a copper sample holder (avoiding interference with chemical composition of the particle) equipped with a beam trap (maximising the characteristic-peak-to-background ratio).

Chemical composition of all elements with atomic number higher than 3 (Li) was determined with energy-dispersive X-ray microanalysis. A sorting step after ccSEM was performed to remove particles with low X-ray counts (due to shading effects) and features of the TEM grid. Between 159 and 776 aluminosilicates were detected per sample, with the highest abundance of particles at an average diameter of 200 nm.

The traditional method for reporting the composition of aerosol particles involves the classification of particles into compositional groups using a variety of elemental ratios and boundary rules, e.g. Kandler et al. (2007, 2011b); Young et al. (2016). However, these classification systems are impossible to apply to SPMS due the matrix effects that skew and suppress elemental ratios. We therefore choose to display the SEM composition as ratios of Al/Si, (K + Na)/Si and (Fe + Mg)/Si, which leverages the quantitative ability to produce a representation of the interstitial cation and aluminosilicate structure that can be intuitively compared to the ternary diagrams obtained by SPMS.

A scatterplot of single-particle average chemical composition is plotted in Fig. 5a. This demonstrates that pure minerals can potentially be differentiated using quantitative Al/Si ratio and the (K + Na)/Si (cation to silicate) ratio. For example, the pure kaolinite clay mineral has the highest Al/Si ratios (≈ 1) but no (K + Na) content. In general, the decreasing Al/Si ratio must be balanced by increasing cation/Si ratio in clay minerals.

2.3 INUIT09 laboratory-suspended dust experiment

2.3.1 Experiment setup

For the aerosol generation during the INUIT09 campaign, the natural dust samples were sieved to diameters less than 75 µm and injected in either the AIDA cloud chamber or the aerosol preparation and characterisation (APC) chamber. For injection, a rotating brush generator linked to a cyclone im-

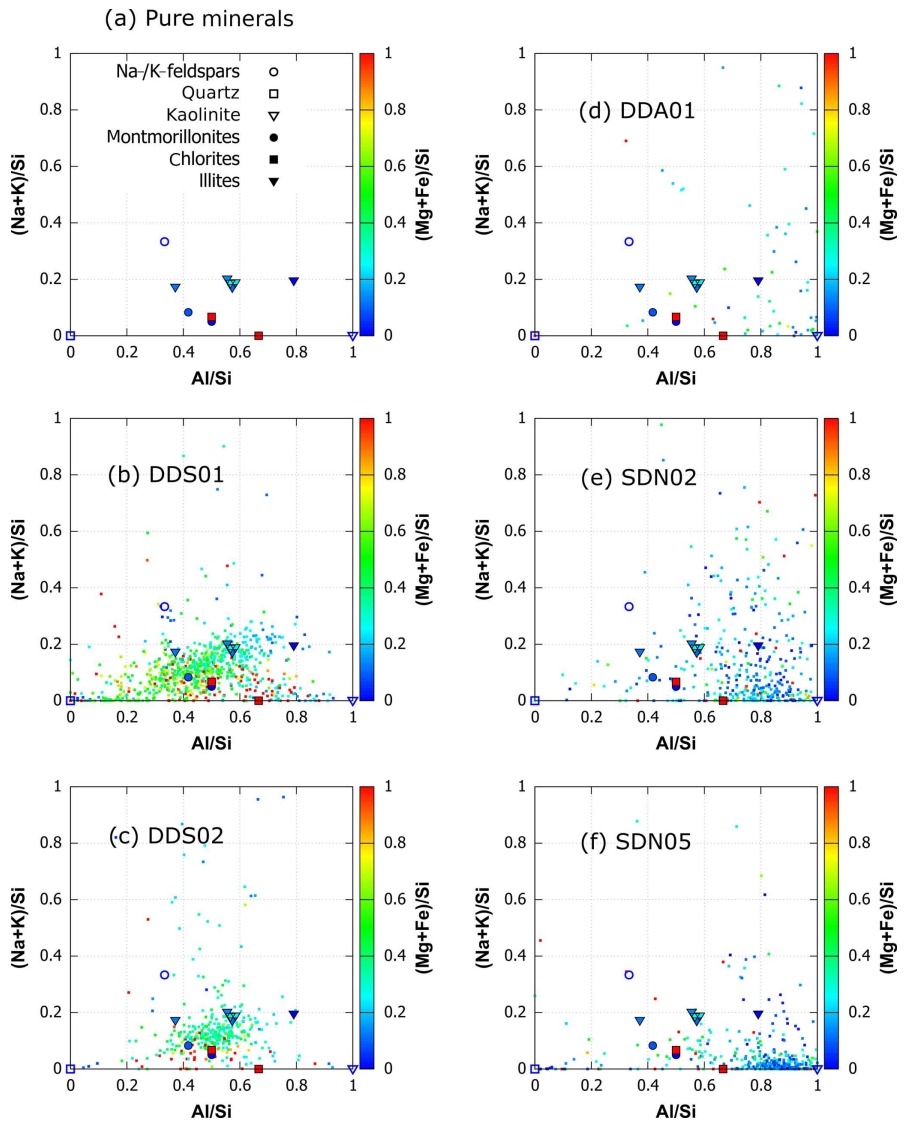

Figure 5. Elemental subcomposition diagrams of suspended natural soil samples (INUIT09) by SEM EDX analysis: **(a)** average composition of nominally pure mineral samples, **(b)** DDS01, **(c)** DDS02, **(d)** DDA01, **(e)** SDN02 and **(f)** SDN05. Ratios are calculated from atomic percentage.

pactor was used, resulting in aerosol particles with aerodynamic diameters of less than about 5 µm. The dust number concentration in the AIDA chamber was initially between 200 and 300 cm^{-3} and in the APC chamber between 1000 and 5000 cm^{-3}. The number concentrations and size distribution of the dispersed aerosol are detailed in Sect. S2 in the Supplement.

During this study, the single-particle mass spectrometer LAAPTOF was either connected to the AIDA chamber or the APC, and sampled for about 1 h during each experiment. During the sampling time, both the AIDA chamber and APC chamber were held to nearly constant temperature (either −16 or −21 °C in AIDA and 25–27 °C in APC) and pressure (998–1010 hPa in AIDA and 990–1005 hPa in APC) conditions.

2.3.2 Soil sampling locations

Soil samples from two specific ecoclimatic zones were suspended at the AIDA facility: the mountainous north-west margin of the Sahara and the west-central Sahel beyond the southern margin of the Sahara (hereafter named Sahel dust). These PSAs were chosen because there are likely to be differences in mineralogical composition between the two zones. Analyses of surface material across north Africa are scarce, but the available studies demonstrate a north–south decease in illite/kaolinite (I/K) ratio in the clay fraction (Caquineau et al., 2002; Scheuvens et al., 2013; Formenti et al., 2014)

mainly due to differences in diagenetic history between dry and wet climate zones.

The sampling locations (Table 1) of the natural arid soils are displayed in Fig. 6. Moroccan dust samples were collected in the Mhamid region, on the upper Draa Valley, Morocco, during the Saharan mineral dust experiment (SAMUM) (Ansmann et al., 2011). The Draa Valley is a large geographical feature on the southern edge of the Anti-Atlas Mountains, beyond which is the Sahara desert of Algeria. All sampling locations fall within unit 1336 in the Digital Soil Map of the World (DSMW), compiled by the Food and Agriculture Organization (FAO) of the United Nations.

The samples of Sahel soil were collected from diverse geographical locations in Niger and Burkina Faso. All three sampling locations fall within the zone of kaolinite-rich soil (Fig. 6), where the DSMW indicates cation exchange capacity (CEC) $< 35\,\mathrm{cmol\,kg^{-1}}$.

2.4 Ambient measurement at Cabo Verde during ICE-D

The Cabo Verde archipelago is a favourable location for remote marine measurements. Situated some 800 km off the west coast of north Africa (Fig. 6), it is a site at which long-term measurements of greenhouse gases, trace gases and aerosol properties are recorded (Carpenter et al., 2010). Notable studies of mineral dust composition in the area include long-term filter sample collection at Cabo Verde atmospheric observatory (CVAO) (Patey et al., 2015) and Praia, Santiago Island (Salvador et al., 2016), and filter collection at Praia airport, Santiago Island, for the SAMUM campaign in January–February 2008 (Kandler et al., 2011a).

Ground-based ambient measurements during ICE-D took place in the mobile Manchester Aerosol Laboratory located within the perimeter of Praia International Airport, Santiago Island, Cabo Verde (14°57′ N, 23°29′ W; 100 m a.s.l.), approximately 1500 m from the coast and 150 m from the airport runway. The main airport terminal and the outskirts of the city of Praia were 400 and 2500 m downwind of the prevailing NE wind, respectively. Aerosol was sampled via a 15.24 cm plastic inlet fixed to a 10 m tower and pumped at $185\,\mathrm{L\,min^{-1}}$. The flow was distributed to a suite of online instruments, including the LAAPTOF, via a system of 48 mm ID lines isokinetically sampled from the main inlet, and heated to 19 °C.

3 Results and discussion

3.1 Single-particle analysis of laboratory-suspended natural soil (INUIT09)

The sampling of particles took place after dispersing the source material in the APC chamber using a rotating brush generator. The resulting particle concentration and size distribution were dynamic but was typically on the order of $1000\,\mathrm{cm^{-3}}$ with a particle size mode at 200 nm (see Sect. S2 in the Supplement), which is below the lower size cut of the LAAPTOF, but not the filter collection. Therefore, the two measurement techniques are not performed on the exact same particle sizes. Still, both measurements represent the fine fraction ($< 2.5\,\mu\mathrm{m}$) of the dispersed dust.

3.1.1 Silicate mineralogy of laboratory-suspended soil (INUIT09)

SEM EDX analysis of the suspended soil shows that the composition of single particles within each soil type varies in a continuous distribution rather than in distinct clusters (Fig. 5). A distinct difference in the elemental composition of soil from the northern Sahara and the Sahel exists in these diagrams, particularly with respect to the Al/Si ratio. The Moroccan soils (Fig. 5b–c) have a spread in compositions close to the illite plotted on the diagram, with the DDS01 samples being more diverse than the DDS02. In contrast, the soil from the Sahel (Fig. 5c–f) consists of material with a higher Al/Si ratio which approaches the composition of the plotted kaolinite. This is in agreement with CEC measurements of sediments which show that kaolinite fraction in soils increases in the Sahel region compared to the northern region of the Sahara (Scheuvens et al., 2013).

SPMS mineralogical analysis proceeded by considering the relative abundance between K, Na and Al + Si, which together define the phase of many minerals in the continental crust. This subcompositional analysis was previously applied to nominally pure mineral samples from the Clay Minerals Society (CMS) to provide a fingerprint reference for the common clay mineral phases (Fig. 7a). The same analysis applied to Moroccan dust (Fig. 7a–c) and Sahelian dust (Fig. 7e–g) shows key differences between the composition of the two ecoclimatic zones, with Moroccan dust tending towards an illite composition and Sahelian dust tending to a kaolinite composition, in agreement with the SEM EDX analysis.

Application of the crystal structure analysis (colour function in Fig. 7) to each particle indicates that the majority of the particles are of a 2 : 1 clay structure, even in Sahelian dust particles that have a kaolinite-like (1 : 1 clay structure) composition. This may suggest an impure kaolinite or montmorillonite that is not captured in the cation subcomposition due to the relatively high sensitivity to K^+ in the LAAPTOF measurement. A comparison of the subcomposition (Al+Si)/(Al+Si+K+Na) obtained by SPMS and SEM (Fig. 8) demonstrates a much greater sensitivity to alkali metals in the SPMS measurement (due to low ionisation energy) than in the established filter technique. The SEM technique reports a lower (Al + Si)/(Al + Si + K + Na) ratio in the Moroccan sample (DDS01; Fig. 8a) compared to the Sahel sample (SDN02; Fig. 8c), but this is greatly exaggerated in the SPMS analysis (Fig. 8b and d) due to selective ionisation of K and Na and the matrix effect.

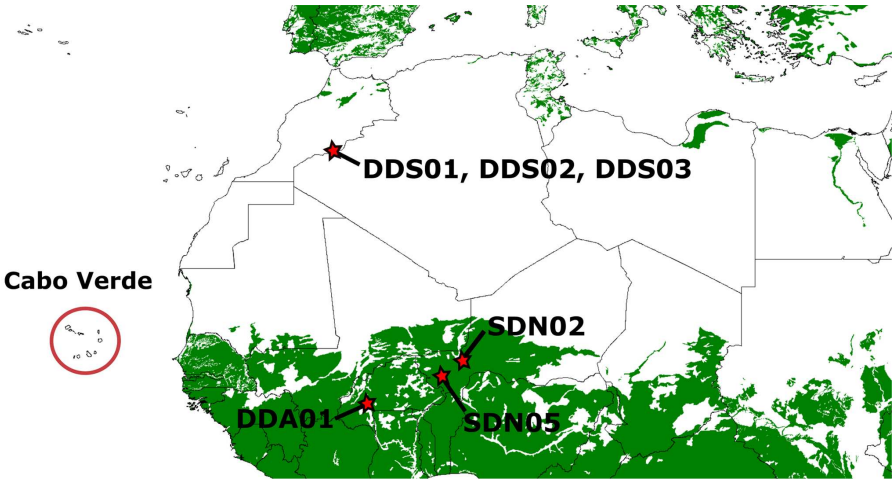

Figure 6. Sampling locations of natural soil (stars) and transported dust at Cabo Verde (circle). The green colour indicates soils that have a cation ion exchange capacity (CEC) of less than 35 cmol kg^{-1} indicating kaolinite-rich soil. This figure is produced from the Digital Soil Map of the World.

Table 1. Sampling location of natural soils for laboratory experiments.

Sample	Location	Notes
DDS01	29.83773° N, −5.76143° E	River sediments
DDS02	29.84957° N, −6.01508° E	Hamada with large amounts of dust
DDS03	29.86202° N, −6.156760° E	Border of dry salt/silt plain
SDN02	13.516667° N, 2.633333° E	Banizoumbou, Niger
SDN05	13.522203° N, 2.133011° E	Grand Mosque, Niamey, Niger
DDA01	NA	Dano, Burkina Faso

NA: not available.

In general, our analysis suggests that the fine fraction of these north African soil samples consists of K-rich and Al-rich clay minerals. This agrees somewhat with a comprehensive study of soil samples using many techniques by Engelbrecht et al. (2016) that concluded suspended mineral dust particles were primarily made up of two types of mineral assemblages: (i) fragments of micas, clays, oxides and ions of potassium-rich (K^+), calcium-rich (Ca^+) and sodium-rich (Na^+) colloids in amorphous clay-like material, and (ii) kaolinite with individual oxide mineral grains. The exception is that our measurements indicate that the potassium and sodium are retained in a 2 : 1 clay structure rather than in amorphous clay.

In order to explore the composition of potentially amorphous and feldspar matrix, we extracted particles with τ values of 0.58–0.8 into separate plots (Fig. 9). Perhaps unsurprisingly, the composition of these types of particles reflects the composition of clay particles (Fig. 7), with samples from the Sahel showing a greater loss of alkali metals due to weathering and diagenesis. It is not possible to separate felsic and amorphous material with any confidence, but it is reasonable to say that any feldspars that may be present in the Moroccan samples are fresher (unaltered) than their counterparts from the Sahel due to the higher potassium content. It is known that K-feldspar is progressively altered to quartz and kaolinite if the potassium is removed by dissolution in the soil.

The sample that potentially has the most feldspar grains is DDS01, which shows a small number of particles with a felsic composition in the SEM EDX analysis (Fig. 5b) and may be a reflection of the river sediment containing freshly eroded rock from the Anti-Atlas mountain range. This sample also displays a distinct mode in the SPMS τ histogram in the felsic/amorphous region (Fig. 7d). In general, the SPMS crystal structure analysis in the τ histograms agrees with the SEM EDX analysis of the distribution of composition in the samples. For example, the τ histogram of DDS02 indicates a predominately illite composition which is also reported in the narrow composition distribution in the SEM EDX analysis.

3.1.2 Internal mixing state of suspended natural soil

Unlike the mineralogical composition, the mixing state of the natural soil samples varied quite a lot within the same PSA (Fig. 10). Sample DDS03, collected close to a salt/silt

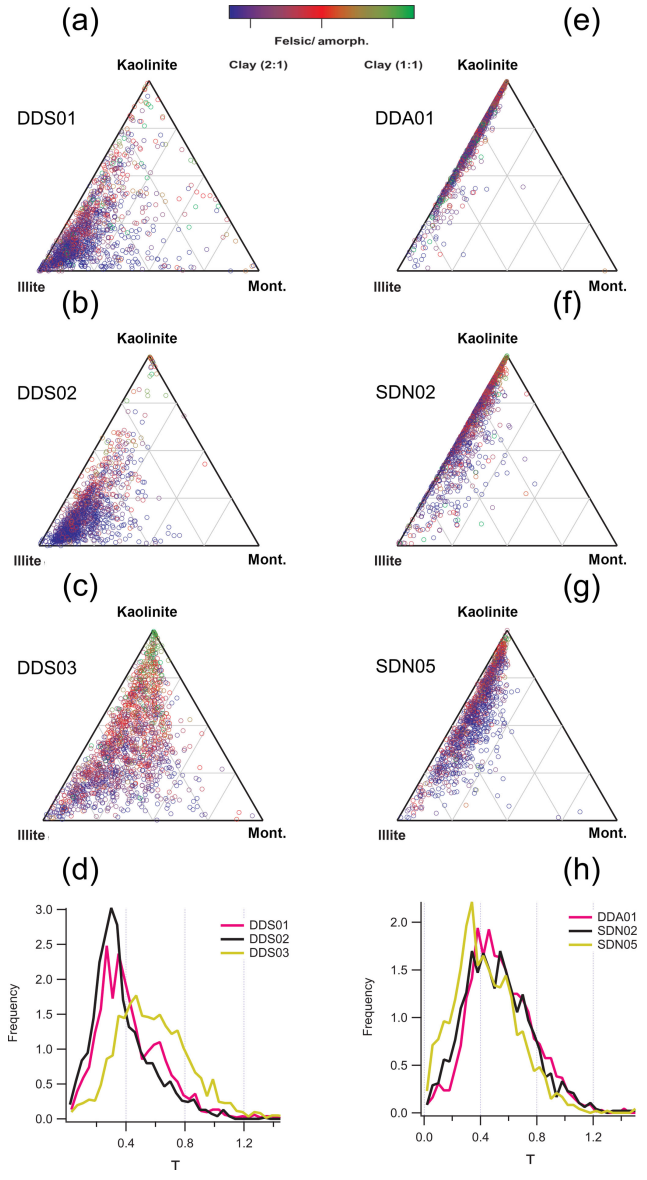

Figure 7. Subcompositional analysis of suspended natural soil samples (INUIT09) by SPMS. The ternary diagrams are referenced to the inferred kaolinite, illite, Na-montmorillonite endmembers of the clay mineral series using the Al+Si, K and Na ratios from reference minerals (Fig. 3). Samples from Morocco are in the left column **(a, b, c)** and samples from the Sahel in the right column **(e, f, g)**. The colour function is proportional to the τ parameter as defined by the crystal structure analysis technique, so that the blue dots represent 2 : 1 clay minerals. The distribution of τ for each sample is also displayed as a histogram **(d, h)** (2000 particles analysed in each sample).

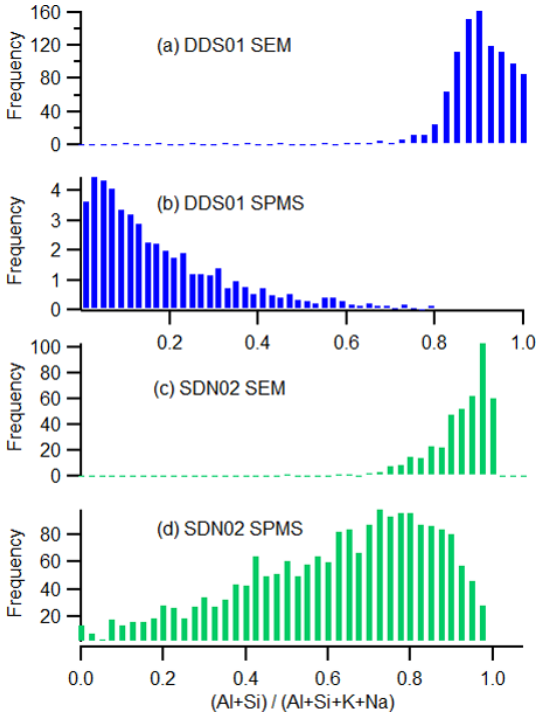

Figure 8. A comparison of the relative sensitivity of the SEM and SPMS techniques to the principal elements in silicate minerals. Histograms represent the sensitivity to alkali metals of the interstitial complex with respect to the Al and Si of the silicate structure (Al+Si)/(Al+Si+K+Na) in single particles. Moroccan soil sample DDS01 **(a, b)** compared to Sahelian soil sample SDN02 **(c, d)** using the SEM and SPMS techniques, respectively.

plain, shows a relatively high sulfate content, probably associated with evaporite deposits. The biggest difference, however, is the relative amount of org–bio internally mixed in the particles. This is further demonstrated in the histograms of the normalised org–bio content displayed in Fig. 11. Most samples contain particles with significantly less org–bio than chlorine, but samples DDS01 and SDN02, collected from a dry river bed and agricultural land, respectively, have a number of particles where the org–bio signal is even stronger than that of chlorine, which is significant given the high electron affinity of the later. All laboratory-suspended soil samples contained a significant amount of chlorine, demonstrating that chlorine can be internally mixed with silicate particles before emission and transport. This makes the Al/Cl ratio used by Sullivan et al. (2007b) in ambient Asian dust an unreliable measure of heterogeneous reaction of silicate with atmospheric HCl in ambient Saharan dust.

3.2 The composition and transport history of transported dust (ICE-D)

In order to examine the properties of the transported dust in the ambient measurement, the mass spectra of silicate particles were first extracted from the general aerosol population. This was achieved using the fuzzy c-means clustering supplied with the data analysis software (LAAPTOF data analysis v1.0.2). The analysis was performed on positive and negative ion spectra and on negative ion spectra only. In both

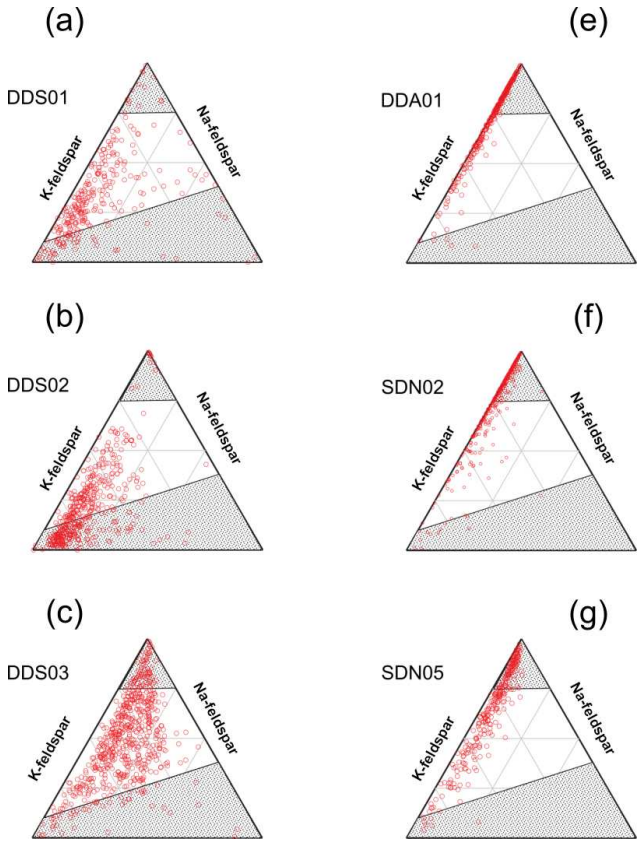

Figure 9. Subcompositional analysis of the feldspar/amorphous content in suspended natural soil samples (INUIT09) by SPMS. The felsic/amorphous fraction was selected by crystal structure analysis ($0.58 < \tau < 0.8$). The ternary diagrams are referenced to the inferred K and Na endmembers of the feldspar series using the Al+Si, K and Na ratios from reference minerals (see Fig. 3). The greyed out area represents unlikely composition of feldspar as demonstrated by the reference minerals. Samples from Morocco are in the left column **(a, b, c)** and samples from the Sahel in the right column **(e, f, g)**.

cases, silicate and calcium classes of particles were reported along with sulfate, carbonaceous and abundant sea-salt particles. Analysis using only negative ion spectra proved more useful in the evaluation of mixing state because it was not subject to false class divisions caused by greater peak position shifting in positive ion spectra. A full description of the clustering analysis, including mass spectra of the cluster centres, is provided in Sect. S3 in the Supplement.

Averaged detection rate of the silicate and calcium particle types, as determined by the fuzzy clustering analysis, is displayed in Fig. 12a with a 1 h resolution. A previous comparison with an aerodynamic particle sizer indicated that the silicate particle count represented approximately 1 % of the actual silicate present due to instrument function (Marsden et al., 2016). Nevertheless, the temporal evolution of the particle classes is representative and compares well to the dust fraction of incandescent particles identified in tandem soot photometer (SP2) measurement (Liu et al., 2018).

3.2.1 Calcium-rich particles

Calcium carbonate ($CaCO_3$) is the most abundant non-silicate material in arid soils and is expected to be a major constituent in mineral dust aerosol. However, pure calcium carbonate particles were not observed in this ambient measurement. Alkaline calcium carbonate particles are expected to readily react with acid gases in the atmosphere to form calcium salts. The reaction of calcium carbonate with nitric acid has been offered as a mechanism to explain $Ca(NO_3)_2$ on filters exposed to dusty environments (Krueger et al., 2004; Laskin et al., 2005; Matsuki et al., 2005; Hwang and Ro, 2006; Sobanska et al., 2012). More recently, it has been suggested that, in remote marine environments, a prevalence of HCl over HNO_3 would favour the formation of $CaCl_2$ as the principal calcium salt (Tobo et al., 2009; Kim and Park, 2012).

A distinct calcium chloride particle class is reported in this ambient measurement. These particles are characterised by signals of Ca^+ (m/z 40), CaO^+ (m/z 56) and $CaCl^+$ (m/z 75, 77) in positive ion spectra, and Cl^- (m/z −35, −37) and $CaCl_3^-$ (m/z 145, 147, 149) in negative ion spectra (see Sect. S3.2 in the Supplement). The temporal evolution of this particle class is similar to that of the silicate particle class (Fig. 12a) but is very different to that of the sea-spray particles (see Sect. S3.5 in the Supplement); therefore, we conclude that it has a similar source to the silicate and probably represents calcium carbonate that has been processed in the atmosphere.

3.2.2 Temporal evolution of the silicate particle mineralogy (ICE-D)

In order to create a concise time series of the single-particle mineralogy for the entire time period, the silicate class of particles (previously identified by cluster analysis) was differentiated into a simple binary system of ISCM and non-ISCM using the crystal structure analysis (τ parameter) to produce a time series of the ISCM ratio (Fig. 12b). The ISCM ratio is the number of particles which have $\tau < 0.58$ divided by the number of silicate particles which have $\tau > 0.58$, representing ISCM and non-ISCM (feldspar, amorphous and pure kaolinite), respectively (see Sect. 2.1.1). The average detection rates of silicate- and calcium-containing particles were combined to produce an hourly average of the ISCM, non-ISCM and calcium number fractions in mineral dust (Fig. 12c). Note that these fractions are relative to the detection efficiency of the instrument to each particle type (see Sect. 2.1), so that ratios presented here are semi-quantitative only, but the temporal evolution is representative of changes in particle composition.

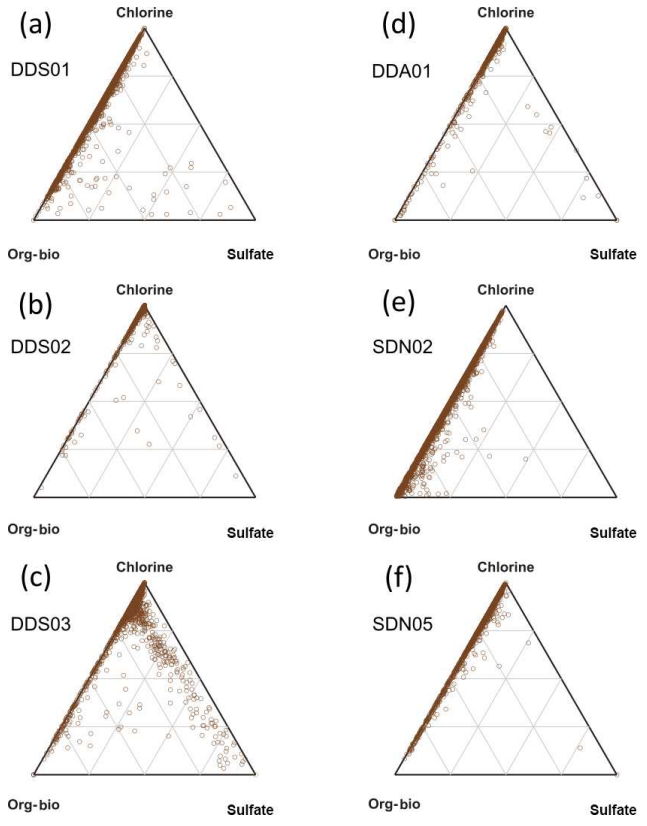

Figure 10. Subcompositional analysis of the non-silicate content in suspended natural soil samples (INUIT09) by SPMS. Ternary plots of the Cl, organic–biological and sulfate marker peak areas in Moroccan **(a, b, c)** and Sahelian **(c, d, e)** resuspended soil dust (2000 particles analysed in each sample).

Most of the measurement period was characterised by a relatively high ISCM ratio which is generally $\gg 1$. This is consistent with continuous long-term offline measurements of elemental composition around Cabo Verde by Patey et al. (2015), who concluded that illite was the most abundant clay mineral type. However, these conditions changed 17 August when the ISCM ratio was much lower than in the previous period (ISCM ratio < 1) and the fraction of calcium-containing particle increased. We used the time series to define two dust events (D1 centred on 00:00 LT, 11 August 2015 and D2 centred on 15:00 LT, 17 August 2018) which were analysed in more detail with subcompositional analysis, using the same method applied to the soil dust samples.

Silicate dust in event D1 contained a high fraction of ISCM-type mineral composition with 2 : 1 phyllosilicate structure (blue circles in Fig. 13a), that plotted close to the illite composition in the ternary diagram, similar to that observed in Moroccan soils DDS01 and DDS02 (Fig. 7b, c). In contrast, these ISCM particles are much reduced in dust event D2, which has a higher proportion of non-ISCM (felsic or amorphous material (red circles in Fig. 13e) and shifts away from the illite composition on the diagram. The actual mineral phase of these particles is less clear, but from the large fraction of these particle types and their central position on the ternary diagram, it would be reasonable to assume a mixed amorphous matrix. It is clear, however, that the large fraction of particles with illite matrix present in D1 is absent in D2. The potential source and transport history of these materials in these dust events is discussed in more detail after consideration of the mixing state below.

3.3 Temporal evolution of the mixing state of silicate particles (ICE-D)

The mixing of silicate and non-silicate within single particles may result from processes within the native soil (primary) or during atmospheric transport (secondary). The internal mixing state of transported silicate dust (ICE-D) is reported with the subcomposition chlorine – Org–bio – nitrate, similar to the treatment of suspended dust (INUIT09) in Sect. 3.1.2, except we target nitrate in ambient particles instead of sulfate because nitrate was present in low quantities in suspended soil. An increase in nitrate aerosol has previously been observed in association with air masses passing through Europe and Africa to Cabo Verde (Fomba et al., 2014), so this may be a useful indicator of the history of transported dust. The analysis of the suspended soil dust showed mineral particles in north African soils are already mixed, particularly with varying quantities of chlorine, sulfate and organic–biological material. Therefore, the internal mixing state observed in transported dust may be derived from primary or secondary sources.

In transported dust, nitrate mixing with the silicate dust was varied, with the subcomposition of nitrate markers indicating a relatively greater quantity of nitrate mixing with silicate particles during the period between the defined dust events. This showed a similar trend to the number concentration of nitrate sea-spray aerosol particle types extracted by fuzzy clustering (Sect. S3.5 in the Supplement), which suggest the particles may have coexisted in the same air mass for some period of time. There was a distinct drop in nitrate subcomposition during dust period D2 when we also measured a change in silicate mineralogy.

Although it is not possible to conclude a primary or secondary source of organic–biological mixing, we observed less variation in mixing state in the transported dust than in the laboratory-generated reference material. The number of particles whose mixing state subcomposition contained more than 20 % organic–biological material (org–bio > 0.2) varies with the dust concentration (Fig. 12d), and the median amount of the organic–biological marker signal is fairly stable, with the exception of a 24 h period following dust event D1 (Fig. 12e). This may be informative of how well mixed local sources of dust become after emission but could also be a reflection of atmospheric processing.

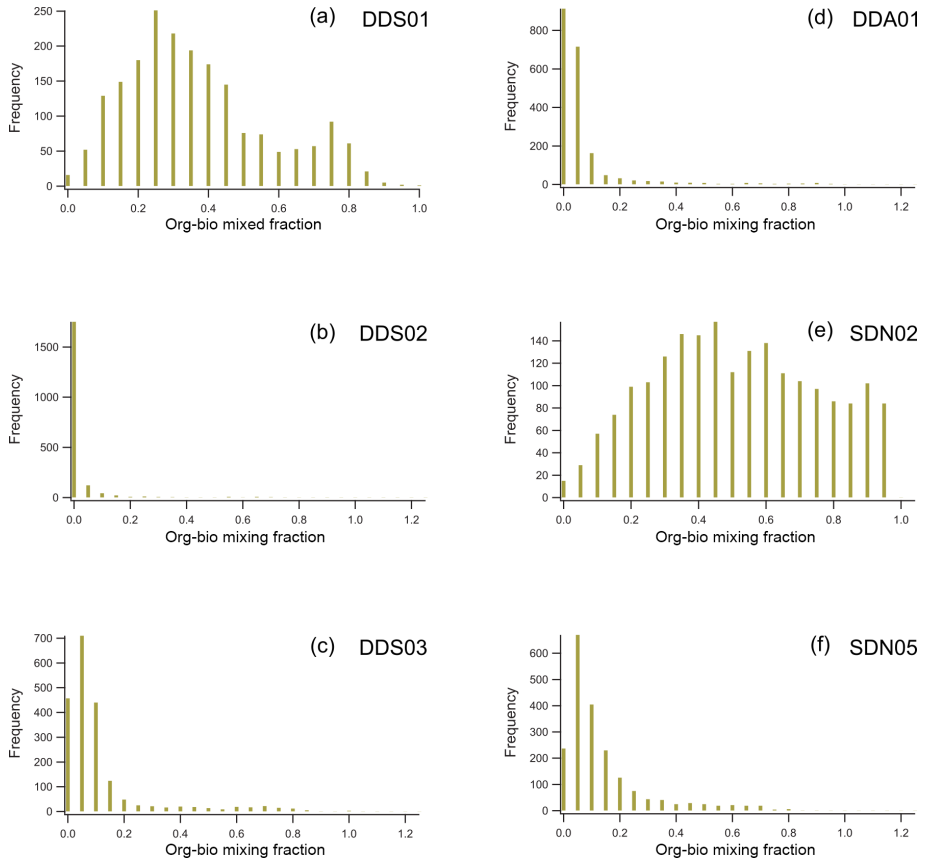

Figure 11. A comparison of the relative organic–biological content in the non-silicate portion in suspended natural soil samples (INUIT09). Histograms are of the normalised org–bio fraction in single particles of Moroccan **(a, b, c)** and Sahelian **(d, e, f)** samples.

Particle mixing is important because the efficient ice-nucleating properties of proteinaceous INPs can be transferred to dust particles after mixing (Augustin-Bauditz et al., 2016; O'Sullivan et al., 2016). It is interesting to note that Price et al. (2018) did not see significant variation in INP concentration in aircraft-based studies of the Saharan air layer during ICE-D, despite geographically widespread sources of that dust. The origin of the organic–biological markers CN^- and CNO^- in these dust particles requires further investigation. Zawadowicz et al. (2017) demonstrated a method of distinguishing between biogenic and inorganic ion signals using a different SPMS instrument (PALMS), but it is not yet proven to be transferable to other instruments' designs.

3.4 Potential source areas and transport history

Dust transport to Cabo Verde is controlled by the position of the Azores High pressure system, whose anticyclonic flow results in persistent north-easterly trade winds along the coast of Morocco, western Sahara and Mauritania (Carpenter et al., 2010). Dust concentrations at ground level are influenced by the dust deposition rate, which is strongly dependent on the horizontal and vertical dust distribution (Schepanski et al., 2009a). We used back-trajectory analysis, satellite observations and our measurement of dust mineralogy and mixing state to give potential source areas and transport history of two dust events observed at Cabo Verde in the summer of 2015.

Back-trajectory analysis of both dust events (D1 and D2, defined in the analysis above), shows transport in the trade winds within the marine boundary (Fig. 13c, g). Influence from the African continent is evident during D1 when some of this air mass was lofted over the Atlas Mountains, Morocco, before descending into the marine boundary layer (MBL). The high ISCM ratio we measure (68 %) is consistent with Scheuvens et al. (2013), who suggested illite/kaolinite ratio > 2 is indicative of the PSA that comprises the northern part of the west coast of Africa and the south-eastern slopes of the Atlas Mountains. Satellite observations at the time showed a plume of dust developing in Algeria and crossing the Atlas Mountains and then above the Atlantic Ocean in the days proceeding dust event D1 (Sect. S5 in the Supplement). However, source activation observed by remote satellite is subject to errors associated with the temporal resolution of the measurement (Schepanski et al., 2012). Dust emission associated with density currents

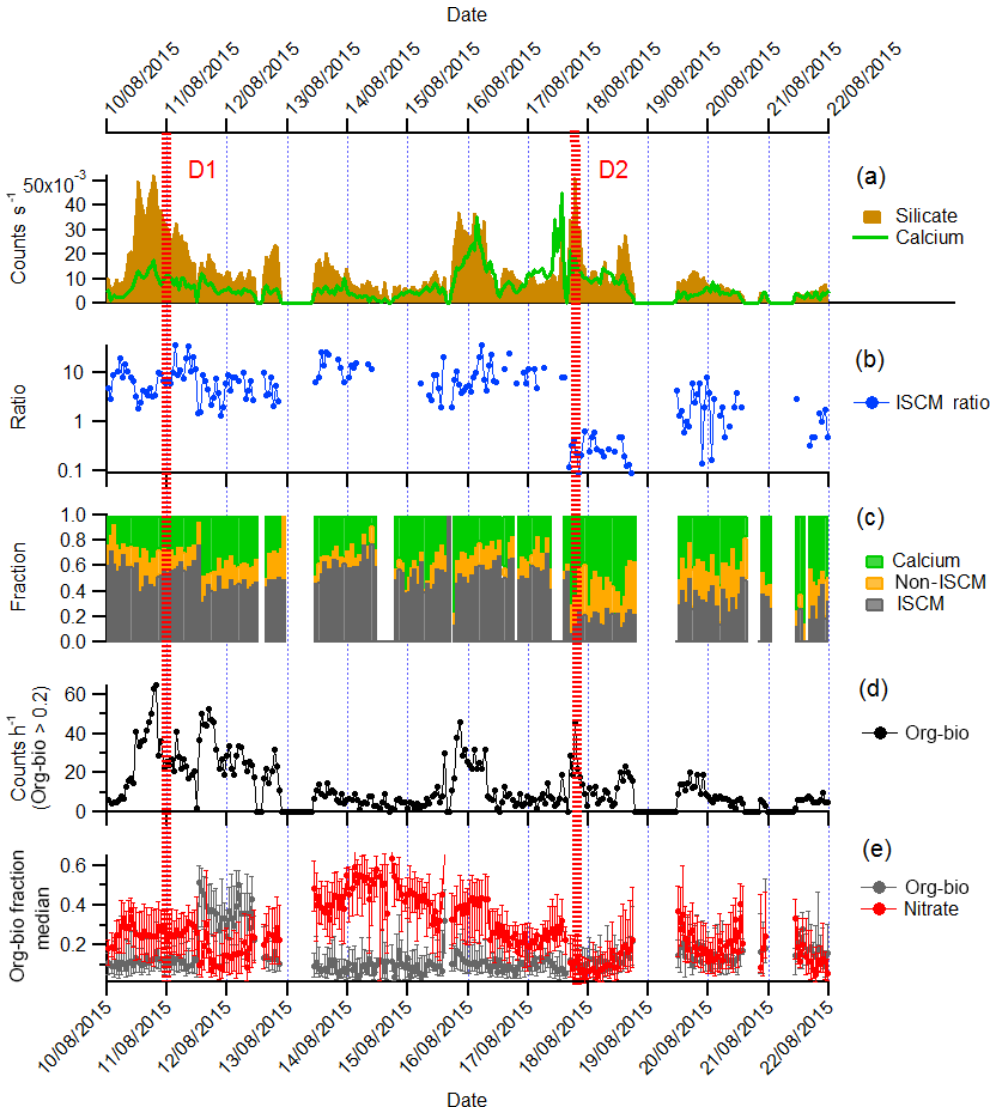

Figure 12. Time series (1 h resolution) of ambient dust properties measured at Cabo Verde during the ICE-D campaign by LAAPTOF SPMS. **(a)** Concentration of silicate- and calcium-rich particles (from 12 698 silicate and 6837 calcium particles measured). **(b)** Hourly average ratio of ISCM to non-ISCM minerals (ISCM ratio) determined by crystal structure. **(c)** Hourly particle number fraction of calcium, ISCM and non-ISCM particles. **(d)** Hourly concentration of silicate particles with organic–biological subcomposition > 0.2. **(e)** Hourly median org–bio and nitrate subcomposition marker quantity. Error bars are at the 25th and 75th percentiles.

related to moist convection had been previously observed on the Sahara side of the Atlas mountain chain by Knippertz et al. (2007), where the soil mineral content is a close match to the material we report in this dust event. The Anti-Atlas Mountains were also suggested as a source of micronutrients in sediment traps in the north-east Atlantic Ocean by Chavagnac et al. (2007).

In contrast, back trajectories for D2 suggest this air mass was never lofted over Africa but came into direct contact with the coastline of Mauritania. This is a possible source of dust that could explain the relatively low ISCM content and relatively high calcium fraction which is consistent with source sediments of the Atlantic coastal basin (Moreno et al., 2006). In offline filters collected at Praia, Cabo Verde, Kandler et al. (2011b) reported an illite/kaolinite ratio of between 1 : 2 and 1 : 4 during winter transport of dust from coastal Mauritania and Mali, respectively.

The nitrate mixing state of particles also suggests different transport pathways for the two dust events. The mixing of nitrate with silicate during and after D1 indicates contact with polluted air and is consistent with transport from the north, as reported by Salvador et al. (2016), whilst the cleaner particles in D2 indicate that no such mixing took place. An increase in the fraction of sulfate-containing sea-spray aerosol in D2 on the other hand (Sect. S3.5 in the Supplement) may be associated with organosulfur-containing compounds from

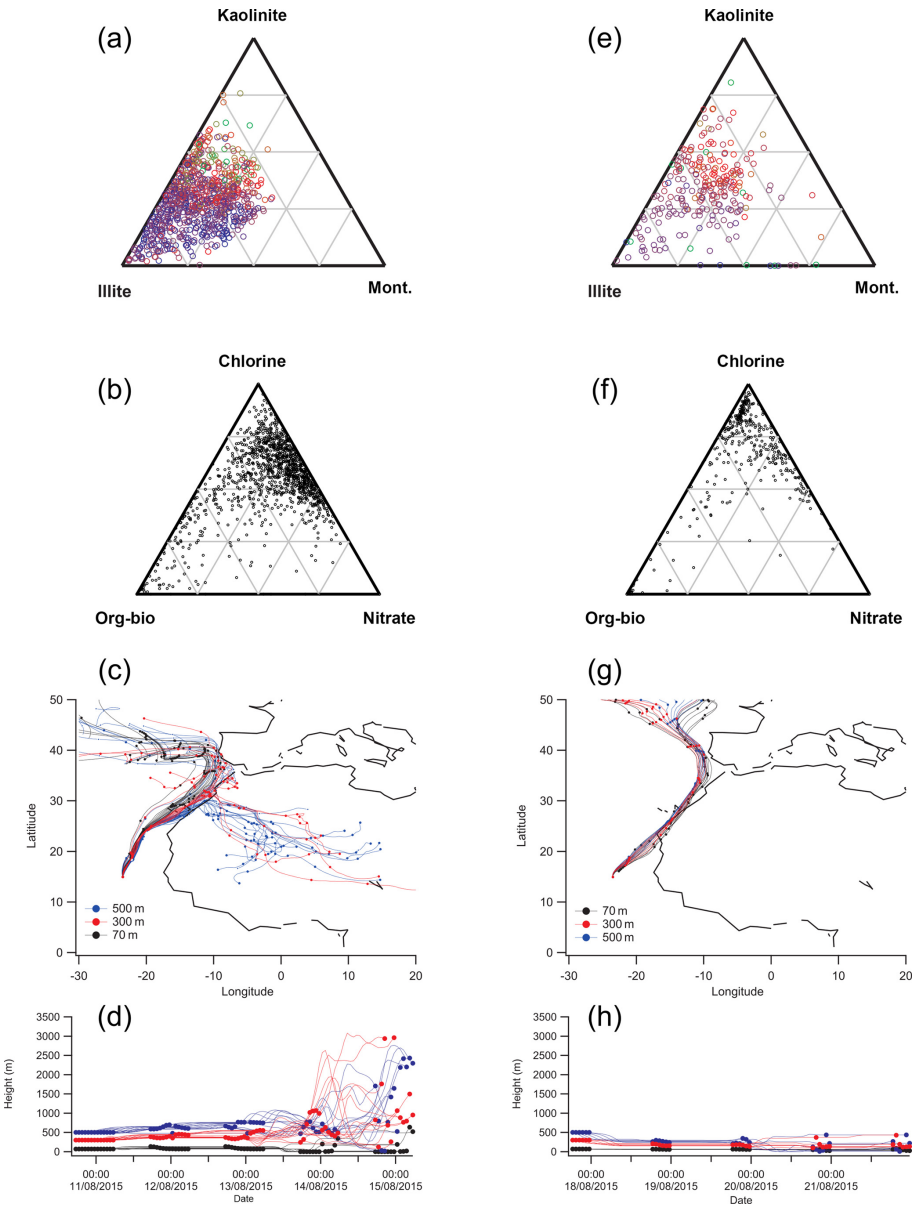

Figure 13. Analysis of the mineralogy and mixing state of dust events D1 in the left column **(a–d)** (1301 particles analysed) and D2 in the right column **(e–f)** (378 particles analysed). Mineralogical analysis by SPMS shows the high number of illite particles (blue circles) present in D1 **(a)** is absent in D2 **(e)**. In addition, mixing state analysis shows a higher proportion of particles mixed with nitrate in D1 **(d)** than in D2 **(f)**. Hybrid Single-Particle Lagrangian Integrated Trajectory (HYSPLIT) back-trajectory analysis suggests influence of air masses from the Sahara during D1 **(c, d)** and coastal Mauritania during D2 **(g, h)**.

biogenic sources in the coastal upwelling region off the coast of Mauritania. In addition, the particle size distribution of the silicate from D2 also suggests that this dust may have been transported a relatively short distance compared to D1 (see Sect. S4 in the Supplement). The silicate from D1 has a well-defined mode at approximately 1 µm, which is in contrast to the broader distribution of D2 particle sizes, which extends above 2 µm.

Our high-resolution measurements show that the mineralogy and mixing state of dust can change on a hourly basis, suggesting that changes in dust source, transport pathways and particle composition are lost in offline data. For example, in XRD analysis of material captured in marine sediment traps of Cape Blanc, Mauritania, Friese et al. (2017) concluded that seasonal variation in mineralogy occurred due to changes in transport pathways: from long-distance transport in the SAL during summertime to local transport in the trade winds in winter. Our measurements also suggest two pathways for dust arriving at Cabo Verde that change over a much shorter time period of hours rather than months. We

propose that, in August 2015, illite-rich dust from the NW margin of the Sahara was advected into the free troposphere and became mixed in to the MBL off the coast of Morocco before several days of transport to Cabo Verde. An eastward shift in the Azores High results in the direct entrainment of dust into the MBL from the coast of Mauritania, producing a relatively illite-poor and calcium-rich dust event in Cabo Verde on 17 August that lasted for a few hours. In all the above offline studies, filters were exposed for around 1 day, resulting in insufficient temporal resolution of the data.

4 Conclusions

We have presented a detailed characterisation of the mineralogy and mixing state of the fine fraction ($< 2.5\,\mu m$) of north African mineral dust using a novel combination of subcomposition and crystal structure analysis with a single-particle mass spectrometer. Despite the fact that the technique provides incomplete coverage in terms of particle number, elemental composition and mineralogy, it was possible to detect regional differences in the mineralogy in single particles of suspended soil and ambient transported dust.

The following conclusions were made under the reasonable assumption that single particles in the fine fraction were composed of either clay minerals or feldspars/amorphous matrix, a distinction that can be realised by our novel crystal analysis technique. Although the SPMS technique has been shown to be generally non-quantitative with respect to the elemental subcomposition of pure mineral phases such as illite and K-feldspar, a semi-quantitative (relative) measurement of elemental composition can be achieved after particles are separated into mineral groups based on crystal structure. Differentiation of the mineral phase can then be made by comparison to pure mineral fingerprints from within the mineral group. This indicates the importance of particle structure in addition to particle composition in the matrix effect in SPMS.

The sensitivity of the technique to potassium, sodium and aluminum makes it particularly useful for differentiating illite (potassium-rich clay), montmorillonite (sodium-rich clay) and kaolinite (aluminum-rich clay) clay mineral assemblages. Comparison with offline SEM EDX analysis of the suspended soil confirms the observations that a composition close to illite is observed in Moroccan samples compared to a kaolinite composition in samples from the Sahel, in agreement with geology of these regions. SPMS is less effective than SEM EDX at identifying particles rich in magnesium and calcium due to suppression by the matrix effect and interference from poorly resolved peaks, but it is likely that these elements are derived from carbonates and oxides and are not strictly necessary to classify the silicate minerals. This makes the assumption that Mg, Fe and Ca are of minor importance in silicate mineralogy in continental sediment, which is certainly not true on a local level. However, our measurements show it is not necessary to include these elements when considering the genesis and subsequent weathering history of the clay fraction in soil on a continental scale.

These results show that the SPMS and SEM EDX techniques are complementary, with SPMS providing a high-resolution online indication of mineralogy and mixing state of the principal particle matrix, and SEM EDX providing semi-quantitative elemental composition of all particles, including material that the SPMS may not vaporise. In most cases, both techniques show the distribution of mineralogical composition is more continuous than clustered in distinct mineral phases, and only laboratory-suspended river sediment from the Anti-Atlas Mountains, Morocco, contained a distinct mode of fine particles with a feldspar matrix.

The detailed analysis of laboratory-suspended dust provided useful reference data for the interpretation of the origins and transport history of ambient dust in the remote North Atlantic. Although semi-quantitative in terms of particle number fractions due to number-counting bias effects associated with instrument function, the relative temporal trends are very informative. A relatively large number of illite-rich particles (ISCM ratio > 5) suggests a dust source on the NW margins of the Sahara during the summer. However, a rapid change (< 1 h) towards a felsic/amorphous particle matrix (ISCM ratio < 1) was observed in silicate particles when back trajectories suggested direct emission into the marine boundary layer from the west African coast. This episode lasted only a few hours and challenges previous findings from offline measurements that the source and composition of transported dust only change on a seasonal basis.

Internal mixing state was of some use to understanding transport history of ambient dust but must be used with caution because some degree of mixing was already present in the primary soil. However, variations in internally mixed nitrate suggested dust from the NW margins of the Sahara was deposited into the marine boundary layer after transport in the Saharan air layer. In contrast, the relative concentration of organic–biological markers did not vary significantly in transported dust but had significant local variation in suspended soil samples, making them less useful for interpreting transport pathways but potentially informative of how well mixed local sources become after emission. The primary and secondary origins of these chemical markers and how they change the physiochemical properties of dust particles require further investigation.

The combination of online mineralogy and mixing state of ambient dust has potential for resolving the complexity of dust emission, transport and deposition, but more high-resolution measurements at varying distance from potential dust sources are required to fully understand the complexity of these processes. The example of transported dust provided here should also be useful for studies of ice nucleation, radiative effects and heterogeneous reactions involving mineral dust.

Data availability. LAAPTOF soil dust characterisation data collected for the INUIT09 campaign at the AIDA facility are available at https://data.eurochamp.org/data-access (last access: 15 February 2019). Data collected during the ICE-D campaign are available from the British Atmospheric Data Centre, Centre for Environmental Data Analysis (2018, http://www.ceda.ac.uk/, last access: 15 February 2019), at the following URL: http://catalogue.ceda.ac.uk/uuid/d7e02c75191a4515a28a208c8a069e70 (last access: 15 February 2019) (Bennett, 2015).

Supplement. The supplement related to this article is available online at: https://doi.org/10.5194/acp-19-2259-2019-supplement.

Author contributions. The document was principally written by NAM with input from RU and SEH. The INUIT09 project was devised and managed by RU and OM, with SPMS data acquired by NAM. The ICE-D field data were acquired by NAM and PIW with support from MJF, JDA and HC. Data processing was performed by NAM (SPMS) and SEH (ESEM) with support from KK. Back-trajectory analysis was done by DL and ZC.

Competing interests. The authors declare that they have no conflict of interest.

Special issue statement. This article is part of the special issue "Fifth International Workshop on Ice Nucleation (FIN)". It is not associated with a conference.

Acknowledgements. ICE-D was supported by the Natural Environment Research Council (grant number NE/M001954/1), during which Nicholas A. Marsden was supported by a PhD studentship (NERC M113463J). This project/work has received funding from the European Union's Horizon 2020 research and innovation programme through the EUROCHAMP-2020 Infrastructure Activity under grant agreement no. 730997. We thank the AIDA engineering and technical team for maintaining and operating the cloud chamber facility. Romy Ullrich and Ottmar Möhler acknowledge funding by the Deutsche Forschungsgemeinschaft (DFG) through the research unit INUIT (FOR 1525, project MO 668/4-2). Konrad Kandler and Stine Eriksen Hammer acknowledge financial support from the Deutsche Forschungsgemeinschaft (DFG, German Research Foundation) – 264907654, 264912134 and 416816480 (KA 2280) as well as FOR 1525.

Edited by: Barbara Ervens
Reviewed by: three anonymous referees

References

Ahern, A. T., Subramanian, R., Saliba, G., Lipsky, E. M., Donahue, N. M., and Sullivan, R. C.: Effect of secondary organic aerosol coating thickness on the real-time detection and characterization of biomass-burning soot by two particle mass spectrometers, Atmos. Meas. Tech., 9, 6117–6137, https://doi.org/10.5194/amt-9-6117-2016, 2016.

Ansmann, A., Petzold, A., Kandler, K., Tegen, I., Wendisch, M., Müller, D., Weinzierl, B., Müller, T., and Heintzenberg, J.: Saharan Mineral Dust Experiments SAMUM-1 and SAMUM-2: what have we learned?, Tellus B, 63, 403–429, https://doi.org/10.1111/j.1600-0889.2011.00555.x, 2011.

Atkinson, J. D., Murray, B. J., Woodhouse, M. T., Whale, T. F., Baustian, K. J., Carslaw, K. S., Dobbie, S., O'Sullivan, D., and Malkin, T. L.: The importance of feldspar for ice nucleation by mineral dust in mixed-phase clouds, Nature, 498, 355–358, https://doi.org/10.1038/nature12278, 2013.

Augustin-Bauditz, S., Wex, H., Denjean, C., Hartmann, S., Schneider, J., Schmidt, S., Ebert, M., and Stratmann, F.: Laboratory-generated mixtures of mineral dust particles with biological substances: characterization of the particle mixing state and immersion freezing behavior, Atmos. Chem. Phys., 16, 5531–5543, https://doi.org/10.5194/acp-16-5531-2016, 2016.

Baker, A. R., Kelly, S., Biswas, K., Witt, M., and Jickells, T.: Atmospheric deposition of nutrients to the Atlantic Ocean, Geophys. Res. Lett., 30, 2–5, https://doi.org/10.1029/2003GL018518, 2003.

Baustian, K. J., Cziczo, D. J., Wise, M. E., Pratt, K. A., Kulkarni, G., Hallar, A. G., and Tolbert, M. A.: Importance of aerosol composition, mixing state, and morphology for heterogeneous ice nucleation: A combined field and laboratory approach, J. Geophys. Res., 117, D06217, https://doi.org/10.1029/2011JD016784, 2012.

Bennett, L.: UK ICE-D: atmospheric measurements dataset collection, Facility for Airborne Atmospheric Measurements, Centre for Environmental Data Analysis, available at: http://catalogue.ceda.ac.uk/uuid/d7e02c75191a4515a28a208c8a069e70 (last access: 15 February 2019), 2015.

Bhave, P. V., Allen, J. O., Morrical, B. D., Fergenson, D. P., Cass, G. R., and Prather, K. A.: A field-based approach for determining ATOFMS instrument sensitities to ammonium and nitrate, Environ. Sci. Technol., 36, 4868–4879, 2002.

Cahill, J. F., Suski, K., Seinfeld, J. H., Zaveri, R. A., and Prather, K. A.: The mixing state of carbonaceous aerosol particles in northern and southern California measured during CARES and CalNex 2010, Atmos. Chem. Phys., 12, 10989–11002, https://doi.org/10.5194/acp-12-10989-2012, 2012.

Caponi, L., Formenti, P., Massabó, D., Di Biagio, C., Cazaunau, M., Pangui, E., Chevaillier, S., Landrot, G., Andreae, M. O., Kandler, K., Piketh, S., Saeed, T., Seibert, D., Williams, E., Balkanski, Y., Prati, P., and Doussin, J.-F.: Spectral- and size-resolved mass absorption efficiency of mineral dust aerosols in the shortwave spectrum: a simulation chamber study, Atmos. Chem. Phys., 17, 7175–7191, https://doi.org/10.5194/acp-17-7175-2017, 2017.

Caquineau, S., Gaudichet, A., Gomes, L., and Legrand, M.: Mineralogy of Saharan dust transported over northwestern tropical Atlantic Ocean in relation to source regions, J. Geophys. Res.-Atmos., 107, 4251, https://doi.org/10.1029/2000JD000247, 2002.

Carpenter, L. J., Fleming, Z. L., Read, K. A., Lee, J. D., Moller, S. J., Hopkins, J. R., Purvis, R. M., Lewis, A. C., Müller, K., Heinold, B., Herrmann, H., Fomba, K. W., Van Pinxteren, D., Müller, C., Tegen, I., Wiedensohler, A., Müller, T., Niedermeier,

N., Achterberg, E. P., Patey, M. D., Kozlova, E. A., Heimann, M., Heard, D. E., Plane, J. M. C., Mahajan, A., Oetjen, H., Ingham, T., Stone, D., Whalley, L. K., Evans, M. J., Pilling, M. J., Leigh, R. J., Monks, P. S., Karunaharan, A., Vaughan, S., Arnold, S. R., Tschritter, J., Pöhler, D., Frieã, U., Holla, R., Mendes, L. M., Lopez, H., Faria, B., Manning, A. J., and Wallace, D. W. R.: Seasonal characteristics of tropical marine boundary layer air measured at the cape verde atmospheric observatory, J. Atmos. Chem., 67, 87–140, https://doi.org/10.1007/s10874-011-9206-1, 2010.

Carslaw, K. S., Lee, L. A., Reddington, C. L., Pringle, K. J., Rap, A., Forster, P. M., Mann, G. W., Spracklen, D. V., Woodhouse, M. T., Regayre, L. A., and Pierce, J. R.: Large contribution of natural aerosols to uncertainty in indirect forcing, Nature, 503, 67–71, https://doi.org/10.1038/nature12674, 2013.

Chavagnac, V., Waniek, J. J., Atkin, D., Milton, J. A., Leipe, T., Green, D. R., Bahlo, R., Hayes, T. E., and Schulz-Bull, D. E.: Anti-Atlas Moroccan Chain as the source of lithogenic-derived micronutrient fluxes to the deep Northeast Atlantic Ocean, Geophys. Res. Lett., 34, 1–5, https://doi.org/10.1029/2007GL030985, 2007.

Christopoulos, C. D., Garimella, S., Zawadowicz, M. A., Möhler, O., and Cziczo, D. J.: A machine learning approach to aerosol classification for single-particle mass spectrometry, Atmos. Meas. Tech., 11, 5687–5699, https://doi.org/10.5194/amt-11-5687-2018, 2018.

Claquin, T., Schulz, M., and Balkanski, Y. J.: Modeling the mineralogy of atmospheric dust sources, J. Geophys. Res., 104, 22243, https://doi.org/10.1029/1999JD900416, 1999.

Connolly, P. J., Möhler, O., Field, P. R., Saathoff, H., Burgess, R., Choularton, T., and Gallagher, M.: Studies of heterogeneous freezing by three different desert dust samples, Atmos. Chem. Phys., 9, 2805–2824, https://doi.org/10.5194/acp-9-2805-2009, 2009.

Creamean, J. M., Suski, K. J., Rosenfeld, D., Cazorla, A., Demott, P. J., Sullivan, R. C., White, A. B., Ralph, F., Minnis, P., Comstock, J. M., Tomlinson, J. M., and Prather, K. A.: Dust and Biological Aerosols, Science, 339, 1572–1578, https://doi.org/10.1126/science.1227279, 2013.

Cziczo, D. J., DeMott, P. J., Brock, C., Hudson, P. K., Jesse, B., Kreidenweis, S. M., Prenni, A. J., Schreiner, J., Thomson, D. S., and Murphy, D. M.: A Method for Single Particle Mass Spectrometry of Ice Nuclei, Aerosol Sci. Technol., 37, 460–470, https://doi.org/10.1080/02786820300976, 2003.

Cziczo, D. J., Thomson, D. S., Thompson, T. L., DeMott, P. J., and Murphy, D. M.: Particle analysis by laser mass spectrometry (PALMS) studies of ice nuclei and other low number density particles, Int. J. Mass Spectr., 258, 21–29, https://doi.org/10.1016/j.ijms.2006.05.013, 2006.

Cziczo, D. J., Froyd, K. D., Gallavardin, S. J., Moehler, O., Benz, S., Saathoff, H., and Murphy, D. M.: Deactivation of ice nuclei due to atmospherically relevant surface coatings, Environ. Res. Lett., 4, 044013, https://doi.org/10.1088/1748-9326/4/4/044013, 2009.

Dall'Osto, M., Harrison, R. M., Highwood, E. J., O'Dowd, C., Ceburnis, D., Querol, X., and Achterberg, E. P.: Variation of the mixing state of Saharan dust particles with atmospheric transport, Atmos. Environ., 44, 3135–3146, https://doi.org/10.1016/j.atmosenv.2010.05.030, 2010.

DeMott, P. J.: African dust aerosols as atmospheric ice nuclei, Geophys. Res. Lett., 30, 1732, https://doi.org/10.1029/2003GL017410, 2003.

DeMott, P. J., Prenni, A. J., Liu, X., Kreidenweis, S. M., Petters, M. D., Twohy, C. H., Richardson, M. S., Eidhammer, T., and Rogers, D. C.: Predicting global atmospheric ice nuclei distributions and their impacts on climate, P. Natl. Acad. Sci. USA, 107, 11217–22, https://doi.org/10.1073/pnas.0910818107, 2010.

Di Biagio, C., Formenti, P., Balkanski, Y., Caponi, L., Cazaunau, M., Pangui, E., Journet, E., Nowak, S., Caquineau, S., Andreae, M. O., Kandler, K., Saeed, T., Piketh, S., Seibert, D., Williams, E., and Doussin, J.-F.: Global scale variability of the mineral dust long-wave refractive index: a new dataset of in situ measurements for climate modeling and remote sensing, Atmos. Chem. Phys., 17, 1901–1929, https://doi.org/10.5194/acp-17-1901-2017, 2017.

Doherty, O. M., Riemer, N., and Hameed, S.: Saharan mineral dust transport into the Caribbean: Observed atmospheric controls and trends, J. Geophys. Res.-Atmos., 113, 1–10, https://doi.org/10.1029/2007JD009171, 2008.

Dunion, J. P. and Marron, C. S.: A reexamination of the Jordan mean tropical sounding based on awareness of the Saharan air layer: Results from 2002, J. Climate, 21, 5242–5253, https://doi.org/10.1175/2008JCLI1868.1, 2008.

Engelbrecht, J. P., Moosmüller, H., Pincock, S., Jayanty, R. K. M., Lersch, T., and Casuccio, G.: Technical note: Mineralogical, chemical, morphological, and optical interrelationships of mineral dust re-suspensions, Atmos. Chem. Phys., 16, 10809–10830, https://doi.org/10.5194/acp-16-10809-2016, 2016.

Eriksen Hammer, S., Mertes, S., Schneider, J., Ebert, M., Kandler, K., and Weinbruch, S.: Composition of ice particle residuals in mixed-phase clouds at Jungfraujoch (Switzerland): enrichment and depletion of particle groups relative to total aerosol, Atmos. Chem. Phys., 18, 13987–14003, https://doi.org/10.5194/acp-18-13987-2018, 2018.

Evan, A. T., Flamant, C., Fiedler, S., and Doherty, O.: An analysis of aeolian dust in climate models, Geophys. Res. Lett., 41, 5996–6001, https://doi.org/10.1002/2014GL060545, 2014.

Fitzgerald, E., Ault, A. P., Zauscher, M. D., Mayol-Bracero, O. L., and Prather, K. A.: Comparison of the mixing state of long-range transported Asian and African mineral dust, Atmos. Environ., 115, 19–25, https://doi.org/10.1016/j.atmosenv.2015.04.031, 2015.

Fomba, K. W., Müller, K., van Pinxteren, D., Poulain, L., van Pinxteren, M., and Herrmann, H.: Long-term chemical characterization of tropical and marine aerosols at the Cape Verde Atmospheric Observatory (CVAO) from 2007 to 2011, Atmos. Chem. Phys., 14, 8883–8904, https://doi.org/10.5194/acp-14-8883-2014, 2014.

Formenti, P., Schütz, L., Balkanski, Y., Desboeufs, K., Ebert, M., Kandler, K., Petzold, A., Scheuvens, D., Weinbruch, S., and Zhang, D.: Recent progress in understanding physical and chemical properties of African and Asian mineral dust, Atmos. Chem. Phys., 11, 8231–8256, https://doi.org/10.5194/acp-11-8231-2011, 2011.

Formenti, P., Caquineau, S., Desboeufs, K., Klaver, A., Chevaillier, S., Journet, E., and Rajot, J. L.: Mapping the physicochemical properties of mineral dust in western Africa: miner-

alogical composition, Atmos. Chem. Phys., 14, 10663–10686, https://doi.org/10.5194/acp-14-10663-2014, 2014.

Friese, C. A., van Hateren, J. A., Vogt, C., Fischer, G., and Stuut, J.-B. W.: Seasonal provenance changes in present-day Saharan dust collected in and off Mauritania, Atmos. Chem. Phys., 17, 10163–10193, https://doi.org/10.5194/acp-17-10163-2017, 2017.

Gallavardin, S. J., Froyd, K. D., Lohmann, U., Moehler, O., Murphy, D. M., and Cziczo, D. J.: Single Particle Laser Mass Spectrometry Applied to Differential Ice Nucleation Experiments at the AIDA Chamber, Aerosol Sci. Technol., 42, 773–791, https://doi.org/10.1080/02786820802339538, 2008.

Gaston, C. J., Quinn, P. K., Bates, T. S., Gilman, J. B., Bon, D. M., Kuster, W. C., and Prather, K. A.: The impact of shipping, agricultural, and urban emissions on single particle chemistry observed aboard the R/V Atlantis during CalNex, J. Geophys. Res.-Atmos., 118, 5003–5017, https://doi.org/10.1002/jgrd.50427, 2013.

Gemayel, R., Hellebust, S., Temime-Roussel, B., Hayeck, N., Van Elteren, J. T., Wortham, H., and Gligorovski, S.: The performance and the characterization of laser ablation aerosol particle time-of-flight mass spectrometry (LAAP-ToF-MS), Atmos. Meas. Tech., 9, 1947–1959, https://doi.org/10.5194/amt-9-1947-2016, 2016.

Glaccum, R. A. and Prospero, J. M.: Saharan aerosols over the tropical North Atlantic – Mineralogy, Mar. Geol., 37, 295–321, https://doi.org/10.1016/0025-3227(80)90107-3, 1980.

Griffin, D. W.: Atmospheric movement of microorganisms in clouds of desert dust and implications for human health, Clin. Microbiol. Rev., 20, 459–77, https://doi.org/10.1128/CMR.00039-06, 2007.

Gross, D. S., Gälli, M. E., Silva, P. J., and Prather, K. A.: Relative sensitivity factors for alkali metal and ammonium cations in single-particle aerosol time-of-flight mass spectra, Anal. Chem., 72, 416–22, 2000.

Gross, D. S., Atlas, R., Rzeszotarski, J., Turetsky, E., Christensen, J., Benzaid, S., Olson, J., Smith, T., Steinberg, L., and Sulman, J.: Environmental chemistry through intelligent atmospheric data analysis, Environ. Model. Softw., 25, 760–769, https://doi.org/10.1016/j.envsoft.2009.12.001, 2010.

Harrison, A. D., Whale, T. F., Carpenter, M. A., Holden, M. A., Neve, L., O'Sullivan, D., Vergara Temprado, J., and Murray, B. J.: Not all feldspars are equal: a survey of ice nucleating properties across the feldspar group of minerals, Atmos. Chem. Phys., 16, 10927–10940, https://doi.org/10.5194/acp-16-10927-2016, 2016.

Hatch, L. E., Pratt, K. A., Huffman, J. A., Jimenez, J. L., and Prather, K. A.: Impacts of Aerosol Aging on Laser Desorption/Ionization in Single-Particle Mass Spectrometers, Aerosol Sci. Technol., 48, 1050–1058, https://doi.org/10.1080/02786826.2014.955907, 2014.

Heinold, B., Knippertz, P., Marsham, J. H., Fiedler, S., Dixon, N. S., Schepanski, K., Laurent, B., and Tegen, I.: The role of deep convection and nocturnal low-level jets for dust emission in summertime West Africa: Estimates from convection-permitting simulations, J. Geophys. Res.-Atmos., 118, 4385–4400, https://doi.org/10.1002/jgrd.50402, 2013.

Hinz, K.-P., Erdmann, N., Grüning, C., and Spengler, B.: Comparative parallel characterization of particle populations with two mass spectrometric systems LAMPAS 2 and SPASS, Int. J. Mass Spectr., 258, 151–166, https://doi.org/10.1016/j.ijms.2006.09.008, 2006.

Hiranuma, N., Augustin-Bauditz, S., Bingemer, H., Budke, C., Curtius, J., Danielczok, A., Diehl, K., Dreischmeier, K., Ebert, M., Frank, F., Hoffmann, N., Kandler, K., Kiselev, A., Koop, T., Leisner, T., Möhler, O., Nillius, B., Peckhaus, A., Rose, D., Weinbruch, S., Wex, H., Boose, Y., DeMott, P. J., Hader, J. D., Hill, T. C. J., Kanji, Z. A., Kulkarni, G., Levin, E. J. T., McCluskey, C. S., Murakami, M., Murray, B. J., Niedermeier, D., Petters, M. D., O'Sullivan, D., Saito, A., Schill, G. P., Tajiri, T., Tolbert, M. A., Welti, A., Whale, T. F., Wright, T. P., and Yamashita, K.: A comprehensive laboratory study on the immersion freezing behavior of illite NX particles: a comparison of 17 ice nucleation measurement techniques, Atmos. Chem. Phys., 15, 2489–2518, https://doi.org/10.5194/acp-15-2489-2015, 2015.

Hoose, C. and Möhler, O.: Heterogeneous ice nucleation on atmospheric aerosols: a review of results from laboratory experiments, Atmos. Chem. Phys., 12, 9817–9854, https://doi.org/10.5194/acp-12-9817-2012, 2012.

Hwang, H. J. and Ro, C. U.: Direct observation of nitrate and sulfate formations from mineral dust and sea-salts using low-Z particle electron probe X-ray microanalysis, Atmos. Environ., 40, 3869–3880, https://doi.org/10.1016/j.atmosenv.2006.02.022, 2006.

Jeong, G. Y. and Chun, Y.: Nanofiber calcite in Asian dust and its atmospheric roles, Geophys. Res. Lett., 33, 1–5, https://doi.org/10.1029/2006GL028280, 2006.

Jeong, G. Y. and Nousiainen, T.: TEM analysis of the internal structures and mineralogy of Asian dust particles and the implications for optical modeling, Atmos. Chem. Phys., 14, 7233–7254, https://doi.org/10.5194/acp-14-7233-2014, 2014.

Jeong, G. Y., Park, M. Y., Kandler, K., Nousiainen, T., and Kemppinen, O.: Mineralogical properties and internal structures of individual fine particles of Saharan dust, Atmos. Chem. Phys., 16, 12397–12410, https://doi.org/10.5194/acp-16-12397-2016, 2016.

Jickells, T. D., An, Z. S., Andersen, K. K., Baker, A. R., Bergametti, C., Brooks, N., Cao, J. J., Boyd, P. W., Duce, R. A., Hunter, K. A., Kawahata, H., Kubilay, N., LaRoche, J., Liss, P. S., Mahowald, N., Prospero, J. M., Ridgwell, A. J., Tegen, I., and Torres, R.: Global iron connections between desert dust, ocean biogeochemistry, and climate, Science, 308, 67–71, https://doi.org/10.1126/science.1105959, 2005.

Journet, E., Balkanski, Y., and Harrison, S. P.: A new data set of soil mineralogy for dust-cycle modeling, Atmos. Chem. Phys., 14, 3801–3816, https://doi.org/10.5194/acp-14-3801-2014, 2014.

Kandler, K., Benker, N., Bundke, U., Cuevas, E., Ebert, M., Knippertz, P., Rodríguez, S., Schütz, L., and Weinbruch, S.: Chemical composition and complex refractive index of Saharan Mineral Dust at Izaña, Tenerife (Spain) derived by electron microscopy, Atmos. Environ., 41, 8058–8074, https://doi.org/10.1016/j.atmosenv.2007.06.047, 2007.

Kandler, K., Schütz, L., Deutscher, C., Ebert, M., Hofmann, H., Jäckel, S., Jaenicke, R., Knippertz, P., Lieke, K., Massling, A., Petzold, A., Schladitz, A., Weinzierl, B., Wiedensohler, A., Zorn, S., and Weinbruch, S.: Size distribution, mass concentration, chemical and mineralogical composition and derived optical parameters of the boundary layer aerosol at Tinfou, Morocco, during SAMUM 2006, Tellus B, 61, 32–50, https://doi.org/10.1111/j.1600-0889.2008.00385.x, 2009.

Kandler, K., Lieke, K., Benker, N., Emmel, C., Küpper, M., Müller-Ebert, D., Ebert, M., Scheuvens, D., Schladitz, A., Schütz, L., and Weinbruch, S.: Electron microscopy of particles collected at Praia, Cape Verde, during the Saharan Mineral Dust Experiment: particle chemistry, shape, mixing state and complex refractive index, Tellus B, 63, 475–496, https://doi.org/10.1111/j.1600-0889.2011.00550.x, 2011a.

Kandler, K., Schütz, L., Jackel, S., Lieke, K., Emmel, C., Müller-Ebert, D., Ebert, M., Scheuvens, D., Schladitz, A., Šegvic, B., Wiedensohler, A., and Weinbruch, S.: Ground-based off-line aerosol measurements at Praia, Cape Verde, during the Saharan Mineral Dust Experiment: Microphysical properties and mineralogy, Tellus B, 63, 459–474, https://doi.org/10.1111/j.1600-0889.2011.00546.x, 2011b.

Kaufman, Y. J., Koren, I., Remer, L. A., Tanré, D., Ginoux, P., and Fan, S.: Dust transport and deposition observed from the Terra-Moderate Resolution Imaging Spectroradiometer (MODIS) spacecraft over the Atlantic Ocean, J. Geophys. Res.-Atmos., 110, 1–16, https://doi.org/10.1029/2003JD004436, 2005.

Kemppinen, O., Nousiainen, T., and Jeong, G. Y.: Effects of dust particle internal structure on light scattering, Atmos. Chem. Phys., 15, 12011–12027, https://doi.org/10.5194/acp-15-12011-2015, 2015.

Kim, J.-S. and Park, K.: Atmospheric Aging of Asian Dust Particles During Long Range Transport, Aerosol Sci. Technol., 46, 913–924, https://doi.org/10.1080/02786826.2012.680984, 2012.

Knippertz, P. and Todd, M. C.: Mineral dust aerosols over the Sahara: Meteorological controls on emission and transport and implications for modeling, Rev. Geophys., 50, RG1007, https://doi.org/10.1029/2011RG000362, 2012.

Knippertz, P., Deutscher, C., Kandler, K., Müller, T., Schulz, O., and Schütz, L.: Dust mobilization due to density currents in the Atlas region: Observations from the Saharan Mineral Dust Experiment 2006 field campaign, J. Geophys. Res.-Atmos., 112, 1–14, https://doi.org/10.1029/2007JD008774, 2007.

Kok, J. F., Ward, D. S., Mahowald, N. M., and Evan, A. T.: Global and regional importance of the direct dust-climate feedback, Nat. Commun., 9, https://doi.org/10.1038/s41467-017-02620-y, 2018.

Krueger, B. J., Grassian, V. H., Cowin, J. P., and Laskin, A.: Heterogeneous chemistry of individual mineral dust particles from different dust source regions: The importance of particle mineralogy, Atmos. Environ., 38, 6253–6261, https://doi.org/10.1016/j.atmosenv.2004.07.010, 2004.

Laskin, A., Iedema, M. J., Ichkovich, A., Graber, E. R., Taraniuk, I., and Rudich, Y.: Direct observation of completely processed calcium carbonate dust particles, Faraday Discuss., 130, 453–468, https://doi.org/10.1039/b417366j, 2005.

Liu, D., Taylor, J. W., Crosier, J., Marsden, N., Bower, K. N., Lloyd, G., Ryder, C. L., Brooke, J. K., Cotton, R., Marenco, F., Blyth, A., Cui, Z., Estelles, V., Gallagher, M., Coe, H., and Choularton, T. W.: Aircraft and ground measurements of dust aerosols over the west African coast in summer 2015 during ICE-D and AER-D, Atmos. Chem. Phys., 18, 3817–3838, https://doi.org/10.5194/acp-18-3817-2018, 2018.

Marsden, N., Flynn, M. J., Taylor, J. W., Allan, J. D., and Coe, H.: Evaluating the influence of laser wavelength and detection stage geometry on optical detection efficiency in a single-particle mass spectrometer, Atmos. Meas. Tech., 9, 6051–6068, https://doi.org/10.5194/amt-9-6051-2016, 2016.

Marsden, N. A., Flynn, M. J., Allan, J. D., and Coe, H.: Online differentiation of mineral phase in aerosol particles by ion formation mechanism using a LAAP-TOF single-particle mass spectrometer, Atmos. Meas. Tech., 11, 195–213, https://doi.org/10.5194/amt-11-195-2018, 2018.

Matsuki, A., Iwasaka, Y., Shi, G., Zhang, D., Trochkine, D., Yamada, M., Yoon-Suk, K., Chen, B., Nagatani, T., Miyazawa, T., Nagatani, M., and Nakata, H.: Morphological and chemical modification of mineral dust: Observational insight into the heterogeneous uptake of acidic gases, Geophys. Res. Lett., 32, 1–4, https://doi.org/10.1029/2005GL024176, 2005.

Möhler, O., Benz, S., Saathoff, H., Schnaiter, M., Wagner, R., Schneider, J., Walter, S., Ebert, V., and Wagner, S.: The effect of organic coating on the heterogeneous ice nucleation efficiency of mineral dust aerosols, Environ. Res. Lett., 3, 025007, https://doi.org/10.1088/1748-9326/3/2/025007, 2008.

Moreno, T., Querol, X., Castillo, S., Alastuey, A., Cuevas, E., Herrmann, L., Mounkaila, M., Elvira, J., and Gibbons, W.: Geochemical variations in aeolian mineral particles from the Sahara-Sahel Dust Corridor, Chemosphere, 65, 261–270, https://doi.org/10.1016/j.chemosphere.2006.02.052, 2006.

Murphy, D. M.: The design of single particle laser mass spectrometers, Mass Spectr. Rev., 26, 150–165, https://doi.org/10.1002/mas, 2007.

Nickovic, S., Vukovic, A., Vujadinovic, M., Djurdjevic, V., and Pejanovic, G.: Technical Note: High-resolution mineralogical database of dust-productive soils for atmospheric dust modeling, Atmos. Chem. Phys., 12, 845–855, https://doi.org/10.5194/acp-12-845-2012, 2012.

Niedermeier, D., Shaw, R. A., Hartmann, S., Wex, H., Clauss, T., Voigtländer, J., and Stratmann, F.: Heterogeneous ice nucleation: exploring the transition from stochastic to singular freezing behavior, Atmos. Chem. Phys., 11, 8767–8775, https://doi.org/10.5194/acp-11-8767-2011, 2011.

Nousiainen, T., Zubko, E., Niemi, J. V., Kupiainen, K., Lehtinen, M., Muinonen, K., and Videen, G.: Single-scattering modeling of thin, birefringent mineral-dust flakes using the discrete-dipole approximation, J. Geophys. Res.-Atmos., 114, 1–12, https://doi.org/10.1029/2008JD011564, 2009.

O'Sullivan, D., Murray, B. J., Ross, J. F., and Webb, M. E.: The adsorption of fungal ice-nucleating proteins on mineral dusts: a terrestrial reservoir of atmospheric ice-nucleating particles, Atmos. Chem. Phys., 16, 7879–7887, https://doi.org/10.5194/acp-16-7879-2016, 2016.

Patey, M. D., Achterberg, E. P., Rijkenberg, M. J., and Pearce, R.: Aerosol time-series measurements over the tropical Northeast Atlantic Ocean: Dust sources, elemental composition and mineralogy, Mar. Chem., 174, 103–119, https://doi.org/10.1016/j.marchem.2015.06.004, 2015.

Pawlowsky-Glahn, V. and Egozcue, J. J.: Compositional data and their analysis: an introduction, Geological Society, London, Special Publications, 264, 1–10, https://doi.org/10.1144/GSL.SP.2006.264.01.01, 2006.

Peckhaus, A., Kiselev, A., Hiron, T., Ebert, M., and Leisner, T.: A comparative study of K-rich and Na/Ca-rich feldspar ice-nucleating particles in a nanoliter droplet freezing assay, Atmos.

Chem. Phys., 16, 11477–11496, https://doi.org/10.5194/acp-16-11477-2016, 2016.

Perlwitz, J. P., Pérez García-Pando, C., and Miller, R. L.: Predicting the mineral composition of dust aerosols – Part 1: Representing key processes, Atmos. Chem. Phys., 15, 11593–11627, https://doi.org/10.5194/acp-15-11593-2015, 2015a.

Perlwitz, J. P., Pérez García-Pando, C., and Miller, R. L.: Predicting the mineral composition of dust aerosols – Part 2: Model evaluation and identification of key processes with observations, Atmos. Chem. Phys., 15, 11629–11652, https://doi.org/10.5194/acp-15-11629-2015, 2015b.

Pratt, K. A., DeMott, P. J., French, J. R., Wang, Z., Westphal, D. L., Heymsfield, A. J., Twohy, C. H., Prenni, A. J., and Prather, K. A.: In situ detection of biological particles in cloud ice-crystals, Nat. Geosci., 2, 398–401, https://doi.org/10.1038/ngeo521, 2009.

Price, H. C., Baustian, K. J., McQuaid, J. B., Blyth, A., Bower, K. N., Choularton, T., Cotton, R. J., Cui, Z., Field, P. R., Gallagher, M., Hawker, R., Merrington, A., Miltenberger, A., Neely, R. R., Parker, S. T., Rosenberg, P. D., Taylor, J. W., Trembath, J., Vergara-Temprado, J., Whale, T. F., Wilson, T. W., Young, G., and Murray, B. J.: Atmospheric Ice-Nucleating Particles in the Dusty Tropical Atlantic, J. Geophys. Res.-Atmos., 123, 2175–2193, https://doi.org/10.1002/2017JD027560, 2018.

Rebotier, T. P. and Prather, K. A.: Aerosol time-of-flight mass spectrometry data analysis: a benchmark of clustering algorithms, Anal. Chim. Acta, 585, 38–54, https://doi.org/10.1016/j.aca.2006.12.009, 2007.

Reilly, P. T. A., Lazar, A. C., Gieray, R. A., Whitten, W. B., and Ramsey, J. M.: The Elucidation of Charge-Transfer-Induced Matrix Effects in Environmental Aerosols Via Real-Time Aerosol Mass Spectral Analysis of Individual Airborne Particles, Aerosol Sci. Technol., 33, 135–152, https://doi.org/10.1080/027868200410895, 2000.

Reinard, M. S. and Johnston, M. V.: Ion formation mechanism in laser desorption ionization of individual nanoparticles, J. Am. Soc. Mass Spectr., 19, 389–99, https://doi.org/10.1016/j.jasms.2007.11.017, 2008.

Reitz, P., Spindler, C., Mentel, T. F., Poulain, L., Wex, H., Mildenberger, K., Niedermeier, D., Hartmann, S., Clauss, T., Stratmann, F., Sullivan, R. C., DeMott, P. J., Petters, M. D., Sierau, B., and Schneider, J.: Surface modification of mineral dust particles by sulphuric acid processing: implications for ice nucleation abilities, Atmos. Chem. Phys., 11, 7839–7858, https://doi.org/10.5194/acp-11-7839-2011, 2011.

Ro, C. U., Hwang, H., Kim, H., Chun, Y., and Van Grieken, R.: Single-particle characterization of four "Asian Dust" samples collected in Korea, using low-Z particle electron probe X-ray microanalysis, Environ. Sci. Technol., 39, 1409–1419, https://doi.org/10.1021/es049772b, 2005.

Rosenfeld, D., Rudich, Y., and Lahav, R.: Desert dust suppressing precipitation: a possible desertification feedback loop, P. Natl. Acad. Sci. USA, 98, 5975–80, https://doi.org/10.1073/pnas.101122798, 2001.

Ryder, C. L., Highwood, E. J., Lai, T. M., Sodemann, H., and Marsham, J. H.: Impact of atmospheric transport on the evolution of microphysical and optical properties of Saharan dust, Geophys. Res. Lett., 40, 2433–2438, https://doi.org/10.1002/grl.50482, 2013.

Salvador, P., Almeida, S. M., Cardoso, J., Almeida-Silva, M., Nunes, T., Cerqueira, M., Alves, C., Reis, M. A., Chaves, P. C., Artíñano, B., and Pio, C.: Composition and origin of PM_{10} in Cape Verde: Characterization of long-range transport episodes, Atmos. Environ., 127, 326–339, https://doi.org/10.1016/j.atmosenv.2015.12.057, 2016.

Scanza, R. A., Mahowald, N., Ghan, S., Zender, C. S., Kok, J. F., Liu, X., Zhang, Y., and Albani, S.: Modeling dust as component minerals in the Community Atmosphere Model: development of framework and impact on radiative forcing, Atmos. Chem. Phys., 15, 537–561, https://doi.org/10.5194/acp-15-537-2015, 2015.

Schepanski, K., Tegen, I., and Macke, A.: Saharan dust transport and deposition towards the tropical northern Atlantic, Atmos. Chem. Phys., 9, 1173–1189, https://doi.org/10.5194/acp-9-1173-2009, 2009a.

Schepanski, K., Tegen, I., Todd, M. C., Heinold, B., Bönisch, G., Laurent, B., and Macke, A.: Meteorological processes forcing Saharan dust emission inferred from MSG-SEVIRI observations of subdaily dust source activation and numerical models, J. Geophys. Res.-Atmos., 114, 1–18, https://doi.org/10.1029/2008JD010325, 2009b.

Schepanski, K., Tegen, I., and Macke, A.: Comparison of satellite based observations of Saharan dust source areas, Remote Sens. Environ., 123, 90–97, https://doi.org/10.1016/j.rse.2012.03.019, 2012.

Scheuvens, D., Schütz, L., Kandler, K., Ebert, M., and Weinbruch, S.: Bulk composition of northern African dust and its source sediments – A compilation, Earth-Sci. Rev., 116, 170–194, https://doi.org/10.1016/j.earscirev.2012.08.005, 2013.

Schmidt, S., Schneider, J., Klimach, T., Mertes, S., Schenk, L. P., Kupiszewski, P., Curtius, J., and Borrmann, S.: Online single particle analysis of ice particle residuals from mountain-top mixed-phase clouds using laboratory derived particle type assignment, Atmos. Chem. Phys., 17, 575–594, https://doi.org/10.5194/acp-17-575-2017, 2017.

Shen, X., Ramisetty, R., Mohr, C., Huang, W., Leisner, T., and Saathoff, H.: Laser ablation aerosol particle time-of-flight mass spectrometer (LAAPTOF): performance, reference spectra and classification of atmospheric samples, Atmos. Meas. Tech., 11, 2325–2343, https://doi.org/10.5194/amt-11-2325-2018, 2018.

Silva, P. and Prather, K.: Interpretation of mass spectra from organic compounds in aerosol time-of-flight mass spectrometry, Anal. Chem., 72, 3553–3562, 2000.

Sobanska, S., Hwang, H., Choël, M., Jung, H. J., Eom, H. J., Kim, H., Barbillat, J., and Ro, C. U.: Investigation of the chemical mixing state of individual asian dust particles by the combined use of electron probe X-ray microanalysis and raman microspectrometry, Anal. Chem., 84, 3145–3154, https://doi.org/10.1021/ac2029584, 2012.

Sodeman, D. A., Toner, S. M., and Prather, K. A.: Determination of single particle mass spectral signatures from light-duty vehicle emissions, Environ. Sci. Technol., 39, 4569–4580, https://doi.org/10.1021/es0489947, 2005.

Sullivan, R. C. and Prather, K. A.: Recent advances in our understanding of atmospheric chemistry and climate made possible by on-line aerosol analysis instrumentation, Anal. Chem., 77, 3861–3885, https://doi.org/10.1021/ac050716i, 2005.

Sullivan, R. C., Guazzotti, S. A., Sodeman, D. A., and Prather, K. A.: Direct observations of the atmospheric processing

of Asian mineral dust, Atmos. Chem. Phys., 7, 1213–1236, https://doi.org/10.5194/acp-7-1213-2007, 2007a.

Sullivan, R. C., Guazzotti, S. A., Sodeman, D. A., Tang, Y., Carmichael, G. R., and Prather, K. A.: Mineral dust is a sink for chlorine in the marine boundary layer, Atmos. Environ., 41, 7166–7179, https://doi.org/10.1016/j.atmosenv.2007.05.047, 2007b.

Sullivan, R. C., Miñambres, L., Demott, P. J., Prenni, A. J., Carrico, C. M., Levin, E. J. T., and Kreidenweis, S. M.: Chemical processing does not always impair heterogeneous ice nucleation of mineral dust particles, Geophys. Res. Lett., 37, 1–5, https://doi.org/10.1029/2010GL045540, 2010a.

Sullivan, R. C., Petters, M. D., DeMott, P. J., Kreidenweis, S. M., Wex, H., Niedermeier, D., Hartmann, S., Clauss, T., Stratmann, F., Reitz, P., Schneider, J., and Sierau, B.: Irreversible loss of ice nucleation active sites in mineral dust particles caused by sulphuric acid condensation, Atmos. Chem. Phys., 10, 11471–11487, https://doi.org/10.5194/acp-10-11471-2010, 2010b.

Tobo, Y., Zhang, D. Z., Nakata, N., Yamada, M., Ogata, H., Hara, K., and Iwasaka, Y.: Hygroscopic mineral dust particles as influenced by chlorine chemistry in the marine atmosphere, Geophys. Res. Lett., 36, L05817, https://doi.org/10.1029/2008GL036883, 2009.

Tsamalis, C., Chédin, A., Pelon, J., and Capelle, V.: The seasonal vertical distribution of the Saharan Air Layer and its modulation by the wind, Atmos. Chem. Phys., 13, 11235–11257, https://doi.org/10.5194/acp-13-11235-2013, 2013.

Usher, C. R., Michel, A. E., and Grassian, V. H.: Reactions on mineral dust, Chem. Rev., 103, 4883–4939, https://doi.org/10.1021/cr020657y, 2003.

Wonaschuetz, A., Kallinger, P., Szymanski, W., and Hitzenberger, R.: Chemical composition of radiolytically formed particles using single-particle mass spectrometry, J. Aerosol Sci., 113, 242–249, https://doi.org/10.1016/j.jaerosci.2017.07.012, 2017.

Worringen, A., Kandler, K., Benker, N., Dirsch, T., Mertes, S., Schenk, L., Kästner, U., Frank, F., Nillius, B., Bundke, U., Rose, D., Curtius, J., Kupiszewski, P., Weingartner, E., Vochezer, P., Schneider, J., Schmidt, S., Weinbruch, S., and Ebert, M.: Single-particle characterization of ice-nucleating particles and ice particle residuals sampled by three different techniques, Atmos. Chem. Phys., 15, 4161–4178, https://doi.org/10.5194/acp-15-4161-2015, 2015.

Yamaguchi, N., Ichijo, T., Sakotani, A., Baba, T., and Nasu, M.: Global dispersion of bacterial cells on Asian dust, Sci. Rep.-UK, 2, 525, https://doi.org/10.1038/srep00525, 2012.

Young, G., Jones, H. M., Darbyshire, E., Baustian, K. J., McQuaid, J. B., Bower, K. N., Connolly, P. J., Gallagher, M. W., and Choularton, T. W.: Size-segregated compositional analysis of aerosol particles collected in the European Arctic during the ACCACIA campaign, Atmos. Chem. Phys., 16, 4063–4079, https://doi.org/10.5194/acp-16-4063-2016, 2016.

Yuan, H., Rahn, K. A., and Zhuang, G.: Graphical techniques for interpreting the composition of individual aerosol particles, Atmos. Environ., 38, 6845–6854, https://doi.org/10.1016/j.atmosenv.2004.09.010, 2004.

Zawadowicz, M. A., Froyd, K. D., Murphy, D. M., and Cziczo, D. J.: Improved identification of primary biological aerosol particles using single-particle mass spectrometry, Atmos. Chem. Phys., 17, 7193–7212, https://doi.org/10.5194/acp-17-7193-2017, 2017.

Zelenyuk, A., Yang, J., Choi, E., and Imre, D.: SPLAT II: An Aircraft Compatible, Ultra-Sensitive, High Precision Instrument for In-Situ Characterization of the Size and Composition of Fine and Ultrafine Particles, Aerosol Sci. Technol., 43, 411–424, https://doi.org/10.1080/02786820802709243, 2009.

Zelenyuk, A., Imre, D., Wilson, J., Zhang, Z., Wang, J., and Mueller, K.: Airborne Single Particle Mass Spectrometers (SPLAT II & miniSPLAT) and New Software for Data Visualization and Analysis in a Geo-Spatial Context, J. Am. Soc. Mass Spectr., https://doi.org/10.1007/s13361-014-1043-4, 2015.

Zhu, A., Ramanathan, V., Li, F., and Kim, D.: Dust plumes over the Pacific, Indian, and Atlantic oceans: Climatology and radiative impact, J. Geophys. Res.-Atmos., 112, 1–20, https://doi.org/10.1029/2007JD008427, 2007.

Zimmermann, F., Weinbruch, S., Schütz, L., Hofmann, H., Ebert, M., Kandler, K., and Worringen, A.: Ice nucleation properties of the most abundant mineral dust phases, J. Geophys. Res.-Atmos., 113, D23204, https://doi.org/10.1029/2008JD010655, 2008.